MINERAL CARBONATION TO SEQUESTER CO_2 WITH CONCURRENT METAL SULFIDIZATION

by

FEI WANG

B.Eng., Wuhan University of Science and Technology, 2011
M.Eng., Wuhan University of Science and Technology, 2014

A DISSERTATION SUBMITTED IN PARTIAL FULFILLMENT OF THE REQUIREMENTS FOR THE DEGREE OF

DOCTOR OF PHILOSOPHY

in

THE FACULTY OF GRADUATE AND POSTDOCTORAL STUDIES

(Materials Engineering)

THE UNIVERSITY OF BRITISH COLUMBIA

(Vancouver)

October 2019

The following individuals certify that they have read, and recommend to the Faculty of Graduate and Postdoctoral Studies for acceptance, the dissertation entitled:

Mineral carbonation to sequester CO_2 with concurrent metal sulfidization

submitted by Fei Wang in partial fulfillment of the requirements for

the degree of Doctor of Philosophy

in Materials Engineering

Examining Committee:

Dr. David B Dreisinger, Materials Engineering
Supervisor

Dr. David G Dixon, Materials Engineering
Supervisory Committee Member

Dr. Wenying Liu, Materials Engineering
Supervisory Committee Member

Dr. Gregory M Dipple, Earth, Ocean and Atmospheric Sciences
University Examiner

Dr. Bern Klein, Mining Engineering
University Examiner

Additional Supervisory Committee Members:

Dr. Brend Wassink, Materials Engineering
Supervisory Committee Member

Supervisory Committee Member

Abstract

Global warming is an urgent issue all over the world and mineral carbonation for CO_2 sequestration is one of the best methods to permanently store CO_2 gas. To make the mineral carbonation process profitable, it is suitable to combine with metal sulfidization for valuable metal recovery by utilizing the carbonation process since there are increasing demands of valuable metals around the world as well. This dissertation established the theoretical system for the potentially successful development of mineral carbonation for permanent CO_2 storage and utilization for metal sulfidization. The fundamental mechanisms and kinetics of mineral carbonation of olivine have been elucidated. The most important factors affecting the mineral carbonation process were the temperature, CO_2 partial pressure (PCO_2), specific surface area, aqueous ionic strength (I) and addition of sodium bicarbonate. The effects of these parameters on the mineral carbonation of olivine have been quantified. The mechanism can vary under different conditions and mainly depended on PCO_2 and the aqueous I. The increase of the aqueous I and PCO_2 can help prevent passivation of the mineral carbonation reaction by preventing formation of a silica-rich layer or a uniform carbonate layer respectively. Once the aqueous I and PCO_2 are high enough, the mineral carbonation of olivine is always controlled by chemical reaction of the dissolution of olivine. Under the chemical reaction control, a quantitative kinetic model has been developed, which can be used to predict the mineral carbonation efficiency and also the requirements of carbonation conditions. It is possible to utilize the mineral carbonation process for recovery of the released valuable metal from the dissolution of olivine by in-situ sulfidization. The key for the in-situ metal sulfidization is to continuously supply sulfide ions in the mineral carbonation system in order to selectively convert the released valuable bivalent metal ions to recoverable metal sulfides.

Lay Summary

Excessive CO_2 emission by anthropogenic activities has resulted in global warming. Mineral carbonation that converts the greenhouse gas CO_2 to stable solid carbonates is regarded as the only way to permanently sequester CO_2. It has attracted world-wide attention since the 1990s but this technology has not been successfully applied yet thus far since there is no profit for industries in this application. This dissertation bridges the mineral carbonation technology and the potential application in mineral processing industries by utilizing the mineral carbonation process to enhance valuable metal recovery and to potentially compensate the costs of carbonation. The corresponding theoretical system has been successfully established and confirmed that it is possible to recover the valuable metals released from silicate minerals during the mineral carbonation by selectively sulfidizing the valuable metals as potentially recoverable metal sulfides.

Preface

This dissertation is original, independent work by Fei Wang. This research was to utilize mineral carbonation for CO_2 sequestration to enhance valuable metal conversion for potential recovery enhancement, as a collaboration project between the University of British Columbia (UBC) and Giga Metals Corporation under the supervision of Professor David Dreisinger. The original idea of this project was proposed by Professor David Dreisinger and Mr. Mark Jarvis. The author Fei Wang designed the research framework, carried out all the tests and analyzed all the data. Dr. Bérend Wassink provided the safety support throughout the project. Professor Edouard Asselin provided the stainless steel autoclave for this research. The LECO carbon and sulfur analysis and chemical composition analysis were provided by the Bureau Veritas Mineral Laboratories, Vancouver and SGS Canada Inc., Burnaby. The mineral composition measured through Quantitative X-ray diffraction with Rietveld refinement analysis was conducted by the Department of Earth, Ocean and Atmospheric Sciences, UBC. Sample lithology analysis among Turnagain samples was provided by Giga Metals Corporation. The specific surface area through BET analysis was analyzed by Ms. Sally Finora, Department of Mining Engineering, UBC. All the other tests and analysis were carried out by the author Fei Wang.

Partial contents in Chapter 2 and 5 have been published in the following peer-reviewed journals. The author Fei Wang wrote all the original journal articles. Professor David Dreisinger contributed to the major suggestions of revisions. All other co-authors provided less contribution to the interpretation and revisions.

1. Fei Wang, David Dreisinger, Jarvis Mark, Tony Hitchins, Devy Dyson, 2019. Quantifying kinetics of mineralization of carbon dioxide by olivine under moderate conditions. Chemical Engineering Journal, 360: 452-463. Portion of this paper appears in Chapter 5.

2. Fei Wang, David Dreisinger, Jarvis Mark, Tony Hitchins, 2019. Kinetics and mechanism of mineral carbonation of olivine for CO_2 sequestration. Minerals Engineering, 131: 185-197. Portion of this paper appears in Chapter 5.

3. Fei Wang, David Dreisinger, Jarvis Mark, Tony Hitchins, 2018. The technology of CO_2 sequestration by mineral carbonation: Present status and future prospects. Canadian Metallurgical Quarterly, 57(1): 46-58. Portion of this paper appears in Chapter 2.

Table of Contents

List of Tables

List of Figures

List of Rocks and Minerals

Lithology

Clinopyroxenite: An ultramafic rock, containing ≥90% clinopyroxene

Dunite: A subdivision of peridotites, also known as olivinite, containing ≥90% olivine

Peridotite: Ultramafic rock(<45% SiO_2), mainly containing olivine and clino-/ortho-pyroxene

Wehrlite: A subdivision of peridotites, mainly containing olivine and clinopyroxene

Mineralogy

Anorthite: $CaAl_2Si_2O_8$

Calcite: $CaCO_3$

Clinopyroxene: Monoclinic pyroxene

Diopside: $CaMgSi_2O_6$

Enstatite: $MgSiO_3$

Fayalite: Fe_2SiO_4

Forsterite: Mg_2SiO_4

Magnesite: $MgCO_3$

Melilite: $(Ca,Na)_2(Al,Mg,Fe^{2+})[(Al,Si)SiO_7]$

Nesquehonite: $MgCO_3\ 3H_2O$

Olivine: $(Mg,Fe)_2SiO_4$

Pentlandite: $(Fe, Ni)_9S_8$

Pyroxene: $XY(Si,Al)_2O_6$. X represents Ca, Na, Mg, Fe(II) etc.; Y represents Fe(III), Al, etc.

Serpentine: $(Mg, Fe)_3Si_2O_5(OH)_4$

Siderite: $FeCO_3$

Silica: SiO_2

Sulfides: MS, M represents metals, such as Fe, Ni, etc.

Tremolite: $Ca_{2(}Mg_{5\text{-}4.5}Fe_{0\text{-}0.5})Si_8O_{22}(OH)_2$

Wollastonite: $CaSiO_3$

Acknowledgements

First of all, I would like to give my most thanks to my supervisor Professor David Dreisinger. Thank you so much for giving me the precious opportunity to come to UBC and to lead this amazing project! Thanks to you, I have the chance to broaden my views in academic research and personally re-define the hydrometallurgy area. I feel like that I am contributing myself to the world and realizing my personal and social values. Thank you so much for all your support and patience! You always give me your kindest support and best wishes since the first time we met. I am really grateful! Thank you so much for your guidance and suggestions not only for the research project but also for my life confusion and my future academic plan. I am highly honoured to have you as my life mentor. All your support and help have been deeply appreciated!

I would like to express my sincere gratitude to Dr. Bérend Wassink for your support in safe working in the laboratory and professional suggestions to advance my work. I also want to thank Professor Edouard Asselin and Dr. Jianming Lu for your technical support. Thanks to all the members in our hydrometallurgy group, Chihwei, Brighty, Chulho, Jackie, Maryam M., Maryam R., Martin, Hiroki, Jamie, Roselyn, Junichi, Renaud and Ryan, Hongxing, Pablo, Baseer, and others. Thank you very much for your friendship!

Thanks to the financial support from the Natural Sciences and Engineering Research Council of Canada (NSERC) (CRDPJ 523097 - 17) and (505580 2016). Thanks to Giga Metals Corporation, especially Mr. Mark Jarvis and Mr. Tony Hitchins for your technical support and encouragement, I am proud to participate in this wonderful project. Special thanks to the Natural Sciences and Engineering Research Council of Canada (NSERC) (CRDPJ 523097 - 17) for financial support and Sibelco Europe for providing the high-grade olivine for free.

I also want to thank my PhD committee members, Professor David Dixon and Professor Wenying Liu for all your professional support and suggestions. Thanks to all the staff in the Department of Materials Engineering, Fiona, Michelle, Mary, Norma, Sherry, Marlon, Ross, Carl, Wonsang, Heli and Jacob for all your help.

Finally I own a great debt of gratitude to my dearest family, my wife Jenny, my daughter Ricky, my parents Xumei and Hongjian. Without your support, I cannot pursue my dream and cannot finish my PhD research. Especially, Jenny and Ricky, thank you very much for accompanying me to Canada from our home country. I am deeply grateful to you!

I would like to dedicate this dissertation to my wife, my daughter, my mum and dad

who are always supporting me!

1 Introduction

According to the reports of the International Panel on Climate Change (IPCC)[1], it is postulated that the global climate is changing rapidly in recent times[2]. Changes which have been observed include the rising of global average sea level[3–6], the decreasing of global ice thickness[3,6,7], and the acidification of oceans[8,9]. All these changes have the potential to affect human health and welfare. As a result of these changes and potential detrimental impacts, it may be desirable to control or decrease the CO_2 concentration in the atmosphere[10,11]. The Paris Agreement has been signed by 197 countries in 2015[12,13], whereby the global goal has been set to control the global temperature increase below 2 ℃ and 1.5 ℃ at the best[5,14]. Among the available methods, CO_2 removal by sequestration by mineral carbonation is considered as the most promising permanent method[15–21]. In fact, mineral carbonation is a natural and exothermic process, which has been observed naturally all over the world[22–24]. In essence, the mineral carbonation process transforms CO_2 gas into carbonates and the most important reactions are through silicate minerals, shown in Table 1.1. More importantly, the formed carbonates are stable and will not be affected by weakly acidic rain[22]. Theoretically, the carbonates will be stable through long geological periods[25,26].

Table 1.1 $\triangle G°$ of the most important mineral carbonation reactions at 25 ℃.

Reactions	$\triangle G°$, kJ/mol CO_2
$Mg_2SiO_4 + 2CO_2 = 2MgCO_3 + SiO_2$	-18.59
$Mg_3Si_2O_5(OH)_4 + 3CO_2 = 3MgCO_3 + 2SiO_2 + 2H_2O$	-1.93
$CaSiO_3 + CO_2 = CaCO_3 + SiO_2$	-40.56
$Fe_2SiO_4 + 2CO_2 = 2FeCO_3 + SiO_2$	-11.45

However, these natural processes are kinetically unfavourable under atmospheric temperature and pressure conditions though they are thermodynamically favoured[23] as Table 1.1 shows. The

time frame for the reaction may range from hundreds of years to millennia[27]. Since the 1990s[15,16], the current mineral carbonation research mainly focuses on how to accelerate this natural process. Thus far, the research mainly focuses on the ex-situ direct mineral carbonation, which means that CO_2 reacts with the silicate minerals after removal from the original deposit in the presence of H_2O. Researchers have obtained many significant breakthroughs[15,23,28–30], but the key limitations are the slow kinetics, high energy requirements and high costs. In order to make it cost-effective, some researchers have developed the idea that the products after mineral carbonation may be recovered for sale, such as high-purity silica and carbonates. However, it is difficult to effectively separate the individual mineral products from the whole mineral carbonation product mass. There is no successful large-scale application of CO_2 sequestration by mineral carbonation thus far mainly due to the lack of profit for the industry. Therefore, the development of an effective and low-cost process for CO_2 sequestration by mineral carbonation is urgently required. If the mineral carbonation can be achieved as an economically favourable technology, it will attract the attention of industry and facilitate the industrial application.

In addition, some mineral companies have to operate beyond the limits of the current electrical grid. For example, Giga Metals intends to develop power from the combustion of liquid natural gas in order to recover valuable metal sulfides mineral concentrates from ores. However, the majority of the gangue minerals in the ore are olivine and serpentine[31], which are regarded as two of the main minerals suitable for mineral carbonation. It may be possible to combine sulfide mineral recovery with mineral carbonation to achieve valuable carbon sequestration at the mineral processing site. This combination can share the costs and earn the carbon credits for the mineral companies while addressing the significant emission of CO_2 gas from combustion of natural gas. Furthermore, some valuable metals that may exist in the olivine and serpentine

mineral phases may be unrecoverable by simple beneficiation. These metal values will enter the final tailings in a conventional flotation plant. For Giga Metals, up to 41% of the nickel and up to 50% of the cobalt are in the form of silicates and therefore the overall nickel and cobalt flotation recovery is only around 55%-60%[32] due to the abundance of nickel and cobalt in silicates. If the unrecoverable metals can be converted into easily recoverable metal sulfides as part of a mineral carbonation process, Giga Metals may obtain improvement of valuable metals recovery and increase economic feasibility. However, the nickel and cobalt in silicates are in the crystal structure by substituting the Fe/Mg atoms of olivine. It is necessary to break down the crystal structures of olivine and to release the valuable metals including nickel and cobalt. Mineral carbonation provides a technical route to achieve this objective.

As a result, the mineral carbonation and metal sulfidization can work together. Therefore, this dissertation focuses on the mineral carbonation technology for the CO_2 storage and the concurrent process of metal sulfidization for metal recovery enhancement.

2 Literature review

Since the 1990s[16], the mineral carbonation technology has been researched intensively. The technology of mineral carbonation has progressed rapidly during this time. The time required for complete mineral carbonation has been shortened from thousands of years to tens of years, hundreds of days, hundreds of hours and finally to several hours[22]. It has been concluded that the presence of water is a significant factor known to accelerate the mineral carbonation process[33,34]. Generally, there are two ways to sequester CO_2 gas as stable carbonates: a passive way[35–38] and an active way[15,23,39–41] as shown in Figure 2.1. The passive way is to sequester the CO_2 gas by mineral carbonation under atmospheric pressure and temperature. The important work in this way is to trap the amount of the sequestered CO_2 gas and to maximize the rate of the natural sequestration. The goal of research in this field is to determine which natural conditions can benefit the carbonation process. The development of the passive way is mainly inspired by two key characteristics of mineral carbonation: the mineral carbonation is a natural weathering process and minimal energy inputs are required to facilitate the mineral carbonation. However, it is still controversial whether the passive method is effective for reducing CO_2 contributions to global warming.

The active way is to accelerate the slow natural process by changing the conditions for mineral carbonation. There are two main methods to accelerate the mineral carbonation according to different schemes where mineral carbonation reaction is happening: in-situ mineral carbonation[42–46] and ex-situ mineral carbonation[47–54]. In-situ mineral carbonation involves injecting CO_2 gas underground and to allow the injected CO_2 gas to react with silicate minerals to form permanently stable carbonates. In contrast, ex-situ mineral carbonation involves pre-

treatment of the silicate minerals for the intensive reaction between CO_2 gas and the pre-treated minerals in a dedicated reactor. Furthermore, the ex-situ mineral carbonation can be further sub-divided into direct and indirect processes. If the mineral carbonation reaction happens directly between CO_2 gas and materials under a specific condition, it is called ex-situ direct mineral carbonation process. If bivalent metals are first extracted from the silicate minerals followed by the reaction between the bivalent metals and CO_2 gas, this process is regarded as ex-situ indirect mineral carbonation. The ex-situ indirect mineral carbonation is an adaptation of the development of the ex-situ direct carbonation technology in order to recover valuable by-products.

Since this dissertation combines the mineral carbonation technology and metal sulfidization for potential enhanced metal recovery, the literature review focuses on the active way of mineral carbonation. Through the analysis and discussion of each method, it is expected to confirm which way is more suitable for the development of mineral carbonation and its utilization for metal sulfidization and recovery.

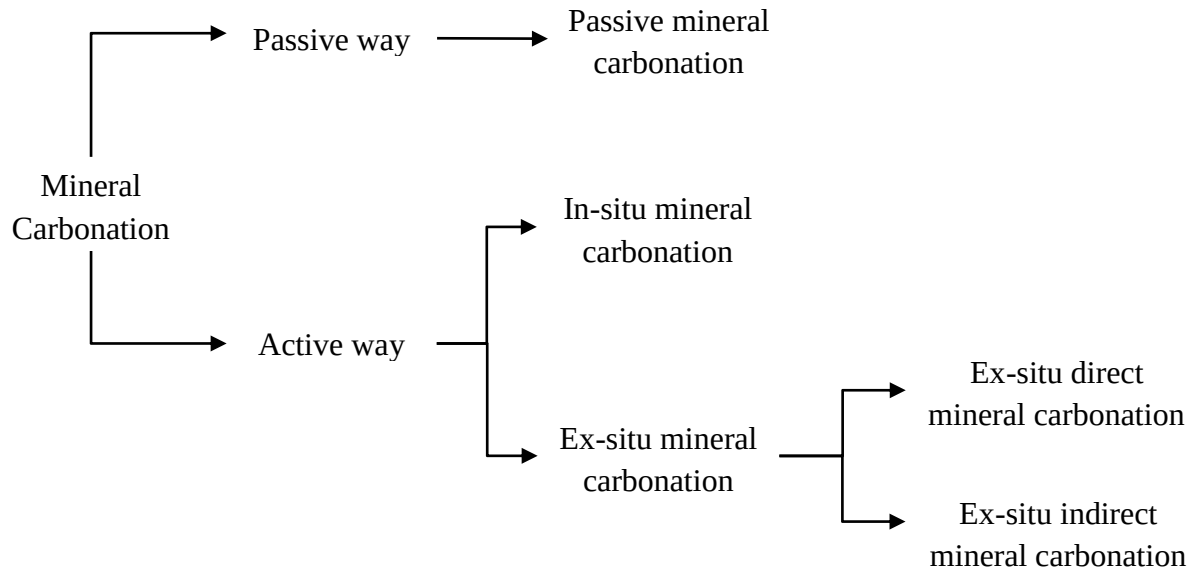

Figure 2.1 Structure of mineral carbonation technology development.

2.1 In-situ mineral carbonation

In-situ mineral carbonation is focused on utilization of Mg-, Fe- and Ca- silicate minerals at present. The Mg-, Fe- and Ca- silicate minerals which are available for mineral carbonation are mainly in the forms of basalts and peridotite[36]. They are called mafic and ultramafic rocks according to their content of SiO_2, 45-52% or <45%, respectively. Both groups of silicate minerals are being researched for carbon dioxide sequestration by carbonation.

Basalts form the top igneous layer in the oceanic crust and occur in large continental provinces, as shown in Figure 2.2. Generally, basalts are more abundant than peridotite.[36]

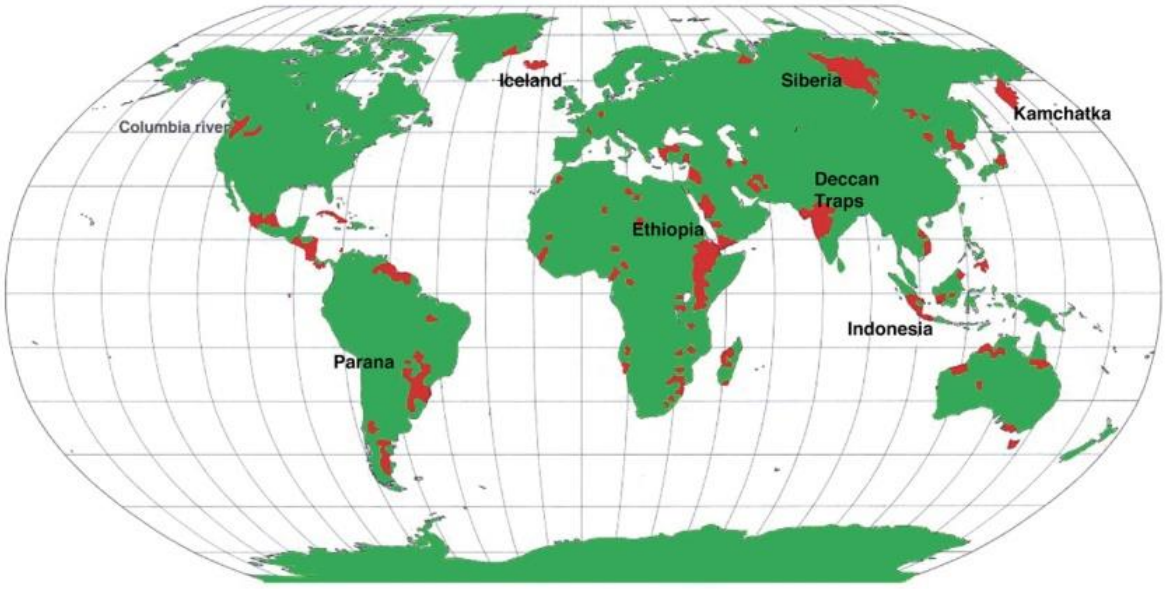

Figure 2.2 Locations of continental basalts that could serve as in-situ mineral carbonation sites[55].

The CarbFix pilot project in Iceland demonstrated the in-situ mineral carbonation by basalts. This project is a cooperation between Iceland and the United Kingdom (UK), the United States of America (USA), France, Netherlands, Australia and Denmark[56–58]. A CO_2-H_2S gas mixture

was injected into a 2000-m-deep well[59]. Mineral carbonation was monitored via 8 monitoring wells ranging in depth from 150 to 1300 m, as shown in Figure 2.3[56]. During the in-situ mineral carbonation, the water temperature and pH were in the range from 20 ℃ to 33 ℃ and from 8.4 to 9.4, respectively[60]. The injected gas was free of oxygen. Furthermore, in order to prevent the CO_2 gas leakage during injection, they developed a novel CO_2 injection system, dissolving the gas mixture into down-flowing water into the well and keeping the CO_2 concentration below its solubility under these conditions[61]. The isotopic analysis method was applied to monitor the mineral carbonation process. Their study demonstrated permanent CO_2 sequestration into carbonates through in-situ mineral carbonation by basaltic rocks is technically feasible. They found that 95% of the CO_2 injected into the CarbFix site had been mineralized in just less than 2 years[56], rather than hundreds to thousands of years thought to be required previously. The conditions used were: 20 ℃-33 ℃, pH=8.4-9.4 with water but without O_2, up to almost 200 bar CO_2 pressure. Thus far, the CarbFix project has successfully sequestered 175 tonnes of pure CO_2 and 73 tonnes of a CO_2-H_2S gas mixture[56]. Lu et al. also verified that O_2 (up to 3.5% of the mixture gas) has no detrimental effect on the mineral carbonation process[62], which means it is unnecessary to use pure CO_2 gas. Based on CarbFix's success, another in-situ mineral carbonation pilot project, Big Sky Regional Partnership, is being conducted in the Columbia River Basalt in the USA, with the support of the CarbFix team (https://www.or.is/english/carbfix-project).

However, Hang et al.[63] reported a different outcome in a study of a natural CO_2 analogue reservoir (CO_2 gas injected into depleted oil reservoirs[64]). They found that the in-situ mineral carbonation was strongly dependent on porosity and permeability and there was no obvious

evidence of the mineral carbonation reaction because of the presence of bitumen coatings preventing the minerals from reaction.

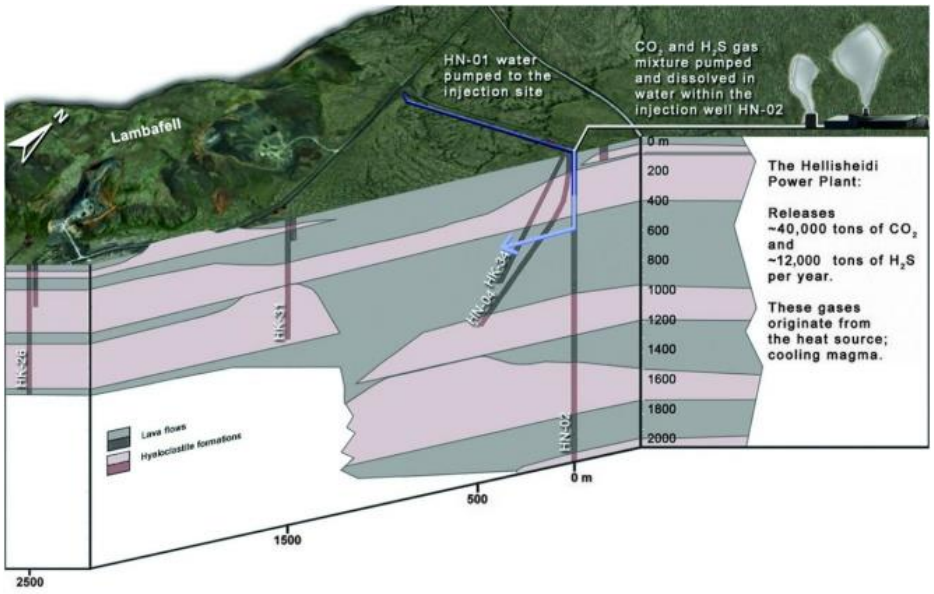

Figure 2.3 Geological cross-section of the CarbFix injection site[56].

Peridotite has a higher divalent metals content with lower silica content. Theoretically, it has great capacity to permanently store CO_2 and is more suitable for mineral carbonation than basalts. Peridotite occurs on almost every continent[36,65]. There are significant peridotite deposits along the east and west coast of North America. Peridotite is theoretically more reactive than basalts[66] owing to its higher content of bivalent metals. However, both porosity and permeability of peridotite are lower (only 10^{-13} to 10^{-10} m^2 permeability for 1% fracture porosity)[36] compared to basalts. These properties hinder the in-situ mineral carbonation development and thus the research of in-situ mineral carbonation by peridotite is still at an early stage[46].

Kelemen and Matter[36,45] have evaluated the mineral carbonation capacity of a deposit of peridotite in Oman. This site alone has a capacity of over 30 trillion tons of CO_2. The passive

carbonation of surface exposed peridotite in Oman is estimated at approximately 10^4 tons of CO_2 per year. Many researchers[24] have studied the passive mineral carbonation occurring with mining tailings and the results are also promising. Lechat et al. [67] simulated in-situ mineral carbonation for ultramafic milling wastes with laboratory scale experiments. They presumed that the diffusion of CO_2 was the dominant transport mechanism and the mineral carbonation reaction close to the surface was the most active. In fact, this process should be regarded as ex-situ mineral carbonation because the milling wastes are the tailings from ore processing, not the original ore.

Schaef et al.[68] developed in-situ High Pressure X-Ray Diffraction (HXRD) and in-situ Infrared (IR) Spectroscopy and applied them to in-situ mineral carbonation studies. With the help of these innovative in-situ analysis methods, nesquehonite, magnesite and calcite formed by mineral carbonation reactions have been identified under variable CO_2 pressures (90-160 bar) and temperatures (35-70 ℃). In addition, they observed that extents of carbonation of peridotite were correlated to the thickness of the mineral surface's water-film measured by in-situ IR. The mineral enstatite was the least reactive mineral observed by in-situ HXRD whereas wollastonite was the most reactive followed by forsterite.

However, there is still no industrially applied in-situ (underground) mineral carbonation project reported thus far, though the CarbFix pilot project has attracted a lot of attention. The limits are mainly the decrease of permeability due to clogging or the decrease in porosity from precipitates and the passivation layers from silica products. Though Zhang and Liu[69] reviewed porosity-permeability relationships in modeling salt precipitation during in-situ mineral carbonation, there is no unequivocal conclusion about the direct relationship between the permeability or porosity

and the precipitation of carbonates. There are still a lot of works to do to advance the in-situ mineral carbonation.

2.2 Ex-situ direct mineral carbonation

The majority of mineral carbonation technology development still focuses on the ex-situ process. Since the 1990s[16,70–75], scientists and engineers have pursued fundamental research on mineral carbonation of peridotite with the goal of accelerating the natural process. At present, the fundamental characteristics of mineral carbonation have been reported. It is hard to accelerate the process except by using more extreme conditions of high temperature, high CO_2 pressure and small particle size[72,76]. If the materials mainly contain serpentine, heat pre-treatment is also needed[77,78] to remove the –OH group and to disintegrate the crystal structure of serpentine for the dissolution of serpentine into solution, because serpentine materials are a weathering product of olivine or other minerals and are more thermodynamically stable than olivine. The $\Delta G°$ of dissolution of olivine and serpentine are -93.28 kJ/mol Mg and -76.61 kJ/mol Mg respectively at 25 ℃ and standard conditions, shown in Table 2.1. This makes serpentine less effective for mineral carbonation. By contrast, heat pre-treatment does not impact the mineral carbonation efficiency of forsterite[77] (Mg_2SiO_4, also called white olivine) since forsterite has no –OH groups in contrast to serpentine. The reasons why such severe conditions are needed may be due to one of a number of potential rate-limiting steps[15] (shown in Figure 2.4): the CO_2 dissolution into solution from gas (Step I) and diffusion in aqueous solution (Step II), the dissolution of Mg- or Ca- silicate minerals into solution (Step V and VI) and the product layer diffusion (for example the generated $MgCO_3$ and SiO_2 layers, Step III and V). However, which step controls the rate and extent of mineral carbonation is controversial[79,80]. There is still a need for a systematic kinetic study.

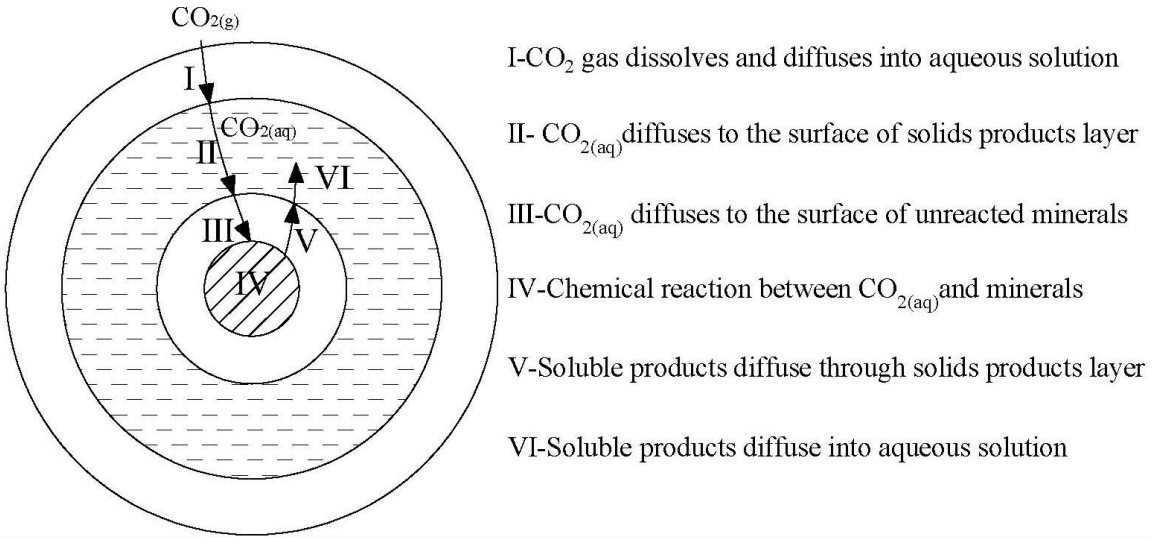

Figure 2.4 Schematic diagram of reaction between CO_2 and Mg-/Ca- silicate minerals[15].

Based on the current kinetic models, the severe conditions required for mineral carbonation can be explained. Firstly, particle size determines the specific surface area which affects the contact between minerals and solution, which controls the dissolution or carbonation of the minerals. Generally with decreasing particle size, the mineral carbonation rate increases. Temperature affects the dissolution of both minerals and the solubility of CO_2 gas in solution, as shown in Table 2.1.

Table 2.1 Thermodynamic data for CO_2 gas dissolution and acid dissolution of forsterite and serpentine into aqueous solution.

△G, kJ/mol	$CO_2(g) = CO_2(a)$					$Mg_2SiO_4+4H^+=$	$Mg_3Si_2O_5(OH)_4+6H^+=$
Temperature	PCO_2, bar					$2Mg^{2+}+SiO_2+2H_2O_{(l)}$	$3Mg^{2+}+2SiO_2+5H_2O_{(l)}$
℃	1	10	30	50	100		
25	7.84	2.14	-0.59	-1.85	-3.57	-186.55	-229.83
60	10.85	4.47	1.43	0.01	-1.91	-180.08	-223.17
100	13.63	6.49	3.08	1.50	-0.65	-172.91	-216.22
140	15.81	7.91	4.13	2.38	0.00	-165.84	-209.69
200	18.04	8.98	4.66	2.65	-0.08	-154.78	-199.62

All data are from HSC Chemistry 7.1.

Thermodynamically, the dissolution of minerals and solubility of CO_2 gas decrease with increasing temperature at temperatures below 200 ℃, according to Table 2.1. But the fact is that the rate of dissolution of minerals increases with increasing temperature[81]. In order to address this issue, high CO_2 pressure is needed. High CO_2 pressure can improve the dissolution of the CO_2 to balance the detrimental effects of high temperature[81]. Furthermore, as the mineral carbonation reaction proceeds, the solid carbonates and silica product will be produced and cover the surface of unreacted minerals, which may hinder the further mineral carbonation reaction. The kinetics of this process may be described by the shrinking core model (SCM) if diffusion of reactants or products through the product layer is rate determining. Therefore, continuous agitation and a low liquid/solid ratio may be helpful as these conditions favour the removal of the product layer by attrition.

The Albany Research Center (ARC) discovered an effective catalyst to accelerate the rate of mineral carbonation. The rate of mineral carbonation increases in the presence of a mixture of $NaHCO_3$ and NaCl[70,72,74,75,82]. The hypothesis for why the mixture enhances the carbonation is indicated in reactions (5-7), though without detailed thermodynamic evidence and the existence of the magnesium-chloride complex[83]: Bicarbonate ions can react with the Mg- or Ca- silicate minerals to form more insoluble carbonates and hydroxyl ions; The hydroxyl ions can immediately absorb CO_2 gas to form bicarbonate ions; Furthermore, the chloride ions can form complex ions with magnesium cations, which can facilitate the dissolution of magnesium silicate minerals by increasing the solubility of magnesium. The NaCl and $NaHCO_3$ additives are not consumed. In addition, the discovery shifted the focus of mineral carbonation development to consideration of basic conditions. Historically the main approach has been to dissolve silicate minerals under acid conditions prior to carbonation[84,85]. The slurry of Mg- or Ca- silicate

minerals is weakly basic. Most current mineral carbonation researchers are studying similar catalytic solutions.

$$Mg_2SiO_4 + 2HCO_3^- \rightarrow 2MgCO_3 + SiO_2 + 2OH^- \quad (5)$$

$$OH^- + CO_2 \rightarrow HCO_3^- \quad (6)$$

$$Mg^{2+} + nCl^- - \rightarrow [MgCl_n]^{2-n} \quad (7)$$

Fundamental research not only promotes the development of ex-situ mineral carbonation but also in-situ mineral carbonation. However, it is also clear that intensive energy is needed for acceptable mineral carbonation efficiency and rates, which of course results in very high costs. It is because of this that there is still no economically successful ex-situ mineral carbonation application. ARC tried to combine ex-situ direct mineral carbonation with in-situ mineral carbonation by injecting mineral slurry and CO_2 gas underground because the ex-situ direct process is too energy-intensive. They calculated costs of US$ 78 and 630 kW ħ per tonne CO_2 sequestered by olivine and US$ 537 and 2200 kW ħ per tonne CO_2 sequestered for serpentine (calculated in 2007)[71,73,75]. This approach may be promising and further study is warranted.

In order to enhance the mineral carbonation efficiency under milder conditions of lower pressure and lower temperature, some researchers[86–94] have started to develop an in-situ grinding mineral carbonation concept. In this concept mineral carbonation occurs during the grinding stage. The mechanism of in-situ grinding mineral carbonation can be explained by Figure 2.5. Park and Fan[95] found that in-situ grinding carbonation can help remove SiO_2 passivation layers that inhibit further carbonation and improve the dissolution of serpentine, especially when there is a Mg-leaching lixiviant in this system. The research was conducted in a 5 cm diameter fluidized bed reactor as shown in Figure 2.6. Verduyn et al.[41] also studied direct contact of flue gas containing

CO_2 with a mineral slurry during grinding. This was an attempt to increase the mineral carbonation efficiency as the flue gas has a lower CO_2 content (about 10% CO_2) as compared to using pure CO_2 gas. Turianicová et al.[86,87,93,96] used a planetary ball mill to do the in-situ grinding mineral carbonation of vermiculites without additives and verified that this method can indeed enhance the structural breakdown of minerals. However, most of researchers have not continued to study in-situ grinding mineral carbonation because there are specific and non-conventional requirements for milling equipment such as sealed systems at higher pressure than atmosphere. These requirements may not only increase investment but also introduce process risks to the grinding step in a mineral processing plant. Nevertheless, in-situ grinding mineral carbonation may still be worth further research.

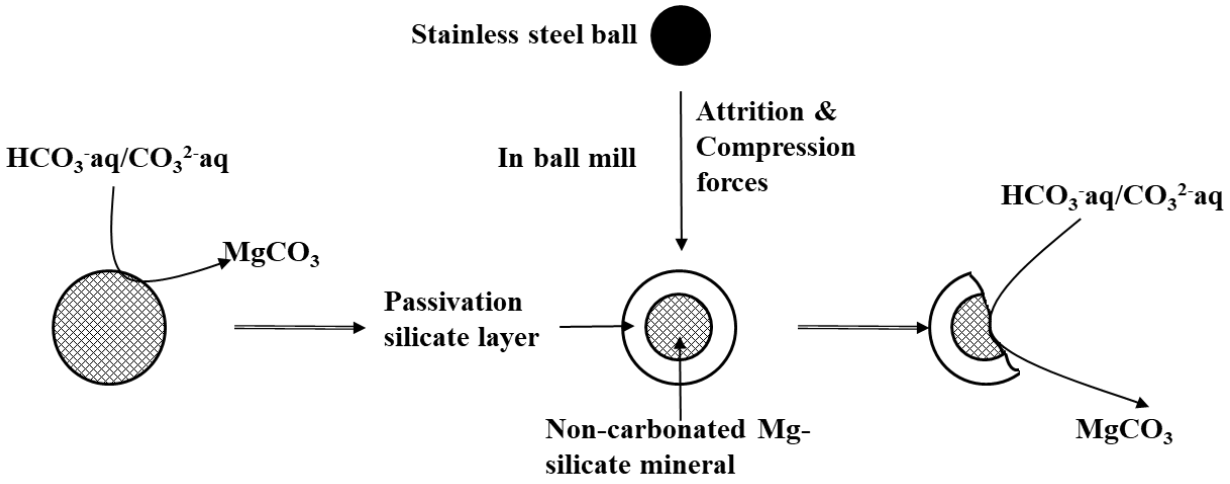

Figure 2.5 Illustrator of the mechanism of in-situ grinding direct aqueous mineral carbonation.

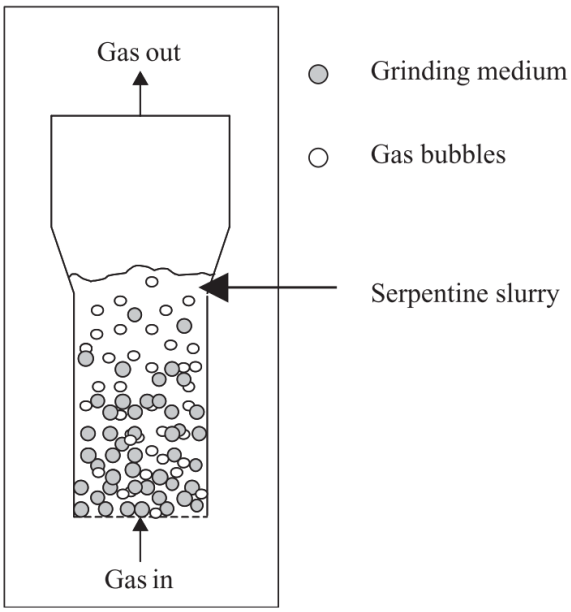

Figure 2.6 Schematic diagram of the internal grinding system[95].

Santos et al.[97] researched ex-situ direct mineral carbonation as a pre-treatment to enhance nickel extraction from pure olivine. The olivine had a nickel content of 0.27%. The majority of the nickel exists in this olivine by replacing magnesium in the Mg-silicate structure as the isomorphous Mg-Ni silicate ($(Mg,Ni)_2SiO_4$). Full carbonation was demonstrated under the following conditions: 35 bar CO_2 pressure, 200 ℃, 20 (wt)% slurry concentration, 86% <80 μm particle size, 0.64 M $NaHCO_3$+1 M NaCl and 72 hours residence time. The leaching behaviour of nickel with HCl or HNO_3 between fresh olivine and fully carbonated olivine was compared and it was found that the leaching efficiency of carbonated olivine was dramatically increased from around 60% to nearly 100%. Carbonation made nickel leaching easier. Nickel was found to be highly dispersed in the carbonated olivine product when studied by electron probe microanalyzer (EPMA) analysis. This research, for the first time, connected ex situ direct mineral carbonation with valuable metal recovery. However, after the carbonation, the mineral carbonates were decomposed by acid leaching. Therefore, CO_2 in the overall process first forms

carbonates and then is released again as CO_2 (for example $CO_2g \rightarrow MgCO_3s \rightarrow CO_2g$). No CO_2 is permanently sequestered. That is to say, in terms of CO_2 sequestration, this process is futile. But the important point is ex-situ mineral carbonation could be connected with valuable metal recovery. Hamilton et al. also shows the similar concept that heap leaching of nickel-containing waste mines followed by passive mineral carbonation is considered to upgrade the nickel content and potentially enhance nickel recovery from waste tailings[98,99].

A number of researchers[23,28,80] believe that the Energy Reactor© invented by Innovation Concepts may be the most promising ex-situ direct mineral carbonation method, as shown in Figure 2.7(a). The Energy Reactor© uses hydrostatic pressure to maintain conditions to contain the high CO_2 pressure required and also utilizes the heat released from mineral carbonation reaction to maintain temperature. These innovations may simplify the equipment for carbonation and reduce the costs considerably. In addition, due to high speed of slurry movement through the Energy Reactor©, particles will be attritted, which may remove the passivation layers of silica and facilitate the successive mineral carbonation reaction. According to the report by Innovation Concepts, the temperature and pressure can be up to 200 ℃ and 90 bar[100]. However, this process is hard to simulate on a laboratory scale. In 2016, there was cooperation between Canada and the Netherlands to do lab-scale CO_2 Energy Reactor© experiments, as shown in Figure 2.7(b). The mineral carbonation achieved through this apparatus was good (approximately 40% carbonation efficiency under conditions of D_{50}=20 μm particle size, 175 ℃, PCO_2=100 bar, 0.64 M $NaHCO_3$+0.056 M organic acids for 3 hours) but it still did not demonstrate all the benefits of the Energy Reactor©. In addition, the results indicated that it is not advisable to obtain maximal mineral carbonation efficiency by increasing the processing costs. The researchers also concluded that the main impetus for mineral carbonation is the value of the products.

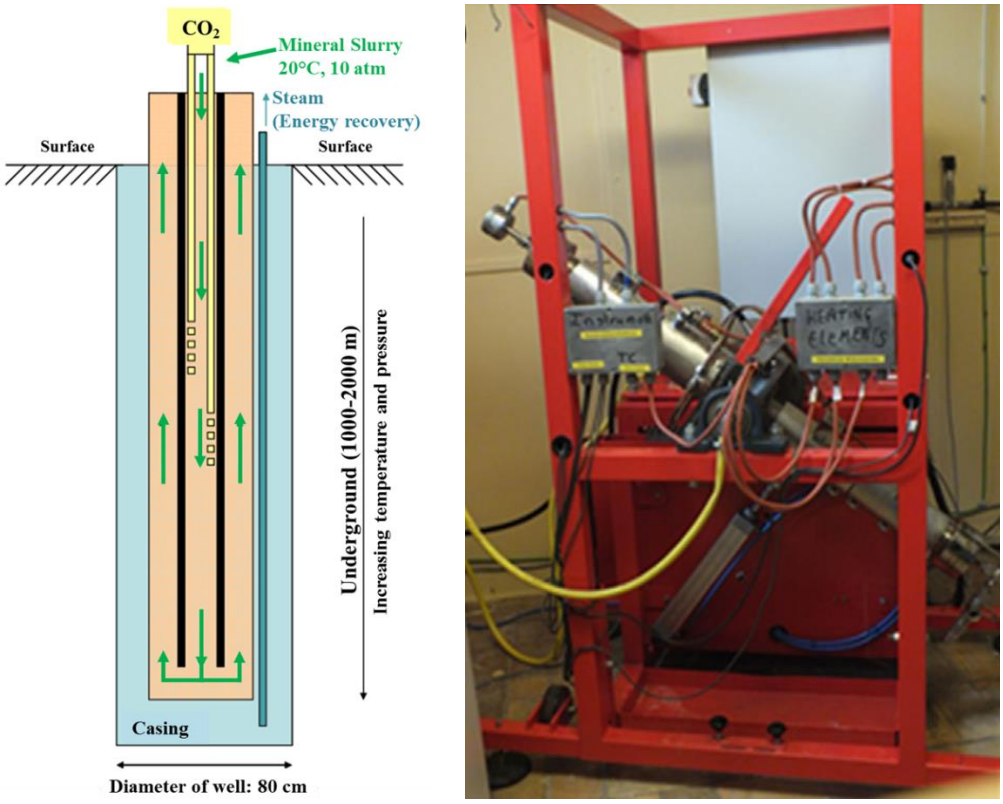

Figure 2.7 (a) Reproduced schematic representation of the CO_2 Energy Reactor[©23] and (b) a lab-scale Energy Reactor: "rocking autoclave" at ~45° position[80].

Various researchers are trying to find a more efficient carbonation catalyst than $NaHCO_3$+NaCl. One of the catalysts is Carbonic Anhydrase (CA). It is a kind of metalloenzyme, symbolized E ZnH_2O. The mechanism by which it enhances mineral carbonation can be seen in reactions (8-12). Compared to the $NaHCO_3$+NaCl, it can enhance not only the dissolution of silicate minerals but also the dissolution of CO_2 gas, both of which may be rate-limiting steps. Power et al.[101–103] used it to accelerate the mineral carbonation by brucite and verified that CA can help address the rate-limiting step of CO_2 dissolution. However, the price of CA is too expensive for widespread use. A price of more than $1000 per 500 mg Bovine CA (No. C3934) has been quoted[104]. Therefore, some researchers believe it is impossible to adopt such an expensive chemical as CA to sequester CO_2[15]. It is also the main reason why there is almost no other research on mineral

carbonation of olivine enhanced by CA. But if the price of CA could become much cheaper artificial CA, mineral carbonation could be reconsidered.

$$\mathrm{E \cdot Zn}H_2O \rightarrow \mathrm{E \cdot Zn}OH^- + H^+ \quad (8)$$

$$\mathrm{E \cdot Zn}OH^- + CO_2 \rightarrow \mathrm{E \cdot Zn}HCO_3^- \quad (9)$$

$$\mathrm{E \cdot Zn}HCO_3^- + H_2O \rightarrow \mathrm{E \cdot Zn}H_2O + HCO_3^- \quad (10)$$

$$Mg_2SiO_4 + 4H^+ \rightarrow 2Mg^{2+} + SiO_2 + 2H_2O \quad (11)$$

$$Mg^{2+} + 2HCO_3^- \rightarrow MgCO_3 + 2H^+ \quad (12)$$

Mineral carbonation by industrial wastes plays a role in mineral carbonation though its capacity is much smaller than that of natural silicate minerals[15,23]. Industrial wastes containing divalent metal usually have higher chemical reactivity and their corresponding mineral carbonation can therefore achieve an acceptable rate of CO_2 conversion under milder conditions[23,105]. Furthermore, industrials wastes can come from various resources, for example, coal fly ash (FA)[106–112] and metallurgical slag[49,54,113,114]. Meanwhile, the applied technology is the same as that of mineral carbonation by silicate minerals.

Mayoral et al.[106] studied the direct mineral carbonation route using lime-rich coal ashe. A carbonation efficiency of 78% was achieved for coal ash and coal waste at 75 ℃, pH=11.5, 60 mL solution/g ash by bubbling 110 mL/min of pure CO_2 gas for only 1 h. Nyambura et al.[108] adopted brine and coal FA to sequester CO_2 and found that fractionated coal FA, especially 20-150 μm particle size, had the best carbonation efficiency (71.84 kg CO_2/t FA) while larger or smaller particle size exhibited less carbonation capacity. Furthermore, carbonation in brine was more efficient than in pure water. Dananjayan et al.[109] compared the direct gas-solid mineral carbonation with direct aqueous mineral carbonation (liquid/solid L/S ratio of 15) at room

temperature with 4 bar CO_2 for 2 h, and found that the dry route is a much slower process. The dry route achieved carbonation of 26.3 kg CO_2/t coal FA (at 10 bar CO_2 for 1 h) while the aqueous route resulted in 50.3 kg CO_2/t coal FA (at 4 bar for 2 h). Hosseini et al.[107] adopted the indirect mineral carbonation route to sequester CO_2. In the first stage, coal FA was leached by NH_4Cl solution. The leachate containing Mg^{2+} and Ca^{2+} was then used to fix carbon dioxide by injecting flue gas containing CO_2 into the leachate. The process produces a carbonate product (a mixed calcium/magnesium carbonate) which can be sold. The leaching residue also can be sold as a cement additive. During this process, ammonium chloride solution can be recycled. Theoretically, this process may be profitable. Han et al.[110] also used coal FA to demonstrate indirect mineral carbonation research at room temperature and pressure and found the capacity was up to 31.1 kg CO_2/t coal FA. Bertos et al.[115] also used the direct mineral carbonation route using municipal solid waste (MSW) incinerator ashes not only to sequester CO_2 but also to stabilize hazardous wastes.

Santos et al.[113] researched the direct mineral carbonation by steel slags which were intensified by ultrasound. They also showed that sonication can facilitate the mineral carbonation reaction by removing the passivation layers of generated carbonates and silica as well as reducing the particle size. Araizi et al.[116] have researched direct mineral carbonation by three kinds of alkaline waste residues, air pollution control residues, cement bypass dust and ladle slag. In each case the carbonation was enhanced by the use of ultrasound. They verified that the application of ultrasound can considerably improve the carbonation efficiency, but needed the help of high L/S ratios (50-100). Huijgen et al.[105] also reported that steel slag was suitable for mineral carbonation. Kasina et al.[49] tried to use blast furnace and steel making slags to sequester CO_2 through the direct mineral carbonation route. It was discovered that steel making slag was much better at

sequestering CO_2 into carbonates than blast furnace slag due to the different mineral compositions (melilite group minerals for blast furnace slags and dicalcium silicates and calcium ferrites for steel making slag). Su et al.[114] utilized basic-oxygen furnace (BOF) slag to sequester CO_2 by direct mineral carbonation as well. However, they claimed that BOF slag was a good CO_2 storage medium. Meanwhile, the valuable vanadium and chromium metals were released into solution during mineral carbonation. This is a further example of carbonation tied to potential additional value recovery. Polettini et al.[54] analyzed the effect of particle size on mineral carbonation by BOF slag. They found the effect was considerable. The difference between carbonation efficiency using particle size of D_{50}=44 μm and D_{50}=88 μm was over 60% (approximately 72% and 8% carbonation respectively) under the same conditions whereas when D_{50}=17 μm, the carbonation efficiency decreased to only 44%. This might be due to the formation of silica gel, preventing the contact with CO_2 and carbonate precipitation. These conclusions are consistent with the work of Nyambura et al.[108] in terms of the importance of particle size.

2.3 Ex-situ indirect mineral carbonation

In order to accelerate the mineral carbonation rate and address the rate-limiting step of dissolution of minerals, as well as to make the mineral carbonation process profitable by increasing the value of products, some researchers have tried to separate the carbonation reaction from the dissolution of Mg-silicate minerals. Some other researchers believe this is not effective as pressurized reactors represent the highest investment costs[117]. At present, the majority of the indirect mineral carbonation employs two-stage mineral carbonation: dissolution of silicate minerals followed by the carbonation reaction[118]. The mechanism of indirect mineral carbonation is based on the knowledge that some minerals range in behaviour from dissolution to

precipitation at different pH values or different temperatures. However ex-situ indirect mineral carbonation does not bypass the requirement of mineral pretreatment by (for example) fine-grinding with or without heat-treatment, which consistently results in non-profitable direct mineral carbonation processes[119–121].

Azdarpour et al.[122] made a review on indirect mineral carbonation through the pH-swing process. Firstly, silicate minerals were dissolved in low-pH solution (with or without ammonium salts), and after L/S separation, carbonates were formed by raising the solution pH[120]. Compared to direct mineral carbonation, it is easier to attain relatively high carbonation efficiency by the pH-swing method. In addition, carbonate products with high purity also can be produced, which can offset the cost of the process. However, mineral carbonation by pH swing, in general, still costs too much because the minerals prior to dissolution also need to be ground which is one of the main costs of mineral carbonation, accounting for more than 50% of the total energy consumption. Furthermore, massive reagent additions are required and it is hard to recycle or regenerate these reagents. In addition, this method cannot utilize the exothermic characteristics of mineral carbonation.

The Åbo Akademi University in Finland[22,123,124] use temperature change for mineral dissolution and carbonation. The direct gas-solid mineral carbonation was previously reported[22,125]. Recently, the ÅA route has been invented[27,123,124,126–128], which has 3 stages and is illustrated in Figure 2.8. The original idea of this technology is to utilize the exothermic heat from mineral carbonation. In the first stage, direct solid-solid reaction between ammonia sulphate and Mg-silicate minerals occurs at 400-440 ℃ to generate solids containing $MgSO_4$ and volatilize NH_3g. The magnesium sulfate is extracted under ambient conditions and $Mg(OH)_2$ is precipitated with recovered NH_3g. The $Mg(OH)_2$ subsequently enters a pressurized fluidized bed under conditions of over 20 bar of

CO_2 pressure and 450-500 ℃ to fix CO_2 as $MgCO_3$. The chemical reactions (13-15) are shown below. It is hard to recover the additive $(NH_4)_2SO_4$ and it is very complicated to achieve heat balance including the hot-cold-hot temperature profile. To solve the heat balance issue, the researchers recently changed the final stage (at ~ 500 ℃) into an aqueous carbonation stage (less than ~100 ℃)[124]. However, the main two disadvantages still exist.

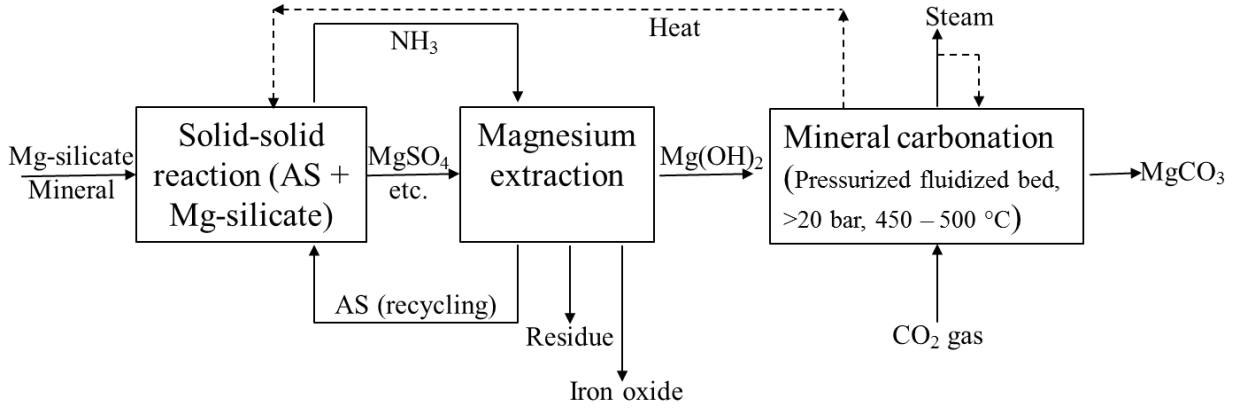

Figure 2.8 Schematic representation of the typical ÅA route (AS $(NH_4)_2SO_4$)[128].

$$Mg_3Si_2O_5(OH)_{4(s)} + 3(NH_4)_2SO_{4(s)} \xrightarrow{400-440℃} 3MgSO_{4(s)} + 2SiO_{2(s)} + 2H_2O_{(g)} + 2NH_{3(g)} \quad (13)$$

$$MgSO_{4(s)} + 2H_2O_{(l)} + 2NH_{3(g)} \xrightarrow{\text{near room temperature}} Mg(OH)_{2(s)} + (NH_4)_2SO_{4aq} \quad (14)$$

$$Mg(OH)_{2(s)} + CO_{2(g)} \xrightarrow{450\sim500℃} MgCO_{3(s)} + H_2O_{(g)} \quad (15)$$

A study on ex-situ indirect mineral carbonation[129] adopted mining wastes for indirect mineral carbonation through crushing, grinding, transportation, heat-treatment, dissolution and precipitation. Finally, two valuable products were obtained: magnetic products containing magnetite, and pure carbonates. Through economic evaluation, they believed that the whole process is profitable. With carbon credits, and through technical evaluation, they concluded that

the whole process needs 1.8252 GJ energy input for sequestering 234 kg CO_2 per tonne of mining waste rock. However, if the input energy is from coal combustion, according to the average energy production value, 6150 kWh/t coal[130], then the whole process will equivalently produce 260 kg CO_2 (assuming 85% content of C in coal), which is more than the amount of CO_2 sequestered. According to the emission factor for electricity produced using coal from IPCC report, 760 g CO_2/kWh[129], the whole mineral carbonation process will release 385 kg CO_2, which is still more than the amount of CO_2 it has sequestered. Therefore, though this process may be profitable, it is no help at all in terms of CO_2 sequestration.

Song et al.[131,132] applied flue gas desulfurization (FGD) gypsum for indirect mineral carbonation to not only sequester CO_2 but form pure carbonate crystals. Xuan et al.[133] adopted direct mineral carbonation to produce environmentally-friendly concrete blocks by recycling concrete aggregates. They discovered that these concrete blocks had higher strength than normal blocks when formed with a CO_2 pressure of 5 bar and a retention time of 24 h. By comparing mineral carbonation by waste concrete and by anorthite tailings, Ghacham et al.[134] further showed that mineral carbonation by waste concrete is much easier than by anorthite tailings along because calcium is effectively locked by in the mineral structure of anorthite and not as available to react with carbon dioxide.

2.4 Potential for product recovery

Many researchers have tried to recover valuable products in order to make the mineral carbonation process profitable. Almost all the products they have tried to recover focus on silica and carbonates[80,117,129], iron oxide by magnetic separation[122] or construction materials as a whole[41,133]. Thus far, it looks like that utilization of mineral carbonation is mainly for building materials. For example, CarbonCure utilizes for sustainable concrete; Mineral Carbonation

International (MCi) for cements and plasterboards; and Carbon8 System for sustainable aggregates. In contrast, it is very hard to obtain high-purity silica or carbonates from solids after mineral carbonation by current traditional technologies, such as flotation or magnetic separation. The iron content in Mg- /Ca- silicate minerals is usually low and the iron is usually in the form of Fe- silicate minerals, for instance, fayalite. These factors have made mineral carbonation processes unprofitable.

The precipitation of metal sulfides may be a new direction for valuable product recovery during mineral carbonation. Metal sulfides are commonly recovered by conventional mineral processing and hence may have an advantage of potentially easy recovery as a co-product from mineral carbonation. Metal sulfide precipitation has fast reaction rates and metal sulfide precipitates have the low solubility[135]. More importantly, sulfide precipitates can be easily recovered by flotation and this, in turn, may make it easier to develop a practical, profitable CO_2 sequestration process. Table 2.2 shows the solubility of metal carbonates and sulfides for comparison. It is clear that the solubility of metal sulfides other than Mg and Ca, is much lower than that of their corresponding metal carbonates. It may be possible for valuable metals to simultaneously convert into corresponding metal sulfide precipitates during the mineral carbonation process by providing a source of sulfide ions.

Table 2.2 Solubility of metal carbonates and sulfides at 25 ℃.

Carbonates	Ksp	Sulfides	Ksp
$MgCO_3$	8.55×10^{-6}	MgS	8.05×10^{4}
$CaCO_3$	5.01×10^{-9}	CaS	1.47×10^{-2}
$FeCO_3$	5.29×10^{-9}	FeS	2.52×10^{-17}
$NiCO_3$	9.74×10^{-12}	NiS	8.60×10^{-24}
$CoCO_3$	4.76×10^{-10}	CoS	5.42×10^{-23}
$ZnCO_3$	1.36×10^{-10}	ZnS	9.01×10^{-25}
$CuCO_3$	1.42×10^{-10}	CuS	1.33×10^{-26}

All data are from HSC Chemistry 7.1.

Table 2.3 shows the Gibbs free energy change for nickel and cobalt species sulfidization at room temperature using soluble sulfide anion or solid troilite (FeS). The $\triangle G^\circ$ values are all negative. It is known that the nickel and cobalt in olivine mineral are in the crystal structure by substituting magnesium or iron atoms. The NiO and CoO in Table 2.3 represent the simplest form of nickel and cobalt in olivine. If the nickel and cobalt can be released as ions during the mineral carbonation process, sulfidization with iron sulfide is thermodynamically favourable. It is interesting that the reactions between nickel and cobalt carbonates and iron sulfide are thermodynamically favourable. The thermodynamics also reveal that it is possible to selectively precipitate the iron and nickel and cobalt as iron carbonate and nickel or cobalt sulfides. The recovery of nickel and cobalt sulfide from iron carbonate would be advantageous. These calculations confirm the possibility of metal sulfidization for potential metal recovery enhancement by utilizing mineral carbonation.

Table 2.3 Thermodynamic data for nickel and cobalt species sulfidization at 25 ℃.

Metal sulfidization reaction	$\triangle G^\circ$, kJ/mol
$NiO + S^{2-} + 2H^+ = NiS + H_2O_{(l)}$	-202.89
$CoO + S^{2-} + 2H^+ = CoS + H_2O_{(l)}$	-205.69
$Ni^{2+} + FeS = NiS + Fe^{2+}$	-36.91
$Co^{2+} + FeS = CoS + Fe^{2+}$	-32.35
$NiCO_3 + FeS = NiS + FeCO_3$	-21.30
$CoCO_3 + FeS = CoS + FeCO_3$	-26.38

All data are from HSC Chemistry 7.1.

Some companies need to produce nickel and cobalt sulfides concentrates from raw ores through a mineral processing process where the majority are magnesium silicate minerals. For example, Giga Metals intend to produce pentlandite concentrates from silicate minerals through a beneficiation process including grinding and sulfide flotation[32,136], as shown in Figure 2.9. The average nickel and cobalt grade in Turnagain deposit in Northern British Columbia is

approximately 0.212% and 0.014%. The estimated resource deposit is approximately 761 Mt with a preliminary treatment rate of 87,000 t/d. The majority of gangue minerals are magnesium silicate minerals including olivine, serpentine and pyroxene, which are amongst the most suitable minerals for mineral carbonation. As a result, the estimated tailings for the Turnagain project are around 756 Mt with the capacity of 86,434 t/d. As discussed in Chapter 1, the total nickel and cobalt recovery are only 55%-60% and about 50% respectively since up to 41% of total nickel is in the crystal structure of silicate minerals[32]. Therefore, there is still great room for improvement for the nickel and cobalt recovery from the silicate minerals; approximately 721 kt nickel and 53 kt cobalt respectively. Based on the current prices CAD$ 7.7/lb Ni and CAD$ 21.27/lb Co, there will be revenue of approximately CAD$ 12 billion from nickel recovery and CAD$ 2.5 billion from cobalt recovery respectively if the nickel and cobalt in silicates are converted to recoverable nickel and cobalt sulfides. In addition, the carbon tax in Canada has been increased to CAD$ 50/t carbon and is expected to continue to increase in the future. Additional approximately CAD$ 5.8 billion in carbon credits can be potentially acquired from the carbon tax if the silicate tailings are completely carbonated. It is obvious that in addition to the carbon credits to offset the costs of mineral carbonation process, the potential of considerably enhanced metal recovery can benefit the company to achieve an economically-profitable mineral processing and carbonation process, if the mineral carbonation process can be combined with the mineral processing and metal sulfidization process. The potential recovery of the metal sulfide products provides a strong possibility for the successful application of mineral carbonation in industry.

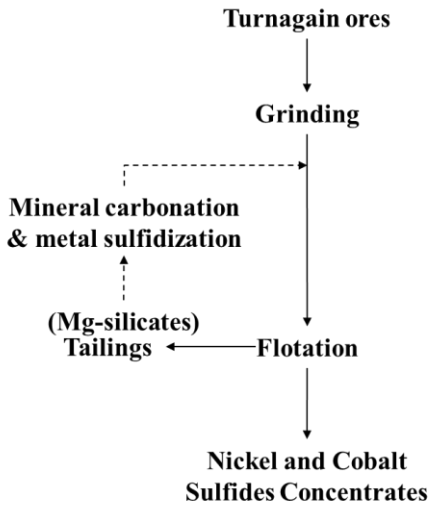

Figure 2.9 Principle mineral processing flowsheet for Turnagain deposit, Giga Metals Corporation.

2.5 Literature conclusions

Overall, in the last 30 years, the technology of CO_2 sequestration by mineral carbonation has been intensively researched. A summary of active mineral carbonation technology research is provided in Table 2.4. Firstly, the fundamental characteristics of mineral carbonation have been discovered. To acquire high mineral carbonation efficiency during a short period, strict conditions are necessary including high temperature, high CO_2 pressure, fine particle size and the addition of a catalyst (such as sodium bicarbonate). Secondly, there has been a technically successful in-situ mineral carbonation pilot study, the CarbFix project based on basalts in Iceland. In-situ mineral carbonation of basalts takes less than 2 years without any additives. Furthermore, in-situ HXRD and in-situ IR analytical technologies have been developed and can be used to monitor actual in-situ mineral carbonation. In addition, with respect to ex-situ mineral carbonation major achievements include the invention of the Energy Reactor©, the in-situ grinding mineral carbonation concept as well as the idea that ex-situ mineral carbonation can be associated with valuable metal recovery.

Table 2.4 Summary of current status and future developments of active mineral carbonation.

Mineral carbonation method	Current status	Future developments
In-situ mineral carbonation	No successful application	Not suitable to combine with metal sulfidization
by basalts	• Strongly encouraged by the successful pilot project, CarbFix. • Complete carbonation in two years. • Develops in-situ HXRD and in-situ IR technology for monitoring in-situ carbonation.	• More in-situ mineral carbonation pilot studies. • Clarify effects of precipitation of carbonates on porosity and permeability.
by peridotite	• At an early stage. • Theoretically more suitable for mineral carbonation compared to basalts owing to larger capacity and higher bivalent metal content. • Less attractive due to lower porosity and permeability.	• In the near future, the in-situ mineral carbonation will be more focused on by basalts rather than by peridotite.
Ex-situ direct mineral carbonation	No successful application	Potentially possible to combine with metal sulfidization
by olivine	• Has been intensively researched. • Preliminary fundamentals of characteristics of mineral carbonation known. • Development of sodium bicarbonate and sodium chloride as an effective catalyst. • Invention of the Energy Reactor© • May result in more CO_2 gas emitted than sequestered.	• Confirm kinetics and mechanism of mineral carbonation of olivine. • Need for a more efficient and economical catalyst, e.g. based on artificial carbonic anhydrase. • Possible combination of mineral processing and carbonation and utilizationformetal sulfidization. • Optimization of equipment such as Energy Reactor©.
by serpentine	• Less attractive due to the necessity of heat pretreatment.	• Can combine with mineral processing and metal recovery.
by industrial wastes	• Suitable under milder conditions with higher chemical reactivity of some industrial wastes. • Potentially address industrial hazards. • Limited contributions to carbonation owing to the smaller capacity than natural silicate minerals.	• Combine mineral carbonation and addressing environmental hazards for potential metal recovery.
Ex-situ indirect mineral carbonation	No successful application • Less attractive due to the intensive energy requirements and no high-value byproducts.	Potentially possible to combine with metal sulfidization

It is believed that mineral carbonation technology will undergo rapid development as concern over carbon emissions intensifies. There will be more studies of in-situ mineral carbonation of basalts. The key challenge of carbonation due to a decrease of porosity and permeability from the precipitation of carbonates will also be investigated with the help of in-situ analysis tools and more in-situ pilot plant research. In-situ mineral carbonation of peridotite will also be promoted.

Ex-situ mineral carbonation will continue to develop where costs can be shared with the main flow sheet of valuable metals recovery[137]. For example, it is easier to couple a mining project treating silicate ores by crushing, grinding and mineral separation with a carbonation process. The energy for mineral size reduction has already been applied in the mining project and therefore this cost is avoided for the carbonation process. Therefore, costs of ex-situ mineral carbonation will be decreased dramatically but the profits of the whole process may be increased due to the carbon credits and possible increases in metal recovery from the mineral deposit. However, it also means that it is not economic to exploit Mg- and Ca- silicate minerals deposits or tailings to only sequester CO_2 by mineral carbonation[75], due to the cost of grinding and heat pre-treatment. Taking this approach, the sequestration process may result in more CO_2 emissions than the amount of CO_2 sequestered! It is suggested that mineral carbonation be combined with recovery of valuable metals from ore deposits which contain suitably high content of divalent metals. The Energy Reactor© may play a key role in the successful application of ex-situ direct mineral carbonation owing to its two outstanding advantages: meeting the high pressure requirement with hydrostatic pressure and utilization of the exothermic heat of mineral carbonation. The use of in-situ grinding for mineral carbonation may also be attractive if mill equipment that can operate at higher pressure can be made economic. In addition to the classic mixture of $NaHCO_3$ and NaCl as a catalyst for carbonation, more efficient and economical

catalysts need to be discovered or manufactured perhaps based on artificial CA. Furthermore, though the capacity of mineral carbonation by industrial wastes is much less than by natural silicate minerals, it is still important, especially if high-value by-products or additional metals recovery can be obtained.

Research on valuable metals recovery during the mineral carbonation process remains at an early stage. To make the mineral carbonation process profitable, it is desirable to combine the mineral carbonation process and the mineral processing process. If the recovery of valuable metals can be increased while also using mineral tailings containing calcium and magnesium silicate minerals for carbonation, it may be possible to increase the economic potential of ex-situ carbonation. It is thermodynamically possible to achieve selective mineral carbonation and valuable metal sulfidization and recovery in an integrated process.

3 Objectives and research framework

The research framework for this dissertation is shown in Figure 3.1. Mineral carbonation and metal sulfidization are the two core research objectives. Mineral carbonation is a precondition necessary for conducting the metal sulfidization tests. There are four important objectives.

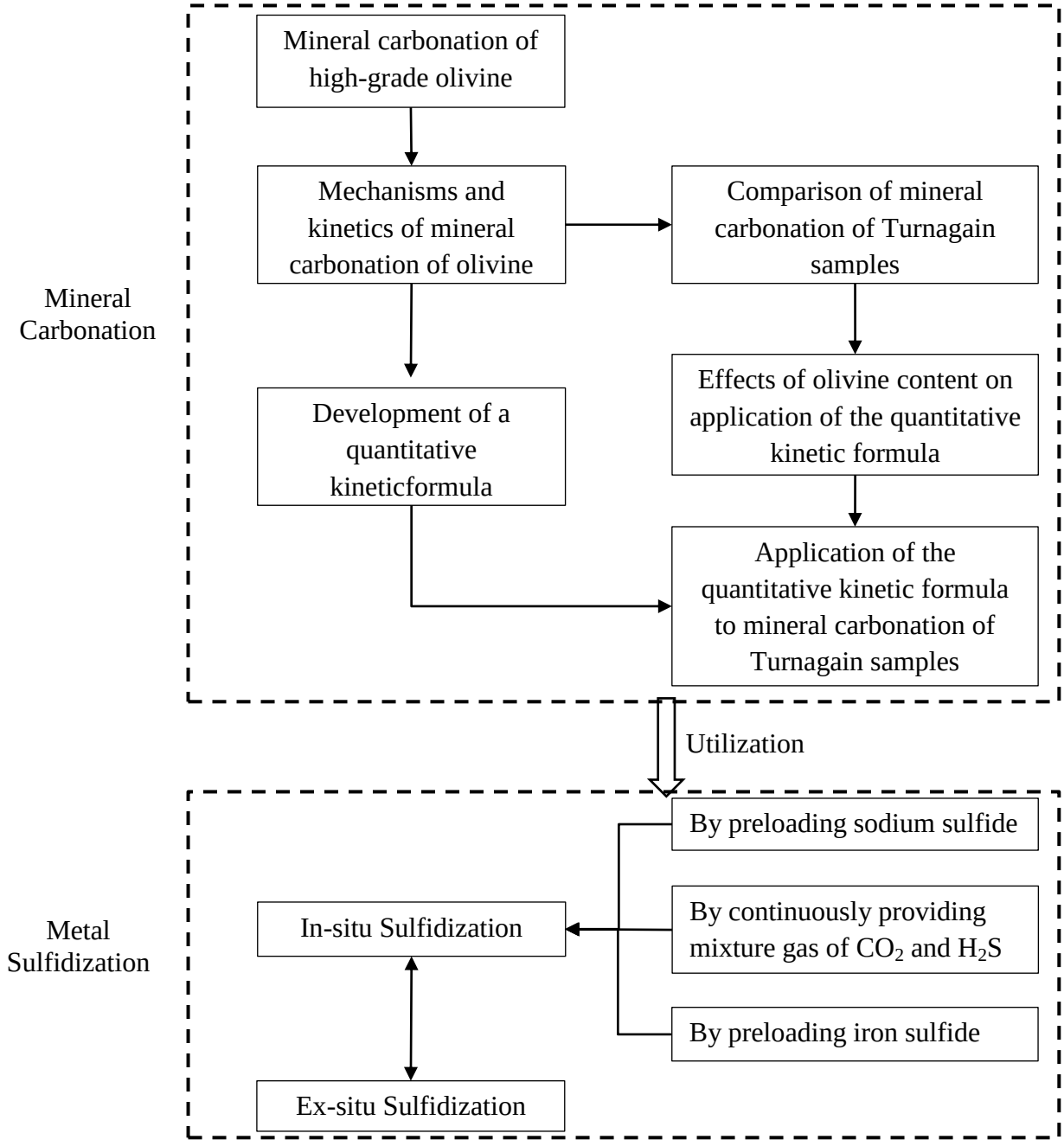

Figure 3.1 Principle research framework of mineral carbonation for CO_2 sequestration and utilization for metal sulfidization.

- **Objective 1: To determine the mechanisms of mineral carbonation of olivine for CO_2 sequestration**

Mineral carbonation is a precondition for metal sulfidization to convert valuable metals in silicates which are not recoverable by flotation to recoverable metal sulfides. How well the mineral carbonation process is understood determines how the mineral carbonation process can be utilized. It is necessary to investigate the effects of various factors (including CO_2 partial pressure, particle size, temperature, addition of salts, agitation speed and solids content) and the relationship between the mechanisms of mineral carbonation and the various factors. High-grade olivine was used for objective 1. As a result, an optimal condition for the mineral carbonation can be determined and the corresponding fundamental mechanism can be investigated.

- **Objective 2: To determine the kinetics of mineral carbonation of olivine**

The mineral carbonation process of olivine is a natural weathering process but of course limited by kinetics at ambient temperature and pressure. It is necessary to carry out the kinetics analysis so as to determine the rate-controlling step. The classical shrinking core model (SCM) of particles was used for the kinetics research. Furthermore, it is necessary to develop a quantitative kinetic formula which can be used to predict the mineral carbonation efficiency under suitable conditions if the mineral carbonation technology is to be applied in industry. Through the kinetic research, the effects of the most important factors on the mineral carbonation efficiency can be quantified. The high-grade olivine was used for the systematically kinetic research. As a result, the rate-controlling step of the mineral carbonation of olivine under the optimal conditions can be determined and a kinetic model developed.

- **Objective 3: To investigate the application of the kinetic model to carbonation of Turnagain samples**

In order to improve the suitability of the kinetic model for potential industrial application, mineral carbonation of the Turnagain mineral samples provided by Giga Metals which have the wide range of mineral compositions and olivine content was investigated. Firstly, the mineral carbonation behaviour of Turnagain samples was compared with that of high-grade olivine under the optimal conditions. The effects of the presence of various minerals including serpentine, pyroxene and iron sulfides on the mineral carbonation were determined. The mechanism and kinetics developed from the high-grade olivine can be applied to explain the different behaviours among the Turnagain samples. As a result, the mineral carbonation model can be refined. Further work was conducted by diluting olivine with a high-purity silica which would not be expected to participate in the mineral carbonation reaction. The objective was to ensure that the kinetic model could apply to relatively pure mineral samples (e.g. high-grade olivine), diluted olivine (with silica) and natural mineral samples (the Turnagain samples).

- **Objective 4: To enhance the valuable metals conversion by utilizing the mineral carbonation process**

The application of the mineral carbonation process was used as a starting point for study of metal sulfidization. The mineral carbonation kinetics can inform on the possibility of nickel and cobalt released from the minerals during the mineral carbonation process. Both the in-situ and ex-situ metal sulfidization processes were studied. In-situ metal sulfidization means that the metal sulfidization happens during the mineral carbonation process. As a result, the metal sulfidization process and mineral carbonation process can be integrated into one process. Ex-situ metal

sulfidization means that the metal sulfidization process was carried out after the mineral carbonation process. The final solids after mineral carbonation are the raw materials for the ex-situ metal sulfidization process. The addition of sodium sulfide or iron sulfide or the continuous injection of a gas mixture of CO_2 and H_2S were used to provide the sulfide ions for the metal conversion to sulfides.

4 Materials and methodology

4.1 Materials

Two different materials were investigated in this work; a high-grade olivine sample and samples from the Turnagain deposit of Giga Metals with a wide range of olivine contents. The high-grade olivine was used for the fundamental research about the mechanisms and kinetics of mineral carbonation of olivine as well as the metal sulfidization which converted the valuable metal nickel to nickel sulfide for enhanced recovery. Turnagain samples were used to verify the mechanisms and kinetics developed from the high-grade olivine as well as the study of metal sulfidization applied to the natural ore.

4.1.1 High-grade olivine

The high grade olivine sample was provided by Sibelco Europe. The chemical composition is shown in Table 4.1. The analysis was via Inductively Coupled Plasma – Optical Emission Spectrophotometry (ICP-OES) analysis after lithium borate fusion. This high-grade olivine contained 0.27% nickel, generally slightly higher than the average nickel content of a Turnagain nickel deposit[31]. The olivine did not contain any measurable carbon or sulfur. All the nickel was in the crystal structure of olivine as an isomorph by substituting the magnesium or iron atoms. Therefore, this high-grade olivine can be considered as very suitable for study of mineral carbonation and metal sulfidization. The mineral composition is indicated in Figure 4.1 and Table 4.2. Figure 4.1 shows the dominant mineral is olivine with a small amount of serpentine. Table 4.2 shows the minerals identified by the quantitative X-ray diffraction (QXRD) method. Olivine and enstatite accounted for 86.4% and 6.3% respectively, approximately 93% of the total. In contrast, serpentine only accounted for 1.4%. This high-grade olivine was used for

fundamental research related to mechanisms and kinetics of mineral carbonation as well as metal sulfidization. The mineral carbonation capacity (m) of the high-grade olivine based on the Mg, Fe and Ca content is 0.554 g CO_2/g high-grade olivine, calculated according to Equation (4.1). However, the carbonation capacity based on only Mg and Ca (0.50 g CO_2/g high-grade olivine, shown in equation (4.2)) was used for the initial analysis of mechanism in Chapter 5 to simplify the calculation since there is still controversy on the contribution of Fe to the carbonation capacity[47].

Table 4.1 Chemical composition of a high-grade olivine.

Elements	Mg	Si	Fe	Al	Cr	Ni	Mn	Ca
Mass, %	27.44	20.76	7.09	0.09	0.21	0.27	0.08	0.11

$$m = \left(\frac{[Mg]}{24.305} + \frac{[Fe]}{55.845} + \frac{[Ca]}{40.078}\right) \times 44.01 \quad (4.1)$$

$$m = \left(\frac{[Mg]}{24.305} + \frac{[Ca]}{40.078}\right) \times 44.01 \quad (4.2)$$

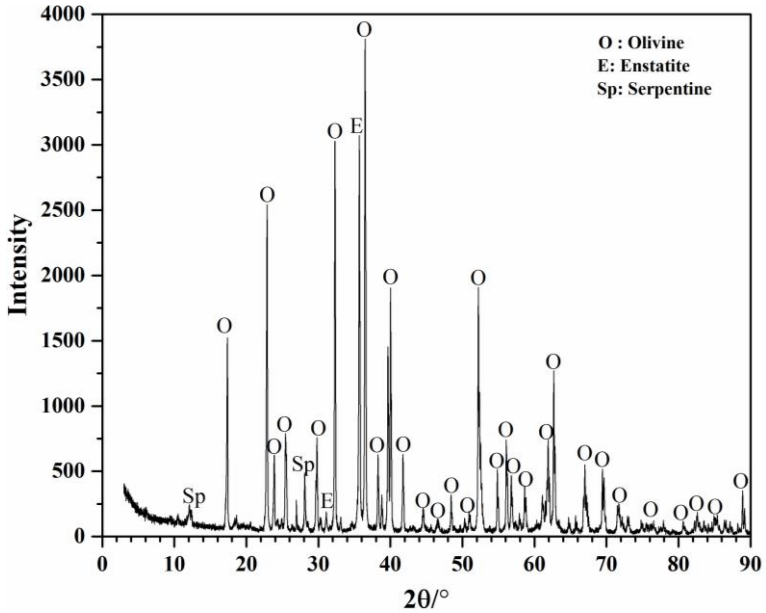

Figure 4.1 X-ray diffraction (XRD) pattern for the high-grade olivine.

Table 4.2 Quantified mineral compositions of the high-grade olivine and Turnagain samples through the quantitative X-ray diffraction (QXRD) analysis.

Samples	High-grade Olivine	Turnagain samples								
Minerals		SN254	SN255	SN256	SN257	SN258	SN259	SN260	SN261	SN262
Olivine $(Mg, Fe)_2SiO_4$	86.4	83.5	78.7	80.4	85.0	79.5	50.5	40.1	30.2	73.3
Enstatite $MgSiO_3$	6.3	-	-	-	-	-	-	-	-	
Magnesiochromite $MgCr_2O_4$	1.3	-	-	-	-	-	-	-	-	-
Brucite $Mg(OH)_2$	-	2.0	2.9	1.3	0.8	-	-	-	-	0.3
Quartz SiO_2	0.5	0.4	0.3	0.3	0.3	-	0.4	-	-	-
Magnetite Fe_3O_4	-	3.8	5.5	5.9	3.9	3.9	6.4	4.4	10.0	4.6
Troilite FeS	-	-	-	0.5	1.7	4.6	0.5	8.1	1.3	2.0
Pyrrhotite $Fe_{1-x}S$	-	-	-	-	-	-	1.3	11.4	1.7	2.8
Calcite $CaCO_3$	-	-	-	0.5	0.4	0.3	0.3	2.5	1.1	0.7
Diopside $CaMgSi_2O_6$	-	-	-	-	-	4.9	29.4	4.9	12.5	9.1
Hydrated silicate minerals										
Serpentine $Mg_3Si_2O_5(OH)_4$	1.4	9.5	12.6	11.2	8.0	6.8	11.1	28.6	43.3	7.2
Others	4.1	0.8	0	-	-	-	-	-	-	-
Total	100.0	100.0	100.0	100.0	100.0	100.0	100.0	100.0	100.0	100.0

4.1.2 Turnagain samples

In order to confirm the theory established with the high-grade olivine, typical bivalent metals-containing silicate samples with a wide range of contents of olivine and other minerals were used for the application and development of mineral carbonation and metal sulfidization theory. Nine Turnagain samples (SN254 – SN262) were provided by Giga Metals Corporation from drill cores obtained from the deposit. The mineral compositions showed a wide range of olivine and other minerals as shown in Table 4.2. The chemical compositions are shown in Table 4.3, obtained through ICP-OES analysis after lithium borate fusion, where the content of carbon and

sulfur were analyzed through LECO CS3200 instrument. There were differences in the contents of sulfur, magnesium and iron among the Turnagain samples. The SN260 sample had the highest content of sulphur and iron (7.19% and 15.62% respectively) but the lowest content of magnesium (18.24%). The sulphur contents in the SN254 and SN255 samples were the lowest, 0.03% and 0.04% respectively. The highest contents of magnesium were for the sample SN254 and SN255, 24.14% and 23.83%, respectively. The carbon content in all Turnagain samples was less than 0.11% and existed as carbonaceous matter. The nickel content generally increased with the increase in the contents of sulfur and iron, in the range of 0.23% (SN259) to 0.40% (SN262) in addition to the exceptionally highest value of 0.70% Ni for sample SN260 which also had the highest sulfur content 7.19%. The other valuable metals (cobalt and copper), in the Turnagain samples were generally very low; less than 0.05% and 0.09%, respectively. There was also an exceptionally high 0.20% copper for sample SN260 that had the highest sulfur content, which was mainly associated with sulfide minerals and was not studied in this dissertation. Compared to the nickel content, quantitative studies involving cobalt and copper would have a high analysis error due to the low content of these elements. Since the cobalt and copper are expected to have similar behaviour to nickel in olivine by substituting magnesium and iron atoms in the crystal structure, the metal sulfidization research was focussed on the nickel conversion from olivine to nickel sulfide with the expectation that copper and cobalt would have similar behaviour.

The XRD patterns (Figure 4.2) and reported lithologies (Table 4.4) show the main mineral compositions of Turnagain samples. The lithologies of sample SN254 – SN258 were predominantly dunite. The corresponding major mineral compositions were olivine, followed by serpentine. In contrast, there were (clino-)pyroxene in samples SN259 – SN262, particularly in sample SN259. Sample SN260 had iron sulfides and high serpentine content. The serpentine

content was highest in sample SN261, accompanied by tremolite. Sample SN262 belonged to the wehrlite lithology and the majority of mineral compositions were olivine followed by serpentine and (clino-) pyroxene.

Table 4.3 Chemical compositions of Turnagain samples.

Samples	SN254	SN255	SN256	SN257	SN258	SN259	SN260	SN261	SN262
S, %	0.03	0.04	0.83	1.30	2.16	1.13	7.19	1.40	2.30
Ni, %	0.28	0.26	0.32	0.35	0.26	0.23	0.70	0.33	0.40
Mg, %	24.14	23.83	22.85	22.74	22.47	18.32	18.24	19.07	21.21
Fe, %	6.60	6.45	8.01	8.99	10.06	7.88	15.62	7.79	9.77
Co, %	0.01	0.01	0.02	0.02	0.02	0.01	0.05	0.02	0.02
Cu, %	<0.01	<0.01	0.04	0.07	0.03	0.03	0.20	0.05	0.09
Al, %	0.04	0.05	0.13	0.04	0.06	0.58	0.22	0.44	0.19
Ca, %	0.21	0.15	0.29	0.24	0.57	3.90	0.51	1.21	1.05
K, %	<0.01	<0.01	0.03	<0.01	<0.01	0.12	0.03	0.09	0.02
Na, %	<0.01	<0.01	<0.01	<0.01	<0.01	0.03	<0.01	<0.01	0.01
C, %	0.06	0.11	0.10	0.05	0.06	0.05	0.03	0.05	0.04

Table 4.4 Lithology of Turnagain samples.

Samples	Lithology	Main minerals
SN254	Green dunite, low sulphur	Olivine, serpentine
SN255	Green dunite, low sulphur	Olivine, serpentine
SN256	Serpentinized dunite	Olivine, serpentine
SN257	Serpentinized dunite	Olivine, serpentine
SN258	Serpentinized dunite	Olivine, serpentine
SN259	Serpentinized wehrlite and olivine clinopyroxenite	Serpentine, olivine, pyroxene
SN260	Serpentinized wehrlite with 20% sulphides	Serpentine, olivine, pyroxene, sulphides
SN261	Serpentinized and tremolite altered wehrlite	Serpentine, olivine, pyroxene
SN262	Wehrlite	Olivine, serpentine, pyroxene

This lithology data was provided by Giga Metals Corporation.

QXRD analysis was used for the Turnagain samples also shown in Table 4.2. The QXRD results were consistent with the XRD images and lithology. Sample SN254 – SN258 had the highest olivine content ranging from 78.7% to 85.0% while the serpentine content ranged from 6.8% and 12.6%. Sample SN259 had the highest pyroxene (diopside) accounting for 29.4%, whereas

olivine and serpentine accounted for 50.5% and 11.1% respectively. Sample SN259 had the highest content of iron sulfides (19.5%), including 8.1% troilite and 11.4% pyrrhotite, and had much higher serpentine content (28.6%) and much lower olivine content (40.1%) compared to sample SN259, whereas the pyroxene content only accounted for 4.9%. Similarly, sample SN261 had the highest serpentine content 43.3% and the lowest olivine content 30.2%, where pyroxene accounted for 12.5%. Sample SN262 which belonged to the wehrlite lithology had the intermediate olivine content of 73.3% compared with dunite and serpentinized wehrlite and 7.2% serpentine and 9.1% pyroxene.

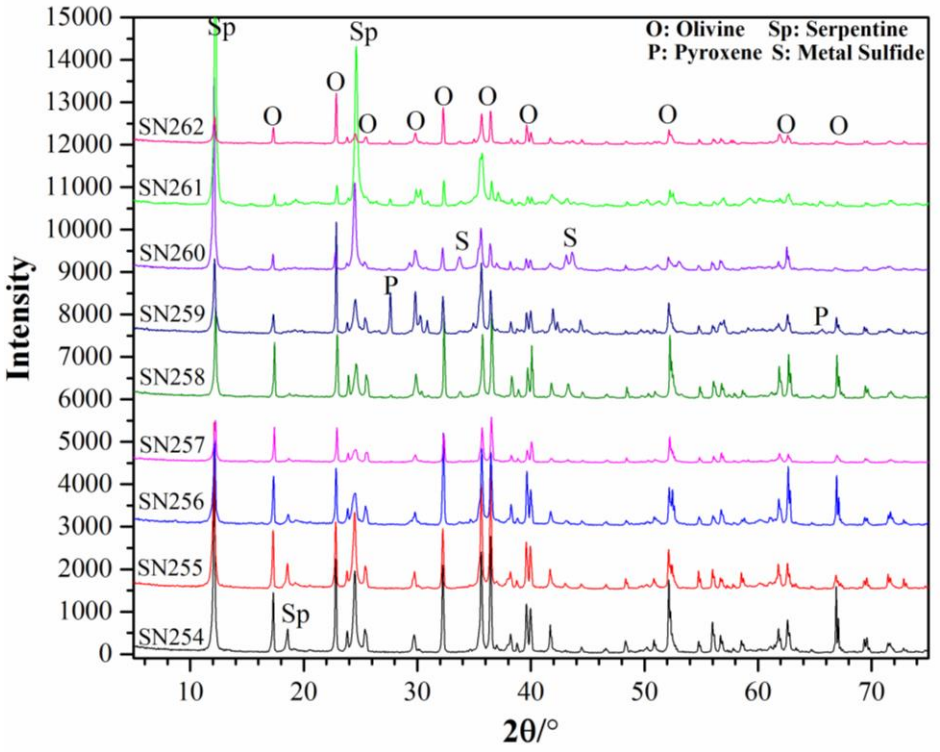

Figure 4.2 XRD images of Turnagain samples.

The general way to calculate the mineral carbonation capacity is based on the Mg, Fe and Ca contents (Equation (4.1)). However, since Turnagain samples have wide ranges of mineral compositions, some bivalent metal-containing minerals other than olivine may have different mineral carbonation behaviours. For example, serpentine may have very low mineral carbonation

rates if treated directly without heat pre-treatment. Iron sulfide would not be expected to participate in the mineral carbonation reaction since iron sulfide is more insoluble than iron carbonate. Therefore, it is necessary to calculate the mineral carbonation capacity in four different ways, based on Mg, Fe and Ca (shown in Equation 4.1) or based on only Mg and Ca (shown in Equation 4.2), with or without consideration of the olivine content, so that there is at least one reasonable way which can reflect the actual mineral carbonation process. The mineral carbonation capacity of Turnagain samples SN254 – SN262 calculated by the four different ways is shown in Table 4.5. It is clear that the olivine content has the most significant effect on the calculation of mineral carbonation capacity for each Turnagain sample. The effect of olivine content on capacity calculations was much larger for the Turnagain samples SN259 – SN261 which have olivine contents less than 50%. The iron content also has a considerable effect on the calculation of mineral carbonation capacity. The most significant effect of iron content is for sample SN260 which has the highest iron sulfides content 19.5%. The carbonation capacity with or without consideration of the iron content is 0.420 and 0.359 g CO_2/g sample SN260 respectively if the olivine content is not considered. The mineral carbonation capacities shown in Table 4.5 were used in work reported in Chapter 6.

Table 4.5 Mineral carbonation capacity of Turnagain samples SN254 – SN262.

Turnagain sample	Mineral carbonation capacity, g CO_2/g Turnagain sample			
	Based on Mg, Fe&Ca without considering olivine content	Based on Mg, Fe&Ca and considering olivine content	Based on Mg&Ca without considering olivine content	Based on Mg&Ca and considering olivine content
SN254	0.491	0.410	0.439	0.367
SN255	0.484	0.381	0.433	0.341
SN256	0.480	0.386	0.417	0.335
SN257	0.485	0.413	0.414	0.352
SN258	0.492	0.392	0.413	0.328
SN259	0.437	0.221	0.375	0.189
SN260	0.459	0.184	0.336	0.135
SN261	0.420	0.127	0.359	0.108
SN262	0.473	0.346	0.396	0.290

In order to facilitate the metal sulfidization research, the Turnagain samples were analyzed for the original nickel sulfide content by bromine-methanol digestion[138,139] followed by atomic absorption spectrometry (AAS). This method was considered as the most selective method for nickel sulfide determination in the presence of nickel as oxide (i.e. in the olivine or serpentine)[138,139]. The results were shown in Table 4.5. The majority of the results from the bromine-methanol digestion were quite similar to the results from the ammonium citrate digestion except for three samples (SN256, SN257 and SN259) where the difference was 3%, 8% and 6%, respectively. The nickel in the sample SN260 which had the highest sulfur content, serpentine content and nickel content was all in the form of nickel sulfide. Sample SN254 had the lowest nickel sulfide content, accounting for 24% of the total nickel, followed by 27% for sample SN255, both of which were green dunite and had the lowest sulfur content. The rest of the Turnagain samples, which had a sulfur content greater than 0.83%, had the more than 72% nickel sulfide as the fraction of the total nickel. The nickel in sample SN261 and SN262 was mainly in the form of nickel sulfide (98% and 97%, respectively) with 1.4% and 2.3% sulfur content, respectively. The nickel sulfide analysis further confirmed the nickel sulfide content was generally related to the sulfur content in the silicate minerals. The bromine-methanol digestion was selected for the nickel sulfide analysis in this dissertation.

Table 4.6 Nickel sulfide analysis of Turnagain samples.

	SN254	SN255	SN256	SN257	SN258	SN259	SN260	SN261	SN262
Total nickel, %	0.28	0.26	0.32	0.35	0.26	0.23	0.70	0.33	0.30
Nickel sulfide, %	0.068	0.071	0.23	0.29	0.22	0.17	0.71	0.33	0.39
Nickel sulfide/ total nickel, %	24.14	27.15	72.47	82.20	85.00	72.83	101.27	97.93	96.73

4.2 Apparatus

The tests of mineral carbonation and metal sulfidization were carried out in a 600 mL stainless steel autoclave (Model 5103 with No. 4842 control system, Parr Instrument Company) with a continuous sampling kit, as shown in Figure 4.3. The maximum pressure for the vessel was 68.95 bar at 22 ℃. A rupture disc (57.71 bar at 185 °C) was used to protect the autoclave vessel and for safe operation of the high temperature and pressure reactor. All the tests were carried out under 50 bar pressure. The continuous sampling kit was used to take representative slurry samples when the high temperature and pressure reactor was running. The reliability and representativeness of these samples are discussed further in Appendix D.

Figure 4.3 The autoclave for the fundamental research on mineral carbonation: (1) temperature and rotation speed controller; (2) sampling kit; (3) inlet of cooling coil; (4) CO_2 inlet; (5) safety pipe connected to a rupture disc; (6) pressure gauge; (7) outlet of cooling coil; (8) CO_2 outlet; (9) thermocouple; (10) mixer shaft; (11) sampling deep tube; (12) cooling coil; (13) thermocouple deep tube; (14) oven for heating and (15) 600 mL stainless-steel reactor vessel.

4.3 Sample preparation

In order to carry out the research of kinetics and mechanism in Chapter 5, the high-grade olivine was ground by a rod mill under the conditions of 60% solids and 1 kg samples/16.5 kg rod charge for 35 minutes. After the grinding process, the samples were wet screened with 500 mesh, 400 mesh, 270 mesh and 200 mesh sieves. The narrow-sized particle fractions -25 μm, 25 – 38 μm, 38 – 53 μm and 53 – 75 μm were collected and used for systematic mineral carbonation tests, including the effects of particle size, temperature, PCO_2, concentration of additives, rotation speed and solids content.

Once the mechanism and kinetics of mineral carbonation of olivine were measured, the quantitative kinetic formula developed in Chapter 5 was first applied with Turnagain sample SN254. Once the application to sample SN254 data was successful, the quantitative kinetic formula was applied to data for Turnagain samples SN255 – SN262. Both narrow-sized particles and full size-range particles were used as discussed in Chapter 6 to test for application. All the Turnagain samples were ground by the same rod mill under the conditions of 60% solids and 1 kg samples/16.5 kg rod charge followed by the wet-screening to obtain the narrow-sized particle fractions. The sieves sizes 500 mesh, 400 mesh, 325 mesh, 270 mesh and 200 mesh were used for the wet-screening to acquire the narrow-sized particle fractions, - 25 μm, 25 – 38 μm, 38 – 45 μm, 45 – 53 μm and 53 – 75 μm. The full size-rangeparticles were the products of grinding without screening. The corresponding particle size distributions and specific surface areas of all the narrow- and full-size particles were determined by the Malvern Mastersizer 2000.

Since the mineral carbonation of olivine represented the majority of the mineral carbonation reactions of all the Turnagain samples studied (which has been confirmed in Chapter 6), the

carbonation and utilization of the high-grade olivine was believed to be representative enough for the Turnagain samples. In addition, the -25 μm particles showed the same carbonation behaviour as the other narrow-sized particle fractions and also the full size-range particles, as shown in Chapter 5 and 6. Studies reported in Chapter 7 mainly used the -25 μm high-grade olivine particles for the study of utilization of mineral carbonation for metal sulfidization. The Turnagain sample SN254 which had the lowest nickel sulfide content among the Turnagain samples was also used for a part of this study to verify the sulfidization findings from the study of high-grade olivine.

4.4 Test procedures

The carbonation tests were carried out in a 600 mL high temperature reactor with a continuous sampling kit (shown in Figure 4.3). Prior to the tests, the solid samples were loaded into the reactor vessel with 400 mL of aqueous solution which contained sodium bicarbonate or sodium chloride. The vessel was mixed at room temperature with 300 rpm agitation speed. High-purity CO_2 gas was introduced into the vessel to the total pressure of 6.89 bar and then released to 0.14 bar pressure followed by increasing the total pressure to 1.38 bar. This method was used first to remove most of the air from the autoclave and second to seal the reactor, respectively. The reactor was then heated to the pre-determined temperature within approximately 20 minutes. Once the desired temperature was reached, the reaction time started to be recorded. The agitation speed was increased up to the target and high-purity CO_2 gas was introduced to the pre-determined target pressure in approximately one minute, where the CO_2 partial pressure was the difference between the total pressure and the water vapour pressure. When the test was finished, the reactor was cooled down to around 30 ℃ and the pressure was released starting from when the temperature was around 50 ℃. After the reaction, the cooled slurry was vacuum filtered. The

solids were washed five times with deionized water. The solid was dried to remove free moisture in an oven at 60 ℃ for 12 hours, weighed and analyzed for LECO total carbon content. According to the weight of solids before and after the reaction as well as the total carbon content, the carbonation efficiency can be calculated. In order to perform the kinetics analysis, slurry samples were collected at specified times. The collected slurry sample was taken using the continuous sampling kit. First a sample was collected and disposed of to flush the sample line. Then a second slurry sample was collected and centrifuged. The solid was rinsed by deionized water (twice the mass of the solids) and then dried in the oven. Total carbon analysis was performed on the dried solids. The obtained aqueous solution was immediately diluted by a factor of 5 and contained 2% nitric acid. These were analyzed by ICP-OES. The detailed experimental conditions are described beginning on Section 5.1.

The sulfidization tests were also carried out in the same autoclave. Two types of sulfidization tests were considered, in-situ sulfidization and ex-situ sulfidization. The in-situ sulfidization means that metal sulfidization occurred concurrently with the mineral carbonation process by providing the sulfide sources including the sodium sulfide, hydrogen sulfide gas or iron sulfide. The in-situ sulfidization all used the same test procedure except for the supply of sulfide sources: the sodium sulfide or iron sulfide was added into the slurry before the vessel was charged whereas the hydrogen sulfide was provided as the mixture gas of CO_2 and H_2S. The ex-situ sulfidization was used to convert the valuable metals in the carbonated products to metal sulfides after the mineral carbonation by providing sodium sulfide. In consideration of effectively controlling the use of sodium sulfide and avoiding the potential environmental pollution, the concentration of sodium sulfide during the ex-situ sulfidization was controlled to less than 0.012 m and the corresponding solid content was less than 1%.

4.5 Analysis methods

The chemical compositions of the high-grade olivine and the nine Turnagain samples were analyzed by the ICP-OES analysis after lithium borate fusion. However, the copper (Cu) and cobalt (Co) contents of the Turnagain samples were obtained by ICP-OES after four acid (hydrochloric acid, nitric acid, hydrofluoric acid and perchloric acid) digestion. The centrifuged solutions were also analyzed by ICP-OES after 5 times dilution into 2% nitric acid. The total carbon and sulfur contents of solids were analyzed by LECO CS3200 instrument for the calculation of mineral carbonation efficiency. The carbon and sulfur were analyzed with precision ±0.5%.

The mineral compositions of all the samples used in this thesis were analyzed using a Rigaku MultiFlex XRD instrument with Cu-Kα radiation over the range of 3 °- 90° of 2θ. In contrast, the quantitative XRD analyses (shown in Table 4.2) were performed as follows: The ten samples were reduced to the optimum grain-size range for quantitative X-ray analysis (<10 μm) by grinding under ethanol in a vibratory McCrone Micronizing Mill for 10 minutes; Continuous-scan X-ray powder-diffraction data were collected over a range 3 °- 80° of 2θ with Co-Kα radiation on a Bruker D8 Focus Bragg-Brentano diffractometer equipped with an Fe monochromator foil, 0.6 mm (0.3 °) divergence slit, incident- and diffracted- beam Sollor slits and a LynxEye detector; The long fine-focus Co X-ray tube was operated at 35 kV and 40 mA, using a take-off angle of 6 °. The X-ray diffractograms were analyzed using the International Centre for Diffraction Database PDF-4 and Search-Match software by Bruker; X-ray powder-diffraction data of the samples were refined with Rietveld program Topas 4.2 (Bruker AXS). In addition, the amounts of serpentine were analyzed based on the PONKCS method[140,141] for samples SN260-SN261 and the Rietveld refinement using the lizardite-1T crystal structure[142] for

all the other samples with Rwp values less than 6.0. All the Rwp values for the QXRD analysis are less than 6.0.

The detailed particle size distribution of narrow-sized particle fractions were analyzed by a laser method on the Malvern Mastersizer 2000. A scanning electron microscope with an energy dispersive X-ray detector (SEM-EDX) analysis was used to investigate the process of the mineral carbonation. The surface and the transverse surface of particles were the analysis targets. To analyze the surface of particles, the dry particles were first coated by gold-palladium using the Denton Desk II sputter coater, followed by the SEM-EDX analysis. To analyze the transverse surface of particles, the samples needed to be prepared in the following steps. The carbonated solids after mineral carbonation were first dispersed well in pure carbon powders as the mechanical dispersant to prevent particles from sticking together. Then EpoFix resin and hardener were added with the weight ratio 25/3, followed by subsequently mixing with the mineral solids plus carbon powders. The mixture was then placed under vacuum to remove air bubbles which remained in the mixture and then it was left under ambient conditions for more than 48 hours to cure. The polishing steps started with the 400 grit sand paper, followed by 600 grit, 800 grit and 1200 grit sand papers until there were no obvious scratches on the polished surface. Subsequently, the 6-micron grade sand paper was further used to polish the sample with 6-micron monocrystalline diamond suspension, followed by washing with soapy water. The 1-micron grade sand paper was also used to further polish it with 1-micron monocrystalline diamond suspension, followed by thorough washing with soapy water. After further washing with ethyl alcohol, the mixture was coated with carbon to make the sample conductive for the SEM-EDX analysis. The FEI Quanta 650 instrument was used for the SEM-EDX analysis through measuring the molar ratio of Mg, Fe versus Si.

The nickel sulfide content and the molar ratio of iron sulfide/nickel sulfide of the raw materials and the sulfidized products were analyzed by Atomic Absorption Spectrometry (AAS) after the bromine-methanol digestion which is highly selective for the dissolution of metal sulfides away from oxides[138,139]. The detailed bromine-methanol digestion procedure is described in Appendix.

4.6 Evaluation of mineral carbonation efficiency

The evaluation of mineral carbonation efficiency derives from considering that the final fate of CO_2 gas during the mineral carbonation above 100 ℃, which is formation of non-hydrous carbonates. Physical absorption may result in the removal of some CO_2 gas but this does not persist. The classical way to evaluate the mineral carbonation efficiency is based on the change of the carbon content in the solids before and after the carbonation, illustrated in equation (4.3). During the continuous sampling, the weight after the carbonation is difficult to measure and therefore it is necessary to develop another way to evaluate the mineral carbonation efficiency. Through the fundamental definition of weight change (equation (4.4)) and carbon content (equation (4.5)), the relationship between carbon content and carbonation efficiency can be obtained in equation (4.6). The equation (4.6) can be rearranged to calculate the mineral carbonation efficiency as shown in equation (4.7). It shows that the evaluation of carbonation efficiency is only determined by the total carbon content before and after the reaction as well as the mineral carbonation capacity of the raw materials. Correspondingly, the amount of carbonated CO_2 can be evaluated in equation (4.8).

$$\alpha = \frac{m_2 \times \theta_2 - m_1 \times \theta_1}{m \times m_1} \times \frac{44.0098}{12.011} \times 100\% \tag{4.3}$$

$$m_{CO_2} = \alpha \times m \times m_1 \tag{4.4}$$

$$\theta_2 = \frac{m_1 \times \theta_1 + m_{CO_2} \times \frac{12.011}{44.0098}}{m_1 + m_{CO_2}} \quad (4.5)$$

$$\theta_2 = \frac{\theta_1 + \alpha \times m \times \frac{12.011}{44.0098}}{1 + \alpha \times m} \quad (4.6)$$

$$\alpha = \frac{\theta_2 - \theta_1}{m \times (\frac{12.011}{44.0098} - \theta_2)} \quad (4.7)$$

$$m_{CO_2} = \frac{m_1 \times (\theta_2 - \theta_1)}{\frac{12.011}{44.0098} - \theta_2} \quad (4.8)$$

where, m_1, m_2, and m_{CO2} represents the amount of the raw material, the product solid after carbonation, and carbonated CO_2 respectively, with units of g; m is the mineral carbonation capacity of the raw materials with unit of g CO_2/g material, which is only calculated based on the bivalent metal content of the sample and is not related to the type of minerals or mineral compositions; θ_1 and θ_2 are the total carbon content in %, of the solid before and after carbonation, respectively; and α is the mineral carbonation efficiency in %.

4.7 Evaluation of nickel conversion efficiency

The metals (nickel and cobalt) in the raw materials and products were mainly in two forms. One was metal oxide, including the silicates of olivine and serpentine or crystalline metal carbonate; the other form was metal sulfides. The target of the sulfidization research was to convert the nickel or cobalt in olivine into nickel or cobalt sulfides. The literature[138,139] suggests the bromine-methanol digestion is the best way to selectively dissolve the nickel/cobalt sulfides with only limited dissolution (less than 6%) of olivine. At the same time, the iron is also important part of the work, which was expected to form iron carbonates rather than iron sulfides. Since the

bromine-methnol digestion is selective to dissolve the sulfide minerals, the molar ratio of iron/nickel sulfides was also evaluated.

The nickel conversion efficiency was calculated by equation (4.9).

$$\beta = \frac{m_2 \times \delta_2 - m_1 \times \delta_1}{m_1 \times (1 - \delta_1)} \times 100\% \quad (4.9)$$

Where, β is nickel conversion efficiency, %; δ_1 and δ_2 are the contents of nickel in sulfides before and after carbonation; m_1 and m_2 are the solids weights before and after carbonation. With sampling, $m_2 = m_1 + m_{CO2}$ and m_{CO2} can be calculated by equation (4.8) based on the carbon content after the carbonation.

5 Mechanism and kinetics of mineral carbonation of olivine under moderate conditions

The successful application of a mineral carbonation process requires a detailed understanding of the kinetics and mechanism for optimal application. The improvement of the mineral carbonation theory provides the opportunity to economically enhance the process. This chapter describes the mechanism and kinetics of mineral carbonation of olivine and to develop a novel kinetic model. The tests were carried out under moderate conditions by analyzing the effects of factors including temperature, particle size, addition of salts and additives, PCO_2, rotation speed (rpm) and solids content (pulp density). The mineral carbonation of olivine represents the focus of the majority of the ex-situ mineral carbonation in published research[143]. This research investigated mineral carbonation using narrowly sized particles of olivine and CO_2 pressure lower than 45 bar to avoid excessively high pressure equipment that would have excessively high capital costs[72]. The addition of sodium bicarbonate and sodium chloride was also considered as they are the most classical additives for the mineral carbonation[72,75].

5.1 Effects of comprehensive effects

5.1.1 Effects of particle size

The particle size distribution of narrow-sized particles (- 25, 25 – 38, 38 – 53 and 53 – 75 μm) is shown in Figure 5.1. It is found that there were still the particles over 25 μm. This is mainly because of the difference in particle size analysis methods. The laser analysis depends on the volume of each particle but the sieve screening was closely related to the shape of particles and some over-size particles may still pass the target sieve. The corresponding effects of particle size on the mineral carbonation efficiency are shown in Figure 5.2a.

The mineral carbonation tests were carried out under the conditions of 185 ℃, PCO_2 = 34.5 bar, 10% solids content, 1 m $NaHCO_3$ + 1 m NaCl at 1200 rpm. It is clear that the particle size had a dramatic impact on the efficiency. The finest particle size sample, -25 μm, showed 61% mineral carbonation efficiency in 5 hours. In contrast, the 25 – 38 μm sample only attained 51% in 12 hours, followed by 26% and 22% for particle size ranges of 38 – 53 μm and 53 – 75 μm, respectively. As shown in Figure 5.2b, the specific surface area clearly indicates the marked differences among the narrow-sized particle fractions whereas particle size of P_{80} or P_{50} values cannot obviously show the considerable difference. The specific surface area for the particles sizes, -25 μm, 25 –38 μm, 38 – 53 μm and 53 – 75 μm, were 1.53, 0.27, 0.12 and 0.08 m^2/g, respectively. Comparing the differences of the specific surface area with the considerable effect of the particle size on the mineral carbonation efficiency, it is seen that it was more possible for the mineral carbonation rate is limited by specific surface area.

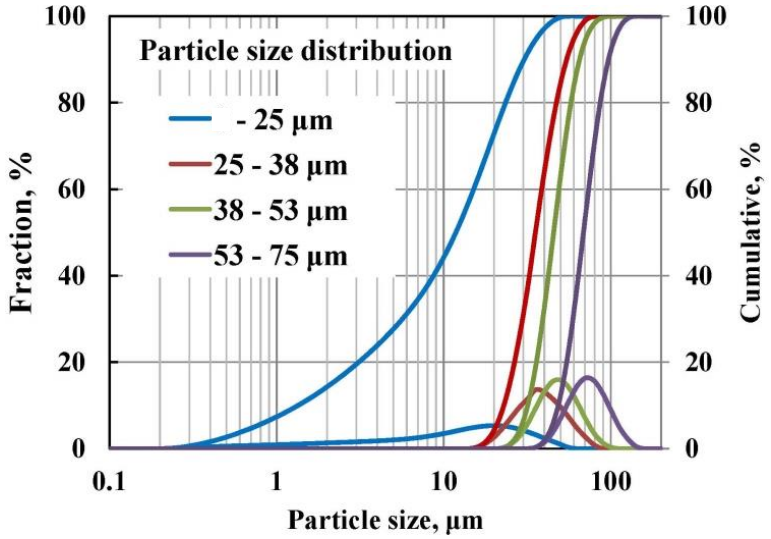

Figure 5.1 Particle size distribution of -25, 25 – 38, 38 – 53 and 53 – 75 μm particles.

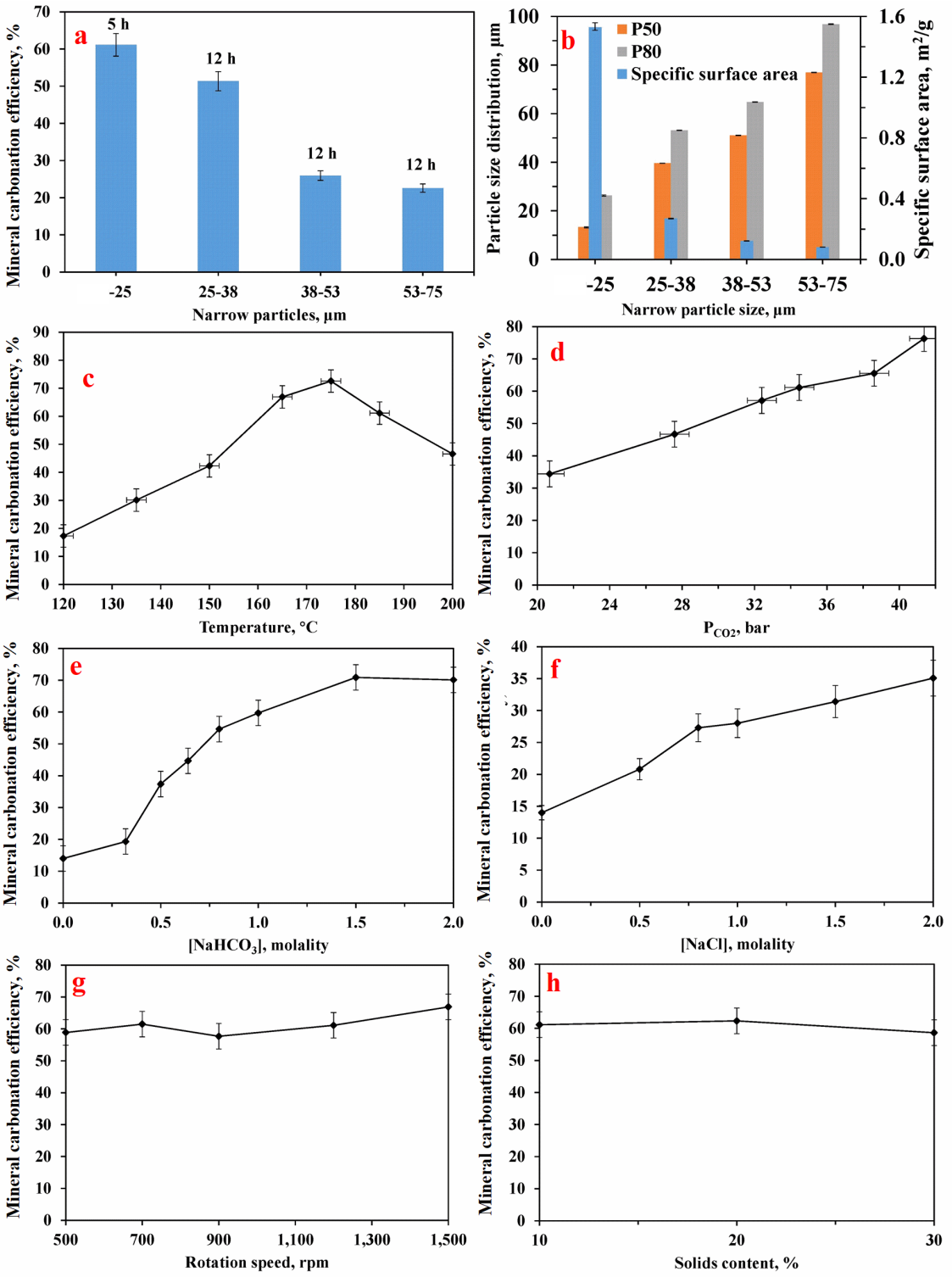

Figure 5.2 Effects of all factors on mineral carbonation under the conditions of -25 μm particle fractions, 185 ℃, PCO_2 = 34 bar, 10% solids content, 1 m $NaHCO_3$ + 1 m NaCl and 1200 rpm: (a) Effect of particle size; (b) Laser particle size distribution and specific surface area of narrow particles; (c) Effect of temperature; (d) Effect of PCO_2; (e) Effect of $NaHCO_3$; (f) Effect of NaCl; (g) Effect of rotation speed; (h) Effect of solids content.

SEM images of the carbonated solids of -25 μm particles under specified conditions are shown in Figure 5.3. According to the analysis of the surface of particles shown in Figure 5.3a and Figure 5.3b, there was obvious generation of cubic to rhomb-shaped minerals and agglomerated amorphous silica on the surface of the particles. The transverse surface analysis of particles, shown in Figure 5.3c and Figure 5.3d, also found that some particles were surrounded by cubic to rhomb-shaped minerals and there was a gap between the particles and the cubic to rhomb-shaped minerals on the outer surface of the particles. In fact, the cubic minerals were crystalline carbonates (magnesite/siderite) and the particles surrounded by carbonates were unreacted olivine. In addition, the amorphous silica was found agglomerated and far away from the olivine particles. Therefore, there may be the generation of aqueous H_4SiO_4 during carbonation that diffused out of the product layer and then the aqueous H_4SiO_4 was decomposed into amorphous silica. Sometimes even hollow particles appeared only consisting of cubic carbonates when the olivine particles were completely carbonated. With the evidence of the SEM-EDX image, it is shown that the shrinking core model (SCM) is suitable for the carbonation reaction process for the particles.

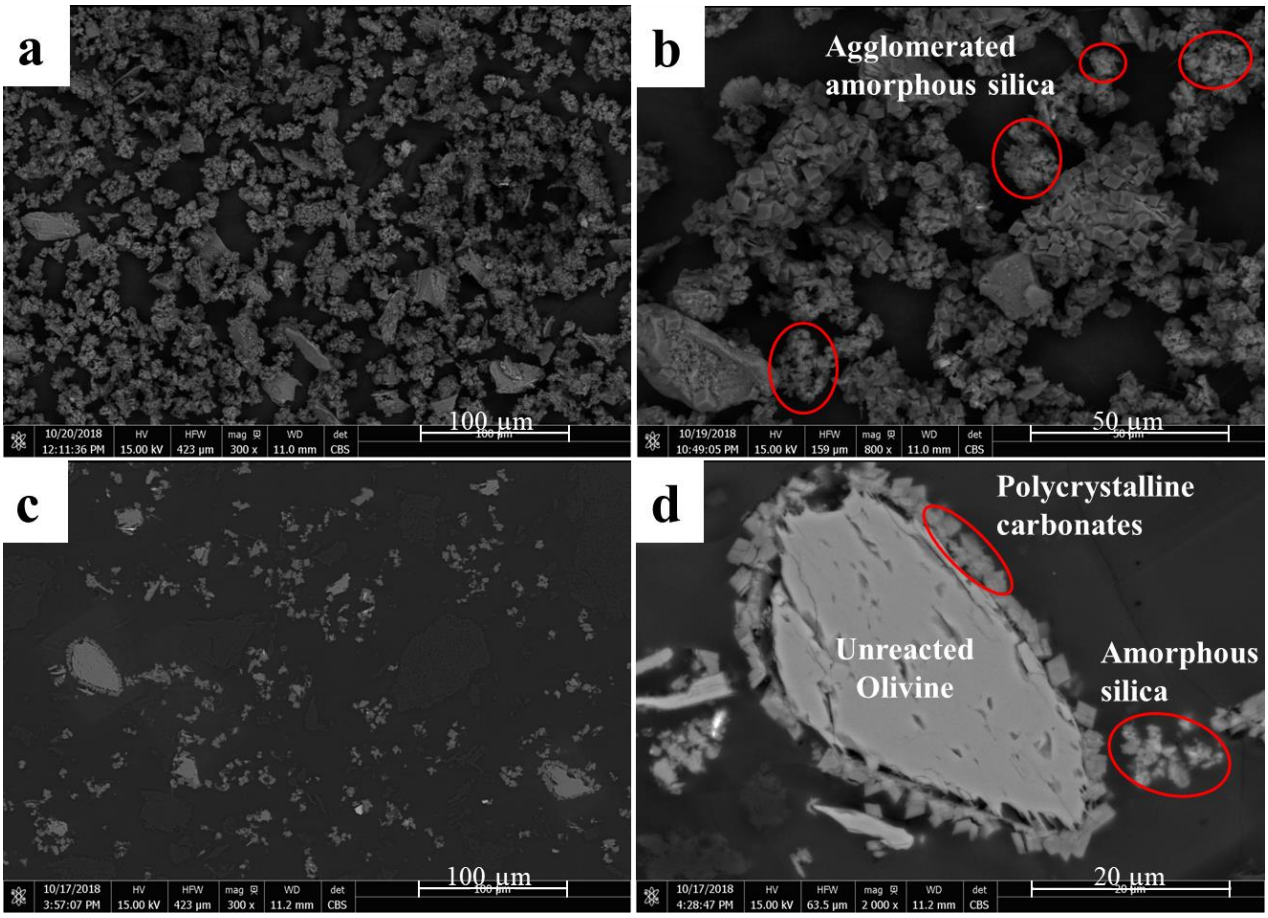

Figure 5.3 SEM images of carbonation solids of -25 µm at the conditions of 185 °C, PCO_2 = 34.5 bar, 10% solids content, 1 m $NaHCO_3$ + 1 m NaCl and 1200 rpm for 5 hours by the scanning electron microscope analysis with a concentric backscatter detector: a, b) Surface of particles; c, d) Transverse surface of particles.

The SCM requires that the overall particle size for the particles remains constant but the size of the unreacted olivine core decreases with time. The solid layer outside of the unreacted silicates is the solid product. There is also a stagnant film for the reacting aqueous ions moving from the aqueous solution to the surface of the solid sphere, which cannot be observed directly. In this research, the unreacted silicates were mainly olivine. The product layer was mainly carbonates. The stagnant film would be for the reacting H^+/HCO_3^- transporting from the solution to the solid surface. The chemical reaction would be expected to be between the unreacted silicates (olivine

core) and the reactive H^+/HCO_3^-. Correspondingly, there are three different possible rate-controlling mechanisms: mass transport, product layer diffusion and chemical reaction[144,145]. The respective kinetic equations[144,145] for the three different process are the following in sequence:

$$t = k_1 \times \alpha \quad (5.1)$$

$$t = k_2 \times [1 - (1 - \alpha)^{1/3}] \quad (5.2)$$

$$t = k_3 \times [1 - 2\alpha/3 - (1 - \alpha)^{2/3}] \quad (5.3)$$

where, t is reaction time, hours; α is the mineral carbonation efficiency, %; k_1, k_2 and k_3 are the rate constants for mass transport control, chemical reaction control and product layer diffusion control, respectively.

5.1.2 Effects of temperature and activation energy

The effects of temperature on the mineral carbonation efficiency was investigated under the conditions of PCO_2 = 34.5 bar, 10% solids content, 1 m $NaHCO_3$ + 1 m NaCl and 1200 rpm, shown in Figure 5.2c. It is clear that temperature had a marked effect on the mineral carbonation efficiency. Figure 5.2c and Figure 5.4a1 are for -25 μm particles. With increasing temperature, the efficiency at five hours of reaction time increased dramatically and peaked (at around 72% of mineral carbonation efficiency) at 175 ℃, followed by a considerable decrease when the temperature continued to rise: 61% and 47% at 185 ℃ and 200 ℃, respectively. Figure 5.4b1 – Figure 5.4c1 showed the same situation, reaching a peak at 175 ℃, at 49% and 43% for 25 – 38 μm and 38 – 53 μm particles, respectively. It is well-known that increasing temperature can considerably accelerate the diffusion rate of effective ions and also the chemical reaction rate between the effective ions and the unreacted olivine. However, once the temperature exceeded 175 ℃, the efficiency significantly decreased. The reason may be related to the applied CO_2

partial pressure and the concentration of bicarbonate ions[32,146]. At this specific PCO_2, high temperature can decrease the effective concentration of bicarbonate ions[146] by making the dissolution of CO_2 gas thermodynamically less favourable (at less than 200 ℃). The Gibbs free energy of the reaction between CO_2 gas and olivine also becomes less favourable as the temperature increases to over 175 ℃ while the higher PCO_2 makes the dissolution of CO_2 gas thermodynamically more favourable. Therefore, it is important to carefully control the temperature in relation to the PCO_2. At 34 bar of PCO_2, a suitable temperature for further study was 175 ℃.

The mineral carbonation efficiency increases with reaction time for all particles and at all temperatures. Plots of α versus time in Figure 5.4a2 to Figure 5.4c2 were linear, indicating that mineral carbonation might be controlled by mass transport under the specified conditions. It is obvious that the mineral carbonation process was not controlled by solid product layer diffusion since plots of $1 - 2\alpha/3 - (1 - \alpha)^{2/3}$ versus time were not linear as shown in Figure 5.4a3 – Figure 5.4c3. By contrast, there was a good relationship between $1 - (1 - \alpha)^{1/3}$ and time, and the corresponding R^2 was always over 0.98 for all particle sizes, as shown in Figure 5.4a4 – 5.4c4. This indicates that the mineral carbonation process is likely controlled by slow chemical reaction. At 185 ℃, there were the same trends for all the particle size fractions indicating chemical reaction control or mass transport control and not product layer diffusion control, as shown in Figure 5.6a2 – Figure 5.6a3.

To determine whether the mineral carbonation was controlled by mass transport or chemical reaction the Arrhenius activation energy was determined. The calculation of activation energy is based on Arrhenius Equation (5.4) and the rearranged form, Equation (5.5).

$$k = A \times e^{-Ea/RT} \quad (5.4)$$

$$\ln k = -Ea/RT + \ln A \quad (5.5)$$

where, k is the rate constant for Equations (5.1 – 5.3); A is the pre-exponential factor; R is the gas constant, 0.008314 $kJ \cdot mol^{-1} \cdot K^{-1}$; T is the reaction temperature, K; and Ea is the activation energy of the mineral carbonation process, kJ/mol. The activation energy is usually below 20 kJ/mol for the diffusion control or mass transport control whereas it is usually more than 40 kJ/mol for chemical reaction control[144,145,147].

Figure 5.5 shows the relationship between lnk and $1/T \times 1000$ according to the mass transport control and chemical reaction control, respectively. It is clear that all of the plots had a good correlation as the R^2 was at least 0.97. The activation energy, i.e. Ea, calculated for the mass transport control plots were 40.7 kJ/mol, 46.1 kJ/mol and 49.1 kJ/mol for 0 – 25 μm, 25 – 38 μm and 38 – 53 μm size ranges, respectively. The activation energy values were too high for mass transport rate control (Ea should be below 12 kJ/mol[144,145]). In contrast, for the chemical reaction rate control plots, the activation energy values were calculated to be 48.0 kJ/mol, 50.8 kJ/mol and 56.5 kJ/mol for -25 μm, 25 – 38 μm and 38 – 53 μm size ranges respectively. These values were with the typical range of the activation energies for chemical reaction rate control. As a result, the mineral carbonation for all narrow-size particles at all temperatures was concluded to be controlled by the chemical reaction between the unreacted olivine and the reactive H^+/HCO_3^- ions. Thus, mass transport control was not considered to be pertinent for the following experiments. Chemical reaction control and the product layer diffusion control were investigated in subsequent work. Furthermore, the smaller particle size will significantly enhance the mineral carbonation efficiency, as shown in Figure 5.6a1.

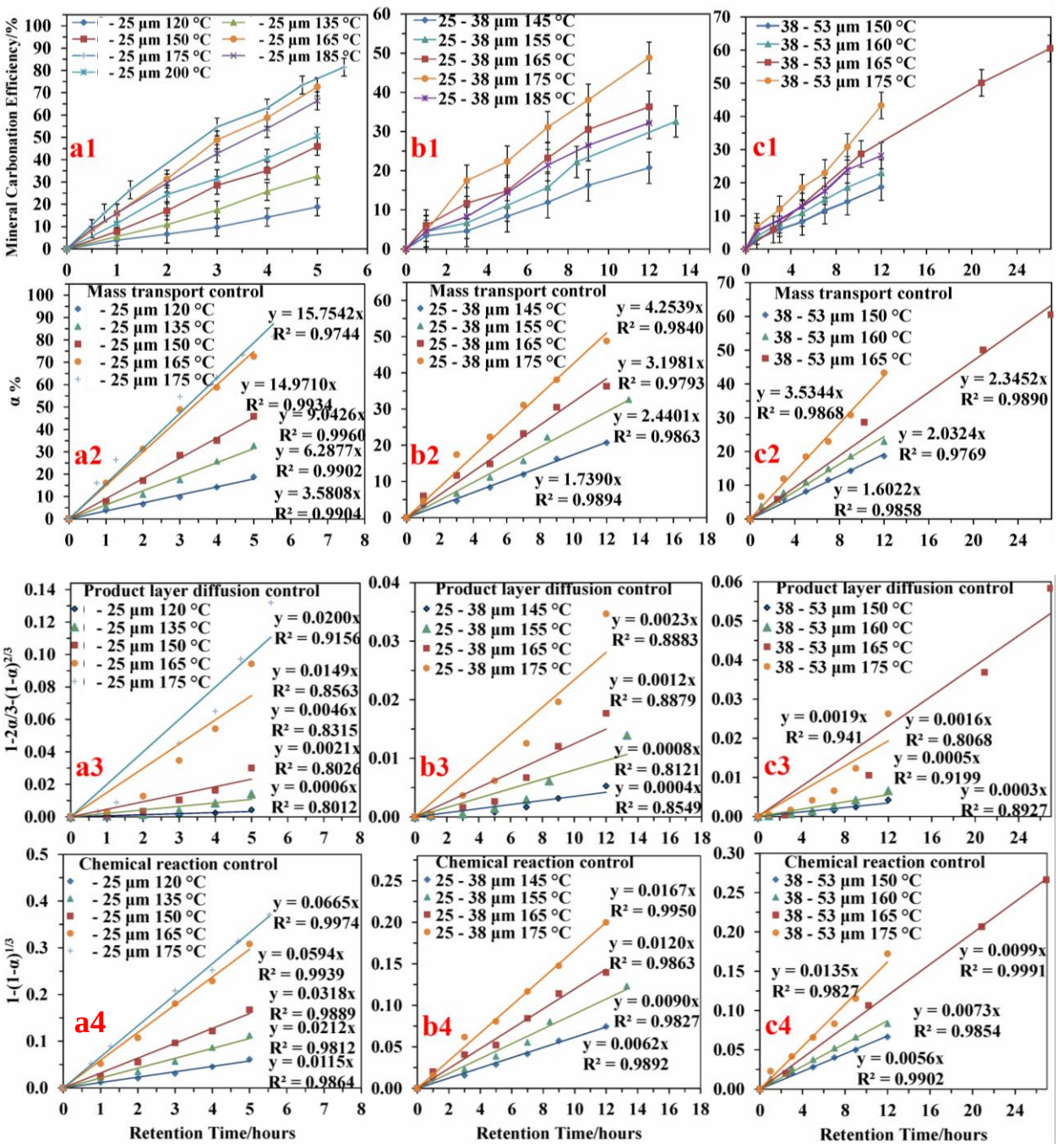

Figure 5.4 Effects of temperature and kinetics plots for narrow-sized particle fractions -25 µm, 25 – 38 µm and 38 – 53 µm, respectively under the conditions of PCO_2 = 34.5 bar, 10% solids content, 1 m $NaHCO_3$ + 1 m NaCl and 1200 rpm: a1, b1, c1) Effects of temperature; a2, b2, c2) mass transport control; a3, b3, c3) product layer diffusion control plots; a4, b4, c4) chemical reaction control plots.

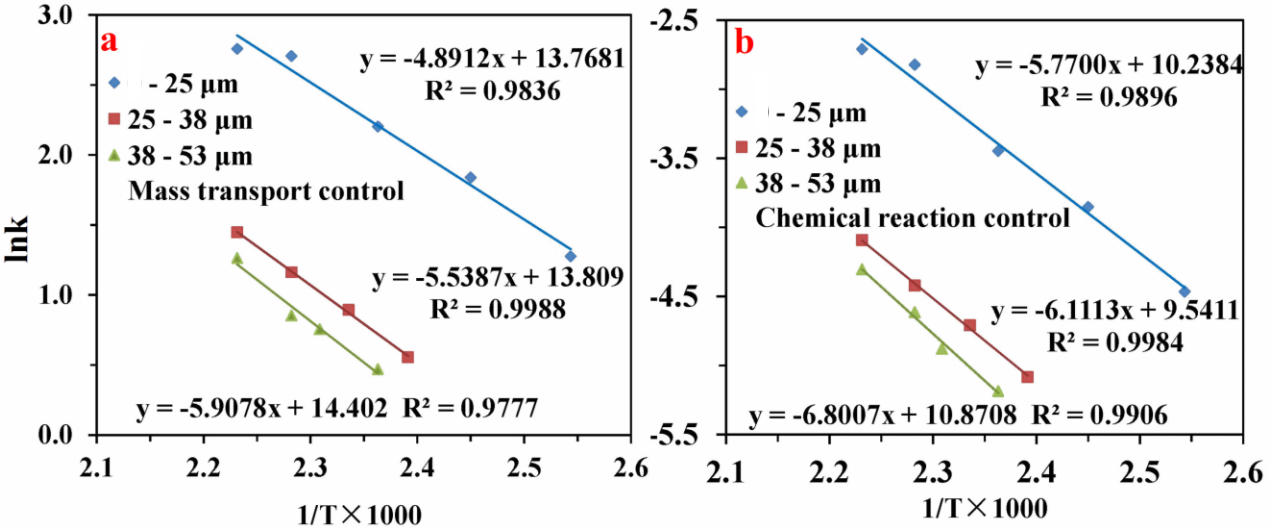

Figure 5.5 Activation energy plots according to the Arrhenius equation based on: (a) mass transport control and (b) Chemical reaction control.

5.1.3 Effects of CO_2 partial pressure

The effects of CO_2 partial pressure on the mineral carbonation efficiency were investigated under the conditions of 0 – 25 µm particle size, 185 ℃, 10% solids content, 1 m $NaHCO_3$ + 1 m NaCl and 1200 rpm, as shown in Figure 5.2d and Figure 5.6b1. The mineral carbonation efficiency was proportional to the CO_2 partial pressure as shown in Figure 5.2d. When the PCO_2 increased from 21 bar to 41 bar, the mineral carbonation efficiency increased markedly from 34% to 76%. Theoretically, it is easier for the mineral carbonation process to proceed at much higher PCO_2. However, the supply of high PCO_2 is an important cost, along with the reactor equipment required[102,148]. It is reasonable to provide a moderate PCO_2 to accelerate the mineral carbonation rate and to control the costs.

The further kinetic modelling of the data, shown in Figure 5.6b2 – Figure 5.6b3, indicates that the reactions were still controlled by chemical reaction except that the reaction at 20.7 bar was controlled by the product layer diffusion as only the R^2 at 20.7 bar was 0.94 for chemical control

(Figure 5.6b2) but 0.98 for the product layer diffusion control (Figure 5.6b3). It is known that increasing CO_2 partial pressure can increase the acidity and the concentration of H^+ or HCO_3^-, which would increase the dissolution rate of olivine. Product layer diffusion control at low CO_2 partial pressure may result from the shortage of the supply of H^+ or HCO_3^-.

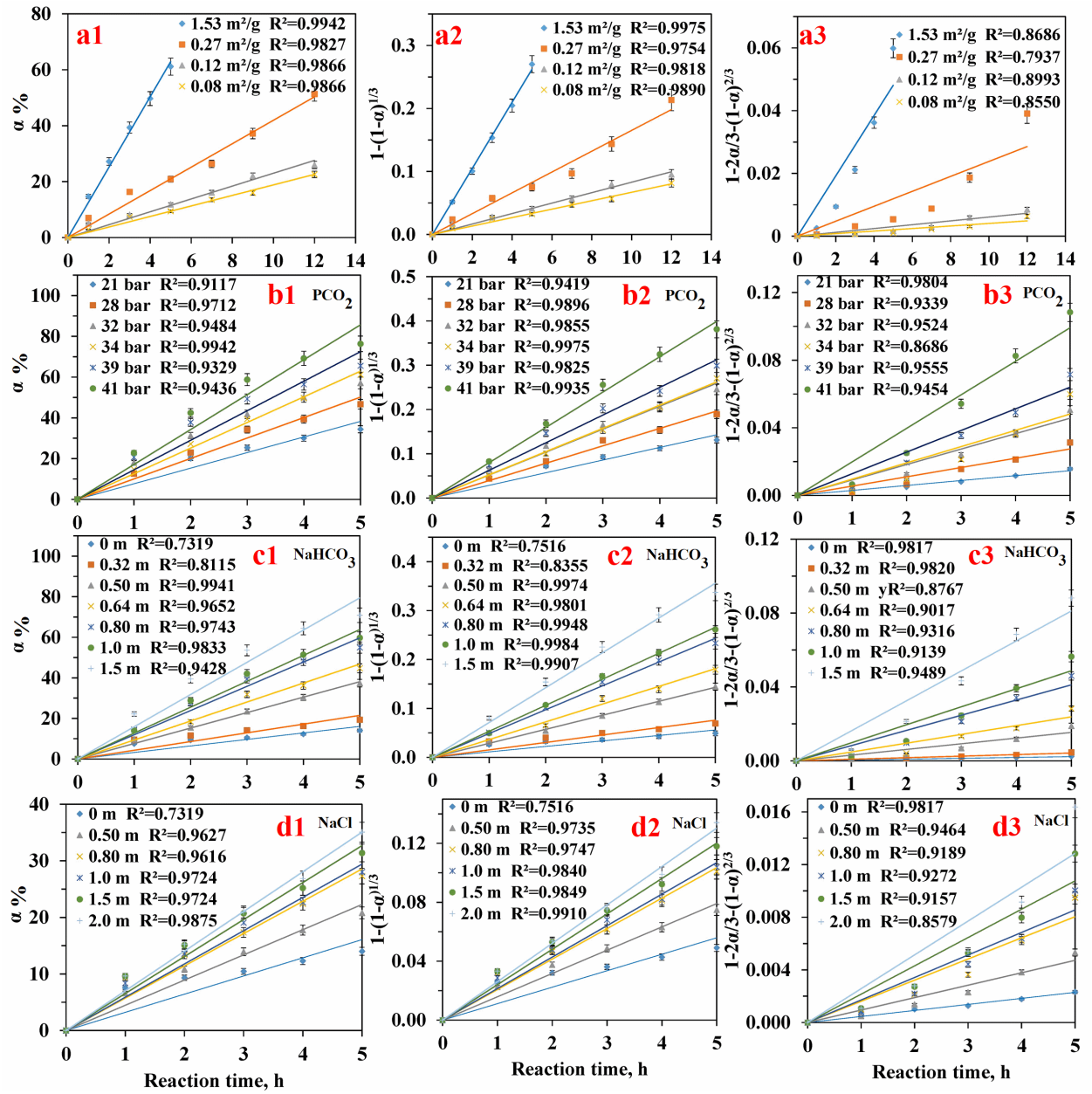

Figure 5.6 Plots of kinetics of mass transport control, chemical reaction control and product layer diffusion control respectively under conditions of -25 μm particles, 185 ℃, PCO_2 = 34 bar, 1 m $NaHCO_3$ + 1 m NaCl: (a) for particle size; (b) for PCO_2; (c) and (d) for $NaHCO_3$ and NaCl respectively.

In order to confirm the change of the control mechanism, further SEM-EDX analysis was used. There is no obvious difference between the images of Figure 5.7a and 5.7b and those of Figure 5.3a and 5.3b. However, it is obvious that the carbonation process has changed markedly by comparing Figure 5.3c-5.3d with Figure 5.7c-5.7d. There was a clear solid layer between the unreacted core and the solid product layer in Figure 5.7d. This clear solid layer was darker (in colour) than the unreacted olivine. In contrast, there was no intermediate layer in Figure 5.3 between the well-crystallized carbonates and the unreacted olivine. This means that there was aqueous H_4SiO_4 generation that diffused out from the product layer when the CO_2 partial pressure was high enough. However, when the CO_2 partial pressure was low, such as 20.7 bar, there was no obvious amorphous silica generation except for the darker minerals (in colour) than olivine, which existed between the well-crystallized carbonates and the unreacted olivine. Through the SEM-EDX analysis (shown in Figure 5.7d), the darker minerals were also carbonates which had no obviously rhomb-shaped crystals. This could indicate that under the lower CO_2 partial pressure conditions, the quick formation and growth of carbonate crystals was inhibited.

Therefore, it is suggested that the mechanism of the mineral carbonation reaction under the conditions of 185 ℃, 10% solids content, 1 m $NaHCO_3$ + 1 m NaCl and 1200 rpm with relatively high CO_2 partial pressure (higher than 20.7 bar), was that the H^+ ions attacked the target olivine particles and the crystal structure of olivine was gradually broken down with release Mg^{2+} and Fe^{2+} ions. Aqueous H_4SiO_4 was generated and diffused out of the solid product layer. The formed carbonates were polycrystalline and remained on the outer layer of the particle sphere where the reactive ions can easily pass through. When the CO_2 partial pressure was lower than 20.7 bar (included), the generated carbonates were not polycrystalline and formed a

relatively uniform solid product layer. Under this condition, the reactive ions cannot easily pass through the uniform layer and the result was apparently product layer diffusion control.

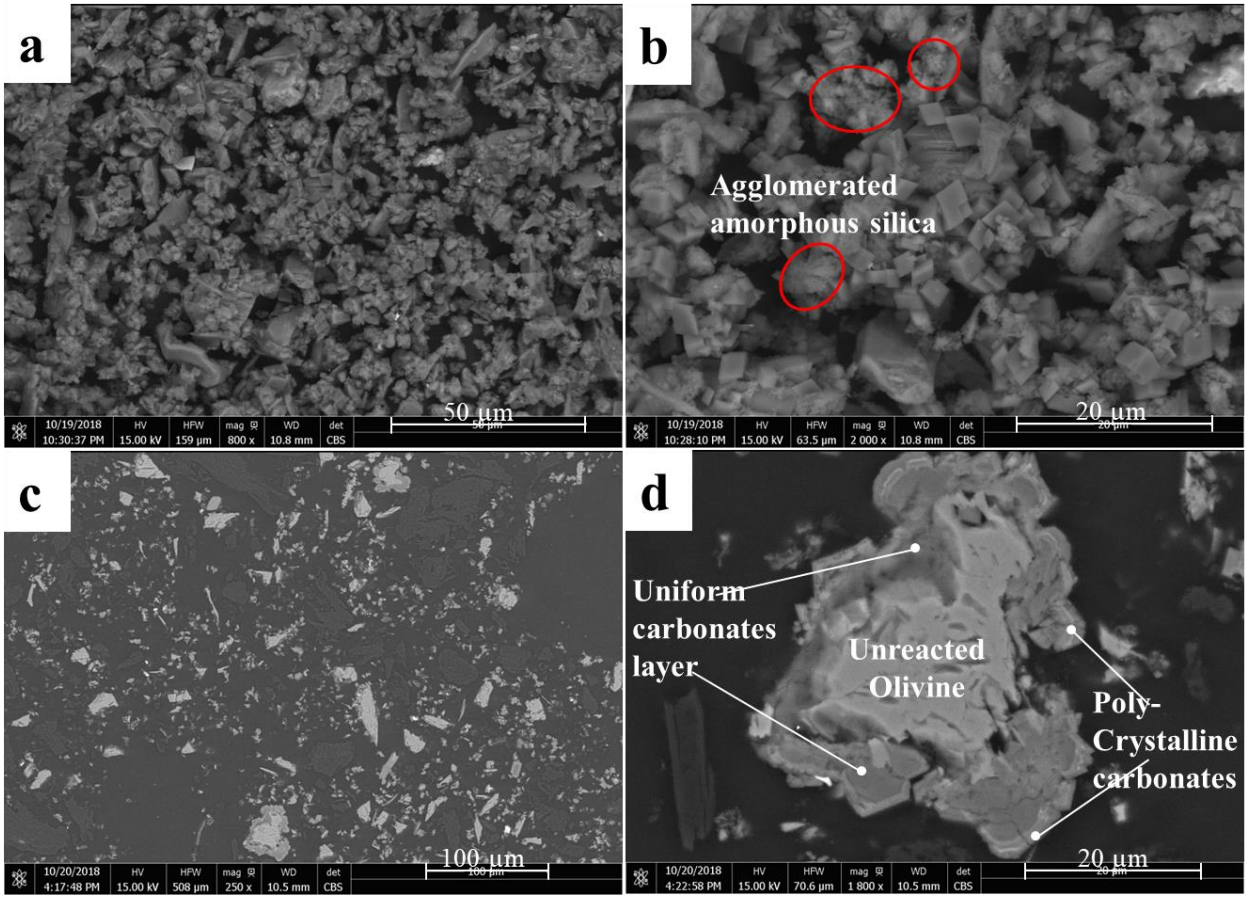

Figure 5.7 SEM-EDX analysis of carbonation solids of -25 µm particle size fractions under the conditions of PCO_2 = 20.7 bar, 185 ℃, 10% solids content, 1 m $NaHCO_3$ + 1 m NaCl and 1200 rpm: a, b) Surface of particles; c, d) Transverse surface of particles.

5.1.4 Effects of $NaHCO_3$

The effects of $NaHCO_3$ on the mineral carbonation efficiency were investigated under the conditions of 0 – 25 µm, 185 °C, PCO_2 = 34.5 bar, 10% solids content and 1200 rpm, as indicated in Figure 5.2e and Figure 5.6c1. It is clear that the $NaHCO_3$ also had a dramatic effect on the carbonation efficiency. The addition of 2 m sodium bicarbonate improved the mineral

carbonation efficiency from 14% to 71 % for 5 hours reaction time. It increased by approximately 57%. There was a slight increase of mineral carbonation efficiency to 19% when 0.32 m sodium bicarbonate was introduced into the system. The efficiency exhibited a logarithmic increase with the further addition of sodium bicarbonate, followed by a plateau after 1.5 m addition at 71% efficiency. It is also noted that the mineral carbonation efficiency with 1.0 m $NaHCO_3$ + 1.0 NaCl and only 1.0 m $NaHCO_3$ was 61% and 60%, respectively under the same conditions. The further addition of sodium chloride only contributed to less than 2% improvement in efficiency for a fixed addition of sodium bicarbonate. The addition of sodium bicarbonate is much more significant than the addition of sodium chloride. It may be unnecessary to add sodium chloride once there is enough sodium bicarbonate.

According to Figure 5.6c2 – Figure 5.6c3, the R^2 value for the fitting of the chemical reaction control model was over 0.98 for experiments with greater than 0.32 m $NaHCO_3$ but below 0.84 for the experiments with lower than 0.32 m (included) $NaHCO_3$. By contrast, the R^2 value for the fitting to the product layer diffusion control model was more than 0.98 for the lower $NaHCO_3$ concentrations but less than 0.90 for the higher concentrations. This shows that the mineral carbonation rate was controlled by the chemical reaction at higher concentrations (>0.32 m) of $NaHCO_3$, whereas the mineral carbonation process was controlled by product layer diffusion when the $NaHCO_3$ concentration was lower than 0.32 m.

SEM-EDX analysis was used to study the change of chemical compositions and particle-product structures, as shown in Figure 5.8. These particles look completely different from those in Figure 5.3 and Figure 5.7. According to the analysis of the surfaces of the particles (Figure 5.8a and 5.8b), there was no obvious generation of individual amorphous silica particle away from the original particle, when there was no addition of any salts. In contrast, there was obvious

generation of a Si-rich layer on the surface. The analysis of the transverse surface of particles also showed that the Si-rich layer surrounded the unreacted olivine as shown in Figure 5.8c and Figure 5.8d. Comparing Figure 5.7 and Figure 5.3, the addition of $NaHCO_3$ appears to accelerate the mineral carbonation process by avoiding control by solid product layer diffusion and facilitating control by chemical reaction. The addition of high concentration of $NaHCO_3$ can enhance the dissolution of olivine and may also result in the formation of aqueous H_4SiO_4 which may be not stable in the bulk solution and decompose to amorphous silica.

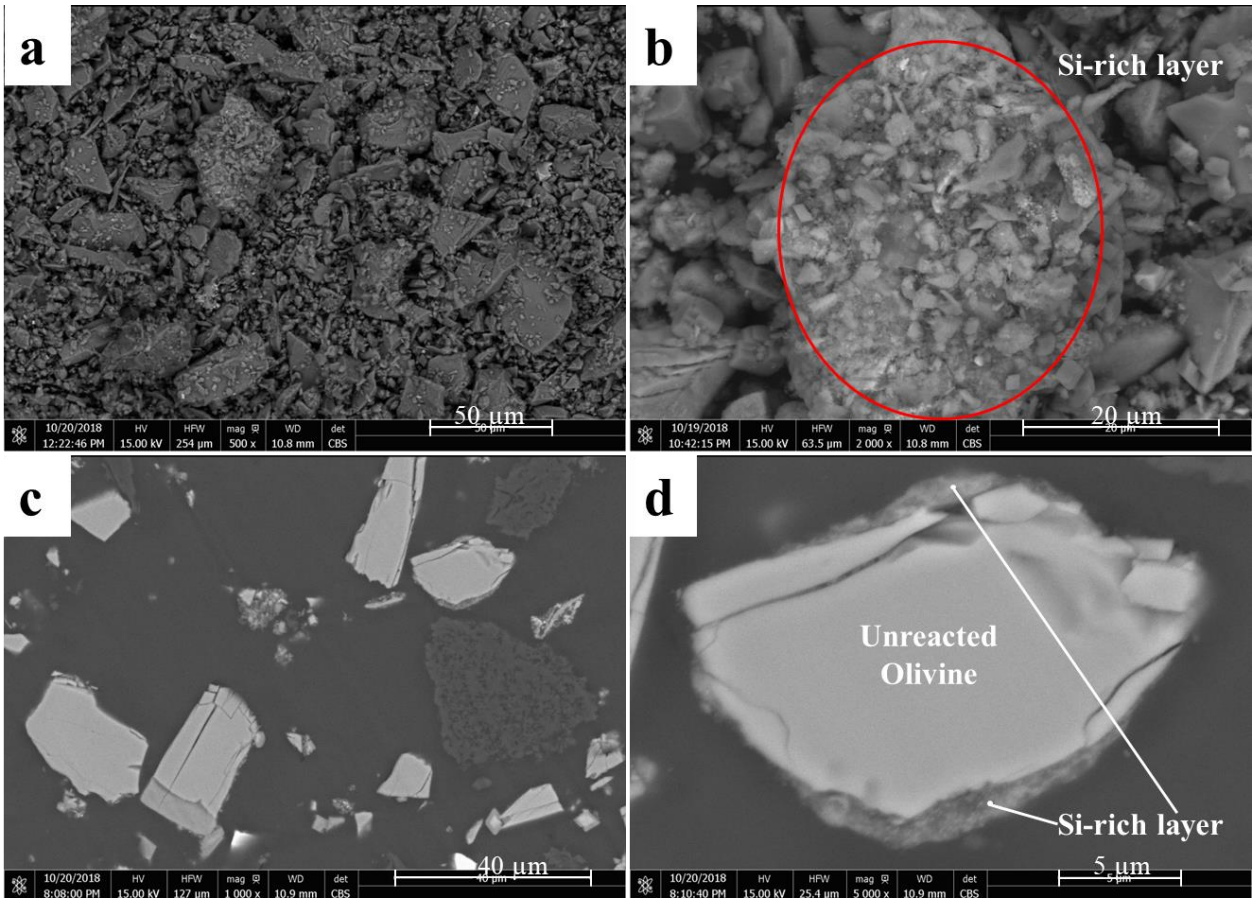

Figure 5.8 SEM-EDX analysis of carbonation solids of -25 µm particle size fractions under the conditions of PCO_2 = 34.5 bar, 185 ℃, 10% solids content and 1200 rpm without any addition of salts: a, b) Surface of particles; c, d) Transverse surface of particles.

5.1.5 Effects of NaCl

Figure 5.2f and Figure 5.6d1 show the effects of NaCl on mineral carbonation efficiencies under the conditions of 0 – 25 μm, 185 °C, PCO_2 = 34.5 bar, 10% solids content and 1200 rpm for 5 hours. It was found that the addition of NaCl had positive effects on mineral carbonation though the effects were less pronounced than those of $NaHCO_3$, which is consistent with the previous research[47,97]. Compared to only 15% of efficiency without NaCl and $NaHCO_3$, the additions of 1 m and 2 m NaCl alone can enhance the mineral carbonation to 28% and 35% (at 5 hours) respectively. The addition of sodium chloride from 0.5 m to 2.0 m also showed a logarithmic improvement in the mineral carbonation efficiency. But unlike sodium bicarbonate, there was no plateau limiting further improvements up to 2.0 m sodium chloride.

In order to try to find the reasons why NaCl can enhance the mineral carbonation process, the further kinetics analysis was performed, as shown in Figure 5.6d2 – 5.6d3. This showed that the carbonation rate was controlled by chemical reaction both at 1 m NaCl and at 2 m NaCl. It is interesting that even though the mineral carbonation efficiency was still lower with addition of NaCl, then with $NaHCO_3$ it was still controlled by chemical reaction rather than product layer diffusion, which controlled the process without the addition of salts and even with the addition low concentrations of $NaHCO_3$. Figure 5.9 shows the effects of addition of sodium salts on the aqueous silicon content during mineral carbonation. It is obvious from Figure 5.9a-5.9b that the aqueous silicon concentration was considerably decreased when sodium chloride was introduced into the system, from approximately 422 mg/L (no salts) to 334 and 283 mg/L with the addition of 1 m and 2 m NaCl, respectively. During the carbonation, the silicon concentration did not significantly change with time of reaction. In addition, the silicon in the aqueous solution only accounted for less than 2% of the total silicon content of the original high-grade olivine. This

means that the great majority of silicon was still in the solids, including in the agglomerated amorphous silica. The addition of sodium salts can increase the instability of aqueous silica and the solubility of aqueous silica is inversely proportional to the addition of sodium salts as shown in Figure 5.9c. The aqueous silica was still not stable though and decomposed into amorphous silica, which was extensively observed in the aqueous solutions after carbonation and settled down for more than one month at room temperature, as shown in Figure 5.9d. In fact, the aqueous silicon is probably in the form of aqueous silica, H_4SiO_4, which can only be temporarily stable in aqueous solution. The reason why the addition of sodium salts can accelerate the mineral carbonation process is mainly because the addition of sodium salts can facilitate the diffusion of dissolved silica generated from the dissolution of olivine through the product layer, which was not stable in aqueous solution and decomposed into amorphous silica in solids.

5.1.6 Effects of agitation speed

The effects of rotation speed on the mineral carbonation efficiencies under the conditions of 0 – 25 μm, 185 °C, PCO_2 = 34.5 bar, 10% solids content and 1 m $NaHCO_3$ + 1 m NaCl were investigated as shown in Figure 5.2g and Figure 5.10a1. It is apparent that the mineral carbonation efficiency increased only slightly with increasing rotation speed. At 5 hours of reaction time, the efficiencies were 59%, 61%, 58%, 61% and 67% respectively for 500 rpm, 700rpm, 900 rpm, 1200 rpm and 1500 rpm. There was no obvious difference in efficiency (less than the systematic error 4%) when the rotation speed was less than 1200 rpm (included). However, the efficiency increased by more than 7% (beyond the systematic error 4%), when the rotation speed increased to 1500 rpm. It might be due to the further milling action due to the too fast mixing. According to the Figure 5.10a2 – 5.10a3, the reactions at all the three rotation

speeds were always controlled by chemical reaction. The curve for the 1500 rpm of rotation speed was slightly steeper than the others. This is consistent with the possible milling action that the very high rotation speed can help remove the loose carbonates layer and make it easier for the reactive ions to pass through the layer and thereby slightly improve the rate of reaction.

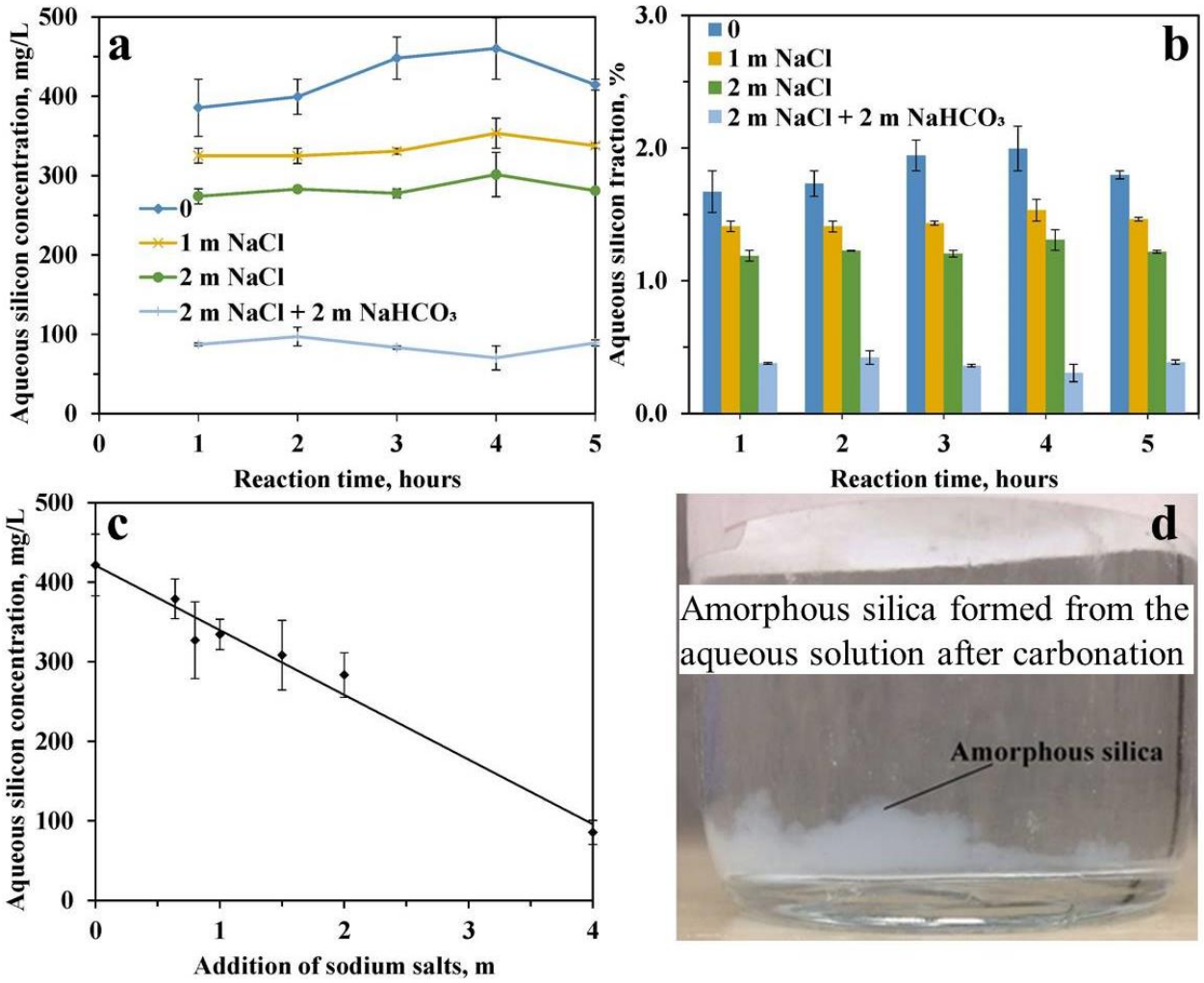

Figure 5.9 Aqueous silicon content during the mineral carbonation under the conditions of -25 μm particle size fractions, PCO_2 = 34.5 bar, 185 ℃, 10% solids content and 1200 rpm: a) Aqueous silicon concentration and b) Aqueous silicon fraction compared to total silicon content of the high-grade olivine; c) Relationship between aqueous silicon concentration and addition of sodium salts and d) Amorphous silica formed from the aqueous solution after carbonation settled down for more than one month at room temperature.

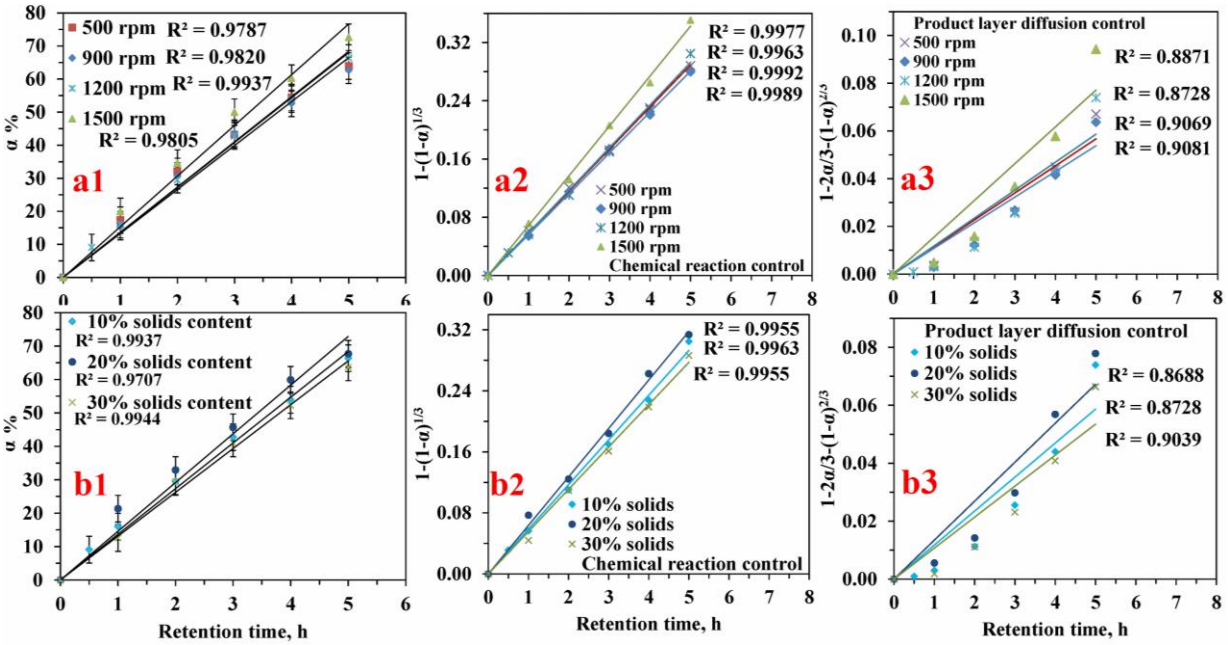

Figure 5.10 Plots of kinetic models function for mass transport control, chemical reaction control and product layer diffusion control: (a) for rotation speed under PCO_2 = 34 bar, 185 ℃, 1 m $NaHCO_3$ + 1 m NaCl; (b) for solids content under -25 μm, 185 °C, 1 m $NaHCO_3$ + 1 m NaCl.

5.1.7 Effects of solids content

The effects of solids content on the mineral carbonation efficiencies under the conditions of 0 – 25 μm, 185 °C, PCO_2 = 34.5 bar, 1200 rpm and 1 m $NaHCO_3$ + 1 m NaCl were investigated and are shown in Figure 5.2h and Figure 5.10b1. It is noted that solids content had only minor effects on the carbonation efficiency: 61%, 62% and 59% for 10% solids, 20% solids and 30% solids respectively at 5 hours reaction time. In fact, the efficiencies for the three solids contents were the same value within 3% relative error, smaller than the overall relative error of the tests. Therefore, it is concluded that the solids content up to 30% almost had no effect on the mineral carbonation. The corresponding kinetic model functions (Figure 5.10b2 – 5.10b3) also showed that all the reactions with different solids contents were still controlled by the chemical reaction. This means that the increase of solids (from 10% to 30%) content did not enhance the product

layer removal by attrition between particles nor hinder the mass transport of the reactive ions under this range of conditions. Fortunately, some mineral companies discharge the final tailings slurry with 30% or higher solids content. This means that the final tailings slurry from a flotation facility might be suitable for the mineral carbonation process.

5.2 Mechanisms of mineral carbonation of olivine

The preceding results and discussion show that all the reactions under all the above conditions were controlled by chemical reaction except for reactions under low CO_2 partial pressure and with little or no addition of $NaHCO_3$ and NaCl. Under these latter conditions mineral carbonation was controlled by product layer diffusion. To summarizing: (1) The reaction rate under 185 ℃, PCO_2 = 34.5 bar, 1 m $NaHCO_3$ + 1 m NaCl, 10% solids content and 1200 rpm was controlled by chemical reaction, no matter what the particle size was and regardless of the mineral carbonation efficiency; (2) The reaction was always controlled by chemical reaction no matter what the temperature, rotation speed and solids content were, so long as there were high enough CO_2 partial pressure and high enough concentrations of $NaHCO_3$ or NaCl; (3) There was the aqueous H_4SiO_4 formation for the chemical reaction control process at high enough concentration of salts ($NaHCO_3$ or NaCl) during the carbonation process even though the unstable aqueous H_4SiO_4 in the bulk solution can decompose into amorphous silica.

The preliminary mechanism of the mineral carbonation of olivine can be summarized from the preceding results and discussion and is illustrated in the schematic diagram shown in Figure 5.11. At low concentration of sodium salts (e.g. <0.32 m $NaHCO_3$ or NaCl), the mineral carbonation was controlled by diffusion through a Si-rich layer, as shown in Figure 5.11a1. The Si-rich layer hindered the diffusion of reactive H^+ from the aqueous bulk solution to the surface of the

unreacted olivine core. It is because of the partial dissolution of Mg out from the olivine structure that the Si-O remained as an incomplete silicate structure to form a Si-rich layer, as shown in Figure 5.11a2. When the concentration of sodium salts was high enough in the carbonation system but the CO_2 partial pressure was low (lower than 20.7 bar), the mineral carbonation process was still controlled by product layer diffusion but the product layer had changed to form uniform carbonates, as shown in Figure 5.11b1. This is because there was enough sodium salts in the system so that the Si-O remaining in the incomplete silicate structure can form aqueous H_4SiO_4 to dissolve into solution followed by decomposition to amorphous silica outside the product layer. However, there was not an adequate and continuous supply of reactive H^+ and CO_3^{2-} ions. As a result, there was neither continuous rapid H^+ formation to attack the olivine structure nor the rapid sufficient CO_3^{2-} formation to accelerate the growth of carbonates. In particular, the carbonates did not apparently grow as separate crystals and simply remained between the already well-crystallized carbonates and the unreacted core. These intermediate carbonates accumulated to form a uniform carbonate layer to hinder the further dissolution of Mg and Fe, as shown in Figure 5.11b2. When the CO_2 partial pressure was high enough and there was adequate concentration of sodium salts, the problem of supply of the rapidly-continuous sufficient CO_3^{2-} and H^+ was addressed. All newly formed carbonates reported to the outer carbonates layer and sequentially the uniform carbonates layer largely disappeared, as shown in Figure 5.11c1. This change benefited the diffusion of reactive H^+ and newly formed aqueous H_4SiO_4 through the carbonates layer. As a result, the concentration of reactive H^+ in the interlayer between the well-crystallized carbonates and unreacted core became quite similar to the concentration in the main aqueous bulk solution. The detrimental effects of solids product

layer diffusion were removed and the mineral carbonation process was accelerated to be controlled by chemical reaction between H^+ and the unreacted olivine, as shown in Figure 5.11c2.

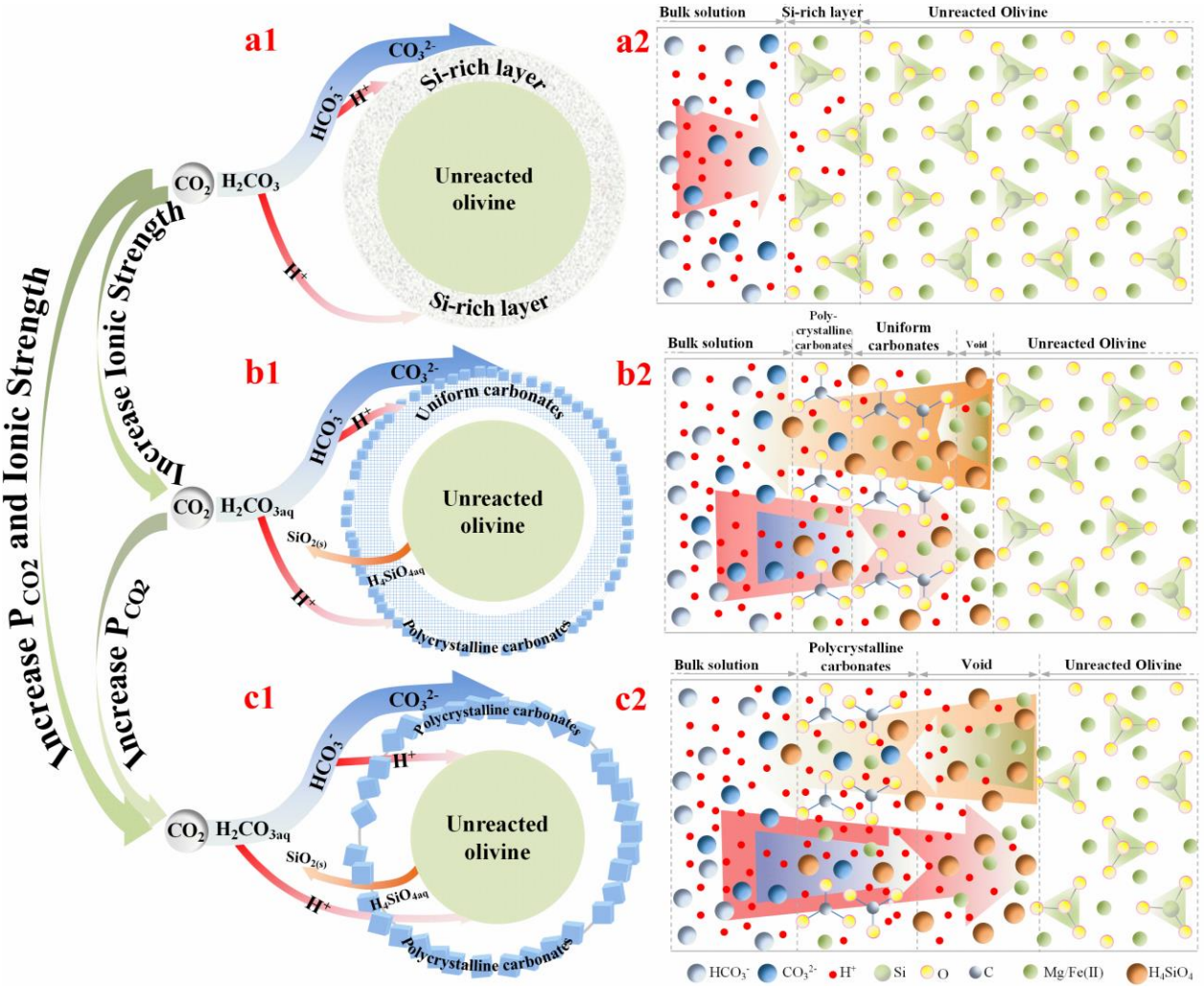

Figure 5.11 Schematic diagram of the mechanisms of mineral carbonation of olivine for CO_2 sequestration: a1) for carbonation at low concentration of sodium salts; a2) gradual process of carbonation at low concentration of sodium salts; b1) for carbonation at low CO_2 partial pressure and high enough concentration of sodium salts; b2) gradual process of carbonation at low CO_2 partial pressure and high enough concentration of sodium salts; c1) for carbonation at high enough CO_2 partial pressure and concentration of sodium salts; and c2) gradual process of carbonation at high enough CO_2 partial pressure and concentration of sodium salts.

Furthermore, the chemical reaction control means that the H^+ reacted with olivine. As we know, the dissolution of silicates is generally sensitive to the acidity of the system. There is higher extent of dissolution of silicates at lower pH values. In order to further elucidate the mechanism of how the various factors affect the mineral carbonation behaviour, OLI Stream Analyzer was used to calculate the theoretical equilibrium pH values and the corresponding ionic strengths under the experimental conditions studied (0.6 L vessel volume and CO_2 gas as the target gas), as shown in Table 5.1. Data of No.1 – 5 show the effects of temperature. It was found that both pH values and ionic strength increased with temperature. Theoretically, the increased pH would detrimentally affect the dissolution of silicates. But as Figure 5.2 showed the increase in temperature (below 175 ℃) can significantly enhance the mineral carbonation efficiency. This may be because increased temperature markedly enhances the chemical reaction rate and the diffusion rate. Too high temperature resulted in a dramatic decrease in mineral carbonation efficiency which may be due to a decrease in the concentration of bicarbonate ions[146] at greater than 175 ℃. It is also noted that the ionic strength rose slightly with temperature and always remained above 1.89 mol/kg H_2O.

The effects of CO_2 partial pressure are shown in No. 6 – 8 and No. 4. It is seen that with increased CO_2 partial pressure, the pH values significantly decreased, which means that more CO_2 gas had been dissolved and more H^+ and HCO_3^- had been generated. Combined with Figure 5.6, the reason why the reaction associated with prediction No. 6 was controlled by product layer diffusion was that under low CO_2 partial pressure (lower than 20.7 bar, included), the generated carbonates layer was uniform and not very porous. Under these conditions, the reactive ions cannot easily pass through the uniform product layer and this resulted in the product layer diffusion control, as shown in Figure 5.11b. With the CO_2 partial pressure increasing, it became

easier to form polycrystalline carbonate products. As a result, the product layer became much looser and porous, which reduced the resistance for the reactive ions to pass through the product layer. Subsequently, the reactive H^+ can be provided more rapidly and easily access the surface of the olivine particles and the mineral carbonation efficiency increased substantially, as illustrated by changes between Figure 5.11b and Figure 5.11c.

Table 5.1 Theoretical equilibrium pH values and ionic strength calculated by OLI Stream Analyzer through autoclave calculation type.

No.	Conditions	pH	Ionic Strength mol/kg H_2O
1	120 ℃, PCO_2 = 34.5bar, 1 m $NaHCO_3$ + 1 m NaCl, 10% solids content	6.69	1.891
2	150 ℃, PCO_2 = 34.5bar, 1 m $NaHCO_3$ + 1 m NaCl, 10% solids content	6.89	1.893
3	175 ℃, PCO_2 = 34.5bar, 1 m $NaHCO_3$ + 1 m NaCl, 10% solids content	7.07	1.910
4	185 ℃, PCO_2 = 34.5bar, 1 m $NaHCO_3$ + 1 m NaCl, 10% solids content	7.14	1.911
5	200 ℃, PCO_2 = 34.5bar, 1 m $NaHCO_3$ + 1 m NaCl, 10% solids content	7.24	1.915
6	185 ℃, PCO_2 = 20.7bar, 1 m $NaHCO_3$ + 1 m NaCl, 10% solids content	7.34	1.919
7	185 ℃, PCO_2 = 27.6bar, 1 m $NaHCO_3$ + 1 m NaCl, 10% solids content	7.23	1.915
8	185 ℃, PCO_2 = 38.6bar, 1 m $NaHCO_3$ + 1 m NaCl, 10% solids content	7.09	1.910
9	185 ℃, PCO_2 = 34.5bar, 10% solids content	5.47	0.0144
10	185 ℃, PCO_2 = 34.5bar, 0.32 m $NaHCO_3$, 10% solids content	6.82	0.323
11	185 ℃, PCO_2 = 34.5bar, 0.64 m $NaHCO_3$, 10% solids content	7.06	0.640
12	185 ℃, PCO_2 = 34.5bar, 1 m $NaHCO_3$, 10% solids content	7.21	0.991
13	185 ℃, PCO_2 = 34.5bar, 2 m $NaHCO_3$, 10% solids content	7.41	1.812
14	185 ℃, PCO_2 = 34.5bar, 1 m NaCl, 10% solids content	5.71	1.029
15	185 ℃, PCO_2 = 34.5bar, 2 m NaCl, 10% solids content	5.73	1.953
16	185 ℃, PCO_2 = 34.5bar, 1 m $NaHCO_3$ + 1 m NaCl, 20% solids content	7.15	1.961
17	185 ℃, PCO_2 = 34.5bar, 1 m $NaHCO_3$ + 1 m NaCl, 30% solids content	7.16	2.029

The theoretical equilibrium pH value and the ionic strength were theoretically only 5.47 and 0.0144 mol/kg H_2O under the conditions of 185 ℃, PCO_2 = 34.5 bar, and 10% solids content without any additives, and the system was controlled by product layer diffusion, as illustrated in Figure 5.11a. Compared to prediction No. 4, the equilibrium pH value dramatically decreased but the efficiency was still much lower. With increase in concentration sodium salts (NaCl or

$NaHCO_3$), the pH values increased considerably but the efficiency was also markedly increased even though the increase in pH values could potentially decrease the dissolution of silicates[85]. It suggests that the significant change in carbonation efficiency may not be due to the change of pH value at the specific high PCO_2 but mainly owing to the increase in ionic strength. The addition of sodium salts can dramatically increase the ionic strength of the aqueous solution and decrease the activity of water, which can enhance the diffusion of aqueous H_4SiO_4[149] arising from the dissolution of Si-O through the product layer. Different from the addition of NaCl, in addition to the effect of ionic strength, the addition of $NaHCO_3$ may have roles as a buffer and a catalyst as well, since it can more significantly promote the carbonation efficiency, to transfer the H^+ and CO_3^{2-} to the surface of unreacted olivine for the dissolution of olivine and precipitation of carbonates respectively to complement the detrimental effect of increase of pH value on the dissolution of olivine.

In order to further verify the effects of the increased the ionic strength alone on the mineral carbonation, the systems with only NaCl addition were considered in predictions No. 14 – 15 and No. 9. It is clear that the pH would increase but not greatly when NaCl was added compared to the system without any additives. But the ionic strength dramatically increased, from only 0.0144 mol/kg H_2O to 1.029 mol/kg H_2O and up to 1.953 mol/kg H_2O for 1 m and 2 m NaCl addition respectively. It is noted that the ionic strength at only 0.32 m $NaHCO_3$ addition was 0.323 mol/kg H_2O and that the mineral carbonation was controlled by diffusion through a Si-rich layer as well. As a result, the mineral carbonation efficiency substantially increased, as shown in Figure 5.2. That is to say, the increase in the ionic strength had beneficial effects on the olivine carbonation. With increasing the ionic strength, the aqueous silica H_4SiO_4 became more unstable[149]. This can produce the stronger attractive force to induce the remaining silica (due to

the dissolution of Mg/Fe) to form the aqueous H_4SiO_4 and pass through the product layer. Subsequently, the Si-rich layer had been removed and only the outer loose carbonates layer remained. As a result, it became easier to get through the product layer. It is the reason why the Si-rich layer diffusion control had been overcome when the ionic strength was increased to high enough, which can be seen from the changes from Figure 5.11a – 5.11c. However, the effect of increase of ionic strength on the carbonation is limited. Although the addition of 2 m $NaHCO_3$ + 2 m NaCl did further decrease the aqueous silica concentration (shown in Figure 5.9a-5.9c), the carbonation efficiency only increased by 2% compared to of the case with 2 m $NaHCO_3$ alone. Once the barrier of the Si-rich layer has been removed, it is limited to considerably improve the efficiency only through increasing the ionic strength. It is also the same reason why there was quite similar mineral carbonation efficiency at 1 m $NaHCO_3$ addition no matter whether the NaCl was introduced or not. Thus, it is unnecessary to add sodium chloride any more once the concentration of sodium carbonate in the mineral carbonation system has been high enough.

Comparing predictions No. 16 and 17 to No. 4, there was no large difference in the pH values and the ionic strength. Thus, there is no obvious effect of solids content on the mineral carbonation efficiency either, neither enhancing the well-crystallized carbonates layer removal by attrition force between particles nor hindering the supply of the reactive H^+ ions.

Generally, the main chemical reactions during the mineral carbonation process are the following (iron atoms in olivine crystal structure have the same role as magnesium atoms):

$$4H^+ + Mg_2SiO_4 = 2Mg^{2+} + H_4SiO_{4(a)} \quad (5.1)$$

$$H_4SiO_{4(a)} = SiO_{2(s)} + 2H_2O_{(l)} \quad (5.2)$$

$$Mg^{2+} + CO_3^{2-} = MgCO_3 \quad (5.3)$$

$$HCO_3^- = H^+ + CO_3^{2-} \quad (5.4)$$

$$H_2CO_{3(a)} = H^+ + HCO_3^- \quad (5.5)$$

$$CO_{2(a)} + H_2O_{(l)} = H_2CO_{3(a)} \quad (5.6)$$

$$CO_{2(g)} = CO_{2(a)} \quad (5.7)$$

Where, reaction (5.1) is the key to the chemical reaction control. It can be promoted by the increase of the H^+ concentration or the decrease of concentration of the Mg^{2+} and $H_4SiO_{4(a)}$. The aqueous $H_4SiO_{4(a)}$ is not stable and will decompose into amorphous silica, shown as reaction (5.2). If the $H_4SiO_{4(a)}$ decomposes into amorphous silica before it diffuses into the aqueous solution, the amorphous silica will accumulate on the product layer and form the Si-rich product layer (Figure 5.8), which hinders the H^+ from reaching the surface of the unreacted olivine core as shown by the results of mineral carbonation with sodium additives below 0.32 m (included). Once there is sufficient concentration of sodium salts in the aqueous solution, the $H_4SiO_{4(a)}$ can more rapidly diffuse into the high ionic strength solution, followed by decomposition into amorphous silica in the aqueous matrix, separate from the reacting particle.

Reaction (5.3) can decrease the Mg^{2+} concentration further and help drive reaction (5.1) to the right. Sufficient supply of CO_3^{2-} ensures the rapid precipitation of $MgCO_3$ as well as the good growth of its crystals as indicated on the polycrystalline carbonates in Figure 5.3. The supply of CO_3^{2-} is mainly from the reaction (5.4) and (5.5), from the decomposition of HCO_3^- and carbonic acid, after a series of chemical reactions (5.6) and the dissolution of CO_2 gas (5.7). However, if the CO_3^{2-} is not supplied fast enough, the formation of polycrystalline carbonates will be limited. By contrast, a uniform and poorly porous carbonates layer will be formed as shown in Figure 5.7

when the PCO_2 was below 21 bar, which also prevented the H^+ and Mg^{2+} from diffusing to their targets.

Once the supply of CO_3^{2-} or HCO_3^- is fast enough and the ionic strength is high enough, the dissolution of olivine (reaction (5.1)) controls the mineral carbonation process. The key is the sufficient supply of H^+. It can be dramatically enhanced by the addition of HCO_3^- and the increase of PCO_2 through reaction (5.4) and (5.5) respectively in addition to providing adequate CO_3^{2-}.

Based on the preceding discussion, the addition of $NaHCO_3$ can not only enhance the supply of CO_3^{2-}, but also provide H^+ through the forward and reverse of reaction (5.4) as well as increase the aqueous ionic strength. It is because of this that the addition of NaCl into the system had the limited effect on the mineral carbonation efficiency once there was enough addition of $NaHCO_3$. The effect of the addition of $NaHCO_3$ was greater than any effect of further addition of NaCl.

Therefore, the effects of NaCl on mineral carbonation can be neglected once there is ≥ 0.5 m $NaHCO_3$ concentration during the following analysis of quantifying the factors affecting the kinetics. When there is no $NaHCO_3$, the effect of NaCl on mineral carbonation is needed to be considered independently.

5.3 Quantification of kinetics on effects of factors

Since the mechanism and the fundamental variation of kinetics of mineral carbonation of olivine have been reported above, it is still necessary for the successful application of the mineral carbonation to quantify the kinetic effects of the important factors. This objective of the work is to develop a quantitative kinetic formula as shown in Formula (5.1). The quantified formula can be theoretically used to predict the mineral carbonation efficiency under specific conditions,

including particle size (R) of raw materials, temperature (T), CO_2 partial pressure (PCO_2), addition of additives (x_1, x_2, ..., x_n), solids content (w), agitation rate of the system (rpm), and reaction time (t).

$$\alpha = F(R, T, P_{CO2}, x_1, x_2, \cdots, x_n, w, rpm, t) \quad (5.1)$$

The choice of a kinetic model is crucial. As indicated above, the classical shrinking core model (SCM) with constant size of particles is a potentially reasonable choice[144,145,147,150–152].

A kinetic formula can provide significant support for the industrial application and the further development of mineral carbonation technology. This work mainly focused on the mineral carbonation process where the rate was controlled by the chemical reaction as discussed above. The data from Figure 5.6 for quantifying the factors affecting the kinetics are shown in Table 5.2. In fact, the key to developing the kinetic formula is to discover the relationship between the constant k_2 and the factors. As the rotation speed and the solids content had very limited effects on the mineral carbonation, the factors that were taken into consideration were only specific surface area, temperature, CO_2 partial pressure, and concentration of sodium bicarbonate and sodium chloride.

It is more effective to use the specific surface area rather than particle size because it is the specific surface area that provides the basis for the chemical reaction between the effective protons and the unreacted olivine. The specific surface area is not only related to the size of particles but also the shape and the surface defects of the particles. The classical way to analyze the specific surface area is by the BET (Brunauer, Emmett and Teller) method. The differences in the results from the BET method and the laser particle size analysis using Malvern Mastersizer, are shown in Table 5.3.

Table 5.2 The data for quantifying the factors affecting the kinetics.

Factors		Kinetic control type					
		Mass transport		Chemical reaction		Product layer diffusion	
		k_1	R^2	k_2	R^2	k_3	R^2
Specific surface area, m^2/g	1.53	12.576	0.994	0.0524	0.998	0.00962	0.869
	0.27	4.192	0.983	0.0165	0.975	0.00238	0.794
	0.12	2.299	0.987	0.00829	0.982	0.000610	0.899
	0.08	1.881	0.987	0.00669	0.989	0.000407	0.855
Temperature, ℃	120	3.581	0.990	0.0115	0.986	0.000543	0.803
	135	6.288	0.990	0.0212	0.981	0.00179	0.805
	150	9.043	0.996	0.0318	0.989	0.00385	0.835
	165	14.971	0.993	0.0594	0.994	0.0121	0.865
	175	15.754	0.974	0.0665	0.997	0.0159	0.926
CO_2 partial pressure, bar	21	7.654	0.912	0.0286	0.942	0.00293	0.980
	28	10.035	0.971	0.0393	0.990	0.00550	0.934
	32	12.579	0.948	0.0518	0.986	0.00913	0.952
	34	12.576	0.994	0.0524	0.998	0.00962	0.869
	39	14.497	0.933	0.0625	0.983	0.0128	0.956
	41	17.129	0.945	0.0798	0.994	0.0198	0.945
$NaHCO_3$, m	0	3.212	0.732	0.0112	0.752	0.000459	0.982
	0.32	4.298	0.812	0.0152	0.836	0.000848	0.982
	0.50	7.622	0.994	0.0286	0.997	0.00307	0.877
	0.64	9.363	0.965	0.0362	0.980	0.00476	0.902
	0.80	11.940	0.974	0.0487	0.995	0.00822	0.932
	1.0	12.764	0.983	0.0532	0.998	0.00975	0.914
	1.5	15.887	0.943	0.0712	0.991	0.0162	0.949
NaCl, m	0	3.212	0.732	0.0112	0.752	0.000459	0.982
	0.50	4.456	0.963	0.0158	0.974	0.000945	0.946
	0.80	5.712	0.962	0.0207	0.975	0.00161	0.919
	1.0	5.882	0.972	0.0214	0.984	0.00171	0.927
	1.5	6.539	0.972	0.0240	0.985	0.00215	0.916
	2.0	7.015	0.988	0.0261	0.991	0.00247	0.858

The specific surface area by the BET method was less than 3.0 times greater than that from Malvern Mastersizer. The results from the BET method were generally higher because the BET method analyzed all surfaces including porous structures through adsorption while the Malvern Mastersizer data was used to calculate the area using the assumption of spherical particles through diffraction. The results from the laser particle size analysis were not less than 1/3 of the

areas by the BET method. There were also repeatable to within ±2% relative error. In addition, the laser particle size analysis has the advantage of convenience and speed and thus is more suitable for application on materials which are less porous (e.g. peridotite). Therefore, the calculated specific surface area based on the laser particle size analysis by using Malvern Mastersizer was used to develop the kinetic formula.

Table 5.3 Comparison of specific surface area of particle size fractions of the high-grade olivine by the laser particle size analysis by the Malvern Mastersizer with the BET analysis.

Narrow particles, um	-25	25 – 38	38 – 53	53 – 75
BET method	4.32	0.32	0.29	0.24
Laser particle size analysis method	1.53	0.27	0.12	0.08
Ratio of BET-to-laser method	2.82	1.19	2.42	3.00

According to the Arrhenius Equation (equation 5.5), the rate constant *k* in the kinetic model is directly related to the pre-exponential factor A, the activation energy Ea and temperature. The discussion around Figure 5.5 showed that the mineral carbonation process was controlled by chemical reaction under most conditions and the corresponding activation energy is 48.0 kJ/mol. Furthermore, according to equation 5.5, the lnk was linear with lnA (the other important factors) at the specific temperature. The logarithmic values of the constant k_2 listed in Table 5.2 were fitted with the logarithmic value of the specific factors, shown in Figure 5.12a – 5.12d. It is clear that the data fit linearly for all the factors. This confirms that the effects of the important factors were independent of each other.

According to Figure 5.12, the order of effects of specific surface area, CO_2 partial pressure and addition of sodium bicarbonate was 0.7, 1.6 and 0.8 also with a relative error ±2.6%, ±4.5% and ±3.5% respectively. The predominant factor was CO_2 partial pressure, approximately twice the order of the effects of the other mainly influential factors. As a result, Formula (5.2) can be

developed. Formula (5.3) can be derived by combining equation (5.2) with formula (5.2). Formula (5.3) can be further transformed into Formula (5.4), which shows the calculation of mineral carbonation efficiency under the specific conditions.

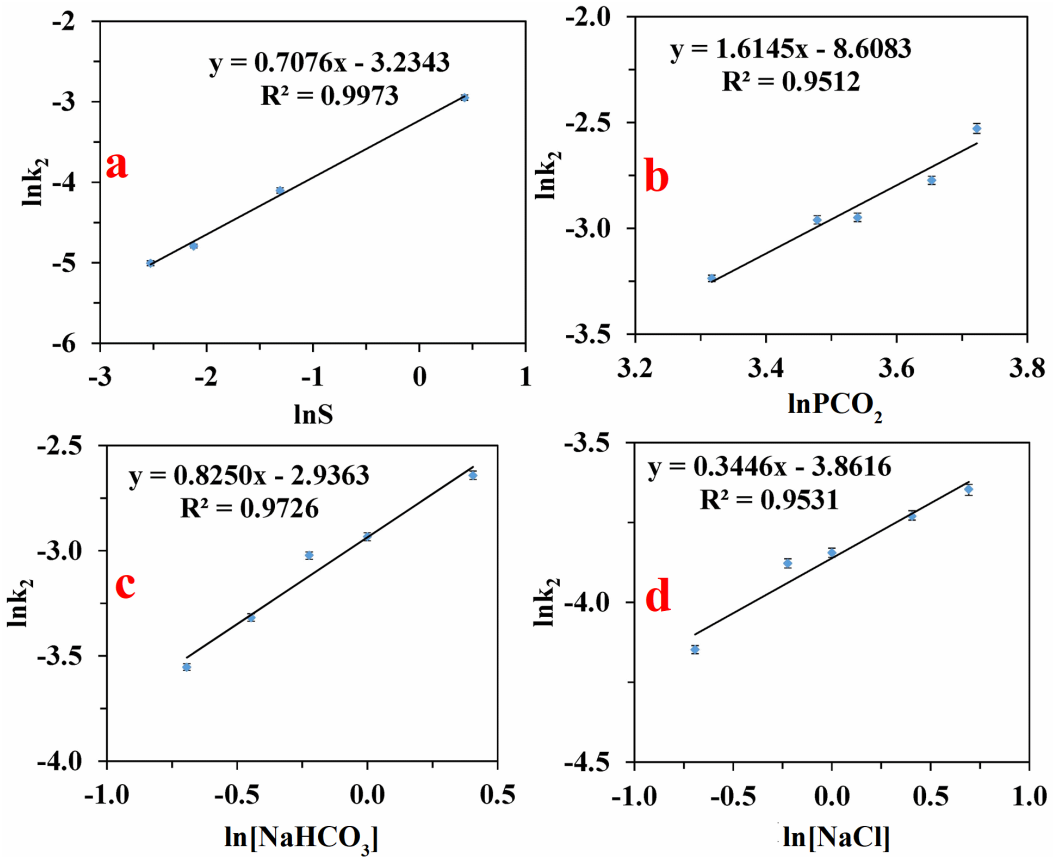

Figure 5.12 Effects of factors on the chemical reaction control rate constant: (a) specific surface area of narrow-sized particle fractions; (b) CO_2 partial pressure; (c) concentration of sodium bicarbonate and (d) concentration of sodium chloride.

$$k_2 = k^o \times [S]^{0.7} \times [P_{CO2}]^{1.6} \times [NaHCO_3]^{0.8} \times e^{(-Ea \times 1000/RT)} \quad (5.2)$$

$$1 - (1 - \alpha)^{1/3} = k^o \times [S]^{0.7} \times [P_{CO2}]^{1.6} \times [NaHCO_3]^{0.8} \times e^{(-Ea \times 1000/RT)} \times t \quad (5.3)$$

$$\alpha = (1 - (1 - k^o \times [S]^{0.7} \times [P_{CO2}]^{1.6} \times [NaHCO_3]^{0.8} \times e^{(-Ea \times 1000/RT)} \times t)^3) \times 100\% \quad (5.4)$$

Where, α is mineral carbonation efficiency, %; S is specific surface area of particles, m^2/g; PCO_2 is CO_2 partial pressure, bar; $NaHCO_3$ is the concentration of sodium bicarbonate in the mineral

carbonation system, molality; Ea is the activation energy of the mineral carbonation of particles, 48.0 kJ/mol; R is the gas constant, 8.314 J/(mol·K); T is the system temperature, K; t is the reaction time, h; k^o is the kinetic factor.

For all the particle size fractions, the kinetic factor k^o will be 72 when the temperature was up to 175 ℃ and 41 when the temperature was 185 ℃, as shown in Formula (5.5) and (5.6) respectively. The different values of the kinetic factor k^o up to 175 ℃ and at 185 ℃ are because the mineral carbonation efficiency decreased at 185 ℃ or higher. The Ea is $48.0 \times (1 \pm 2.5\%)$ kJ/mol due to the relative error bar the above calculation.

$$\alpha = (1 - (1 - 72 \times [S]^{0.7} \times [P_{CO2}]^{1.6} \times [NaHCO_3]^{0.8} \times e^{(-47970/RT)} \times t)^3) \times 100\% \quad (5.5)$$

$$\alpha = (1 - (1 - 41 \times [S]^{0.7} \times [P_{CO2}]^{1.6} \times [NaHCO_3]^{0.8} \times e^{(-47970/RT)} \times t)^3) \times 100\% \quad (5.6)$$

According to Formula (5.5) and (5.6), the predicted data under all conditions are shown in Figure 5.13a – 5.13f under conditions where surface chemical reaction controls mineral carbonation. The predicted data are comparable to the kinetic data acquired from the tests. The deviation is a maximum of only ±5%, which is very close to the range of the precision of carbonation efficiency for the tests, 4%. Therefore, it is suitable for Formula (5.4) to predict the extent of carbonation under specific conditions.

As to the mineral carbonation without $NaHCO_3$ but NaCl alone instead, Formula (5.7) was developed for the mineral carbonation efficiency. The rate constant is proportional to the concentration of sodium chloride to the 0.34 power with a relative error ±5.1% between predicted and experimental results.

$$\alpha = (1 - (1 - k^o \times [S]^{0.7} \times [P_{CO2}]^{1.6} \times [NaCl]^{0.34} \times e^{(-47970/RT)} \times t)^3) \times 100\% \quad (5.7)$$

The kinetic factor k^o is 15 at 185 ℃, around half of the values of k^o when $NaHCO_3$ was added. According to Formula (5.7), the mineral carbonation efficiency can be predicted to within a 2% deviation as shown in Figure 5.13a so long as the process is controlled by reaction (5.1).

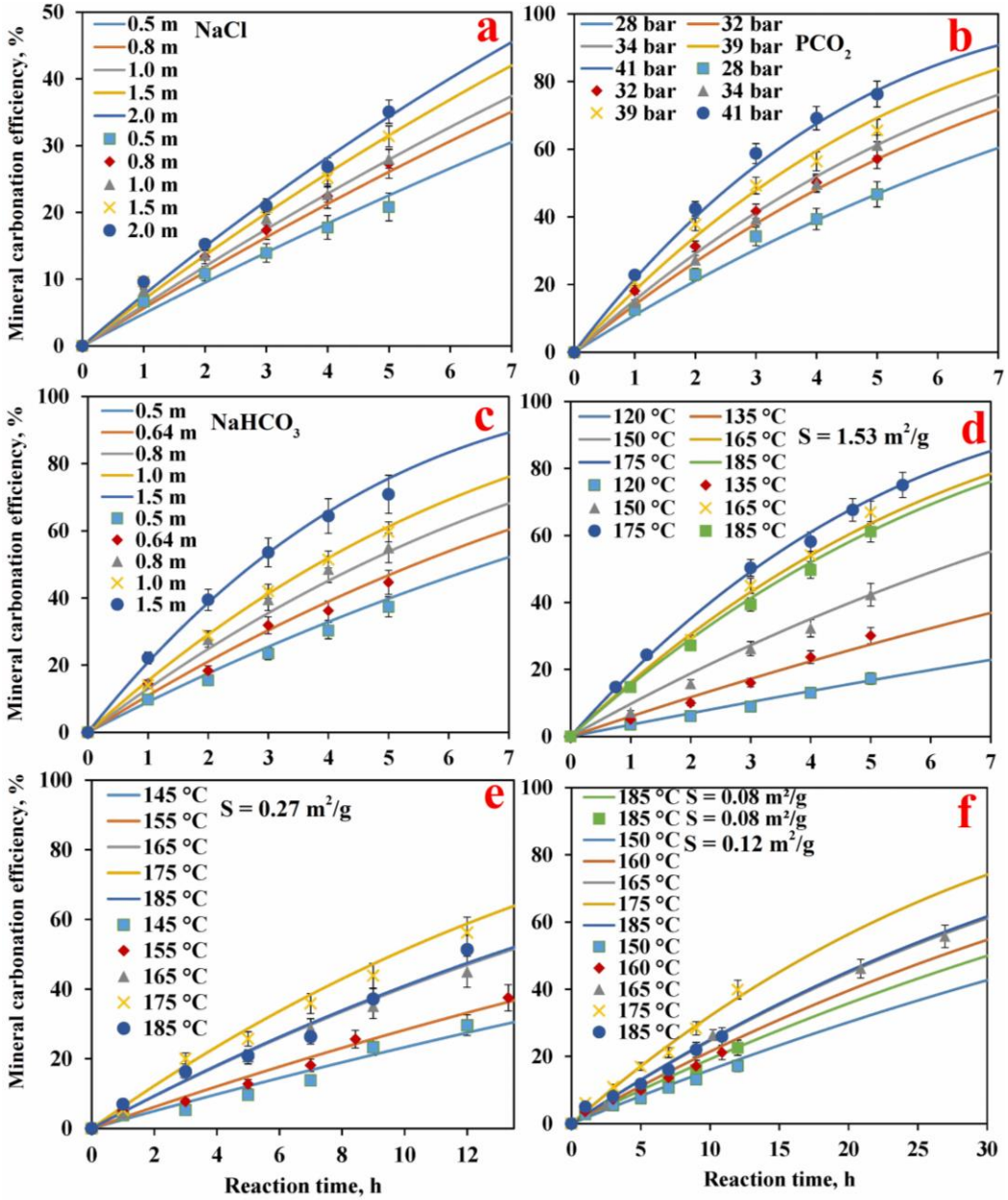

Figure 5.13 Prediction of mineral carbonation efficiency according to the developed formulas and experimental results under conditions of -25 μm particles, 185 ℃, PCO_2 = 34 bar 1 m $NaHCO_3$ or 1 m NaCl: (a) for effects of NaCl; (c) for effects of $NaHCO_3$; (d) for system temperature with -25 μm particles; (e) for system temperature with 25 – 38 μm particles; (f) for temperature with 38 – 53 μm particles and for 53 – 75 μm particles with 185 ℃. (The solid lines are the predicted curves and the marks represent experimental data from the tests.)

5.4 Verification of the quantitative kinetic formula

As discussed above, the developed quantitative kinetic formula (Formula 5.4) can be used to predict the mineral carbonation efficiency according to the listed conditions.

It can be also used to calculate the time needed to reach the acceptable mineral carbonation efficiency under the specific conditions, as shown in Formula 5.8. For example, to achieve 80% of the efficiency of the mineral carbonation for the particles with 1.53 m^2/g specific surface area under PCO_2 = 41 bar, at 175 ℃ and with 1.5 m concentration of sodium bicarbonate, according to Formula 5.8, the required reaction time can be calculated,

$$t \geq (1-(1-\alpha)^{1/3})/(k^o \times [S]^{0.7} \times [P_{CO2}]^{1.6} \times [NaHCO_3]^{0.8} \times e^{(-Ea \times 1000/RT)}) \quad (5.8)$$

The experiments showed that the actual time needed for reaction was 4.29 hours, as shown in Figure 5.14a. The predicted data matched very well.

In addition, the formula can also predict the minimum requirement of a specific factor for acceptable mineral carbonation efficiency. For example, Formula 5.4 can be rearranged into Formula 5.9 to predict the requirement of sodium bicarbonate addition. For the particles with 1.53 m^2/g specific surface area, a mineral carbonation efficiency of 80% under PCO_2 = 41 bar, at 175 ℃ for 5.5 hours, then at least 1.1 m sodium bicarbonate addition is required.

$$[NaHCO_3] \geq ((1-(1-\alpha)^{1/3})/(k^o \times [S]^{0.7} \times [P_{CO2}]^{1.6} \times e^{(-Ea \times 1000/RT)} \times t))^{1/0.8} \quad (5.9)$$

The experimental data shown in Figure 5.14b were well matched with the predicted curve through Formula 5.9.

The same approach may be used to calculate the requirement of the other factors to reach a specific efficiency under the specific conditions for a specific reaction time.

It is known that the requirements for the specific surface area and the CO_2 partial pressure are the major costs for the application of mineral carbonation for CO_2 sequestration. However, it is difficult to reveal the relationship between the requirements of the minimum specific surface area and CO_2 partial pressure. Fortunately, the quantification Formula 5.4 can also be transformed into Formula 5.10 to present the relationship between the required minimum specific surface area and CO_2 partial pressure for specific mineral carbonation efficiency requirement under specified conditions, as long as the mineral carbonation rate is controlled by the chemical reaction.

$$[P_{CO2}] = ((1-(1-\alpha)^{1/3})/(k^o \times [S]^{0.7} \times [NaHCO_3]^{0.8} \times e^{(-Ea\times 1000/RT)} \times t))^{1/1.6} \quad (5.10)$$

For any material with a known specific surface area, the minimum specific surface area requirement can be calculated once the other conditions are set as well. According to Formula 5.10, for instance, for the above dunite, the specific surface area is 1.53 m^2/g, with 80% mineral carbonation efficiency in 5 hours under the conditions of 175 ℃ and 1.5 m concentration of sodium bicarbonate, at least 31 bar of CO_2 partial pressure is needed. The predicted value matched experimental data under the conditions of 31 bar PCO_2, 175 ℃, 1.5 m sodium bicarbonate and 1.53 m^2/g specific surface area well, as shown in Figure 5.14c.

Figure 5.14d shows the relationship more clearly between the required PCO_2 and the specific surface area under the conditions of 175 ℃, 1.5 m concentration of $NaHCO_3$ and 5 hours reaction time. It is assumed that the activation energy Ea and the kinetic factor k^o remain at 48.0 kJ/mol and 72 respectively, even though they might need to be corrected slightly. The kinetic model has also been verified by data for the samples with S = 0.635, 0.655, 0.941 and 1.53 m^2/g under the PCO_2=29, 34, 33, 38 and 31 bar to achieve 50%, 60%, 70% and 80% mineral

carbonation efficiency, respectively. The predicted values matched with the experimental data well in the range of 1.6 bar for PCO_2 and 0.08 m^2/g for specific surface area. Formula 5.4 and Figure 5.14d can be used to support the application of mineral carbonation for CO_2 sequestration.

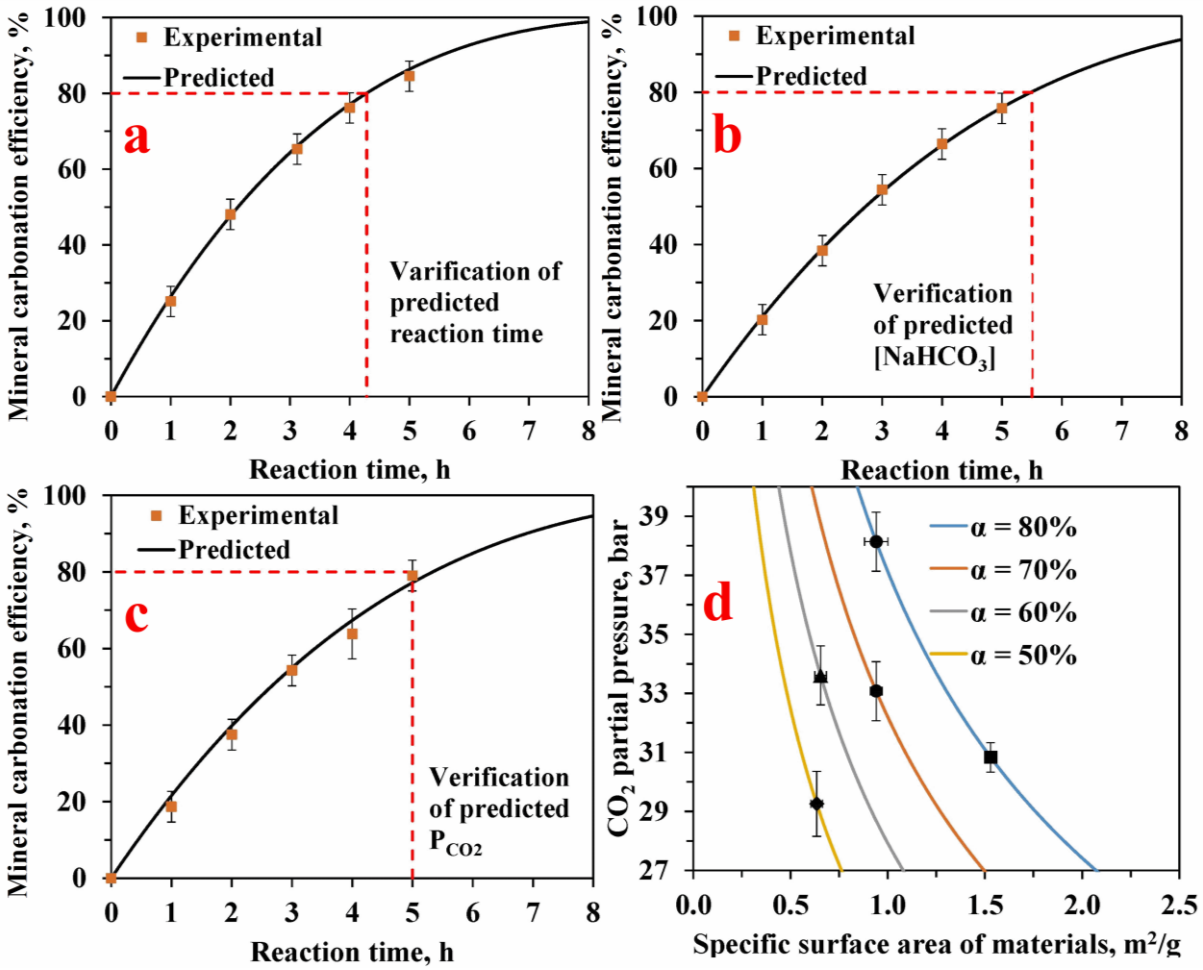

Figure 5.14 Application of quantitative kinetic model: (a) verification of predicted reaction time under the conditions of 1.53 m^2/g of specific surface area, PCO_2 = 41 bar, 175 ℃ and 1.5 m sodium bicarbonate; (b) verification of predicted sodium bicarbonate under the conditions of 1.53 m^2/g of specific surface area, PCO_2 = 41 bar, 175 ℃ and 1.1 m sodium bicarbonate; (c) verification of predicted CO_2 partial pressure under the conditions of 1.53 m^2/g of specific surface area, PCO_2 = 31 bar, 175 ℃ and 1.5 m sodium bicarbonate; (d) relationship between specific surface area of materials and the required minimum CO_2 partial pressure to reach the specific mineral carbonation efficiency under the conditions of 175 ℃, 1.5 m $NaHCO_3$ for 5 hours (assumed that the activation energy and kinetic factor k^o remained 48.0 kJ/mol and 72 respectively) where the shapes ♦, ▲, ● and ■ represented the experimental data for the samples with 0.635, 0.655, 0.941 and 1.53 m^2/g specific surface area respectively.

To this point, Formula 5.4 was only developed from the high grade olivine under the chemical reaction control. It can provide the suitable guidelines for the application of mineral carbonation technology. In principle, the developed Formula 5.4 can be also used for any materials where the olivine is the major mineral. However, this must be confirmed by investigating other sources of olivine for comparison. The k^o value may need to be re-determined through pre-tests because it is related to the capacity of CO_2 sequestration of the materials used and other factors.

5.5 Conclusions

In this chapter, the thorough kinetic research has been carried out on the effects of various factors on the mineral carbonation of olivine for CO_2 sequestration. The mechanisms and kinetics of the mineral carbonation have been elucidated and can be varied under conditions dependent on CO_2 partial pressure and aqueous ionic strength:

With low concentration of sodium salts, the mineral carbonation process was controlled by diffusion through a Si-rich layer. The preferential dissolution of Mg resulted in the formation of this Si-rich layer where Si-O remained as an incomplete silicate structure. The Si-rich layer inhibited the diffusion of reactive H^+ from the aqueous bulk solution to the surface of the unreacted olivine core. Increasing the concentrations of sodium salts can help the diffusion of aqueous H_4SiO_4 from the dissolution of Si-O, followed by decomposition to amorphous silica in the bulk solution. But the process may be still controlled by diffusion through a uniform carbonates under low PCO_2 due to the limited supply of reactive H^+ and CO_3^{2-} ions to continuously attack the olivine structure and for formation of polycrystalline carbonates. The formed uniform and poorly porous carbonate layer hindered the further dissolution of olivine.

With high concentration of sodium salts and high CO_2 partial pressure, the mineral carbonation process was always controlled by the chemical reaction between H^+ and unreacted olivine. Whereas Mg and Fe were preferentially dissolved out from the olivine structure, the Si was also dissolved to form metastable aqueous H_4SiO_4. All new formed carbonates reported to the outer halo of loosely clustered but well-crystallized carbonates. As a result, the reactive H^+ can easily reach the surface of the unreacted olivine core. When the mineral carbonation process was controlled by chemical reaction, the decrease of particle size, increase of temperature, bicarbonate ion concentration and ionic strength can significantly enhance the mineral carbonation efficiency by accelerating chemical reaction rate. The functions of $NaHCO_3$ introduced to the mineral carbonation process can help not only by continuously delivering sufficient dissociated H^+ and CO_3^{2-} from CO_2 gas but also by increasing the ionic strength, which enhanced the dissolution of Mg and Fe and the precipitation of bivalent metal carbonates and the diffusion of metastable aqueous silica respectively.

Furthermore, the effects of the factors (CO_2 partial pressure, specific surface area, concentration of sodium bicarbonate and temperature) on the reaction kinetics were found to be independent of each other and the chemical reaction controlled rate was linearly related to each. The most influential factor was CO_2 partial pressure to the 1.6 power with a relative error ±4.5%. The specific surface area of the particles and addition of sodium bicarbonate showed similar effects, with the 0.7 and 0.8 power with the relative error ±2.6% and ±3.5% respectively. The kinetic formula was finally developed as Formula 5.4. The suitable ranges of PCO_2, temperature and addition of $NaHCO_3$ are 28 bar – 41 bar, 100 ℃ – 175 ℃ and 0.5 m – 1.5 m, respectively. The kinetic factor is related to the mineral carbonation capability of the materials. The developed formula can be applied to predict the mineral carbonation efficiency under specified conditions

and also to calculate the necessary requirements of specific factors. The formula can also show the relationship between the required specific surface area of the material and the minimum CO_2 partial pressure. In principle it can be used for materials where the majority of constituents are olivine; it will be necessary to carry out several pre-tests to calibrate the value of the kinetic factor.

6 Application of quantitative kinetic formula on general samples

A kinetic formula based on the high-grade olivine under the chemical reaction control during carbonation has been developed (Chapter 5). It can predict the carbonation efficiency and could be helpful for the application in industries. However, the commercial ores are usually not high-grade olivine, but may also contain serpentine, pyroxene and other minerals. O'Connor et al.[71,72,83] has reported that the carbonation of serpentine has a slower rate and needs a heat pre-treatment, compared to the olivine carbonation under the same conditions. The presence of the serpentine and pyroxene may affect the successful application of the carbonation formula. Therefore, this Chapter describes the application of the kinetic formula to typical silicate materials and reveals the effects of mineral compositions on the carbonation rate.

6.1 Application of formula on Turnagain sample SN254

The Turnagain sample SN254 which has the lowest sulfur content among the samples received was ground by a rod mill and screened to provide particle size fractions: -25 μm; 25 – 38 μm; 38 – 45 μm; 45 – 53 μm; and 53 – 75 μm. The particle size distributions are shown in Figure 6.1. The corresponding calculated specific surface area is 1.171, 0.178, 0.125, 0.117 and 0.094 m^2/g, respectively, as determined using the Malvern Mastersizer 2000 Instrument. The narrow-sized particles were used for the mineral carbonation tests under the conditions of CO_2 partial pressure PCO_2 = 41 bar, 175 ℃, 10% solids content and with 1.5 m $NaHCO_3$. The results and the comparison with the prediction based on the formula are shown in Figure 6.2a. It is clear that all the experimental results for all the particle size fractions and the predicted data were matched well for the reaction times of 12 hours, 8 hours or 5 hours. It is also noted that the kinetic factor k^o needed to be adjusted to 60 which equals 72 ×olivine content (83.5%) and the activation

energy was in the range of 48.0(1±3.8%) for Turnagain sample SN254. The corresponding XRD images of the carbonated Turnagain SN254 particle size fractions are shown in Figure 6.3. Magnesite was clearly present, which is the desired product of the mineral carbonation process. The peaks of the olivine in the Turnagain SN254 sample were considerably less intense than the initial sample while there was no obvious change in the peaks for serpentine. The peaks for serpentine after the carbonation of the 25 – 38 μm sample were less intense than for the other particle size fractions. This may be due to the long reaction time used to obtain this sample. It is also noticed that there were no peaks for the silica in the XRD images. This is because the silica was in an amorphous form.

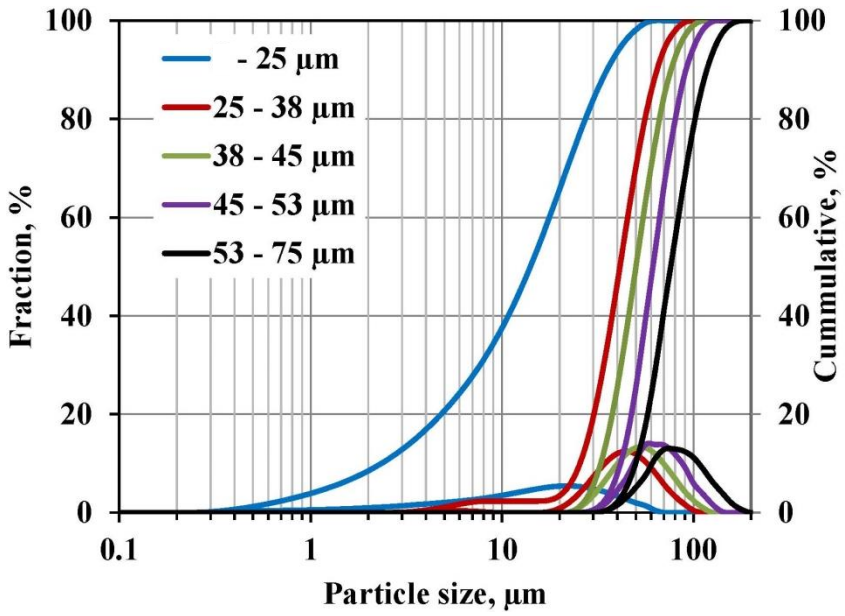

Figure 6.1 Particle size distributions of narrow-sized particle fractions of the typical Turnagain sample SN254.

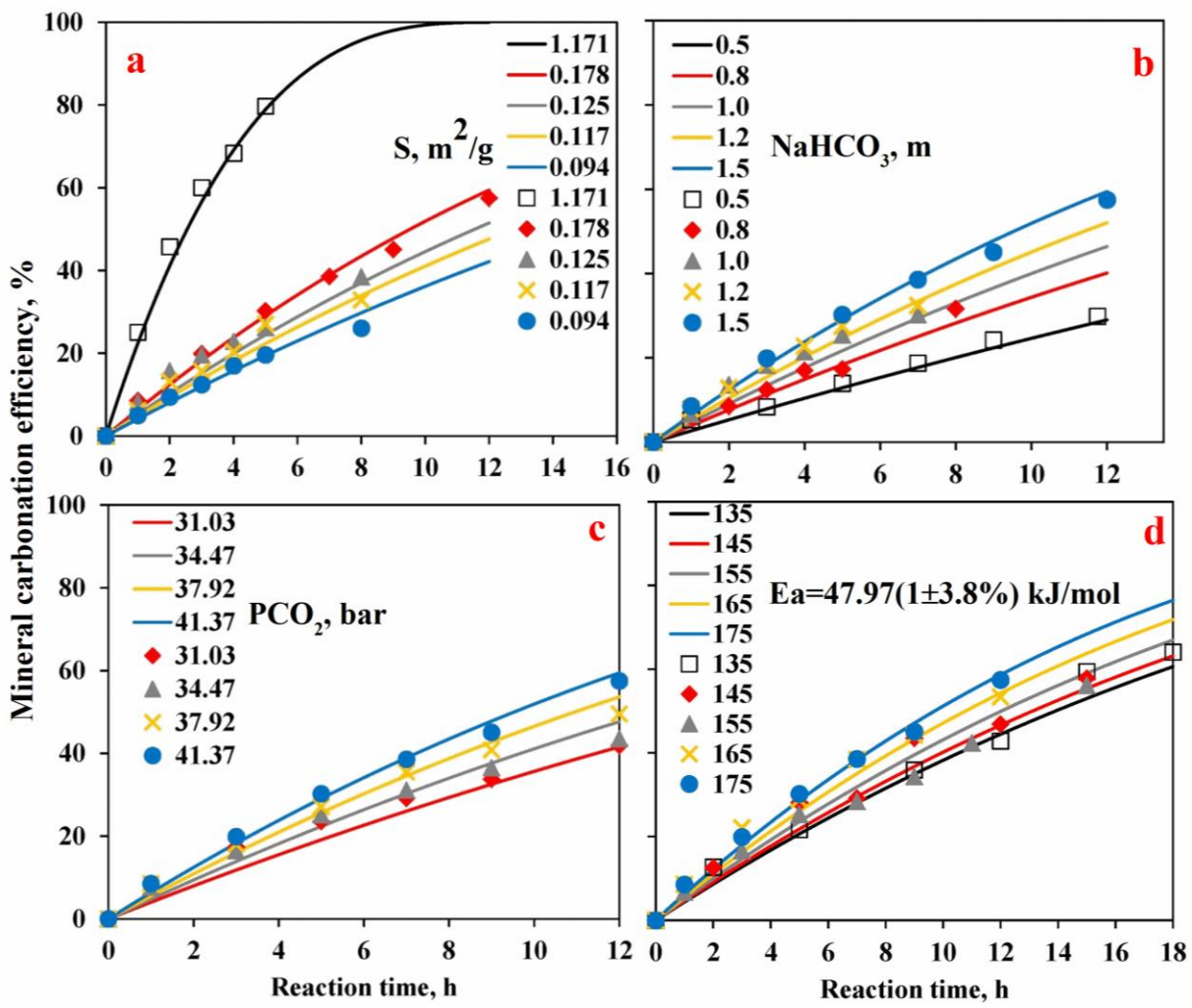

Figure 6.2 Comparison of the experimental data and the predicted data from the kinetic formula under the conditions of 25 – 38 μm particle size fractions, PCO_2 = 41.4 bar, 175 ℃, 10% solids content with 1.5 m $NaHCO_3$: (a) for effects of specific surface area; (b) for effects of addition of $NaHCO_3$; (c) for effects of PCO_2; (d) for effects of temperature. The k_0 is 60 for the typical Turnagain sample SN254.

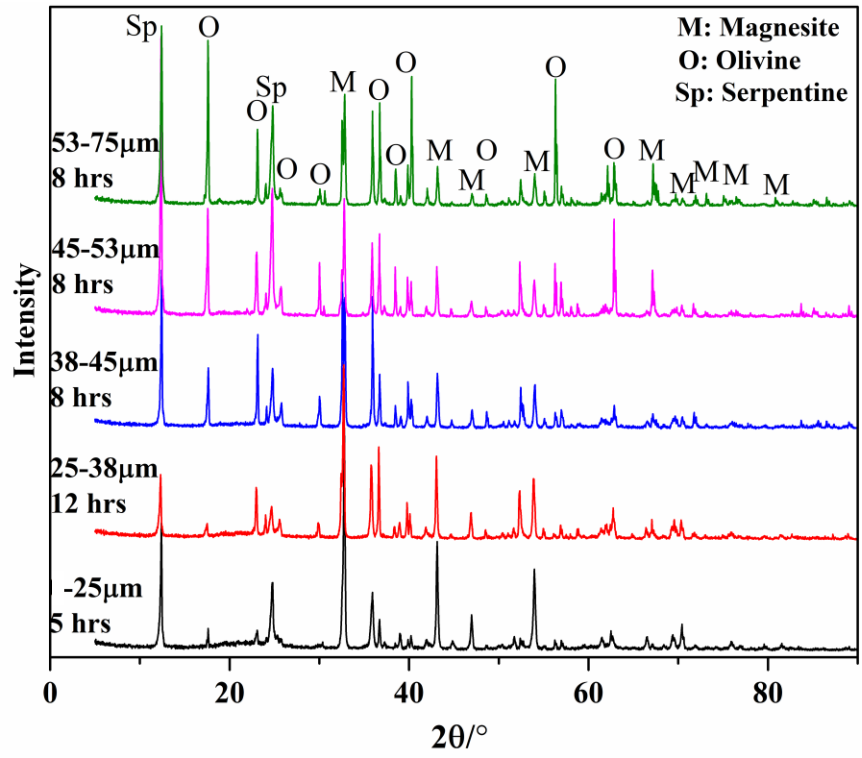

Figure 6.3 XRD images of carbonated Turnagain sample SN254.

The effects of sodium bicarbonate concentration on the mineral carbonation under the conditions of 25 – 38 μm particle size fractions, PCO_2 = 41 bar, 175 ℃ and 10% solids content are shown in Figure 6.2b. In order to make sure the carbonation rate was controlled by chemical reaction, the range of the sodium bicarbonate concentration was from 0.5 m to 1.5 m. It is obvious that the agreement between experimental results and the kinetic formula prediction was good on this Turnagain sample SN254. Similar good matches between the experimental and predicted data were also observed for varying CO_2 partial pressure (Figure 6.2c) and varying temperature (Figure 6.2d). The PCO_2 ranged from 31 bar to 41 bar so that the mineral carbonation process was controlled by the dissolution of olivine rather than by the diffusion through a product layer. The temperature effect was tested under the conditions of PCO_2=41 bar and with 1.5 m $NaHCO_3$, where the carbonation process was still controlled by chemical reaction. Again, the experimental

data and the kinetic formula prediction were very close, though the relative error for the activation energy was also ±3.8% which was determined in the previous research (Chapter 5). As the preceding research shows that temperature, PCO_2, particle size and sodium bicarbonate are the most important factors to affect the mineral carbonation process. Thus far, the Figure 6.2 has proved that the quantified formula can be successfully applied in the carbonation of the Turnagain sample SN254.

However, the model has only been verified on the narrow-sized particle fractions. It would be impractical to use the narrow-sized particles for a metal recovery process in industry. In practical application, the requirement for particle size distribution usually is characterized by the P_{80}, such as P_{80}=75 μm or P_{80}=90 μm. Herein, the full-size range particles were further tested for matching of the formula to experiments under the conditions of PCO_2 = 41.37 bar, 175 ℃, 10% solids content with 1.5 m $NaHCO_3$, as shown in Figure 6.4a. The particle size distribution for the full-sized particles is shown in Figure 6.5. The P_{80} for the four sets of sample was 41 μm, 46 μm, 56 μm and 93 μm with the corresponding specific surface area of 0.93, 0.89, 0.84 and 0.62 m^2/g, respectively. During the tests, a sampling process was controlled by a needle valve. It is interesting that the experimental data for the fine particles, P_{80}=41 μm and 46 μm, and the kinetic formula prediction matched well while the agreement was poor for the coarse particles with P_{80}=56 μm and even worse for the coarsest particles with P_{80}=93 μm, as shown in Figure 6.4a1. The results for the coarse particles suggested the possibility that the process was controlled by diffusion through a product layer. It turns out to be a defect of the sampling method. Evidently, the narrowest sections of the flow path through the needle valve blocked passage of the larger particles. After repeated sampling the particle size distribution was altered, biasing it for larger particles. This would have slowed the reaction. Once the needle valve was replaced with a ball

valve (Figure 6.4b), the problem was corrected. Again, the kinetic model prediction fit well to the experimental data as shown in Figure 6.4b1. All the tests with full-size particle samples were sampled through ball valve.

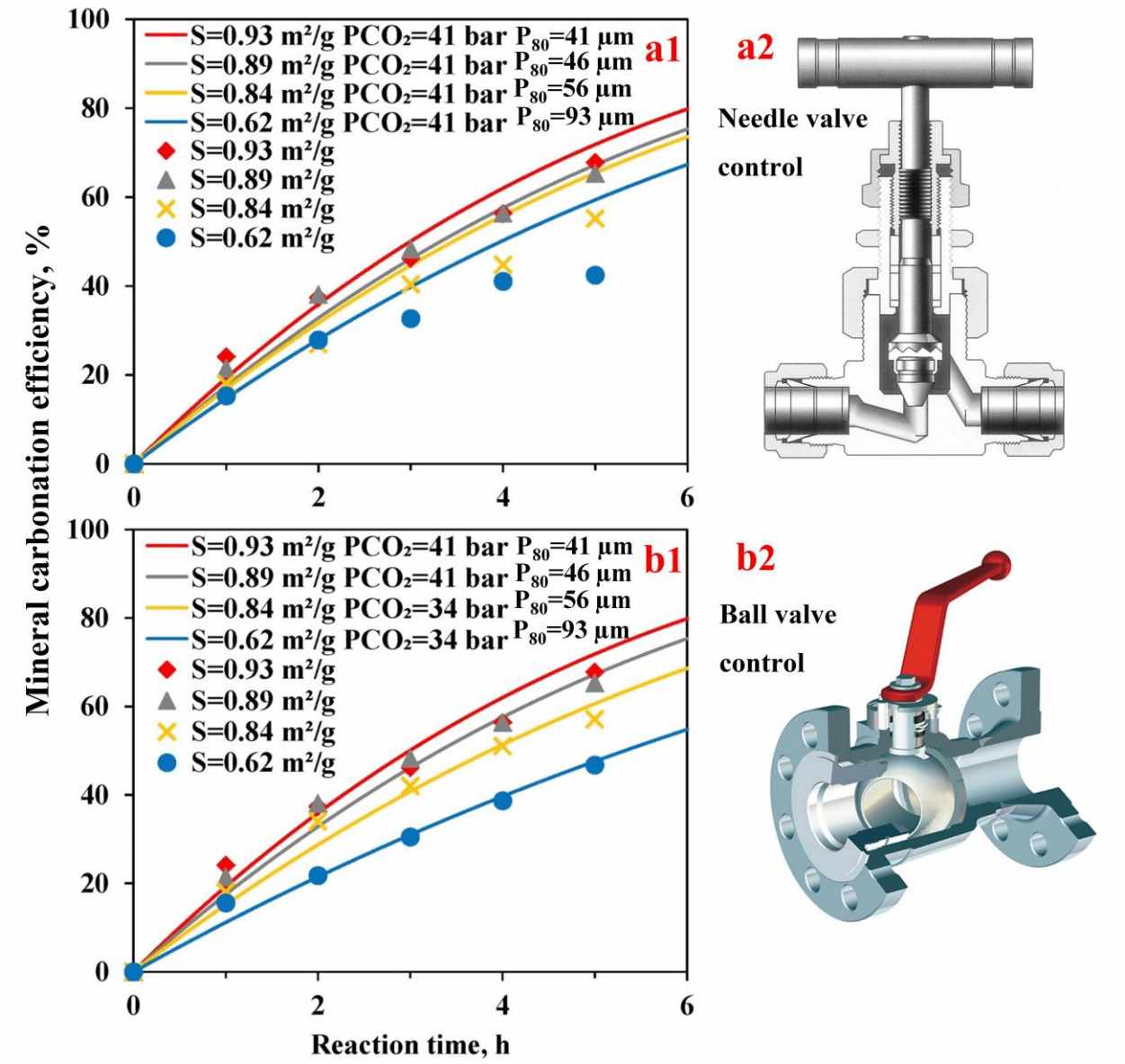

Figure 6.4 Comparison of the experimental data and the predicted data of the quantitative kinetic model for full-size particles of Turnagain sample SN254: (a1) sampling by the control needle valve under PCO_2 = 41.4 bar, 175 ℃, 10% solids content with 1.5 m $NaHCO_3$; (a2) a structure schematic diagram of the control needle valve (http://bit.ly/2DkmlSm); (b1) sampling by the control ball valve under 175 ℃, 10% solids content with 1.5 m $NaHCO_3$; (b2) a structure schematic diagram of the control ball valve (originally from Argus™ EK71).

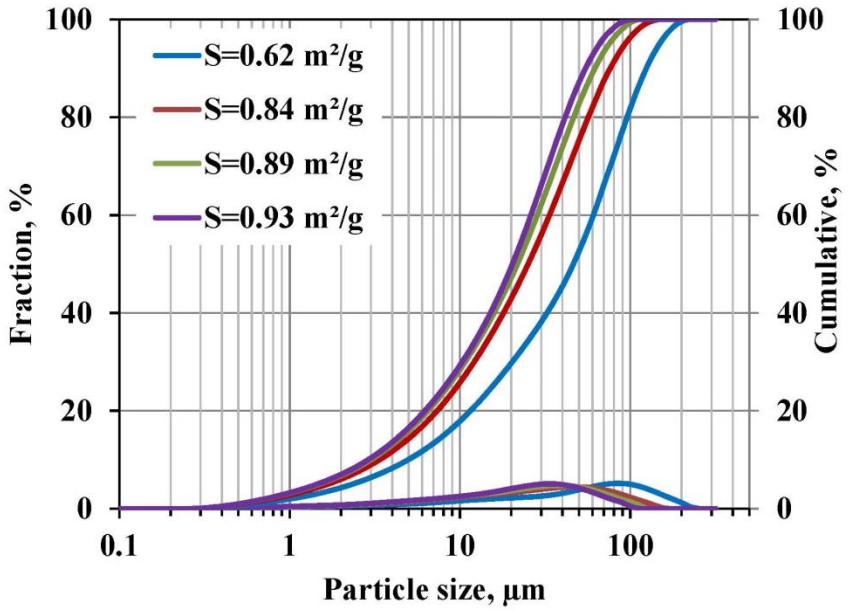

Figure 6.5 Particle size distribution of full-size particles of the Turnagain sample SN254.

SEM-EDX analysis (Figure 6.7) was carried out on the carbonated products of Turnagain SN254 sample under the conditions of -25 µm particle size, PCO_2=41.37 bar, 175 ℃, and with 1.5m $NaHCO_3$ for 5 hours, where the mineral carbonation efficiency was 80%. As seen from the Figure 6.7(a) and (b), there is an obvious porous void between the product carbonate layer and the unreacted olivine core in the carbonated product particles of Turnagain SN254. This means that the carbonation kinetics and the mechanism determined from the high-grade olivine are also applicable for the carbonation of olivine in Turnagain SN254.

It is interesting that the SEM-EDX analysis also showed the carbonation process of other minerals, as shown in Figure 6.7(c) – (j). Figure 6.7(c) and (d) show the results of carbonation of serpentine. The serpentine was also involved in the carbonation process since there were carbonates on the outer surface of the serpentine particles. However, compared to Figure 6.7(b), the carbonation of serpentine occurred to a much lower extent than for olivine under the same

reaction conditions, which is in accordance with the literature[150]. The similar effects were also observed in Figure 6.6(f) and (g).

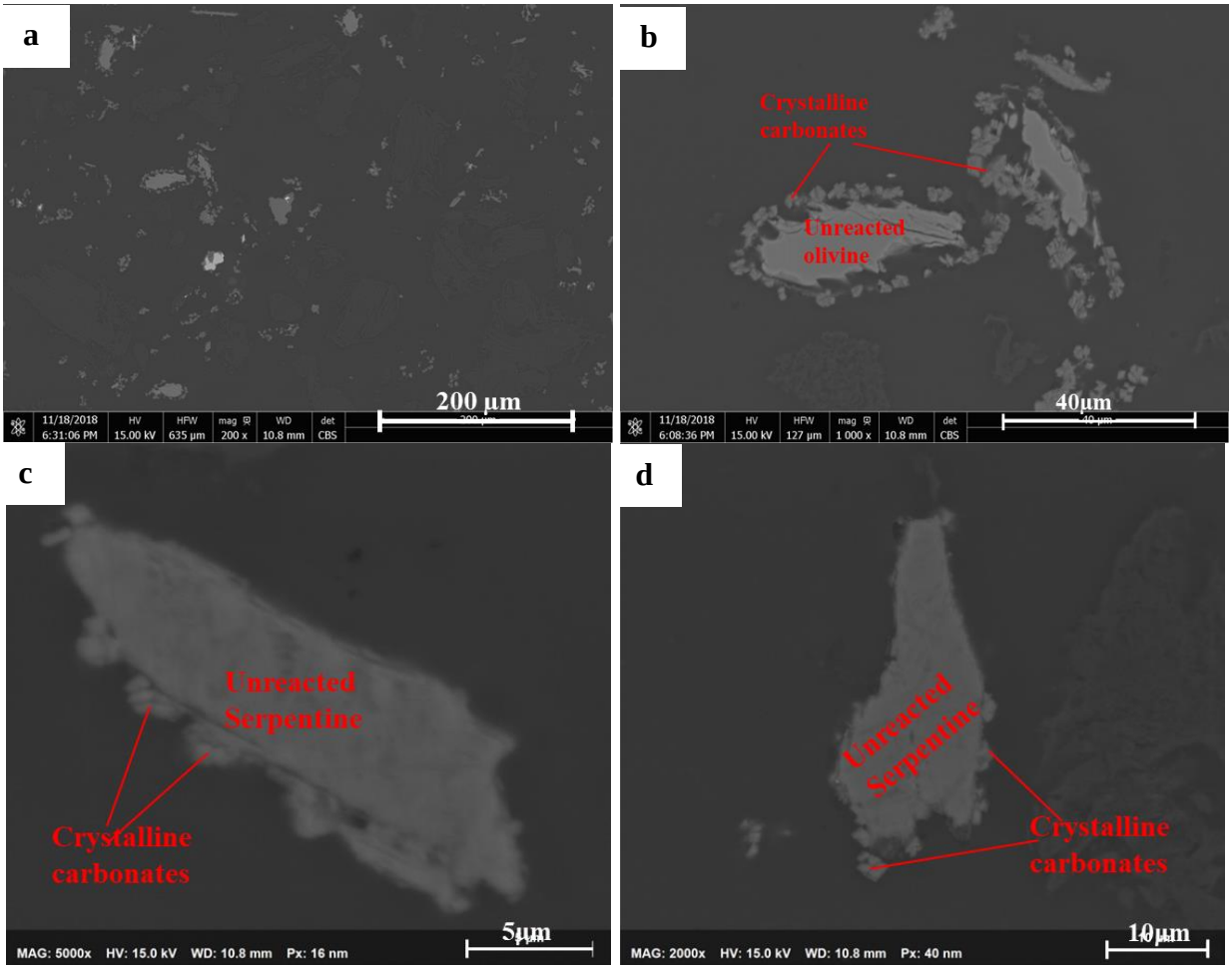

Figure 6.6a-d SEM-EDX images about olivine and serpentine of carbonated products of Turnagain sample SN254 under conditions of -25 µm, PCO_2=41.4 bar, 175 ℃, and with 1.5 m $NaHCO_3$ for 5 hours with mineral carbonation efficiency of 80%.

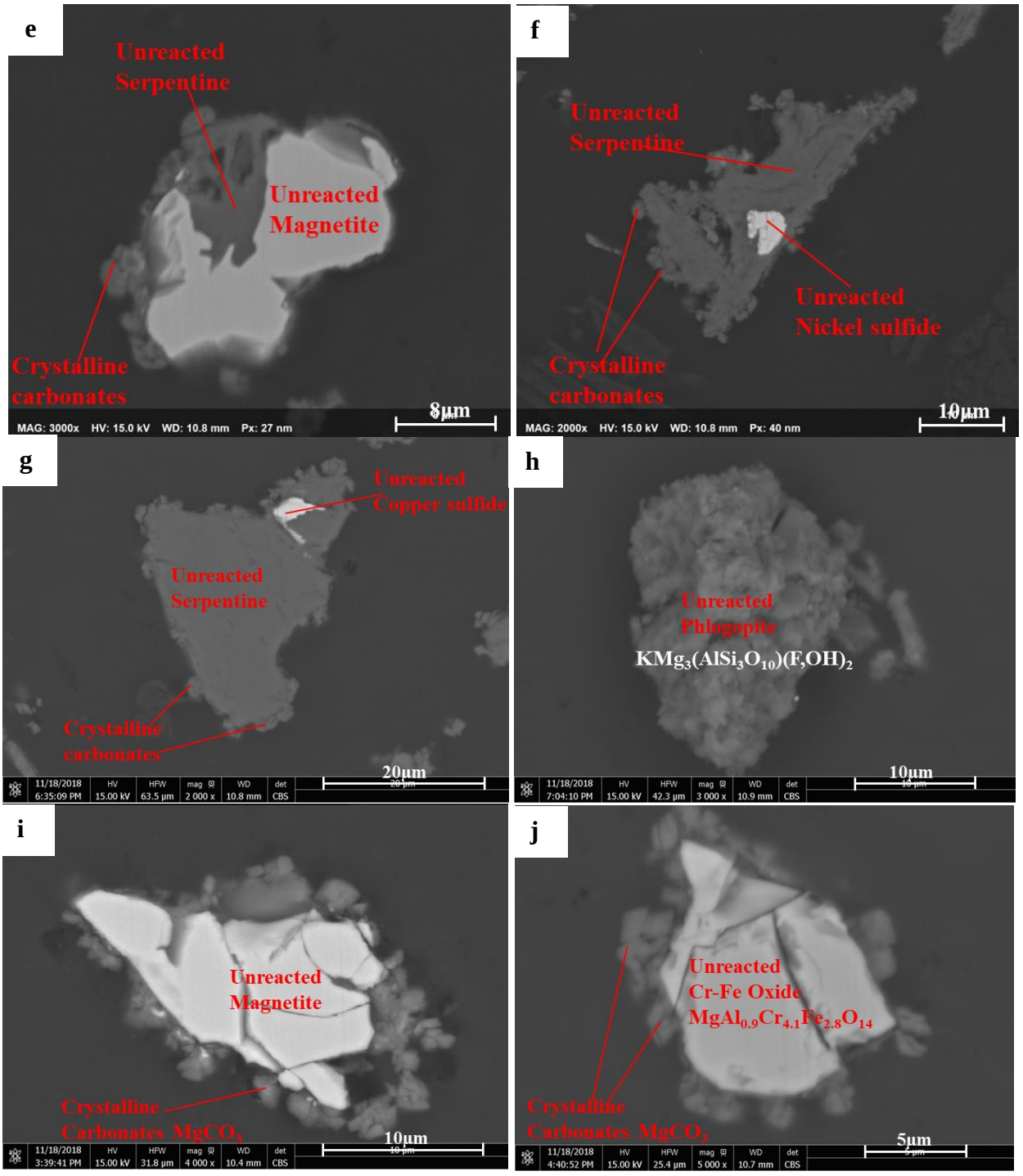

Figure 6.7e-j SEM-EDX images about metal sulfides, magnetite, phlogopite and other minerals of carbonated products of Turnagain sample SN254 under conditions of -25 µm, PCO_2=41.4 bar, 175 ℃, and with 1.5 m $NaHCO_3$ for 5 hours with mineral carbonation efficiency of 80%.

In addition, the magnetite was also been found as seen in Figure 6.7(e) and (i). There were carbonates surrounding the magnetite but they were magnesium-rich carbonates. Considering the possibility that the magnetite was associated with serpentine in the original sample, the carbonates in Figure 6.7(e) may have been formed by the carbonation of serpentine or possibly the carbonation of very little brucite. Another possibility is clear from Figure 6.7(i), namely that the precipitation of carbonates on magnetite may be from the aqueous solution which contained around 40 mg/L magnesium ions, likely dissolved from the olivine during the carbonation. The magnetite may act as the nucleation site for the precipitation of magnesite. A similar process was observed with respect to magnesite precipitation on chromium-iron oxide minerals (as shown in Figure 6.7(j)). Metal sulfides, such as nickel sulfide and copper sulfide, were usually associated with serpentine, as shown in Figure 6.7(f) and (g). The metal sulfides were not involved in the carbonation process because the solubility of the metal sulfides is much lower than the corresponding carbonates. Phlogopite was not involved in the mineral carbonation process as shown by Figure 6.7(h).

As a result, the application of the quantitative kinetic formula on the carbonation of Turnagain sample SN254 was successful under various conditions. The kinetic factor needed to be adjusted in relation to the olivine content of the sample. The mineral carbonation mechanism and kinetic formula developed from the carbonation of a high-grade olivine were applicable to the Turnagain sample SN254. The carbonation of other minerals (for example serpentinite) under the same conditions was much slower compared to the carbonation of olivine. The design and operation of the sampling process was also an important factor in the experimental method.

6.2 Comparison of carbonation of typical Turnagain samples

Turnagain samples SN255-262 were pulverized to the particle size P_{80}=30±3 μm in order to compare the effects of mineral compositions on the mineral carbonation efficiency under a specific set of conditions. It was found that the mineral carbonation efficiency was strongly dependent on the olivine content of the material under the conditions of P_{80}=30±3 μm particle size, specific surface area=2.1 m^2/g, 175 ℃, PCO_2=34.5 bar, with 1.5 m $NaHCO_3$ and 10% solids content for 5 hours. Results are shown in Figure 6.8. The Turnagain samples SN255-SN258 which have an olivine content of approximately 80% had the mineral carbonation efficiencies around 70% based on the magnesium, calcium and iron content, followed by 53% for Turnagain SN262 which had an olivine content of 73%. The samples which had the olivine contents of 51% and 40% had the mineral carbonation efficiencies 45% and 37%, respectively. Turnagain sample SN261 with the lowest olivine content of 30% had the lowest mineral carbonation efficiency 30%. It seems that the carbonation of olivine for the Turnagain samples SN259-SN261 had almost completely carbonated in 5 hours under the indicated conditions. It is also noted that the pyroxene and serpentine contents of the Turnagain samples SN259-261 were 29% and 11%, 5% and 29%, 13% and 43%, respectively. This means that the samples which had the highest content of pyroxene and serpentine had the lowest carbonation efficiency, which accords with the findings indicated in Figure 6.7. The XRD analysis of the carbonated products (Figure 6.9) further demonstrated these conclusions. There were obvious peaks of product carbonates and the decreases for the peak intensities of olivine for the Turnagain samples SN255-SN258. In contrast, the intensity of peaks for pyroxene, serpentine and iron sulfides did not change for the Turnagain samples SN259-261 though there were still the peaks of formation of the carbonates. The intensities of the peaks of the carbonates in the carbonated Turnagain

sample SN262 were lower than those in the carbonated Turnagain SN255-SN258 samples, but higher than those in carbonated Turnagain SN259-SN261 samples. All this further verified that the formation of carbonates was highly dependent on the olivine content rather than on the serpentine, pyroxene and the other minerals.

In addition, because part of the iron content in the Turnagain samples was in the form of magnetite and iron sulfides (troilite and pyrrhotite), which did not participate in the mineral carbonation process, the mineral carbonation efficiency based on only magnesium and calcium content has also been presented in Figure 6.8. Mineral carbonation efficiency based on only magnesium and calcium content was generally around 14% higher than that based on the magnesium, iron and calcium.

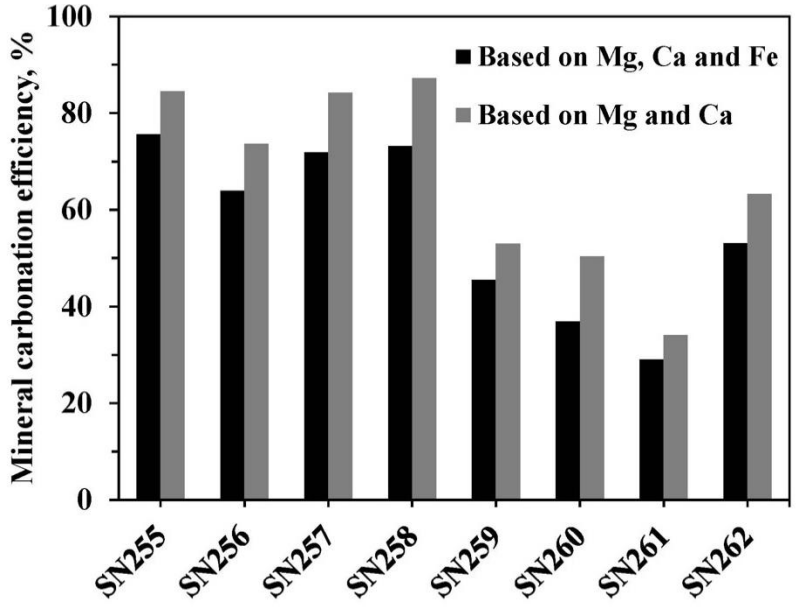

Figure 6.8 Comparison of carbonation efficiencies of Turnagain samples SN255-SN262 under the conditions of P_{80}=30±3 μm particle size, specific surface area=2.1 m^2/g, 175 ℃, PCO_2=34.5 bar, 1.5 m $NaHCO_3$ and 10% solids content for 5 hours (Size reduction by a pulveriser).

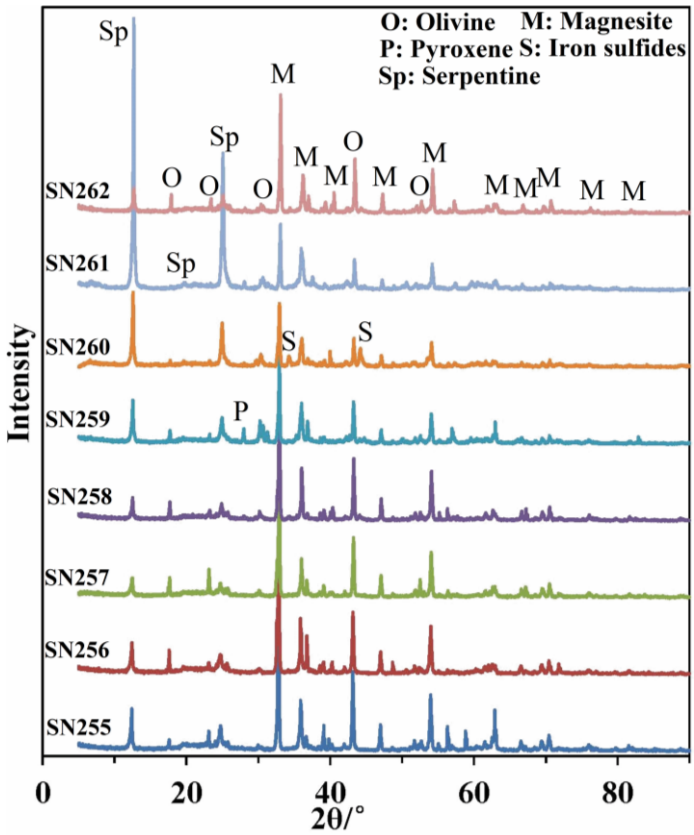

Figure 6.9 XRD images of carbonated Turnagain samples SN255-262.

The SEM-EDX analysis on the transverse surfaces of the carbonated Turnagain samples was carried out as shown in Figure 6.11. The SEM-EDX images in Figure 6.11(a)-(d) and Figure 6.11(h) illustrate the results of the carbonation process for Turnagain SN255-SN258 samples respectively. The porous voids existed between the unreacted olivine core and the outer carbonate layer in the carbonated products of SN255-258 and SN262 samples. This means that the mechanism developed from the carbonation of the high-grade olivine could be extended to the carbonation of the Turnagain samples where the carbonation of olivine was the majority. Turnagain sample SN259 had the highest content of pyroxene and the corresponding Figure 6.9(e) showed the corresponding detailed carbonation process: The pyroxene (the diopside mineral) did not participate in mineral carbonation under the conditions where the olivine was carbonated. In Figure 6.11(e), serpentine and magnetite were also identified. Serpentine was

somewhat involved in the carbonation with some formation of carbonate on the outer mineral surface. There was no obvious carbonation of magnetite associated with the serpentine, which agrees with Figure 6.7. Similar to the pyroxene, the iron sulfides did not carbonate. This can be observed in Figure 6.11(g).

The mechanism of mineral carbonation of olivine developed for the high-grade olivine can be extended to each Turnagain sample in spite of the variable mineral compositions and content of olivine. Additionally, the carbonation of serpentine, pyroxene, metal sulfides, magnetite and other minerals did not occur or was much slower compared to the carbonation of olivine, under the conditions of high concentration of sodium salts and moderate CO_2 partial pressures. It also indicates that the carbonation of the materials would be mainly controlled by the dissolution of olivine since the carbonation of olivine represents the majority of the carbonation reactions.

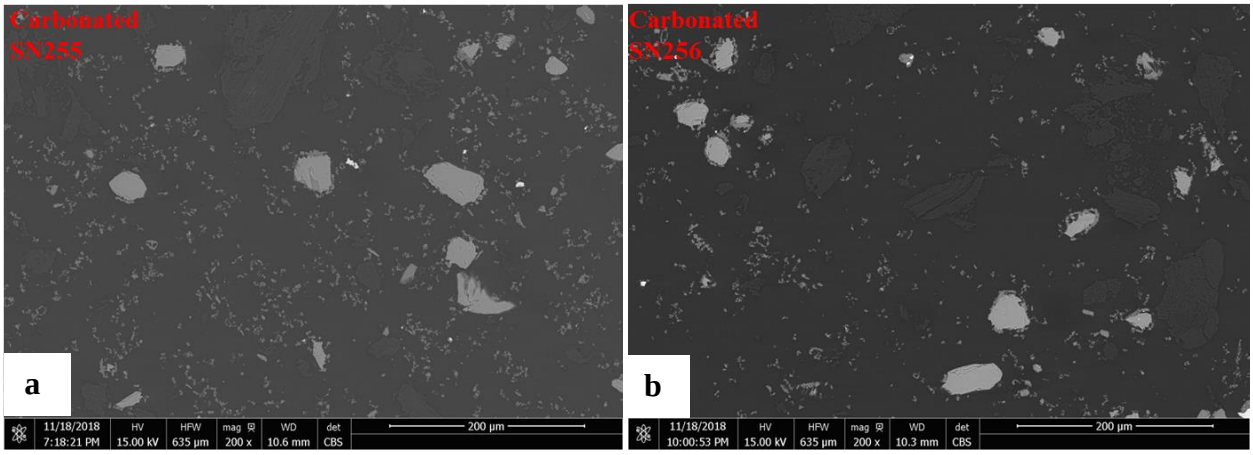

Figure 6.10a-b SEM-EDX images of carbonated products of typical Turnagain samples SN255-SN256 under conditions of P_{80}=30±3 µm particle size, specific surface area=2.1 m^2/g, 175 ℃, PCO_2=34.5 bar, 1.5 m $NaHCO_3$ and 10% solids content for 5 hours (Size reduction by a pulveriser).

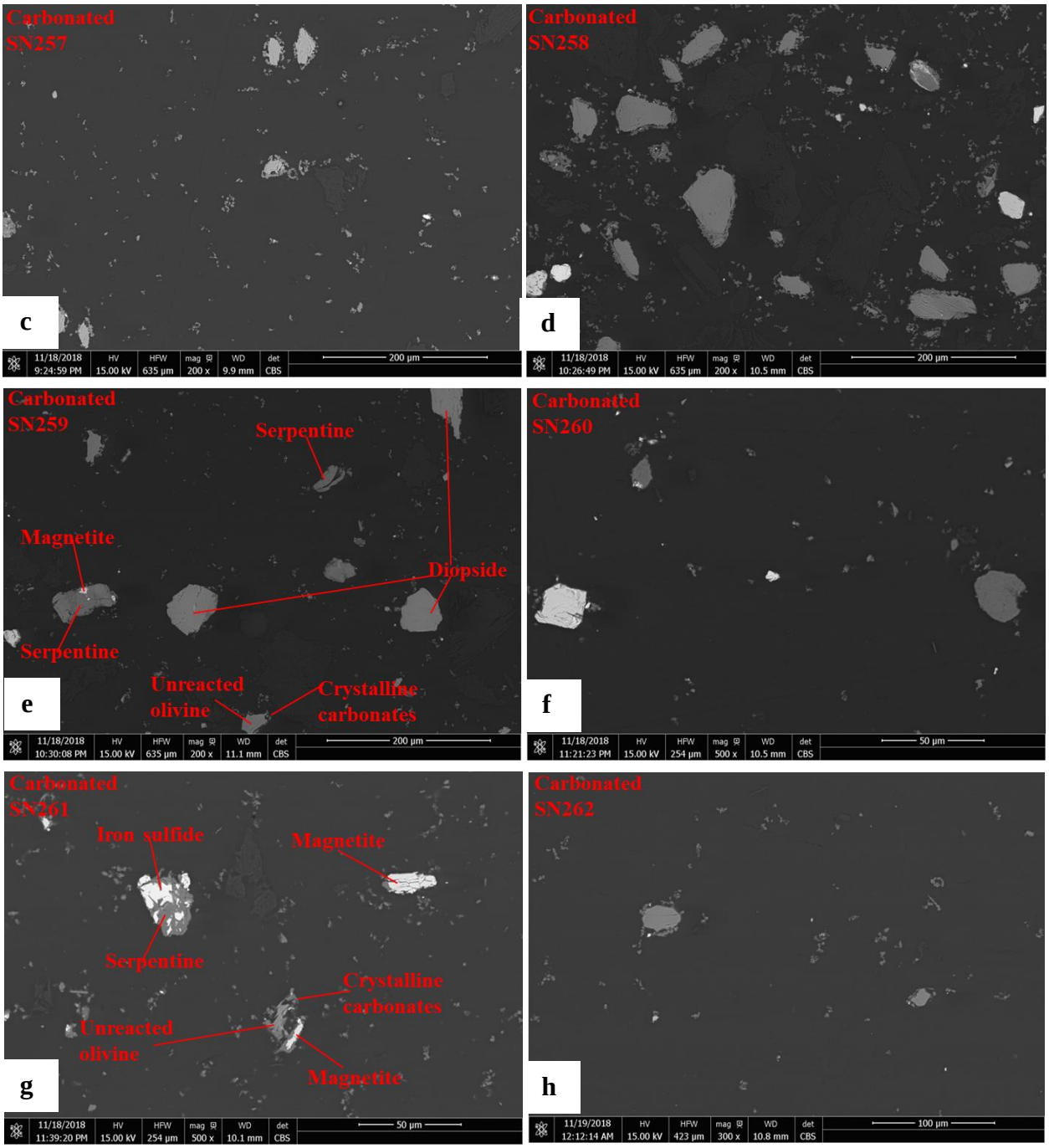

Figure 6.11c-h SEM-EDX images of carbonated products of typical Turnagain samples SN257-SN262 under conditions of P_{80}=30±3 μm particle size, specific surface area=2.1 m^2/g, 175 ℃, PCO_2=34.5 bar, 1.5 m $NaHCO_3$ and 10% solids content for 5 hours (Size reduction by a pulveriser).

6.3 Kinetics of carbonation of typical Turnagain samples

The mechanism and kinetics of the mineral carbonation of olivine has been clearly illustrated in Chapter 5. The carbonation control step of olivine is mainly dependent on the addition of sodium salts and the CO_2 partial pressure. Once the addition of sodium salts is higher than 0.5 m and the CO_2 partial pressure is higher than 27.6 bar, the carbonation rate of olivine is controlled by chemical reaction, that is, the dissolution of olivine. According to the Figure 6.7 and Figure 6.11, the iron sulfides, magnetite and pyroxene are not significantly carbonated under the same conditions of olivine. Besides, the carbonation of serpentine is much slower than olivine if the sample is not heat treated prior to carbonation. In order to test the broader applicability of the kinetic formula, it is necessary to study the kinetics of typical industrial samples. Herein, the kinetics of Turnagain samples SN255-262 were further studied since the samples had various mineral compositions. The samples SN259, SN260 and SN261 were completely different from the others with significant fractions of minerals such as pyroxene, iron sulfides and serpentine. The mineral carbonation behaviour and kinetics could be different. Since some of the iron will be not involved in the carbonation process and there are important contents of other minerals in addition to olivine, the evaluation of mineral carbonation may need to be adjusted as well. The Turnagain samples SN255-262 were the ideal samples to test the effects of mineral compositions on the kinetics of mineral carbonation and also to determine how to more reasonably evaluate the mineral carbonation efficiency.

In order to test the effects of mineral compositions on the kinetics, the Turnagain samples SN255-262 were ground with a rod mill and screened through a 500-mesh sieve to obtain the -25 μm particles. From the kinetic research on the carbonation of high-grade olivine and the Turnagain SN254 sample, the -25 μm particle size fractions were well suited for use in kinetic

studies. To avoid the sampling issues during the continuous sampling, a ball valve was used, as discussed in relation to Figure 6.4. The particle size distributions of the narrow-sized -25 μm particle fractions of Turnagain samples SN255-262 are shown in Figure 6.12a. It can be seen that the particle size distributions were similar to that in Figure 6.1 in general, though sample SN262 was a little different from the others in that the -5 μm fractions accounted for 29% of the mass of -25 μm SN261 sample while it was approximately 20% of the total mass of the others.

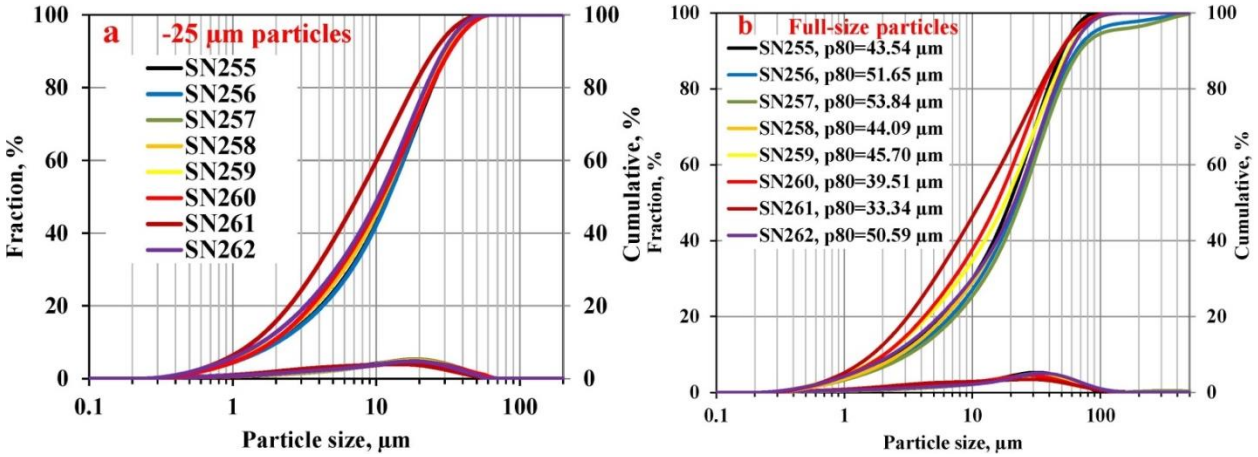

Figure 6.12 Particle size distributions of Turnagain samples SN255-SN262: (a) -25 μm particles and (b) full-size particles.

The kinetic formula was developed from the mineral carbonation of high-grade olivine and under the chemical reaction control (the dissolution of olivine). However, the samples from industry are usually not high-grade olivine. Though the formula has been verified for the Turnagain sample SN254, it still needs to be more fully verified. Turnagain samples contain various minerals and some minerals containing the bivalent metals (iron and/or magnesium) do not readily participate in the mineral carbonation process, as was indicated by Figure 6.7 and Figure 6.11. How to accurately calculate the mineral carbonation efficiency for these typical, naturally occurring samples is still being debated. In this study, four ways to calculate the mineral

carbonation efficiency were explored for the carbonation conditions: -μm particles, 175 ℃, PCO_2=34.5 bar, 10% solids content, and with 1.5 m $NaHCO_3$. These are illustrated in Figure 6.13: (a) based on the magnesium, iron and calcium contents without considering the olivine content, which is the usual method and which has been used for the mineral carbonation of the high-grade olivine in this work: (b) based on the magnesium, iron and calcium contents with considering the olivine content, which disregards the effects of other minerals; (c) based on the magnesium and calcium contents without considering the olivine content, which disregards the effects of magnetite and iron sulfides; and (d) based on the magnesium and calcium contents with considering the olivine content only, which completely removes the effects of all the minerals except for the olivine.

According to Figure 6.13, it is obvious that the mineral carbonation efficiency based on the magnesium and calcium contents with considering the olivine content only always had the highest results for all the tTurnagain samples tested. However, the results were more than 100% for many samples and even up to 120% for Turnagain SN259 and SN260. This means that the carbonation efficiency based on the magnesium and calcium contents and with considering the olivine content only may be not reasonable. The second highest results were always obtained by the method based on the magnesium, iron and calcium contents with considering the olivine content only, which got close to 100% but never greater. This suggests that this method is potentially suitable for the carbonation of Turnagain samples. On the other hand, the carbonation efficiency based on total magnesium and calcium contents was always approximately 2% higher than that based on total magnesium, calcium and iron contents. The effects of consideration of olivine content in the material were generally stronger than those of consideration of iron content for the carbonation capacity. In addition, the difference between the efficiency based on the

consideration of the olivine content and without consideration the olivine content became larger when the olivine content in the Turnagain samples decreased. As a result, the largest difference occurred for the Turnagain sample SN261, followed by Turnagain SN260 and SN259, which had the olivine content of 30%, 40% and 50% respectively. Based on the total magnesium, calcium, and iron contents, the mineral carbonation efficiency of Turnagain SN261 was only down to 27%. In contrast, when with consideration of the olivine content, the corresponding carbonation efficiency based on the magnesium, iron and calcium was up to 91% at four hours, which would indicate almost the complete of the carbonation reaction. Therefore, it is important to choose a suitable way to evaluate the mineral carbonation efficiency.

Therefore, the kinetics analyses based on the shrinking core model, using the four methods to calculate the mineral carbonation efficiencies were performed. Results are shown in Figure 6.14 for Turnagain samples SN255-258 and in Figure 6.15 for Turnagain samples SN259-262. Surprisingly, the chemical reaction control model did not fit the data well, when carbonation efficiency was based on the total magnesium, calcium and iron contents. However, it has been discovered above that the mineral carbonation of olivine was the majority of the reactions for all the Turnagain samples. The porous void structure for chemical reaction control generally was observed in all the carbonated Turnagain samples. There is an obvious conflict between this kinetics and the above discoveries.

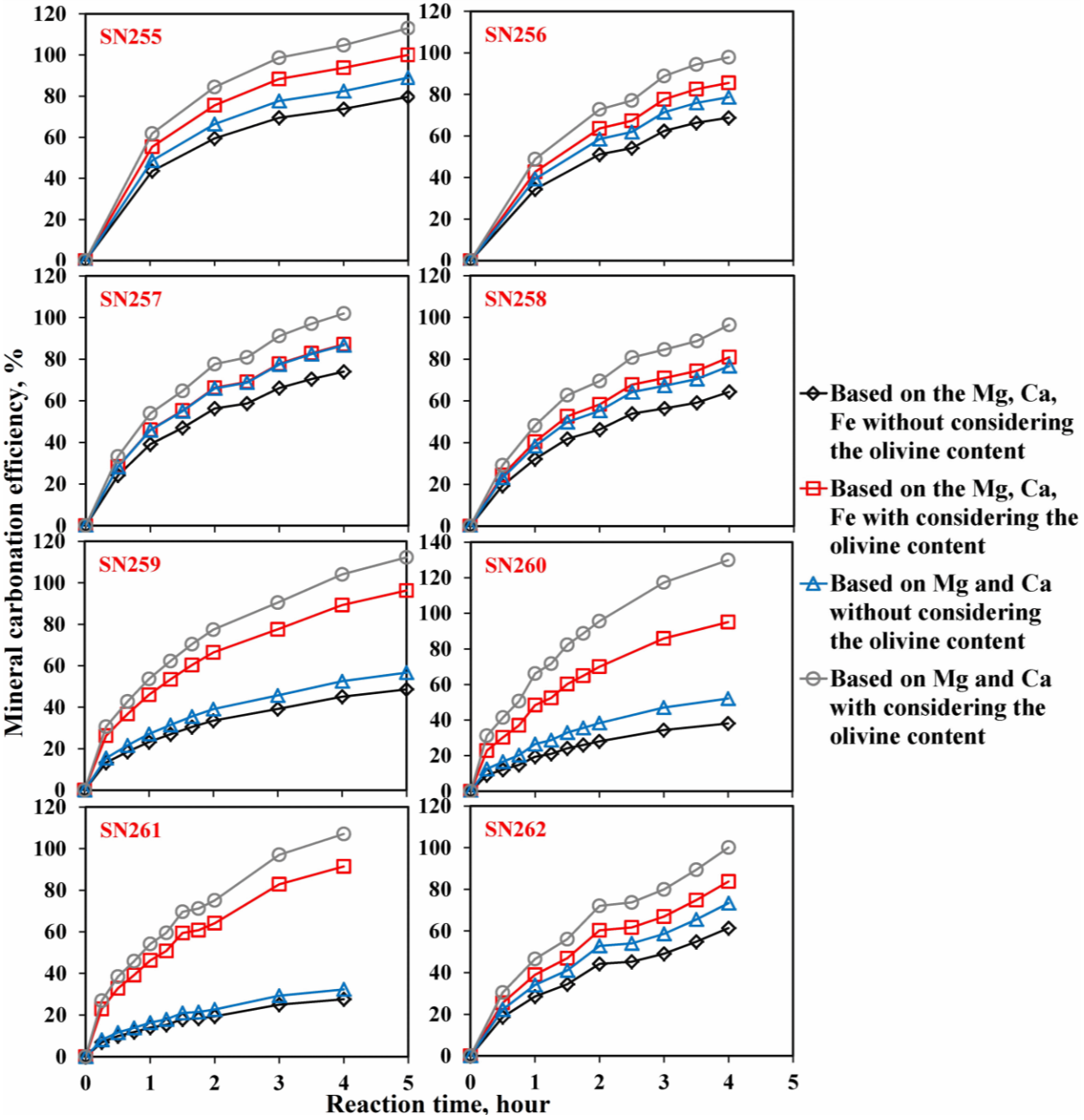

Figure 6.13 Mineral carbonation efficiencies of Turnagain samples SN255-262 according to various evaluation criteria under the carbonation conditions of -25 μm particles, 175 °C, PCO_2=34.5 bar, 10% solids content and with 1.5 m $NaHCO_3$.

This raised a serious question: can the kinetic model developed to date adequately represent the actual kinetics of the carbonation of the various Turnagain samples? In order to address this

conflict, the kinetics analyses were carried out using the other three methods to calculate the mineral carbonation efficiencies:

(1) When the mineral carbonation efficiency was based on the magnesium, iron and calcium contents with considering the olivine content, the degree of the correlation (R^2) for the chemical reaction control increased to over 0.95, while R^2 for the product layer diffusion control was decreased for the samples which had much lower olivine content (in Figure 6.15). This change reflects that the consideration of olivine content of an ore is a very important aspect of the kinetics of the mineral carbonation.

(2) When the carbonation efficiency was calculated based on the total magnesium and calcium contents, the R^2 for the product layer diffusion control was still around 0.98. There was no significant effect on the change of R^2 for the chemical reaction control model. This means that the effect of iron content (if without considering the olivine content) is limited.

(3) Similar to the above discussion (1), when the mineral carbonation efficiency was calculated based on magnesium and calcium contents and with consideration of olivine content, most of the R^2 value was further improved to over 0.98. Although this approach yielded the best fit of the chemical reaction control model to the data, it is not satisfactory since carbonation efficiency can exceed 100% when calculated by this method. The iron content in olivine was also carbonated during the mineral carbonation process, while the iron contents in magnetite, troilite and pyrrhotite did not participate in carbonation. This means that the consideration of the iron content is also significant, if the olivine content alone is considered to calculate the mineral carbonation efficiency. However, compared to the effect of olivine content, the importance of the iron content is limited in involving the mineral carbonation reaction.

Therefore, the considerations of olivine content and the distribution of iron content can benefit the discovery of the kinetics of the detailed mineral carbonation. Nevertheless, the olivine content had the stronger effects on the kinetics analysis than the iron content.

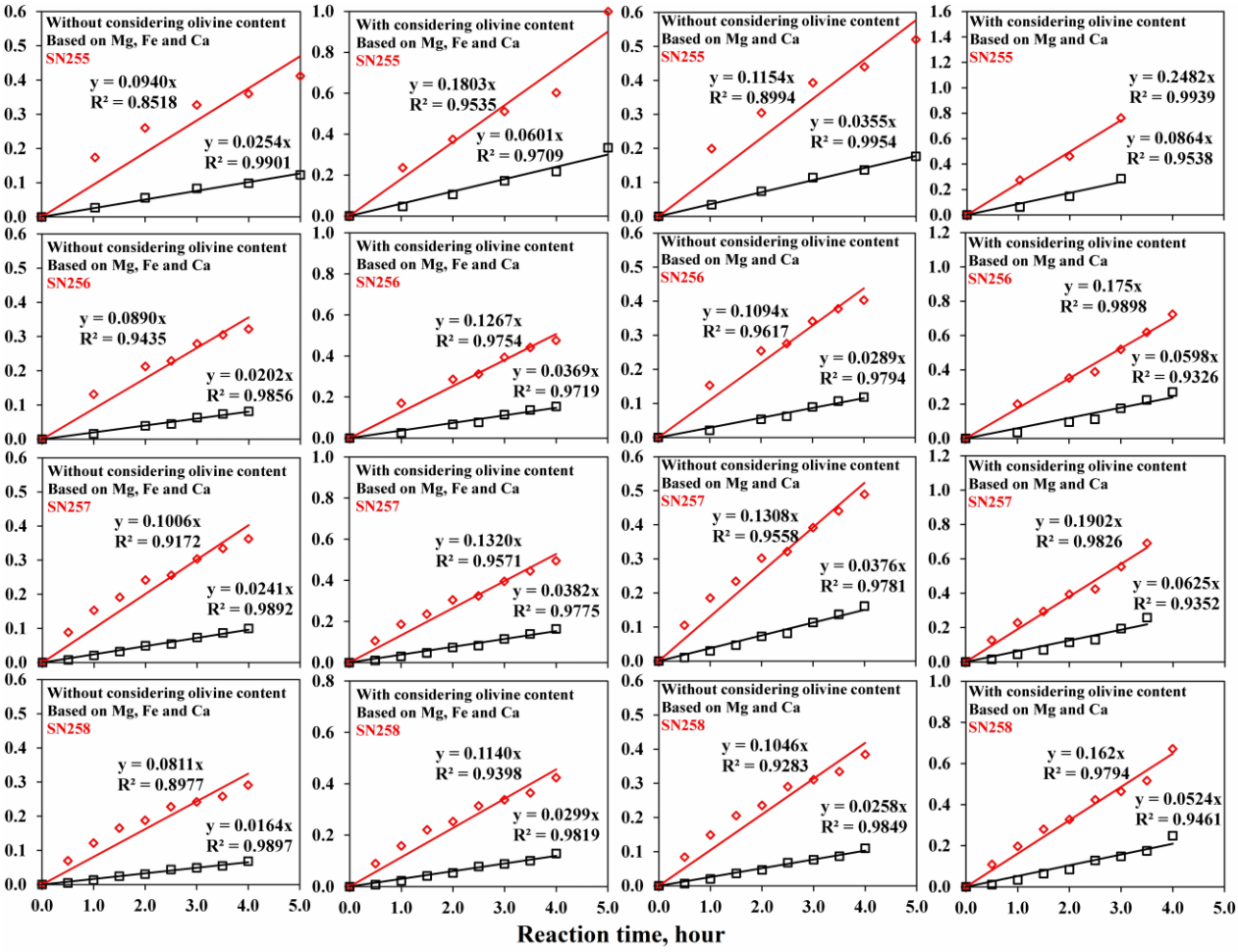

Figure 6.14 Plots of chemical reaction control (in red) and product layer diffusion control (in black) respectively with four evaluation methods of mineral carbonation efficiency for the carbonation of Turnagain samples SN255-SN258 under the conditions of -25 μm particles, 175 ℃, PCO_2=34.5 bar, 10% solids content with 1.5 m $NaHCO_3$: (a) Turnagain SN255; (b) Turnagain SN256; (c) Turnagain SN257 and (d) Turnagain SN258. Red is for chemical reaction control and black is for product layer diffusion control.

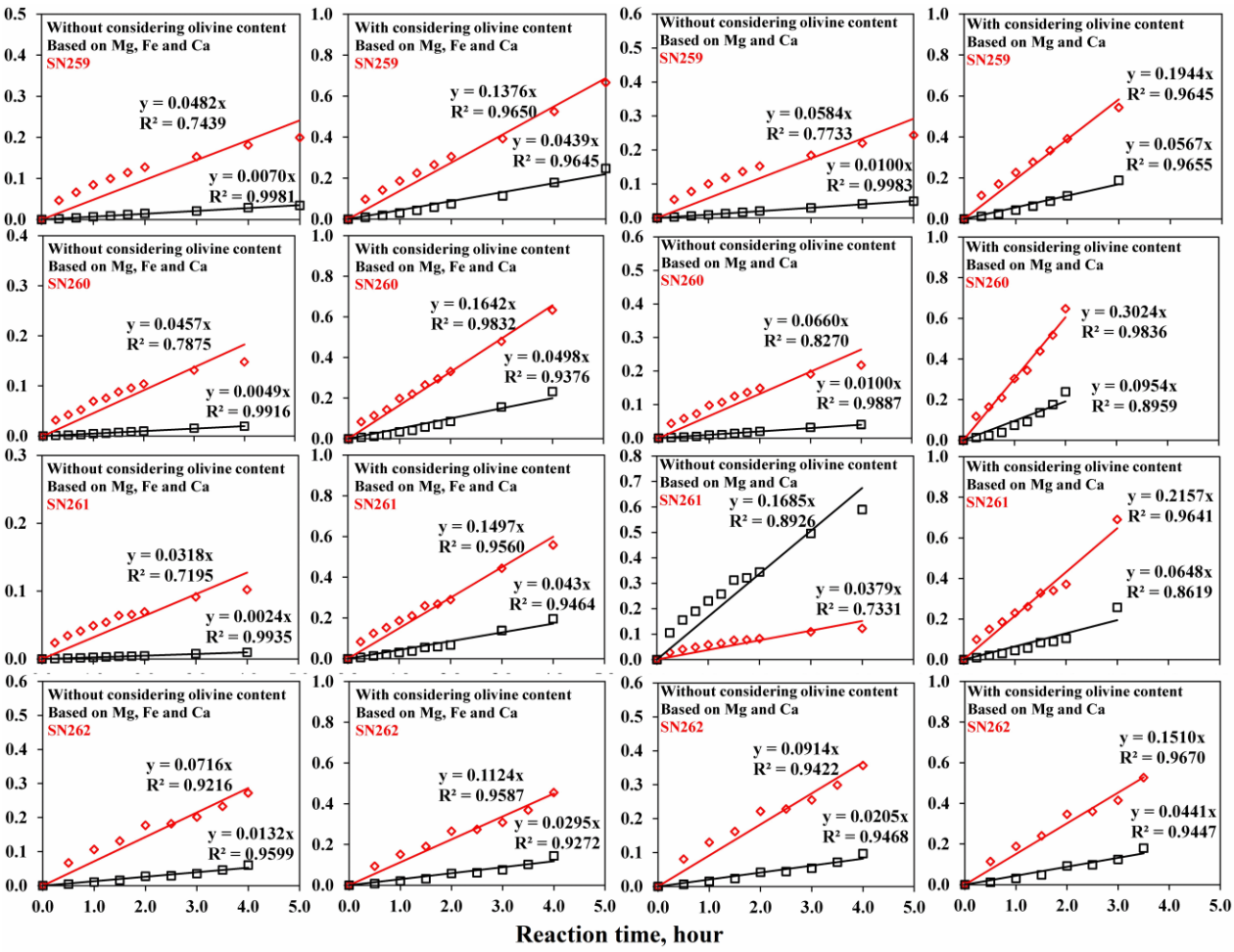

Figure 6.15 Plots of chemical reaction control (in red) and product layer diffusion control (in black) respectively with four evaluation methods of mineral carbonation efficiency for the carbonation of Turnagain samples SN259-SN262 under the conditions of 0 – 25 μm particles, 175 ℃, PCO_2=34.5 bar, 10% solids content with 1.5 m $NaHCO_3$: (a) Turnagain SN259; (b) Turnagain SN260; (c) Turnagain SN261 and (d) Turnagain SN262. Red is for chemical reaction control and black is for product layer diffusion control.

6.4 Effects of olivine content on kinetics

In order to clarify the relationship between the olivine content and the kinetics, a sample of high-purity silica was mixed with a sample of high-grade olivine. The XRD analysis of the silica sample confirmed that SiO_2 was the only mineral present (Figure 6.16). The silica was screened to produce a -25 μm particle size sample. The -25 μm high-purity silica particles were added to a

-25 μm high-grade olivine particles to make the mixed samples which contained an olivine content of 70%, 60%, 50%, 40% and 30%, respectively. There were four main reasons why the -25 μm high-purity silica was chosen for this research: (1) The kinetics plots for the -25 μm olivine particles were the same to those of the narrow-sized particles, as shown in Figure 5.4; (2) The kinetics analysis based on the plots of SCM model was consistent with the SEM-EDX analysis results, as shown in Figure 5.3; (3) Sampling with a ball valve would rise no solids segregation problems, allowing representative samples to be taken (shown in Figure 6.4); and (4) The -25 μm olivine particles had the faster mineral carbonation rate and it is easier to carry out the tests of kinetic analysis.

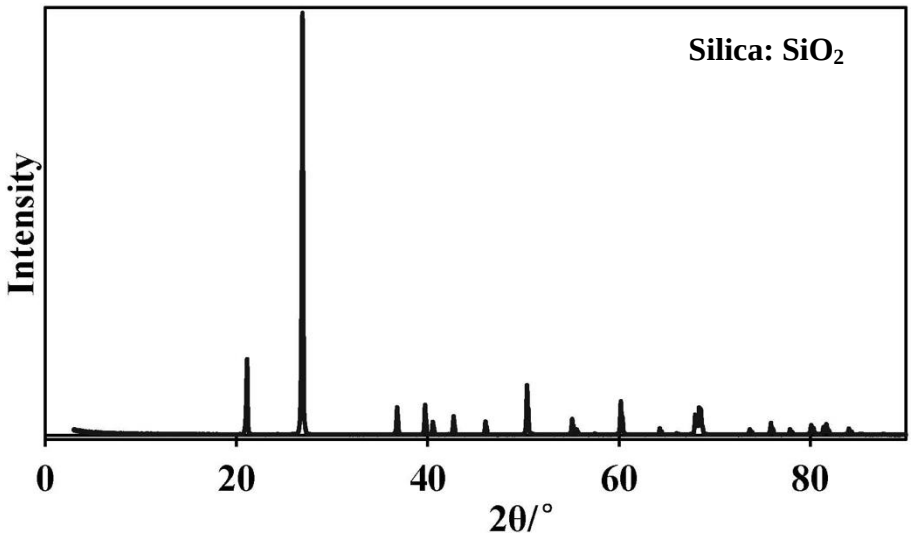

Figure 6.16 XRD image of high-purity silica for the dilution of olivine content.

All the -25 μm mixture samples were carbonated under the following conditions of 175 ℃, PCO_2=34.5 bar, 10% solids content with 1.5 m $NaHCO_3$. The results are shown in Figure 6.17. It is interesting that the decrease of the high-grade olivine content slightly decreased the mineral carbonation efficiency at the same reaction time, but the effect was not proportional to the olivine content in the mixed sample. At 4 hours reaction time, the mineral carbonation efficiency

decreased from 71% for the mixture containing 70% high-grade olivine content to 55% for the 30% high-grade olivine content in mixed sample. The decrease of mineral carbonation efficiency may be because the increase of silica content in mixed sample increased the solubility of aqueous silica in solution and as a result hindered the carbonation process. In spite of the decrease, the experimental mineral carbonation efficiency still matched well with the predicted data from the quantitative kinetic model, shown in Figure 6.17a1-Figure 6.17e1. It is difficult to fully determine the effect of silica on the process since silica exhibited some complex behaviour at high temperature and pressure and may have dissolved and reprecipitated[153,154].

Furthermore, the SCM kinetics analysis was carried out for the mixed samples, as shown in Figure 6.17a2-6.15e2. It is clear that no matter how high the proportion of silica in the mixed sample, the kinetic plots always showed that the chemical reaction control model rather than the product layer diffusion control model. The R^2 correlation coefficient for chemical reaction control was 0.95 to 0.98 for all the mixed samples. The R^2 values confirmed that the process was controlled by the dissolution of olivine as was reported in Chapter 5. In contrast, the R^2 values for the product layer diffusion control model were lower than 0.87. The dilution of the olivine content did not alter the rate-limiting step of mineral carbonation of olivine.

The results suggest that the mineral carbonation of the Turnagain samples should be controlled by the dissolution of olivine. It is necessary to consider the olivine content of the complex materials (not pure olivine) for the kinetics analysis of mineral carbonation. The roles of the magnetite, iron sulfides, pyroxene and serpentine are believed to be the same as those of the pure silica and do not change the rate-limiting step of the mineral carbonation, i.e. no effects on the kinetic analysis.

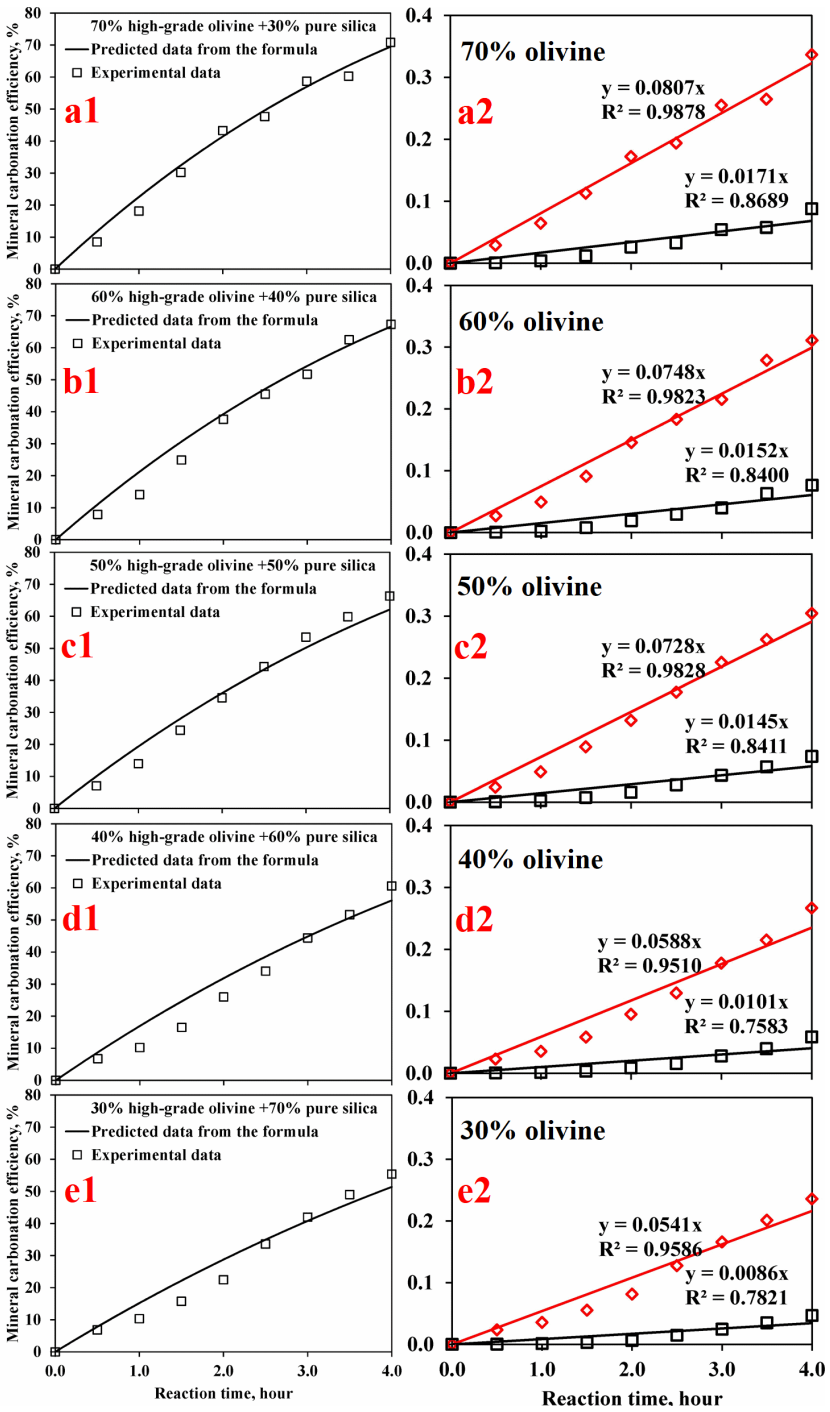

Figure 6.17 Effects of olivine content in the mixture of high-grade olivine and high-purity silica on the kinetics under the conditions of -25 μm particle size, specific surface area=1.53 m2/g of high-grade olivine, 175 ℃, PCO2=34.5 bar, 1.5 m NaHCO3 and 10% solids content for the sample containing 70%, 60%, 50%, 40% and 30% high-grade olivine respectively: (a1-e1) experimental and predicted mineral carbonation efficiencies;(a2-e2) kinetic plots of chemical reaction control (in red) and product layer diffusion control (in black), respectively.

6.5 Application of kinetic formula to carbonation of Turnagain samples

The preceding discussion and analysis have revealed that the rate of mineral carbonation of silicate ores under the high concentration of sodium bicarbonate and moderate CO_2 partial pressure is always controlled by chemical reaction between protons and the unreacted olivine. The kinetic formula, therefore, is potentially applicable to all the Turnagain samples. Sections 6.3 and 6.4 have shown that it is more reasonable for the kinetics to evaluate the mineral carbonation efficiency based on the magnesium, iron and calcium contents and with considering the olivine content. Therefore, the procedure is to compare the difference between the predicted mineral carbonation efficiency and the experimental data that is calculated based on the magnesium, iron and calcium contents and with considering the olivine content, as shown in Figure 6.18. The predicted data had a sufficiently good enough match with all the experimental data for all the Turnagain samples ground to -25 μm particles. The difference between the experimental data and the predicted values was less than 8%. Furthermore, it was also found that all the finely ground Turnagain samples exhibited nearly complete carbonation after five hours reaction, regardless of the specific surface area analyzed by Malvern Mastersizer varying from 1.30 m^2/g to 1.80 m^2/g. The corresponding value of kinetic factor for all the Turnagain samples SN255-262 is shown in Figure 6.17. It seems that there is no clear relationship between the kinetic factor value and the olivine content in the Turnagain samples. The average value of the kinetic factor for all the Turnagain samples is 95. The suitable k^o value for Turnagain samples is in the range of $95(1 \pm 7\%)$ as an empirical fitting constant. The variation of the suitable k^o may be the results of the cumulating errors in specific surface area ($\pm 2.6\%$), CO_2 partial pressure ($\pm 4.5\%$), addition of sodium bicarbonate ($\pm 3.5\%$) and activation energy of olivine ($\pm 2.5\%$).

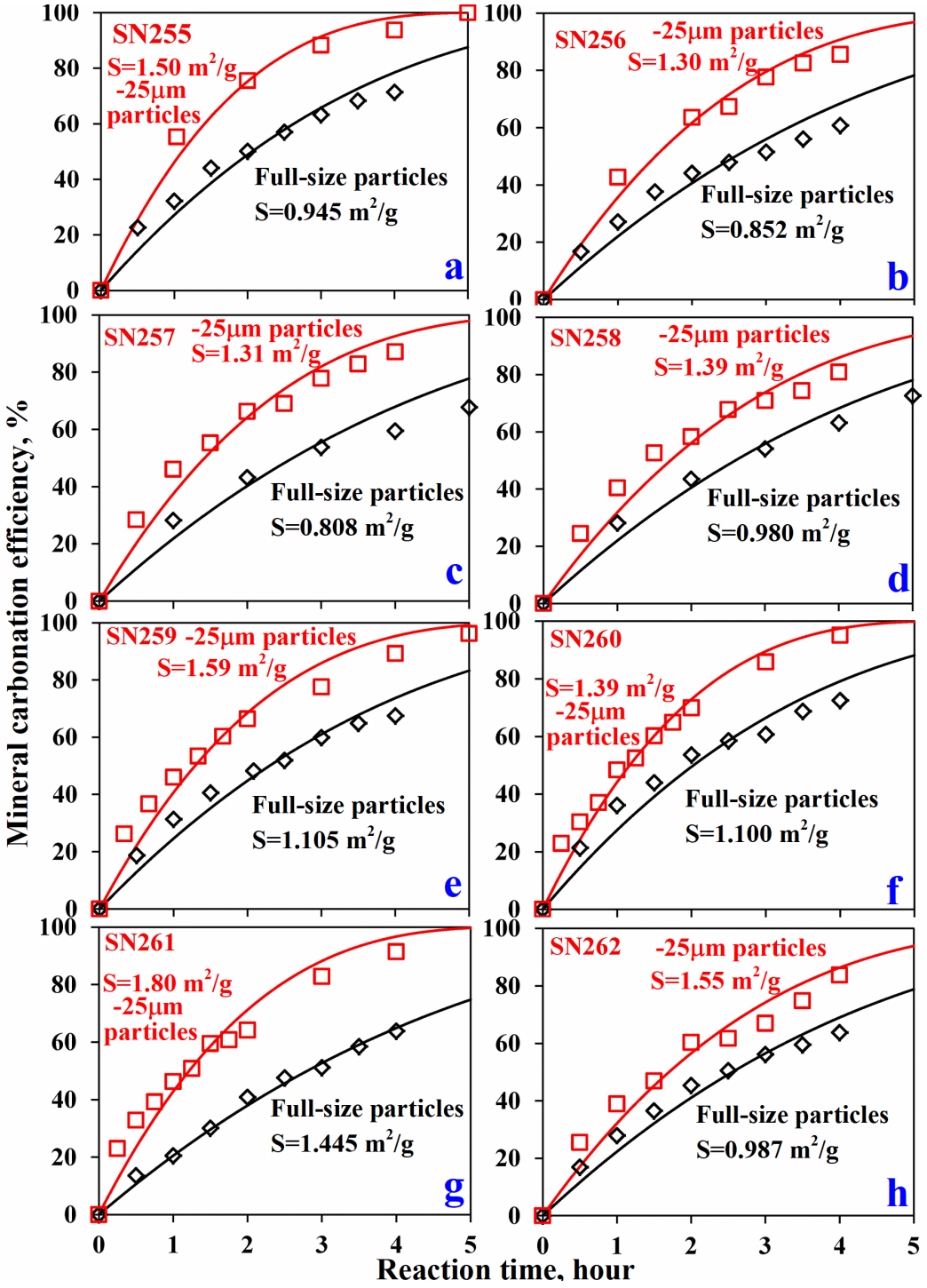

Figure 6.18 Application of the quantitative kinetic formula to carbonation of Turnagain samples with considering olivine content: (a) Turnagain SN255; (b) Turnagain SN256; (c) Turnagain SN257; (d) Turnagain SN258; (e) Turnagain SN259; (f) Turnagain SN260; (g) Turnagain SN261 and (h) Turnagain SN262. Red for -25 μm particles and black for full-size particles.

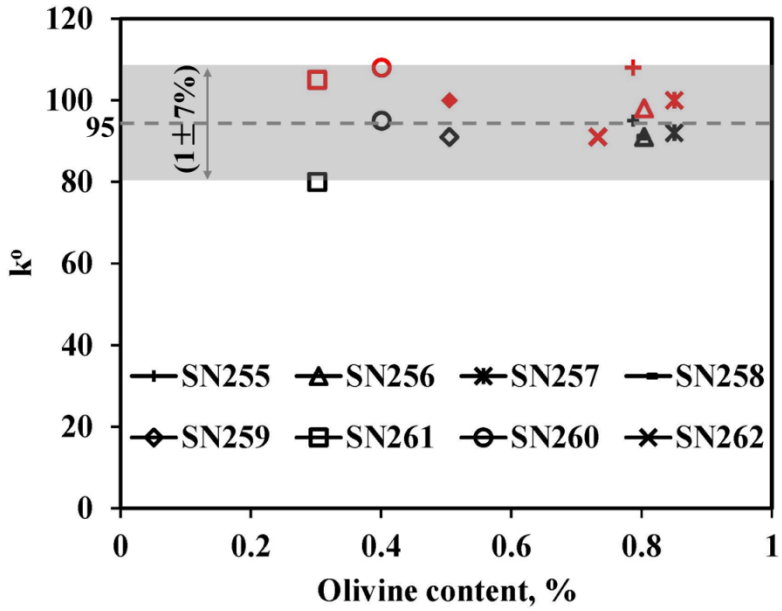

Figure 6.19 Relationship between k^o and olivine content of Turnagain samples SN255-262 (Red is for -25 μm particles and Black is for full-size particles)

In order to test the applicability of the kinetic model to Turnagain samples, the full-size Turnagain samples were also carbonated under the same conditions and the results well fit to the kinetic formula with the same values of parameters as used for the -25 μm particles (as shown in Figure 6.18). The full-size Turnagain particles were ground in a rod-mill and filtered by a pressure filtration. The particle size distribution for the full-size particles of each Turnagain sample is shown in Figure 6.12(b). The P_{80} values of the full-size particles also varied from 33 μm (for Turnagain SN261) to 54 μm (for Turnagain SN257) and the specific surface area analyzed by the Malvern Mastersizer was from 0.808 m^2/g (for Turnagain SN257) to 1.445 m^2/g (for Turnagain SN261), respectively. Sampling during carbonation was done using the ball valve. As seen in Figure 6.18, all the experimental data for the full-size Turnagain particles still matched well to the predicted data based on the same kinetic parameters used. There was one set of data with a difference between the model prediction and the data which reached 14% for the Turnagain SN257 at 5 hours of carbonation reaction time. This might be due to the analysis

errors or sample preparation problems (such as sampling of dried solids for carbon analysis). Except for this data, there was good agreement between the quantitative kinetic model prediction and the experimental data. Even the Turnagain sample SN261 which had the lowest olivine content and the highest serpentine content exhibited good agreement between the experimental data and predicted curves. Therefore, it can be concluded that the quantitative kinetic formula can be still successfully applied on all the Turnagain samples tested, the narrow-size particles and the full-size particles, where the carbonation efficiency is based on the magnesium, iron and calcium contents and with considering olivine content.

Now that the kinetic formula has been verified to be suitable for all the Turnagain samples tested, and for all particle sizes when the mineral carbonation efficiency is based on the magnesium, iron and calcium contents and with consideration of olivine content, it is still necessary to present the results on the same basis as commonly employed in the literature. The universal method which has been generally accepted in the mineral carbonation field is to calculate the mineral carbonation efficiency based only on the total contents of magnesium, iron and calcium and without consideration of the olivine content. The olivine content in a specific sample can be only acquired by the QXRD analysis. Fortunately, there is a simple relationship between the two approaches. The latter mineral carbonation efficiency equals the former value multiplied by the olivine content percentage. Therefore, all the experimental data and the predicted data were re-calculated by simply multiplying the olivine content percentage as shown in Figure 6.20.

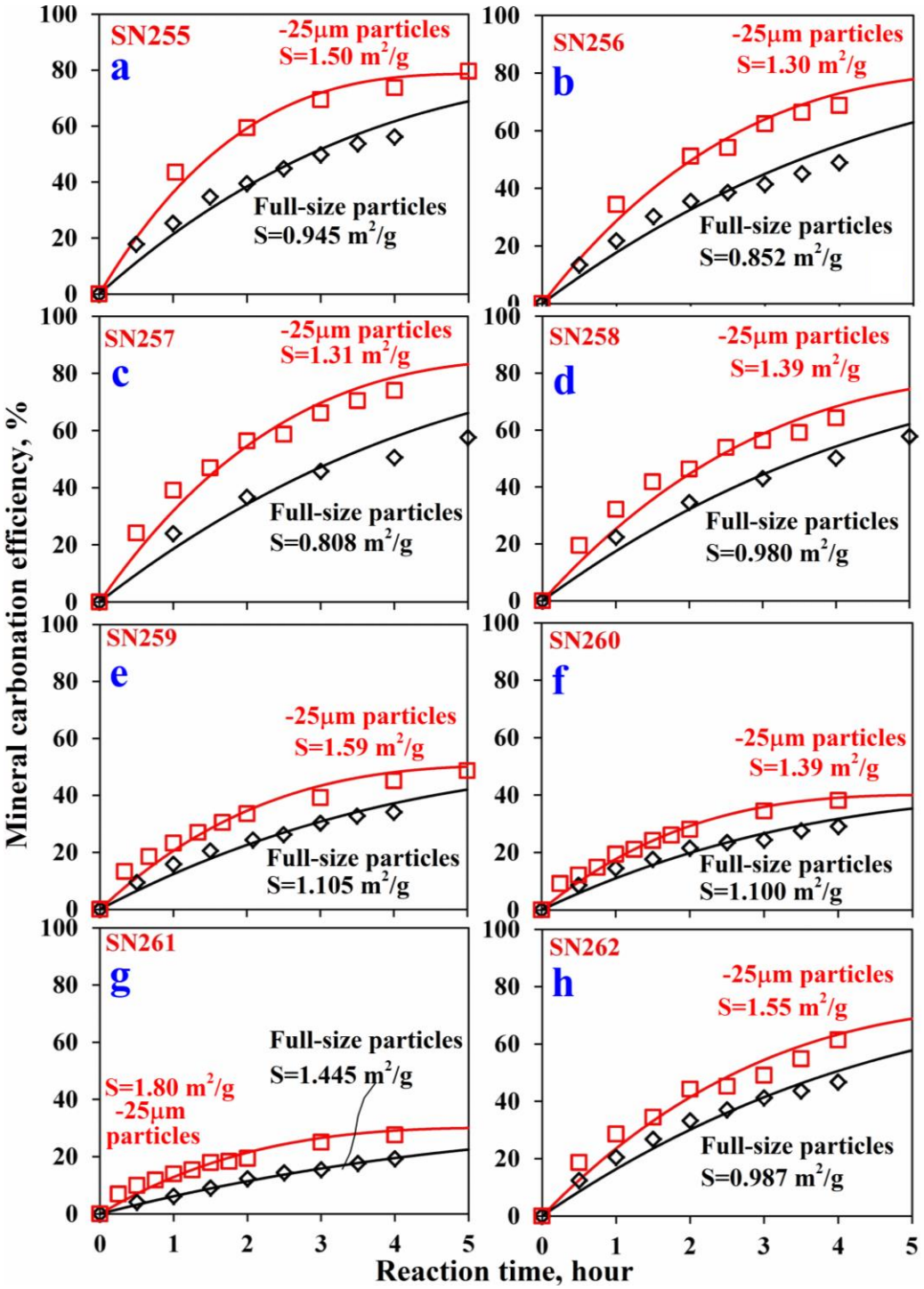

Figure 6.20 Application of the quantitative kinetic formula on the mineral carbonation of Turnagain samples: (a) Turnagain SN255; (b) Turnagain SN256; (c) Turnagain SN257; (d) Turnagain SN258; (e) Turnagain SN259; (f) Turnagain SN260; (g) Turnagain SN261 and (h) Turnagain SN262. Red for -25 μm particles and black for full-size particles.

It is clear that all the experimental data and the predicted curves matched well for all the Turnagain samples. The maximum difference between the experimental data and the predicted data for all the conditions was at most 8% (absolute error) which corresponds to the exceptional data in Figure 6.18. The mineral carbonation efficiency for Turnagain SN261 was only around 20%, but the kinetic model prediction matched the experimental data well.

Thus far, it has been verified that the quantitative kinetic model is suitable for the application to the mineral carbonation of silicate minerals when the carbonation process is controlled by the dissolution of olivine. The applicability of this formula is not affected by the mineral composition, mineral carbonation capacity, specific surface area or the particle size distribution. The variations in the kinetic factor may reflect the cumulative uncertainties in each of the factors that influence the carbonation rate (e.g. PCO_2, activation energy etc.), and perhaps other unaccounted characteristics of the materials. The kinetic formula developed in Chapter 5 can be applied on the carbonation of various minerals with the accuracy ±15% (absolute) where the majority reaction is carbonation of olivine.

In addition, in Chapter 2 it was suggested that the mineral carbonation process and a mineral processing process be combined to make the CO_2 fixation more profitable. In practice, the extent of carbonation of the minerals may be incomplete. To calculate the potential earned carbon credits, it is necessary to directly predict the sequestered CO_2 amount. The carbonation capability (stored CO_2 amount), ε, with unit t CO_2/t material, is calculated by the equation (6.1).

$$\varepsilon = \alpha \times m \tag{6.1}$$

Where, α is the carbonation efficiency shown in Figure 6.18 and m is the carbonation capacity (t CO_2/t material) which is shown in Table 4.5 for Turnagain samples.

For example, the carbonation capability for all the Turnagain samples can be calculated under the mineral carbonation conditions of 175 ℃, PCO_2=34.5 bar, 1.5 m $NaHCO_3$ and 10% solids content, as shown in Figure 6.19. The capabilities of a particular integrated process (mineral carbonation and mineral processing) may need to be re-calculated according to the detailed conditions. Nevertheless, this indicates that the kinetic model can be readily used to estimate the potential of the carbon sequestration for an application.

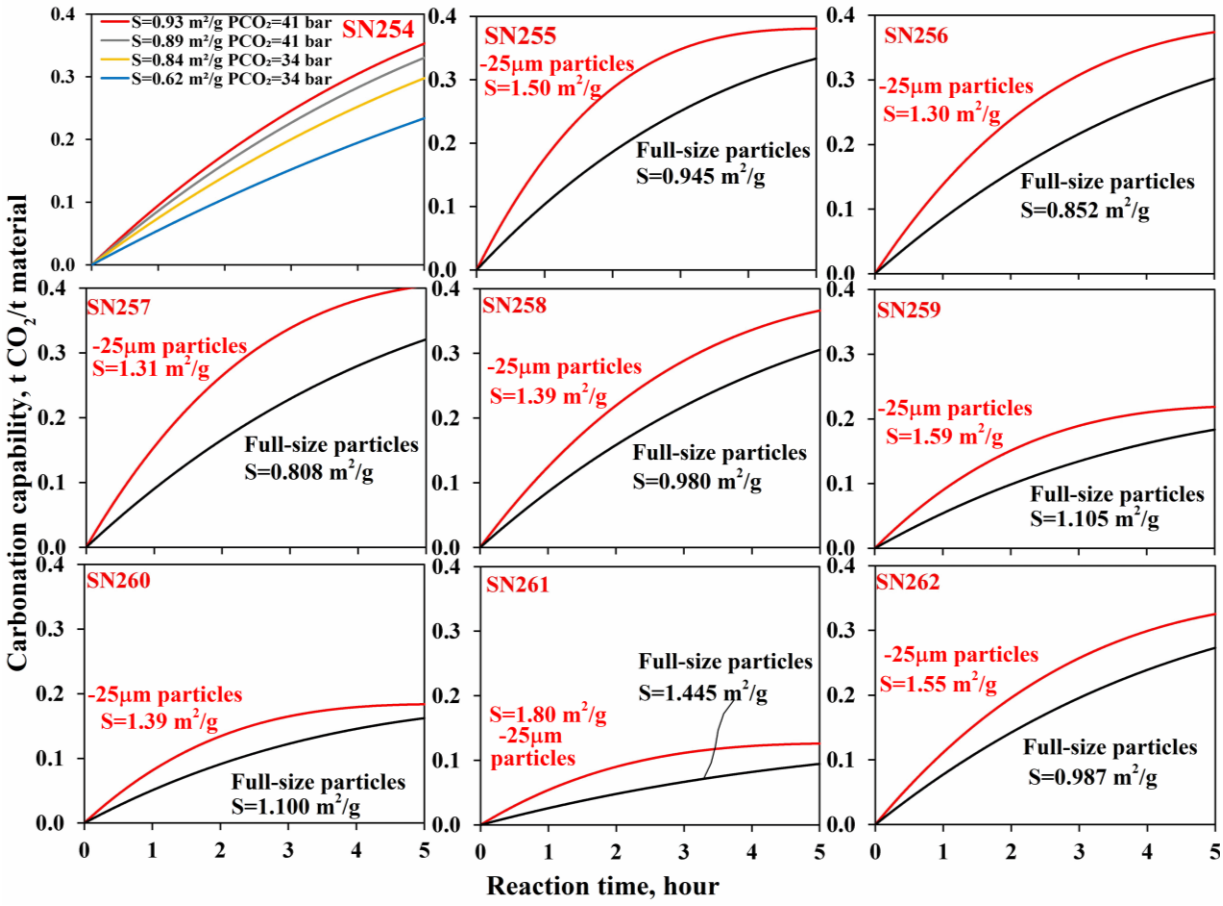

Figure 6.21 Application of the kinetic formula to predicting carbonation capability (t CO_2/t material) of Turnagain samples under the conditions of 175 ℃, PCO_2=34.5 bar, 1.5 m $NaHCO_3$ and 10% solids content.

6.6 Conclusions

The application of the quantitative kinetic formula to Turnagain samples has been developed. The following conclusions can be demonstrated:

(1) The kinetic formula can be applied to mineral carbonation of silicate minerals when the rate was under the chemical reaction control, regardless of the mineral compositions, olivine content, mineral carbonation capacity, specific surface area and the particle size distribution. The effects of specific surface area, CO_2 partial pressure and concentration sodium bicarbonate on the mineral carbonation efficiency were still modelled according to the following formula: $\alpha = (1 - (1 - k^o \times [S]^{0.7} \times [P_{CO2}]^{1.6} \times [NaHCO_3]^{0.8} \times e^{(-47970/RT)} \times t)^3) \times 100\%$. The accuracy of the prediction by the kinetic formula was within 15% of the experimental mineral carbonation efficiency.

(2) The mineral carbonation mechanisms elucidated from the high-grade olivine carbonation were also applicable to the carbonation reaction of the Turnagain samples. The morphology of the carbonated products consisting of a porous void between the polycrystalline carbonate layer and unreacted olivine was universally observed forthe carbonated products of all the Turnagain samples.

(3) The magnetite, iron sulfides (or metal sulfides in general), pyroxene and phologopite did not significantly participate in the mineral carbonation reactions. Naturally occurring serpentine, without heat pre-treatment, had much lower carbonation rates than olivine. Magnetite was observed to act as a nucleation site for the precipitation of the magnesium and/or iron ions and the carbonate ions in the aqueous solution.

(4) The experimental reactor for high temperature and pressure carbonation and especially the choice of the sampling control valve were important for the kinetic analysis. A needle valve control system was not always able to provide a representative sample of the reactor slurry and could change the particle size distribution in the reactor after repeated collection of samples. A ball valve system for the sampling during the elevated temperature and pressure reaction was effective and did provide representative samples.

(5) The direct evaluation of the mineral carbonation efficiency for the mixed mineral samples requires careful consideration of the mineral composition. It is necessary to evaluate the mineral carbonation efficiency by considering the olivine content and the magnesium, iron and calcium contents. The residual content of other silicate minerals which contained bivalent metals but which were not involved in the carbonation reaction, increased with time. This can bias the kinetic analysis based on the shrinking core model and can lead to erroneous conclusions, for example suggesting that product layer diffusion actually control the reaction kinetics. In fact, with a sufficiently high concentration of sodium salts ($NaHCO_3$ or NaCl) and moderate CO_2 partial pressure, the mineral carbonation reaction was always controlled by the chemical reaction of olivine dissolution.

7 Utilization of mineral carbonation for metal sulfidization

Mineral carbonation was found to be controlled by the dissolution of olivine under conditions conductive to the highest reaction rates. The rate can be accelerated under the conditions of high concentration of sodium salts (Na_2CO_3 and/or NaCl) and moderate CO_2 partial pressure. The carbonation of olivine was always responsible for the majority of the mineral carbonation process for natural samples without heat pre-treatment. A kinetic formula was developed and can be applied to predict the mineral carbonation efficiency and also to provide insights for the suitable carbonation parameters. All these findings provide the fundamentals for the development of the utilization of the mineral carbonation. The mineral carbonation process chemically transforms mineral silicates and CO_2 gas into stable carbonate precipitates and silica. The next question that arises is whether the nickel and cobalt values in the silicate minerals can be recovered by a supplemental process. This chapter reports the study of carbonation with sulfidization to form secondary sulfide precipitates for recovery by conventional mineral processing unit operations.

The mechanism and kinetics of mineral carbonation are illustrated in Figure 7.1. The mineral carbonation process is controlled by the chemical reaction between protons and olivine with addition of sodium bicarbonate and moderate PCO_2. The increase of PCO_2 and the concentration of bicarbonate ions enhance the supply of protons to the dissolution of olivine. The addition of sodium bicarbonate also apparently facilitates the diffusion of soluble silica away from the unreacted olivine surface, avoiding any surface obstruction by the formation of a product layer. At the same time, the released bivalent ions, including Mg^{2+}, Fe^{2+}, Ni^{2+} and Co^{2+}, react with the carbonate ions in solution to precipitate as polycrystalline carbonates. The polycrystalline carbonates layer is porous and therefore the product layer did not limit the mineral carbonation

process. There is a porous void between the polycrystalline carbonates and the unreacted olivine core. The bivalent ions formed on attack of the olivine diffused from the olivine surface to precipitate as the polycrystalline carbonates layer.

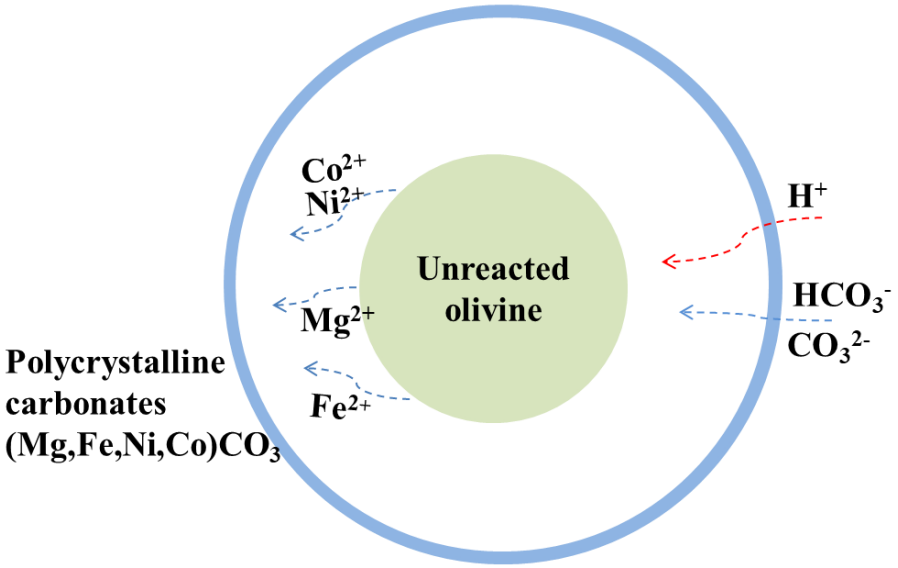

Figure 7.1 Schematic representation of the process of mineral carbonation of olivine under chemical reaction control.

The use of sulfide has been studied as an alternate method to form nickel and cobalt sulfides in place of the carbonate minerals that would naturally form during mineral carbonation. There are two general processes to sulfidize these valuable metals. One is to sulfidize the metal ions before the precipitation as carbonates and after the dissolution of olivine. This is referred to as in-situ sulfidization since the sulfidization happens during the mineral carbonation process. The other is to sulfidize the metal carbonates after the mineral carbonation process. This is referred to as the ex-situ sulfidization since the sulfidization and the mineral carbonation are discrete, sequential processes. The cobalt content in the Turnagain samples and the high-grade olivine sample was low (less than 0.02% Co). It was therefore difficult to accurately evaluate the sulfidization efficiency of cobalt in this work. In contrast, the nickel content was much higher. The nickel

content in the form of silicates in the high-grade olivine was 0.27% Ni, much higher than the cobalt. However, the behaviour of the nickel and cobalt is believed to be similar during the mineral carbonation and sulfidization processes. Therefore, the major criteria to evaluate the sulfidization process were to analyze the nickel sulfides content and the molar ratio of nickel/iron sulfides in the products. The in-situ sulfidization was attempted by two methods. One was by initial addition of sulfide ions using sodium sulfide nonahydrate added to the carbonation slurry. The other was by continuously providing sulfide ions through continuously injecting hydrogen sulfide gas into the carbonation slurry (during carbonation) or through initial addition of iron sulfide minerals. The ex-situ sulfidization experiments used sodium sulfide nonahydrate to sulfidize the products of the mineral carbonation in a subsequent process step.

7.1 In-situ metal sulfidization

The in-situ metal sulfidization tests were carried out by providing sulfide ions during the mineral carbonation process. The sulfide sources for this sulfidization tests were from sodium sulfide, hydrogen sulfide and iron sulfide sample. The work of the in-situ metal sulfidization in this Chapter is summarized in Table 7.1. Test conditions, the main outcomes and problems are summarized. Generally, it presents that it is possible to convert the valuable metals (e.g. nickel) to metal sulfide by utilizing the mineral carbonation process shown in Figure 7.1. The conversion of valuable metals from olivine is directly related to the extent of mineral carbonation. However, the in-situ metal sulfidization has to address the co-precipitation problem of nickel sulfide and iron sulfide.

Table 7.1 Summary of work on in-situ metal sulfidization during mineral carbonation of -25 μm high-grade olivine.

Methods	Sulfide source	Conditions	Results
By pre-addition of sodium sulfide (Na_2S)	Na_2S 0.1 ~ 0.6 m	175 ℃ PCO_2= 34.5 bar 1 m $NaHCO_3$ 5 h	• Nickel conversion efficiency dependent on dosage of Na_2S. • No selectivity for precipitation of nickel sulfide over iron sulfide.
	Reaction time 1 ~ 5 h	175 ℃ PCO_2= 34.5 bar 1 m $NaHCO_3$ 0.5 m Na_2S	• Nickel conversion efficiency dependent on the extent of mineral carbonation. • No selectivity for precipitation of nickel sulfide over iron sulfide.
By continuously providing mixed gas 95% CO_2 + 5% H_2S	PCO_2=26.1 bar + PH_2S=1.4 bar	150 ℃ 1.5 m $NaHCO_3$	• Enhanced selectivity for precipitation of nickel sulfide over iron sulfide. • Limited improvement of Nickel conversion efficiency. • Improvement of up to 25% for mineral carbonation efficiency.
	PCO_2=26.9 bar + PH_2S=1.5 bar	135 ℃ 1.5 m $NaHCO_3$	
	PCO_2=28.2 bar + PH_2S=1.5 bar	115 ℃ 1.5 m $NaHCO_3$	
By pre-addition of iron sulfide mineral	Iron sulfide mineral 30% ~ 70%	175 ℃ PCO_2=34.5 bar 1.5 m $NaHCO_3$ 4 h	• Nickel conversion efficiency dependent on the amount of iron sulfide mineral pre-added. • Enhanced selectivity for precipitation of nickel sulfide.

7.1.1 In-situ metal sulfidization by pre-addition of sodium sulfide during carbonation

The in-situ metal sulfidization experiments by pre-addition of sodium sulfide were carried out under the conditions of -25 μm high-grade olivine particles, 175 ℃, PCO_2=34.5 bar, 10% solid content, with 1 m $NaHCO_3$. The effects of variable dosages of sodium sulfide with 5 hours reaction time on the nickel conversion and carbonation efficiency are shown in Figure 7.2. The addition of sodium sulfide nonahydrate had no detrimental effect on the mineral carbonation efficiency. The carbonation efficiency was 78% compared with the efficiency 74% without addition of sodium sulfide under otherwise identified conditions. Meanwhile, with increasing the

dosage of the sodium sulfide, the nickel conversion efficiency was increased to approximately 63% for addition of 0.6 m sodium sulfides. The nickel conversion efficiency was almost proportional to the dosage of sodium sulfide, shown by R^2=0.96 in Figure 7.2. The apparent nickel conversion efficiency without addition of sodium sulfide was 7.5%. This is a systematic analytical error and is due to the lack of perfect selectivity of the bromine-methanol digestion method for nickel sulfide analysis over nickel in olivine. This method is the most selective for determination of nickel as nickel sulfide, but clearly there is some error in this analysis[138,139]. These results demonstrate that it is possible to sulfidize nickel that is released from the olivine during mineral carbonation.

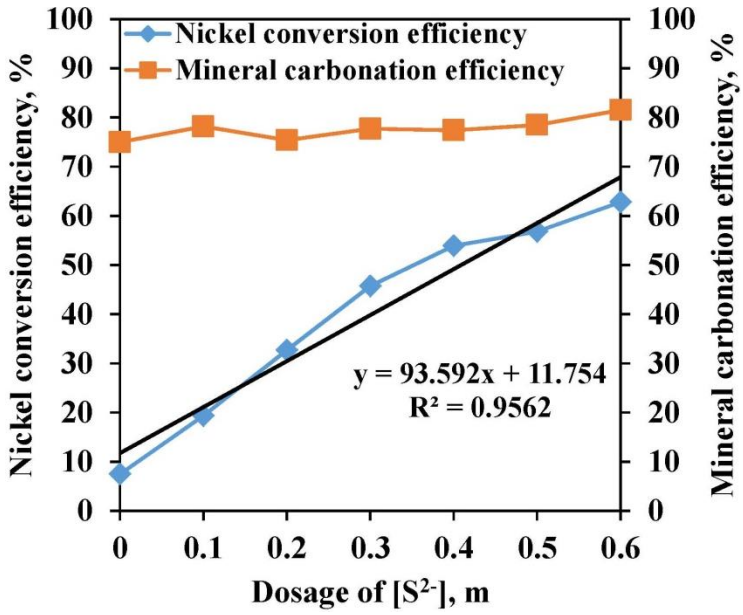

Figure 7.2 Effects of the dosage of sodium sulfide on the nickel conversion for in-situ sulfidization under the conditions of -25 μm high-grade olivine particles, 175 ℃, PCO_2= 34.5 bar, 10% solid content, with addition of 1 m $NaHCO_3$ for 5 hours.

However, it is noted that the added sodium sulfide was very much higher than the stoichiometric value, 0.005 m, which was calculated based on the nickel content 0.27% in the olivine. The some of the additional sulfide formed iron sulfides from the iron released during carbonation. The

corresponding molar ratio of the iron-to-nickel sulfides was analyzed and the results are shown in Figure 7.3. The molar ratio of iron-to-nickel sulfides in the products was around 27. This ratio is almost equal to the molar ratio of the total iron-to-total nickel (28) in the olivine. The molar ratio of iron-to-nickel is less than 1.5 for the bromine-methanol digestion of the untreated olivine. The fluctuation of the molar ratio of the iron-to-nickel sulfides around 27 may be due to experimental variations in the carbonation/sulfidization tests or due to uncertainties in the bromine-methanol analysis procedure. There was no selectivity between the precipitation of nickel sulfides and the precipitation of iron sulfides even though the target nickel in silicates was converted to the nickel sulfides. This presents a serious problem. Even if the sulfidized products may be recovered by flotation, such a high molar ratio of iron/nickel would make it impossible to obtain valuable nickel concentrates. The sulfur content distribution was also analyzed for the in-situ sulfidization by adding the sodium sulfide, as shown in Figure 7.4. It can be seen that the sulfur content in the products increased with increasing the dosage of sodium sulfide to around 5% sulfur for the maximum dosage. This value is so high that the final products after the mineral carbonation and the sulfidization would present environmental and possibly human health risks. When the dosage of sodium sulfide was only 0.1 m, about 75% of the added sulfur reported to the final solid products as metal sulfides. With increasing the sulfide dosage, the percentage of the sulfur found in the final solid products accounting for the total added sulfur decreased to only 38% for the addition of 0.6 m sodium sulfide. A lot of the added sulfur apparently remained in the aqueous solution and/or the gas phase. Both are hazardous to the environment and to human health.

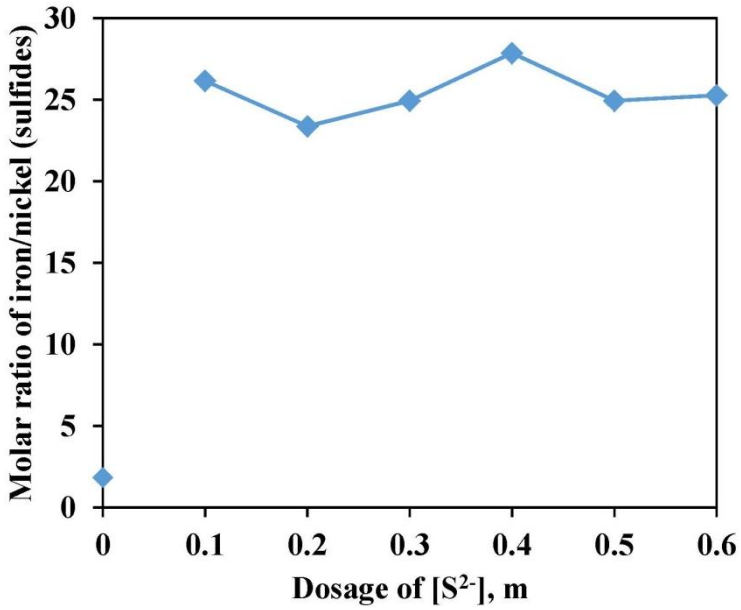

Figure 7.3 Effects of the dosage of sodium sulfide on the molar ratio of iron/nickel sulfides for in-situ sulfidization under the conditions of -25 μm high-grade olivine particles, 175 ℃, PCO_2=34.5 bar, 10% solid content, with addition of 1 m $NaHCO_3$ for 5 hours.

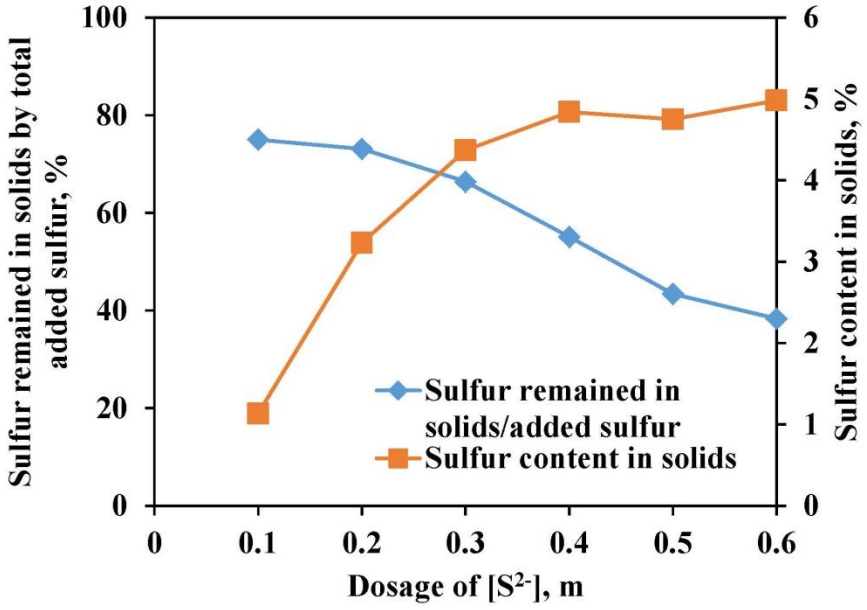

Figure 7.4 Effect of dosage of sodium sulfide on the sulfur content in product solids for in-situ sulfidization under the conditions of -25 μm particles, 175 ºC, PCO_2=34.5 bar, 10% solid content, with addition of 1 m $NaHCO_3$ for 5 hours.

The in-situ sulfidization of metals during mineral carbonation has been demonstrated but there were serious problems including the co-precipitation of iron sulfides and excessive consumption of sodium sulfides. It is necessary to address these deficiencies. The first approach was to further determine if the release of metals through the mineral carbonation process was a pre-condition to successful metal sulfidization. An experiment with sampling under the conditions of -25 μm high-grade olivine particles, 175 ℃, PCO_2=34.5 bar, 10% solid content, with addition of 1 m $NaHCO_3$ and 0.5 m sodium sulfide was carried out to test the assumption. The effects of the reaction time on the nickel conversion and mineral carbonation efficiency are shown in Figure 7.5. The nickel conversion was highly dependent on the mineral carbonation. Before the reaction, the mineral carbonation and the analyzed nickel conversion efficiency were 0 and 7.5% respectively (the latter being a systematic error as described before). At 1 hour of reaction, the mineral carbonation and nickel conversion efficiency increased to 20% and 28%, respectively. With increasing reaction time, the carbonation and nickel conversion efficiency increased to 74% and 60% respectively at 5 hours. Thus, it was confirmed that the mineral carbonation to release the metals ions from the silicates (olivine) is a pre-condition of the metal sulfidization. It is the one that the mineral carbonation can be utilized for the metal recovery enhancement.

The effect of reaction time on the molar ratio of iron/nickel in sulfides under the in-situ sulfidization conditions of -25 μm high-grade olivine particles, 175 ℃, PCO_2=34.5 bar, 10% solid content, with addition of 1 m $NaHCO_3$ and 0.5 m sodium sulfide is shown in Figure 7.6. The molar ratio of iron/nickel sulfides in products was always around 28 regardless of the reaction time. This indicates that iron and nickel were co-precipitated after release during carbonation. The SEM-EDX analysis of the sulfidized products under the conditions of -25 μm olivine particles, 175 ℃, PCO_2=34.5 bar, 10% solid content, with addition of 1 m $NaHCO_3$ and

0.4 m sodium sulfide for 5 hours is shown in Figure 7.7. There was a porous void between the polycrystalline carbonate layer and the unreacted olivine consistent with chemical reaction rate control. There were iron-nickel sulfides particles attached to the surface of the polycrystalline carbonates. There was no indication of separate nickel sulfide particle formation. This finding confirms that it would be difficult to obtain a nickel sulfide concentrate from the non-selective co-precipitated nickel-iron sulfides.

Thus far, it has been confirmed that mineral carbonation releases the valuable metal ions from the olivine and provided the opportunity to form metal sulfides. This in-situ metal conversion depended on the dosage of sulfide ions but nickel sulfides were always co-precipitated with iron sulfides. The co-precipitation of the iron-nickel sulfides obviated the possibility of flotation to selectively produce a selective nickel sulfide concentrate.

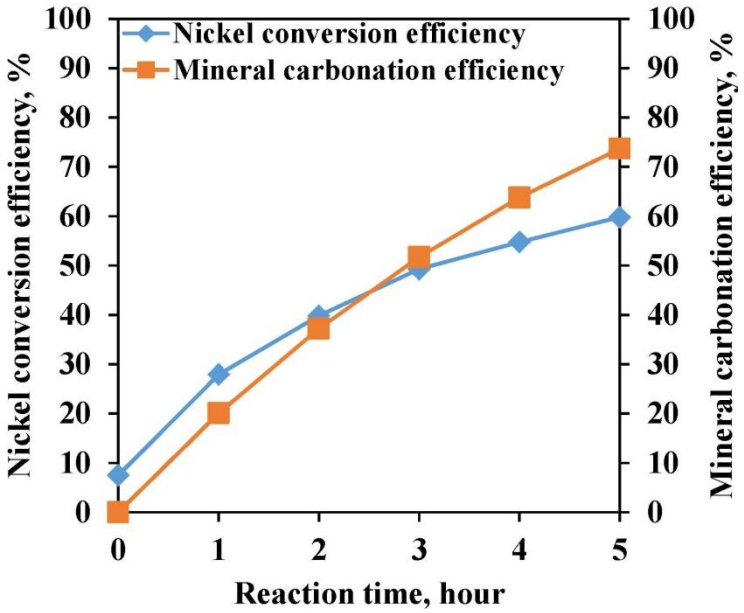

Figure 7.5 Effects of reaction time on the nickel conversion for in-situ sulfidization under the conditions of -25 μm high-grade olivine particles, 175 ℃, PCO_2=34.5 bar, 10% solid content, with addition of 1 m $NaHCO_3$ and 0.5 m sodium sulfide.

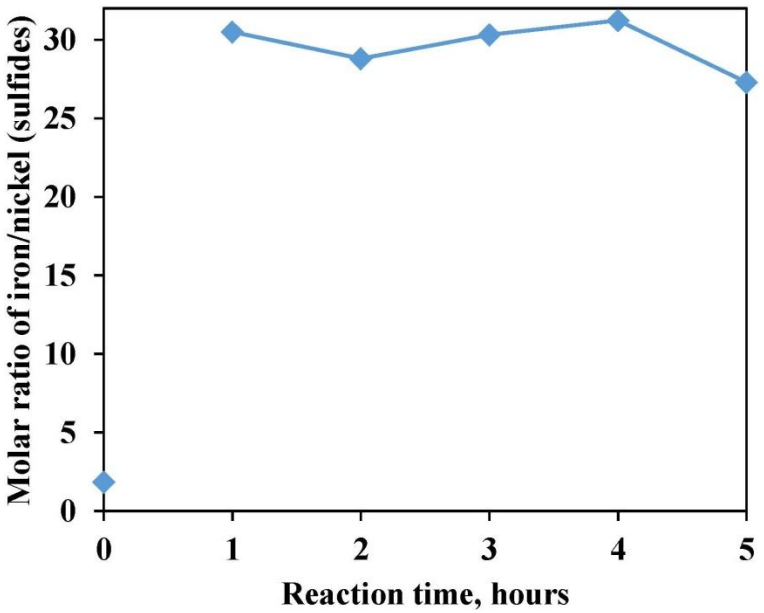

Figure 7.6 Effects of reaction time on the molar ratio of iron/nickel sulfides for in-situ sulfidization under the conditions of -25 μm olivine particles, 175 ºC, PCO_2=34.5 bar, 10% solid content, with addition of 1 m $NaHCO_3$ and 0.5 m sodium sulfide.

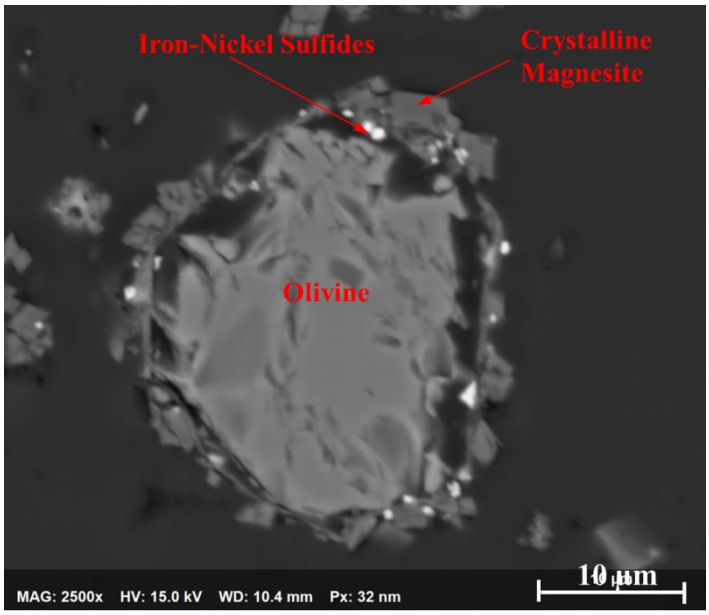

Figure 7.7 SEM-EDX image of products of the in-situ metal sulfidization under the conditions of -25 μm olivine particles, 175 ℃, PCO_2=34.5 bar, 10% solid content, with addition of 1 m $NaHCO_3$ and 0.4 m sodium sulfide for 5 hours.

In order to address this problem, it is necessary to review the fundamentals of carbonation and sulfidization. The key reactions are shown below.

$$Mg^{2+} + CO_3^{2-} = MgCO_3 \quad (7.1)$$

$$Fe^{2+} + CO_3^{2-} = FeCO_3 \quad (7.2)$$

$$Ni^{2+} + CO_3^{2-} = NiCO_3 \quad (7.3)$$

$$Fe^{2+} + S^{2-} = FeS \quad (7.4)$$

$$Ni^{2+} + S^{2-} = NiS \quad (7.5)$$

Reactions (7.1), (7.2) and (7.5) are the desired reactions for mineral carbonation and effective metal recovery. However, Reaction (7.1), (7.4) and (7.5) also occurred during the in-situ sulfidization and mineral carbonation process. Fortunately, Reaction (7.3) has been avoided and Reaction (7.5) has been promoted. Reaction (7.1) has also occurred as the main carbonation process. The key issues are how to hinder Reaction (7.4) and to facilitate Reaction (7.2). Nickel sulfide and cobalt sulfide are much more insoluble than iron sulfide, as shown in Table 2.2. In addition, the nickel, cobalt and iron sulfides are much more insoluble than the corresponding nickel, cobalt and iron carbonates. Therefore, Reactions (7.6) and (7.7) may be considered.

$$NiCO_3 + FeS = NiS + FeCO_3 \quad (7.6)$$

$$CoCO_3 + FeS = CoS + FeCO_3 \quad (7.7)$$

The Reactions (7.6) and (7.7) are based on the principle that the more insoluble substance is preferred during the reactions among insoluble chemicals. The corresponding standard Gibbs free energy changes for the Reaction (7.6) and (7.7) are shown in Figure 7.8. According to Figure 7.8, Reactions (7.6) and (7.7) are thermodynamically favourable between 0 ℃ and 200 ℃. Reaction (7.7) is more favourable than Reaction (7.6) since Reaction (7.7) has the lower

standard Gibbs free energy change. With increasing temperature, there was no obvious change in $\triangle G^{\circ}$ for both Reactions (7.6) and (7.7). This means that it is thermodynamically possible to selectively precipitate nickel (or cobalt) sulfides using the iron sulfide.

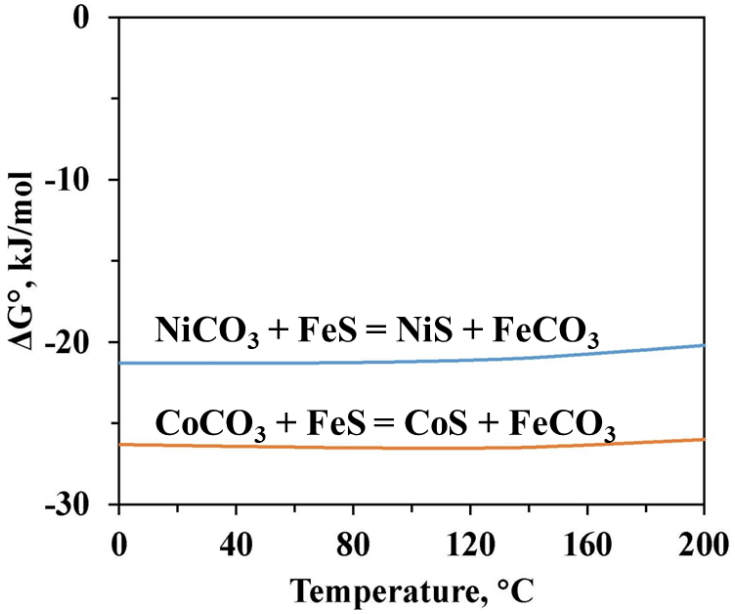

Figure 7.8 Standard Gibbs free energy changes for the reactions between iron sulfide and nickel/cobalt carbonates with temperature (Data from HSC 7.1).

However, what prevented Reactions (7.6) and (7.7) forming NiS and CoS during the in-situ sulfidization by pre-loading sodium sulfide? Why was there still such a high iron sulfide content in the final sulfidization and mineral carbonation products? To answer these questions, the reaction between the pure iron sulfide and crystalline cobalt carbonate was studied under the conditions of 175 ℃, PCO_2 = 34.5 bar, 1.8% solids content, molar ratio of $FeS/CoCO_3$ = 1.2 and [FeS] = 0.09 m. The results are shown in Figure 7.9. The pure cobalt carbonate and the pure iron sulfide were powders with 75% -38 μm particle size as indicated by the laser particle size analysis. The reason for using crystalline cobalt carbonate rather than nickel carbonate were: the reaction of iron sulfide and cobalt carbonate is thermodynamically more favourable than the

reaction between iron sulfide and nickel carbonate and also it is difficult to purchase crystalline nickel carbonate or to make the pure crystalline nickel carbonate products. The reason for choosing the PCO_2=34.5 bar was to simulate the mineral carbonation process. The high-purity iron and sulfide and crystalline cobalt carbonate were analyzed by XRD and the images are shown in Figure 7.10. According to Figure 7.9, it was found that the reaction between pure cobalt carbonate and pure iron sulfide was very slow. The cobalt conversion efficiency was only 19% at 27 hours though the conversion efficiency slowly increased with prolonging reaction time. The apparent initial cobalt conversion efficiency at time zero was 12%. This again represents a limitation of the selectivity of the bromine-methanol digestion analysis method.

In addition, according to the precipitation diagram of the carbonates and sulfides (Figure 7.11), the precipitation lines of nickel sulfide and iron sulfide are always below the corresponding nickel carbonate and iron carbonate lines because the nickel (iron) sulfides are always more insoluble than the corresponding carbonates. The change of the partial pressure of CO_2 gas or H_2S gas has no significant effect on the H_2S-S^{2-} or CO_2-CO_3^{2-} line. With continuous injection of CO_2 gas for the mineral carbonation, the pH values of the aqueous solution may remain stable while the preloading of carbonate ions as $NaHCO_3$ may enhance the precipitation of metal carbonates. It is possible to precipitate nickel sulfide and iron carbonate in a system because the concentration of aqueous sulfide ions and carbonate ions can be controlled. For example, during the in-situ mineral carbonation under the conditions of PCO_2=34.5 bar with addition of 1 m $NaHCO_3$ and 0.4 m Na_2S, the practical carbonate ions concentration can be thermodynamically calculated to be around 0.00039 m and the corresponding log[Fe^{2+}] for $FeCO_3$ is about -8. At this time, if the concentration of sulfide ions can be controlled to less than 10^{-8} m, the corresponding log[Fe^{2+}] for FeS is approximately -7. $FeCO_3$ rather than FeS would be preferentially

precipitated. In contrast, in the same system, the log[Ni^{2+}] for $NiCO_3$ and for NiS is -10 and -12 respectively. Then the NiS rather than $NiCO_3$ would be preferentially precipitated. Another example is for the conditions where with the concentration of carbonate ions and sulfide ions are controlled at $10^{-3.4}$ m and 10^{-9} m, respectively. As a result, the log[Fe^{2+}] for $FeCO_3$ and for FeS is -8 and -6.5 respectively while the log[Ni^{2+}] for $NiCO_3$ and for NiS would be -10 and -11 respectively. Under these conditions, $FeCO_3$ and NiS would preferentially precipitate. The results are expected to be applicable to the mineral carbonation and utilization for metal sulfidization and the conditions are controllable. In fact, there is a suitable range for the reasonable sulfide ions according to Figure 7.11 to selectively sulfidize the released valuable metal ions. The concentration of carbonate ions in the mineral carbonation system with PCO_2 from 28 bar to 41 bar and addition of 1.5 m sodium bicarbonate at 175 ℃ would be very low to around $10^{-3.4}$ m. The log[CO_3^{2-}] should be close to -3.4. As a result, the logarithm of soluble Fe^{2+} and Ni^{2+} from $FeCO_3$ and $NiCO_3$ is approximately -8 and -10, respectively. Therefore, as long as log[Fe^{2+}] and log[Ni^{2+}] for FeS and NiS are more than -8and less than -10, respectively, Ni^{2+} prefers to form NiS while Fe^{2+} prefers to form FeS. The corresponding log[S^{2-}] should be between -9.8 and -7.3. Therefore, the suitable concentration of aqueous sulfide ions which is continuously supplied should be controlled in the range of $10^{-9.8}$ m – $10^{-7.3}$ m.

Therefore, to sulfidize the nickel or cobalt ions and to simultaneously prevent the generation of iron sulfides during mineral carbonation, it is necessary to carefully control the concentration of sulfide ions in the range of $10^{-9.8}$ m – $10^{-7.3}$ m. The reason why the in-situ sulfidization by preloading sodium sulfide succeeded in the formation of nickel sulfides but failed to prevent generation of iron sulfides is that the concentration of the preloading sulfide ions was much higher than $10^{-7.3}$ m. As a result, both NiS and FeS preferred to be precipitated rather than $NiCO_3$

and $FeCO_3$. The precipitation of nickel sulfide and iron sulfide occurred until the concentration of sulfide ions was critically decreased to near to 0. In fact, there may be no way to effectively control the concentrations of sulfide ions and carbonates ions during the in-situ sulfidization through pre-addition of the sulfide ions. Since the release of nickel or cobalt ions from the silicate olivine is a gradual process and depends on the mineral carbonation process, it is believed that the supply of carbonate ions and sulfide ions must be continuous and stable at suitable level throughout the mineral carbonation and in-situ sulfidization process.

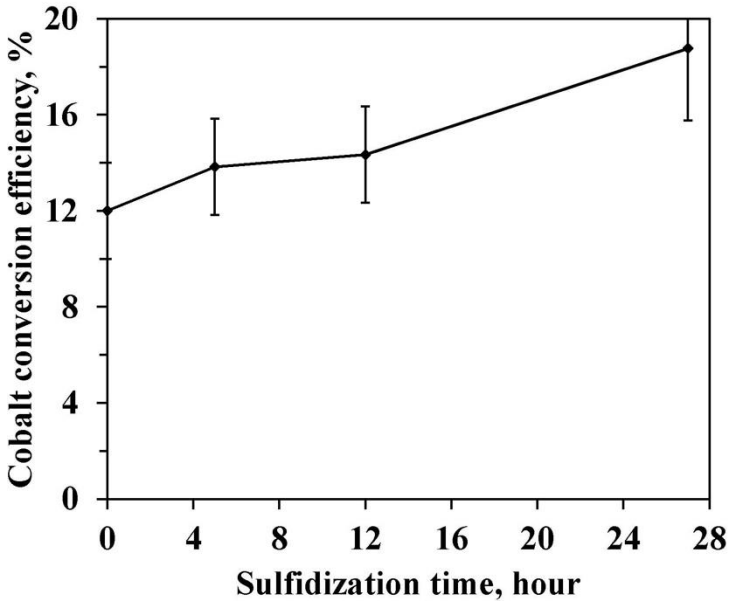

Figure 7.9 Cobalt sulfidization by iron sulfide using crystalline cobalt carbonate under the conditions of 175 ℃, PCO_2 = 34.5 bar, 1.8% solids content, molar ratio of $FeS/CoCO_3$ = 1.2 and [FeS] = 0.09 m.

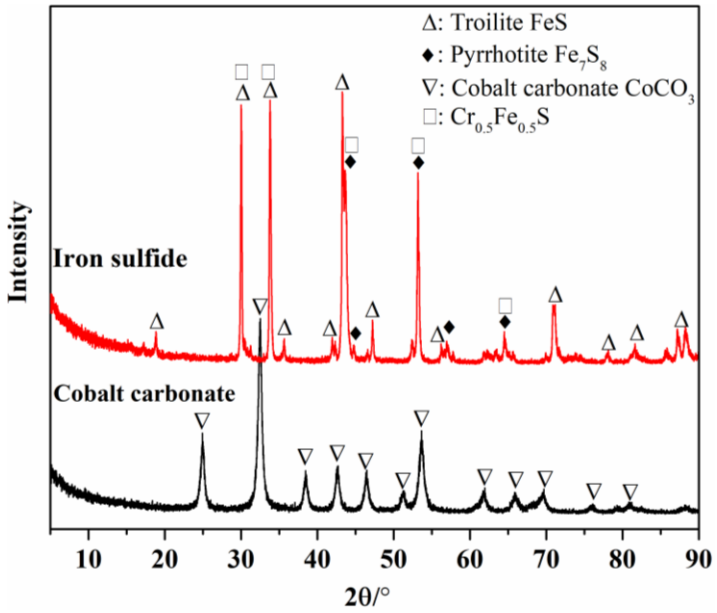

Figure 7.10 XRD patterns for pure crystalline cobalt carbonate and pure iron sulfide.

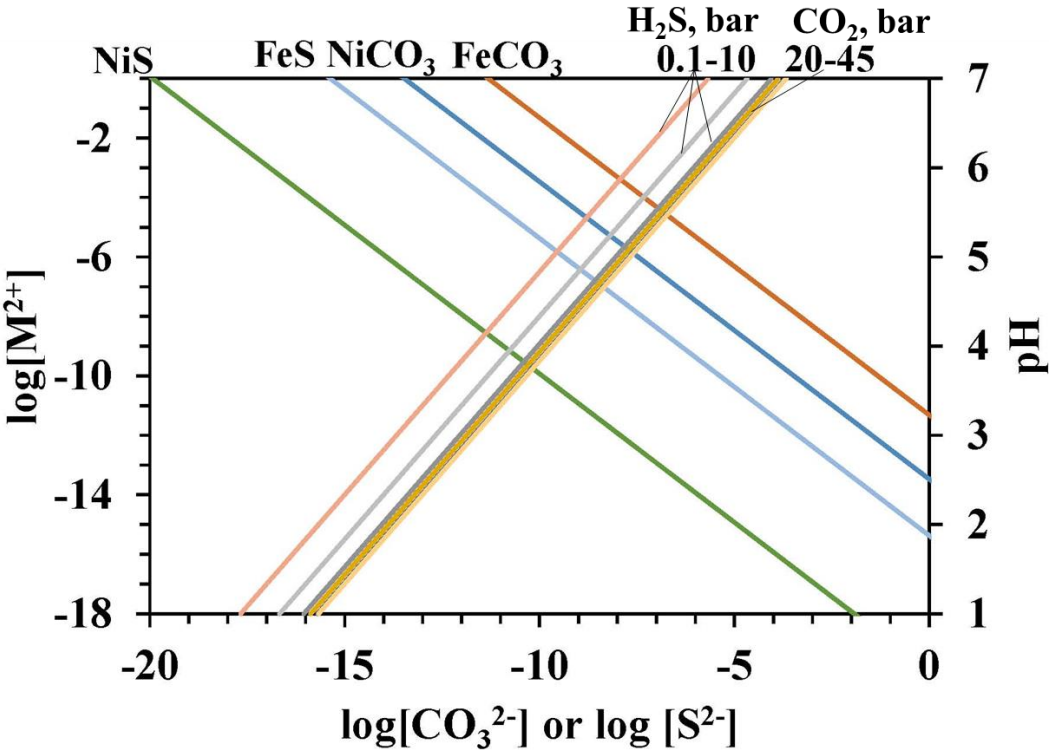

Figure 7.11 Precipitation diagram of metal carbonates and sulfides at 175 ℃.

7.1.2 In-situ metal sulfidization by a mixed gas of H_2S and CO_2

The fundamental review of carbonation and sulfidization confirms that it should be possible to form NiS and $FeCO_3$ by controlling the activity of sulfide. In-situ sulfidization by a mixed gas of CO_2 and H_2S wasused to test the above hypothesis by providing continuous and stable supplies of carbonate ions and sulfide ions. A gas containing of 95% CO_2 and 5% H_2S was obtained from by Praxair Technology, Inc. The maximum total pressure of gas was 41.4 bar. Since the mixed gas contained H_2S, it was necessary to use a corrosion-resistant stainless steel regulator (Praxair model PRS3022 5301330). The maximum outlet pressure of the regulator was 34.5 bar. As a result, in order to maintain the mineral carbonation process under by chemical reaction control, the tests of the in-situ sulfidization by the mixed gas were carried out under the total pressure less than 34.5 bar and the temperature less than 150 ℃. According to Table 5.1, the bulk solution pH value at PCO_2=26 bar should be around 7.2. The solubility of H_2S gas (PH_2S=1.4 bar) at 150 ℃ is calculated to around 5.6×10^{-5} m [S^{2-}] (based on the thermodynamic data from HSC 7.1). However, the dissolution of H_2S gas may decrease the aqueous pH value somewhat. It is difficult to accurately measure pH at high temperature and pressure thus far as well as with the effects of aqueous ionic strength. The actual sulfide ion concentration in the carbonation and sulfidization system may be different from the sample theoretical estimate.

The first test was carried out under the conditions of -25 μm olivine, 150 ℃, 1.5 m $NaHCO_3$, 10% solids content and PCO_2=26.1 bar and PH_2S=1.4 bar. The corresponding nickel conversion efficiency and molar ratio of iron/nickel sulfides in the solid products is shown in Figure 7.12. The nickel conversion efficiency was gradually increased by 24% to approximately 32% at 12 hours of reaction time while the mineral carbonation efficiency was 91%. The nickel conversion efficiency was still positively correlated with the mineral carbonation process. More importantly,

the molar ratio of the iron/nickel sulfides has been decreased to less than 10 from 28 obtained from the experiments on in-situ sulfidization by pre-addition of sodium sulfide. The molar ratio decreased with reaction time from a beginning value of 10.6 at 2 hours to around 1.8 at 12 hours. It is hard to confirm that the molar ratio would decrease further with reaction time; but the average molar ratio was 7.1. It was confirmed that a continuous and steady supply of sulfide ions and carbonate ions using a mixed gas can reduce the formation of iron sulfides and concurrently facilitate the nickel conversion. Unfortunately, the nickel conversion to nickel sulfide was much less than the extent of carbonation.

The second experiment was to further confirm the benefits of the continuous supply of the mixed gas under the conditions of -25 μm olivine, 135 ℃, addition of 1.5 m $NaHCO_3$, 10% solids content and PCO_2=26.9 bar and PH_2S=1.5 bar. In this second test the PCO_2 was increased by decreasing the operating temperature. (A lower operating temperature reduces the water vapour (steam) pressure and increases the PCO_2 for the same total pressure.) The test results are shown in Figure 7.13. Similar to Figure 7.12, Figure 7.13 also reveals that the nickel conversion efficiency gradually increased with the increasing of mineral carbonation efficiency. At 15 hours, the mineral carbonation efficiency and nickel conversion efficiency reached 84% and 19%, respectively. The nickel conversion efficiency was increased by 12% after 15 hours at temperature 135 ℃. Fortunately, the molar ratio of iron/nickel sulfides can be controlled at around 6.5 in spite of the fluctuation in the range from 3 to 9. The molar ratio did not decrease with time.

A third test was conducted with even higher PCO_2 above 27.6 bar by decreasing the system temperature to 115 ℃, so as to overcome the potential control by diffusion through a product layer. The test results under the conditions of -25 μm olivine, 115 ℃, addition of 1.5 m $NaHCO_3$,

10% solids content and PCO_2=28.2 bar and PH_2S=1.5 bar are shown in Figure 7.14. The nickel conversion efficiency was also increased by 9.5% to 18% within 36 hours while the corresponding mineral carbonation efficiency was increased by 88%. The molar ratio of iron/nickel sulfides was controlled much better to 2.7%±1.5%.

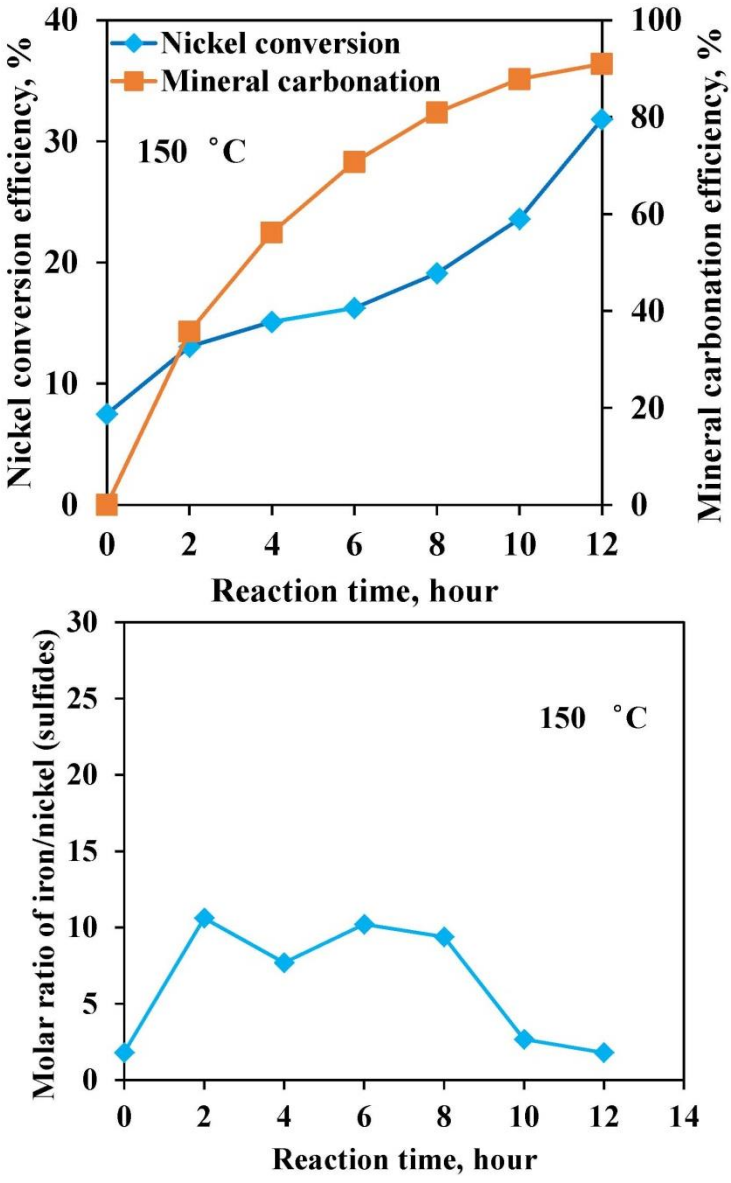

Figure 7.12 In-situ sulfidization by the mixture gas of 95% CO_2 and 5% H_2S under the conditions of -25 μm olivine, 150 ℃, addition of 1.5 m $NaHCO_3$, 10% solids content, PCO_2=26.1 bar and PH_2S=1.4 bar.

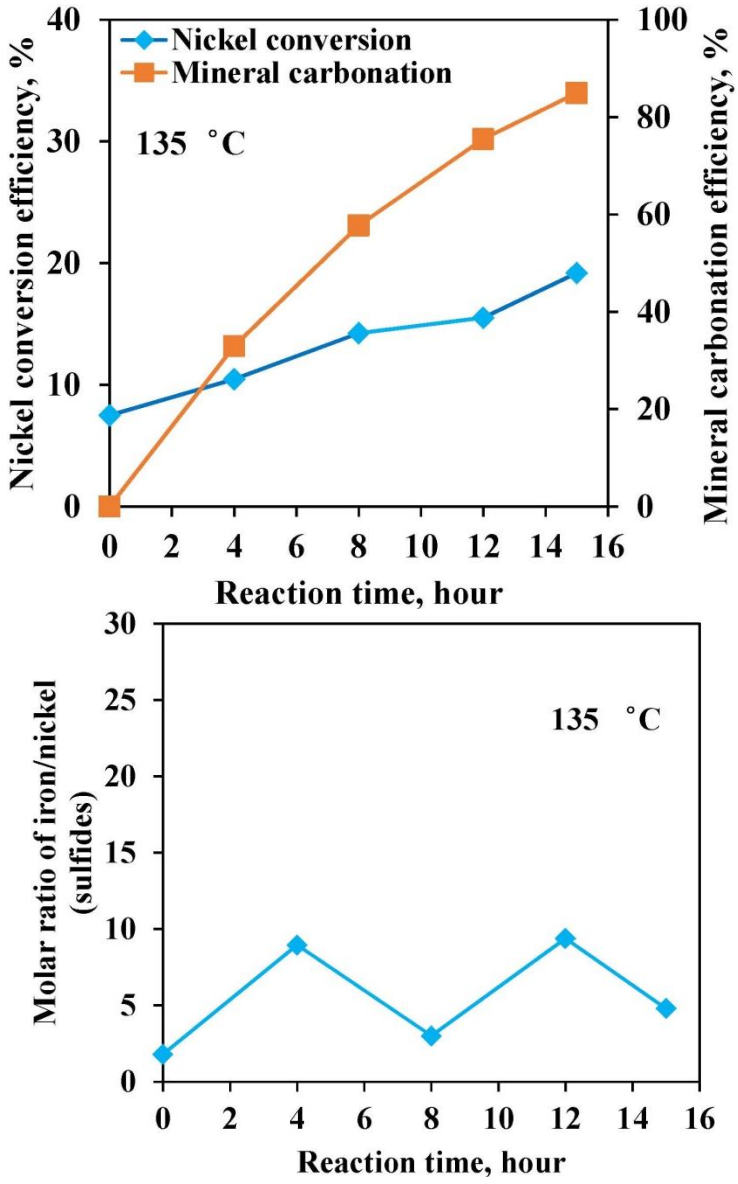

Figure 7.13 In-situ sulfidization by the mixture gas of 95% CO_2 and 5% H_2S under the conditions of -25 μm olivine, 135 ℃, addition of 1.5 m $NaHCO_3$, 10% solids content, PCO_2=26.9 bar and PH_2S=1.5 bar.

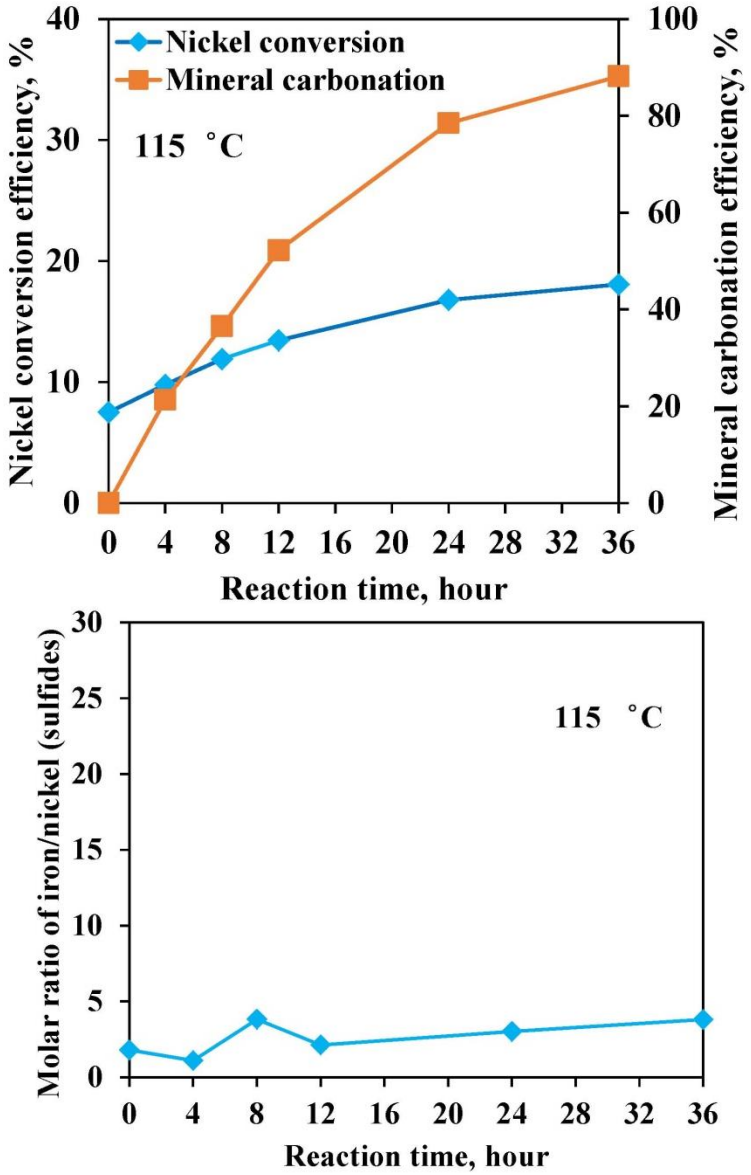

Figure 7.14 In-situ sulfidization by the mixture gas of 95% CO_2 and 5% H_2S under the conditions of -25 μm olivine, 115 ℃, addition of 1.5 m $NaHCO_3$, 10% solids content and PCO_2=28.2 bar and PH_2S=1.5 bar.

With summary of the in-situ sulfidization by the mixture gas of 95% and 5% H_2S, it can be concluded that though the nickel conversion efficiency was low at 32% (shown in Figure 7.12), the molar ratio of iron/nickel sulfides in products was controlled to less than 7.0 compared with 28 for the in-situ sulfidization by pre-addition of sodium sulfide. The in-situ sulfidization has

been much more selective and effective. However, there is a big difference between the mineral carbonation efficiency and the nickel sulfidization efficiency. What is the deportment of the balance of the nickel released during carbonation? According to Figure 7.11, the results can be analyzed. From the discussion in Chapter 5, the added sodium bicarbonate has a role as a catalyst in mineral carbonation of olivine. The sodium bicarbonate can transfer the protons and carbonate ions from the dissolution of CO_2 gas to react with olivine. It was confirmed that 1.5 m sodium bicarbonate is the optimal for olivine carbonation and the further addition is not significant. Therefore, it is believed that the thermodynamically effective carbonate ion concentration for the mineral carbonation is equal to $10^{-3.4}$ m. The corresponding $\log[CO_3^{2-}]$ was maintained around -3.4. Correspondingly, the $\log[Fe^{2+}]$ for $FeCO_3$ and $\log[Ni^{2+}]$ for $NiCO_3$ were -8 and -10, respectively. Owing to the PCO_2 about 27 bar, the corresponding pH value for the carbonation system was approximately 7.3 according to OLI stream simulation. The corresponding $\log[S^{2-}]$ would be approximately -4 which is calculated based on the thermodynamic data from HSC 7.1. Therefore, the $\log[Fe^{2+}]$ for FeS and $\log[Ni^{2+}]$ for NiS were -11.2 and -16, respectively. As a result, in principle, there would still be a problem to effectively precipitate the $[Ni^{2+}]$ as NiS and precipitate the $[Fe^{2+}]$ as $FeCO_3$ under these conditions. However, the experimental results show that the majority of the released both nickel and iron ions were apparently still formed into carbonates. This is because the practical pH values are difficult to accurately measure and the dissolution of H_2S gas may affect the aqueous pH. The practical sulfide ions might be still lower than $10^{-7.3}$ m. In order to address this problem, it is necessary to increase the continuous and stable concentration of sulfide ions to slightly higher level. Unfortunately, there was no way to continue to increase the concentration of sulfide ions with the gas mixture by increasing the PH_2S due to the limits of the tank pressure of the mixed gas and the outlet pressure limit (34 bar).

Nevertheless, from the comparison of the in-situ sulfidization by continuous mixed gas and by preloading sodium sulfide (Figure 7.15), the molar ratio of iron/nickel sulfides was successfully controlled with similar overall nickel conversion efficiency. The in-situ sulfidization both by continuously supplying mixed gas and by preloading 0.1 m sodium sulfide resulted in the nickel conversion efficiency approximately 19%. In contrast, the molar ratio of iron/nickel sulfides for the sulfidization by mixture gas and by preloading 0.1 m sodium sulfide were 4 and 26, respectively, and the sulfur content in the final solids were 0.6 % and 1.1%, respectively.

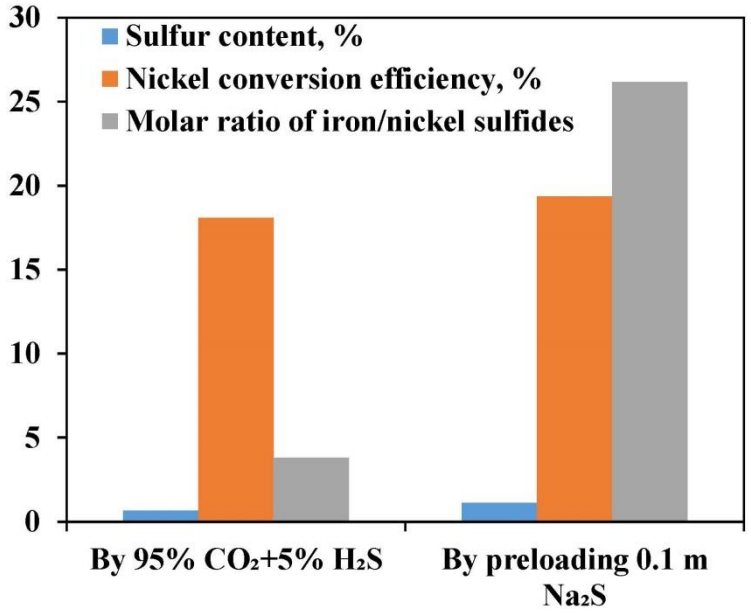

Figure 7.15 Comparison of in-situ sulfidization between by continuous mixture gas of 95% CO_2 + 5% H_2S and by preloading 0.1 m sodium sulfide (conditions for in-situ sulfidization by mixture gas: -25 μm olivine, 115 ℃, PCO_2=28.2 bar, PH_2S=1.5 bar, addition of 1.5 m $NaHCO_3$ for 36 hours; conditions for in-situ sulfidization by preloading sodium sulfide: -25 μm olivine, 175 ℃, PCO_2= 34.5 bar; addition of 1 m $NaHCO_3$ + 1 m NaCl for 5 hours).

In addition to the benefits of the successful control of iron sulfide precipitation, there was another credit for the mineral carbonation process. The mineral carbonation efficiency obtained by using the mixed gas was increased by up to 26% compared to using high-purity CO_2 gas, as shown in Figure 7.16. Both the carbonation processes were still controlled by chemical reaction

control. The reason why there was the significant increase in the mineral carbonation efficiency was possibly because the H_2S gas provided a higher concentration of protons to enhance the rate of dissolution of olivine. In addition, it may be because the H_2S provided a reductive phenomenon to accelerate the mineral carbonation by preventing the competitive oxidation of Fe(II) with dissolved O_2 or H_2O[155].

It is important to continuously supply suitable sulfide ions concentration for the in-situ sulfidization during mineral carbonation. It is possible to supply a mixed gas of CO_2 and H_2S for the in-situ sulfidization, though there is still a challenge to carefully control the H_2S partial pressure to selectively and completely form NiS instead of $NiCO_3$.

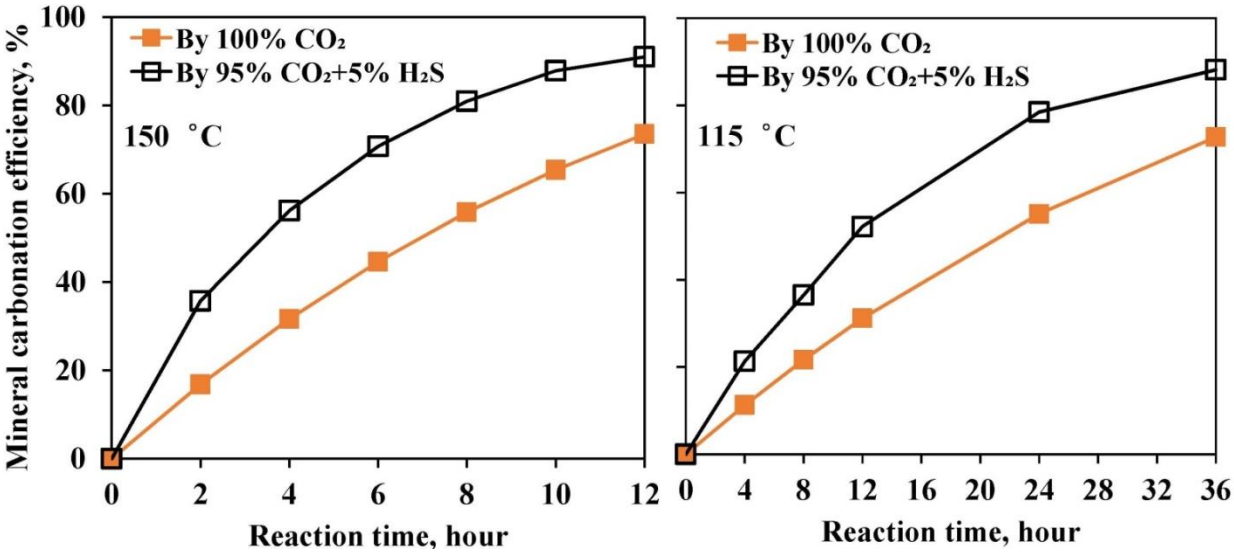

Figure 7.16 Comparison of mineral carbonation efficciency between by using high-purtiy CO_2 gas and by using mixture gas of under the conditions of -25 μm olivine with addition of 1.5 m $NaHCO_3$ (mixture gas at 150 ℃, PCO_2=26.1 bar, PH_2S=1.4 bar and at 115 ℃, PCO_2=28.2 bar, PH_2S=1.5 bar).

7.1.3 In-situ metal sulfidization by pre-addition iron sulfides

The continuous supply of sulfide ions via iron sulfide sample during the carbonation process is an alternate method to provide the necessary reagent to form NiS. The in-situ sulfidization tests by pre-addition of iron sulfide mineral were carried out. The mineral composition by XRD analysis is shown in Figure 7.10. The majority was made up of troilite, pyrrhotite and the compound $Cr_{0.5}Fe_{0.5}S$. The nickel and iron sulfides analysis of this iron sulfide sample using the bromine-methanol digestion-AAS method is shown in Table 7.2. The material contained 0.024% nickel in nickel sulfide and 37.6% iron in the iron sulfide sample. The original molar ratio of iron/nickel sulfides was 1633. This iron sulfide sample was mixed with -25 μm high-grade olivine as the material for the in-situ sulfidization and mineral carbonation. The in-situ sulfidization tests were carried out under the conditions of PCO_2=34.5 bar, 175 ℃ with addition of 1.5 m $NaHCO_3$ for 4 hours. The final solids were analyzed by the bromine-methanol digestion-AAS method to determine the changes in the nickel and iron sulfide contents.

Table 7.2 Nickel and iron sulfide content of the iron sulfide sample by bromine-methanol digestion-AAS analysis.

Nickel sulfide content, %	0.024
Iron sulfide content, %	37.6
Molar ratio of iron/nickel sulfides	1633

The effects of dosage of iron sulfide sample on nickel conversion efficiency, mineral carbonation efficiency and molar ratio of iron/nickel sulfides for the in-situ sulfidization are shown in Figure 7.17. With the increase of dosage of iron sulfide sample in the mixed sample, the conversion efficiency of nickel from the high-grade olivine increased from 29% at 30% dosage of iron sulfide sample to 44% at 70% dosage. If there was no nickel conversion of the olivine, the molar

ratio of iron/nickel sulfides would remain at the original value of 1633. Figure 7.17 shows that the molar ratio of iron/nickel sulfides was reduced to 170, 335 and 534 at the 30%, 50% and 70% dosage respectively. The decrease was due to the conversion of nickel in olivine to nickel sulfides and the conversion of iron sulfide to iron carbonate. Reaction 7.6 represents this reaction. However, it is also noted that there was still obvious gap between the mineral carbonation efficiency and the nickel conversion efficiency. Nickel conversion efficiency was still much lower than mineral carbonation efficiency.

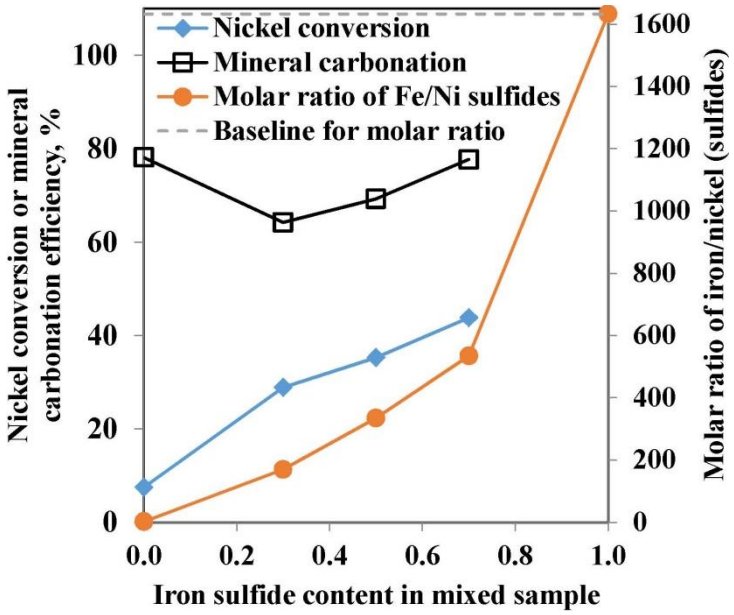

Figure 7.17 Effect of dosage of iron sulfide on nickel conversion efficiency, mineral carbonation efficiency and molar ratio of iron/nickel sulfides for the in-situ sulfidization by pre-addition of iron sulfides under the conditions of mixture sample of -25 μm high-grade olivine and iron sulfide sample, PCO_2=34.5 bar, 175 ℃ with addition of 1.5 m $NaHCO_3$ for 4 hours.

Furthermore, the mineral carbonation efficiency was firstly decreased from the original 78% to 64% at 30% iron sulfide dosage, followed by a significant increase back up to 78% at 70% iron sulfide dosage. Approximately half of the nickel released from the olivine during the mineral carbonation was still precipitated as nickel carbonate. A further increase of the concentration of

sulfide ions is apparently necessary to ensure formation of nickel sulfide. The first decrease of the mineral carbonation efficiency at 30% iron sulfide dosage was observed as well on the research about the effects of olivine content on kinetics (Section 6.4). The mineral carbonation efficiency would be expected to decrease with iron sulfide dosage due to the decrease of olivine content of the mixture. In contrast, the carbonation efficiency gradually increased, possibly due to the contribution of the generated hydrogen sulfide gas (from Fe-S material) and the slightly higher concentration protons available for carbonation (shown in Figure 7.16).

The corresponding changes in nickel sulfide and iron sulfide contents in the products are shown in Figure 7.18. It is interesting that the change between the nickel sulfide content and iron sulfide was significantly different. The experimental nickel sulfide content increased modestly when the dosage of iron sulfide was less than 30% and was subsequently maintained at around 0.05% Ni from 30% to 50% iron sulfide dosage. The difference between the experimental and the theoretical values (based on the nickel sulfide content in the iron sulfide sample) was due to the content of nickel sulfide converted from the high-grade olivine. In contrast, there was no obvious difference between the experimental and the theoretical iron sulfide content. This means that the majority of the preloaded iron sulfide did not react. Figure 7.18 demonstrated that the increase in the molar ratio of iron/nickel sulfides in Figure 7.17 was mainly due to the increase of the percentage of the preloaded iron sulfide in the mixture though the nickel conversion efficiency increased as well.

The preceding discussion of the in-situ sulfidization results indicates that it is possible to continuously supply suitable sulfide ions for the sulfidization during the mineral carbonation process. This continuous supply of sulfide ions can effectively convert the valuable metals released from the olivine to recoverable nickel sulfides with the limits of the precipitation of iron

sulfides. The challenge, thus far, is how to continuously supply the sulfide ions into the high-temperature and high-pressure reaction system in a way that minimize iron sulfide formation.

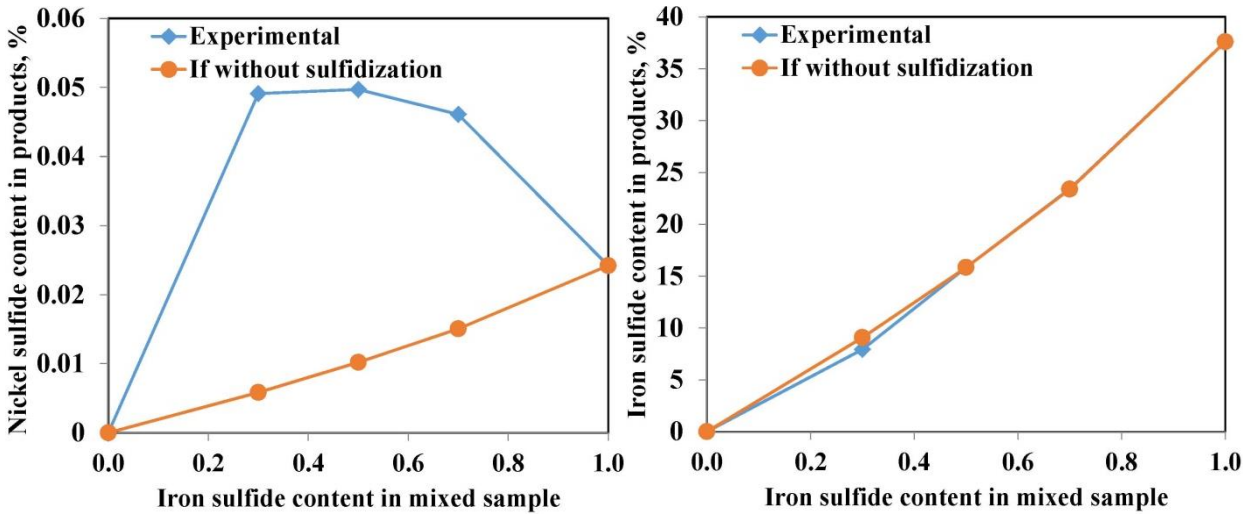

Figure 7.18 Effect of dosage of iron sulfide on nickel and iron sulfides content in the final solids for the in-situ sulfidization by preloading iron sulfides under the conditions of mixture sample of -25 μm high-grade olivine and iron sulfide sample, PCO_2=34.5 bar, 175 ℃ with addition of 1.5 m $NaHCO_3$ for 4 hours.

7.2 Ex-situ metal sulfidization

The ex-situ metal sulfidization tests after the mineral carbonation process were carried out by adding sodium sulfide. The work on the ex-situ metal sulfidization in this Chapter is summarized in Table 7.3. It summarizes the detailed test conditions, the achievements and the challenges. Generally, it presents that it was difficult to convert the nickel carbonate produced during mineral carbonation process into nickel sulfide and to concurrently control the selectivity of metal sulfidization.

Table 7.3 Summary of work on ex-situ metal sulfidization after mineral carbonation.

Samples	Varied conditions	Pre-set conditions	Results
Carbonated high-grade olivine (carbonation conditions: - 25 μm particles, 175 ℃, PCO_2=34.5 bar, 1.5 m $NaHCO_3$, 25% solids content for 5 h with 75% mineral carbonation efficiency)	Temperature 25 ℃ ~ 175 ℃	1% solids content 0.0012 m Na_2S 5 h	• Limited improvement in selective nickel conversion with increase of temperature, dosage of NaCl, dosage of Na_2S or reaction time. • Decreased selectivity of nickel conversion with high dosage of Na_2S or long reaction time.
	Addition of NaCl 0 ~ 0.5 m	1% solids content 175 ℃ 0.0012 m Na_2S 5 h	
	Addition of Na_2S 0 ~ 0.0125 m	1% solids content 175 ℃ 0.5 m NaCl 5 h	
	Reaction time 0 ~ 5 h	1% solids content 175 ℃ 0.5 m NaCl 0.01m Na_2S	
Carbonated Turnagain sample SN254 (carbonation conditions: -25 μm particles, 175 ℃, PCO_2=34.5 bar, with addition of 1.5 m $NaHCO_3$ for 12 h with 95% mineral carbonation efficiency)	Temperature 25 ℃ ~ 175 ℃	1.5% solids content 0.012 m Na_2S 0.5 m NaCl 2 h	• Limited improvement of selective nickel conversion with increase of temperature, reaction time. • Decreased selectivity of nickel conversion with high temperature and long reaction time.
	Reaction time 0 ~ 24 h	1.5% solids content 90 ℃ or 25 ℃ 0.012 m Na_2S 0.5 m NaCl	

7.2.1 Ex-situ metal sulfidization by sodium sulfide after mineral carbonation

Ex-situ metal sulfidization involves sulfidizing the products after the mineral carbonation. The purpose is to sulfidize the nickel and cobalt carbonates in the products to form nickel and cobalt sulfides. In order to test the possibility, the mineral carbonation products from -25 μm high-grade olivine and Turnagain sample SN254 were tested for the ex-situ sulfidization by addition sodium sulfide.

7.2.1.1 High-grade olivine

The mineral carbonation products of the high-grade olivine with carbonation efficiency of 75% under the conditions of -25 μm, 175 ℃, PCO2=34.5 bar, 1.5 m $NaHCO_3$, 25% solids content for 5 hours were used for the ex-situ sulfidization. This means that approximately 75% of the nickel in olivine had been transferred into nickel carbonates. The chemical composition of the carbonated products is shown in Table 7.4. The nickel content is 0.20%, most of which should be nickel carbonate.

Table 7.4 Chemical composition of the mineral carbonation products from high-grade olivine for ex-situ sulfidization.

Elements	Mg	Si	Fe	Al	Cr	Ni	Mn	Ca	C
Mass, %	21.2	12.9	6.2	0.12	0.49	0.20	0.11	0.20	7.9

With a view to efficient use of the sodium sulfides and to avoid the potential environmental pollutions, the concentration of sodium sulfides was controlled to less than 0.012 m and the corresponding solid content was less than 1%. The effects of temperature on the nickel conversion efficiency under the conditions of addition of 0.0012 m [S^{2-}] for 5 hours are shown in Figure 7.19(a). It is clear that the increase of temperature had a positive effect on the nickel conversion from 14% at 25 ℃ to 24% at 175 ℃. The corresponding molar ratio of iron/nickel sulfides was also controlled to less than 5, though it slightly increased with temperature. The addition of sodium chloride also had the slightly beneficial effect on the ex-situ sulfidization, as shown in Figure 7.19(b) under the conditions of 175 ℃, addition of 0.0012m [S^{2-}] for 5 hours.

The addition of 0.5 m sodium chloride further increased the nickel conversion efficiency from 24% to 29% with the iron/nickel sulfides molar ratio of less than 6.

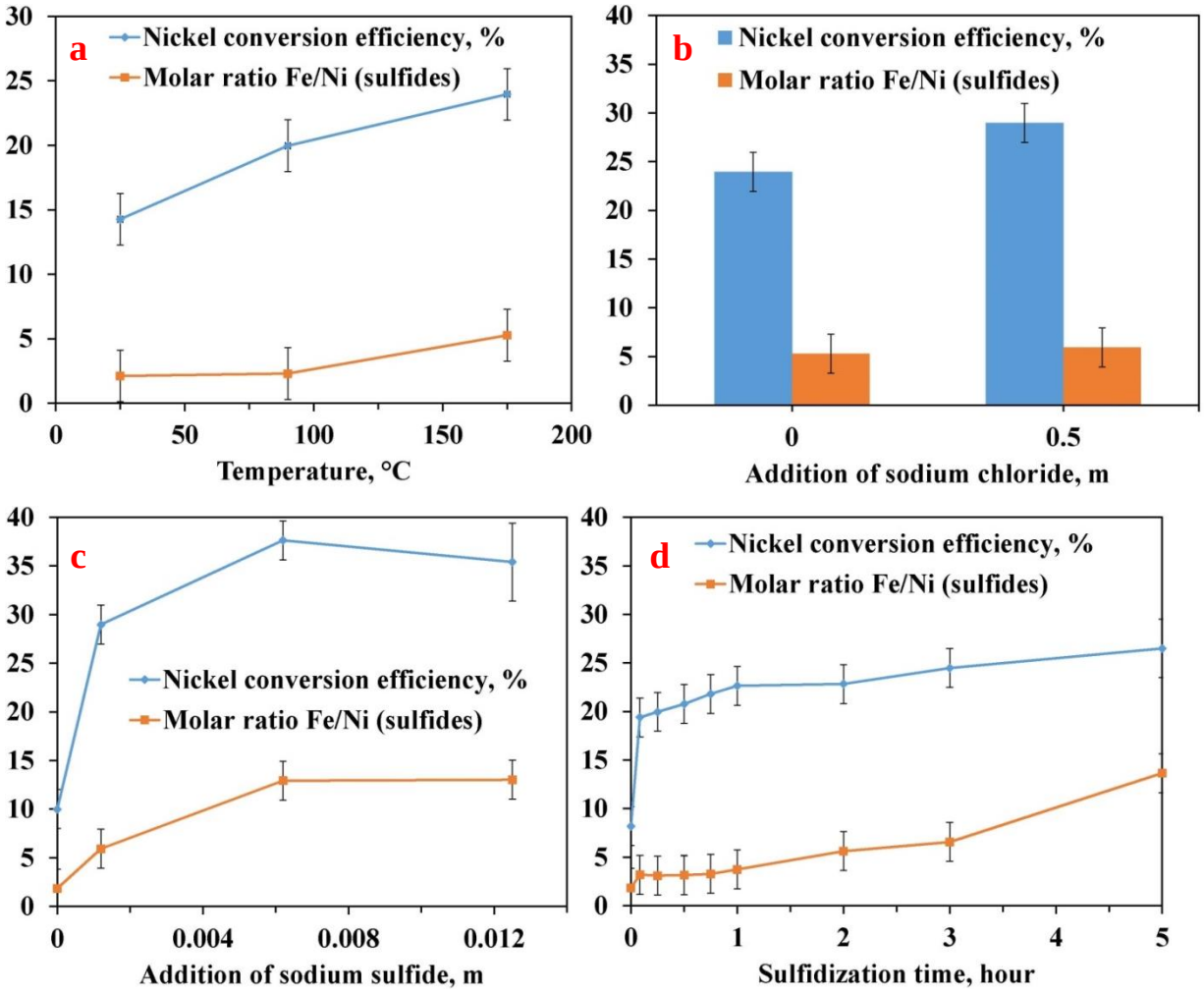

Figure 7.19 Effects of various factors on ex-situ nickel sulfidization efficiency and molar ratio of iron/nickel sulfides in products: (a) effects of temperature under the conditions of 1% solids content, 0.0012 m sodium sulfide for 5 hours; (b) effects of sodium chloride under the conditions of 1% solids content, 175 ℃, 0.0012 m sodium sulfide for 5 hours; (c) effects of sodium sulfide concentration under the conditions of 1% solids content, 175 ℃, 0.5 m sodium chloride for 5 hours; and (d) effects of reaction time under the conditions of 1% solids content, 175 ℃, 0.5 m sodium chloride and 0.01m sodium sulfide.

The effect of dosage of sodium sulfide is shown in Figure 7.19(c). Under the ex-situ sulfidization conditions of addition of 175 ℃, 0.5 m sodium chloride for 5 hours, the nickel conversion

efficiency further increased from 29% at 0.0012 m sodium sulfide to a maximum of 38% at 0.0062 m sodium sulfide. The higher dosage of sodium sulfide did not have any beneficial effect. However, the molar ratio of iron/nickel sulfides increased to 13 from 6. In addition, the change in nickel conversion efficiency and the molar ratio with reaction time were also studied under the conditions of 175 ℃, addition of 0.5 m sodium chloride and 0.01m sodium sulfide, as shown in Figure 7.19(d). Both the nickel conversion efficiency and the molar ratio slightly increased with time. After 3 hours, the nickel conversion efficiency reached 25% with the molar ratio of iron/nickel sulfides of less than 7. The further increase of reaction time did not increase nickel conversion efficiency considerably but resulted in increased the molar ratio to 14 at 5 hours. It was still difficult to reach high nickel conversion efficiency and at the same time to control the sulfidization of iron carbonate.

In order to determine why it was so difficult to effectively sulfidize the carbonated products, two additional approaches were developed. The first was to analyze whether or not the nickel carbonates were discrete grains or intimately associated with other carbonates in the mineral carbonation products. If the nickel carbonates were associated with other carbonate products, it would increase the difficulty of achieving high nickel conversion efficiency and of controlling the co-sulfidization of iron carbonates. The other was to investigate which step controlled the nickel conversion from the nickel carbonates. If it was controlled by chemical reaction, there were several ways to improve the efficiency. If it was controlled by product layer diffusion, it would be more difficult to effectively sulfidize.

The mineral carbonation products of the high-grade olivine with 85% carbonation efficiency under the conditions of -25 μm of high-grade olivine, 175 ℃, PCO_2=41.4 bar, 10% solids content with 1.5 m $NaHCO_3$ for 5 hours were used for the Time-of-Flight Secondary Ion Mass

Spectrometry (ToF-SIMS) analysis. The ToF-SIMS analysis requires conductive samples. However, the solids of mineral carbonation of olivine were not conducting and there is no way to make the polished carbonation solids conductive even with help of resins. The only approach is to analyze the solids by comparing the intensity ratio of magnesium/iron/nickel of individual carbonate crystals. The carbonate crystal was probably independent if the nickel content for carbonate crystal was much higher than the other bivalent metals. The high-spatial resolution mode of the ToF-SIMS analysis result is shown in Figure 7.20. The corresponding intensity ratio values of magnesium/iron/nickel in high-mass resolution mode are shown in Table 7.5.

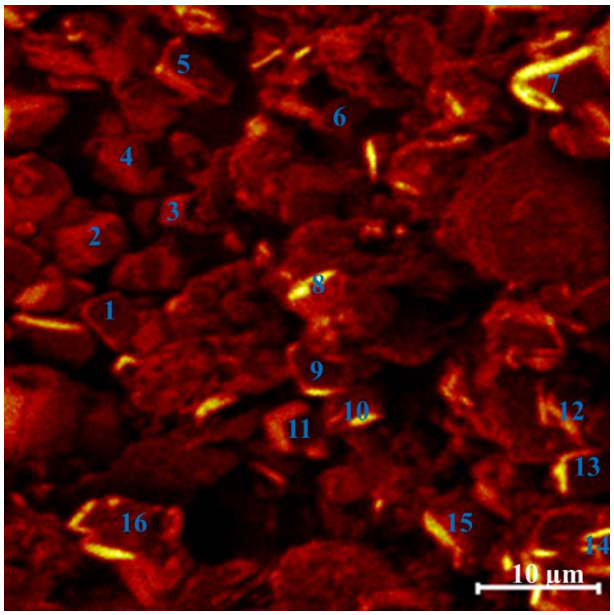

Figure 7.20 The ToF-SIMS analysis image of the mineral carbonated particles from the high-grade olivine in high spacial resolution mode and the analyzed crystal carbonate particles. (see Table 7.5 for data on numbered spots)

Unfortunately, the discrete nickel carbonate crystals were not found through the ToF-SIMS analysis. The highest intensity for nickel was found at spot 7 and the intensity ratio of magnesium/iron/nickel was 4:0.4:1. But this intensity ratio may be because the ToF-SIMS instrument was much more sensitive to nickel other than iron and magnesium. It is noted that the

intensity ratio of iron/nickel was always less than 2 compared to the 28 for analyzed total iron/nickel. Therefore, the exceptional intensity ratio was quite possibly due to the sensitivity of the analysis instrument to specific elements. Furthermore, the similar results were never found for other spots and other areas. Thus, it is believed that the discrete nickel carbonate crystals did not formed but that nickel carbonate was intimately associated with other magnesium or iron carbonates. This increased the difficulty to effectively convert the nickel carbonate to nickel sulfides and also to control the molar ratio of iron/nickel sulfides.

Table 7.5 Intensity ratio of magnesium/iron/nickel for the spots in ToF-SIMS analysis.

Spot	Intensity			Intensity ratio
	Mg	Fe	Ni	Mg:Fe:Ni
1	3521	219	164	22:1.3:1
2	7158	305	212	34:1.4:1
3	1618	95	46	35:2.1:1
4	5083	271	144	35:1.9:1
5	13508	576	452	30:1.3:1
6	4500	220	174	26:1.3:1
7	12176	1164	2747	4:0.4:1
8	6490	259	127	51:2:1
9	7206	462	315	23:1.5:1
10	4071	266	180	23:1.5:1
11	6352	436	252	25:1.7:1
12	8189	427	374	22:1.1:1
13	6743	360	288	23:1.3:1
14	3624	187	132	28:1.4:1
15	10438	470	392	27:1.2:1
16	10428	613	417	25:1.5:1

The other approach was to determine the rate-controlling step of the metal sulfidization between the nickel carbonate and sodium sulfide. The nickel content in the carbonated products from mineral samples was too low for these experiments. A nickel carbonate powder provided by Alfa Aesar was used for this investigation under the conditions of 175 ℃, 1% solids content, addition of 0.09 m sodium sulfide, molar ratio of S/Ni = 1.0 for 2 hours. The SEM-EDX images the

products of the sulfidization process are shown in Figure 7.21. From Figure 7.21(a-c), it is apparent that the sulfidization of nickel carbonate with sodium sulfide was controlled by diffusion through the generated nickel sulfides layer formed on the outer surface of the unreacted nickel carbonate core. The EDX results showed some content of the sulfur even in what was apparently an "unreacted core". The SEM-EDX analysis was difficult because the particles were around 3 microns in diameter. The EDX analysis is not accurate over such small distances. Figure 7.21(d) shows a completely sulfidized particle. The corresponding EDX analysis showed a molar ratio of sulfur/nickel of ~1 over the whole particles surface. It has been confirmed that the sulfidization of nickel carbonate by sodium sulfide was controlled by the diffusion through the product layer, which is consistent with the previous research[156].

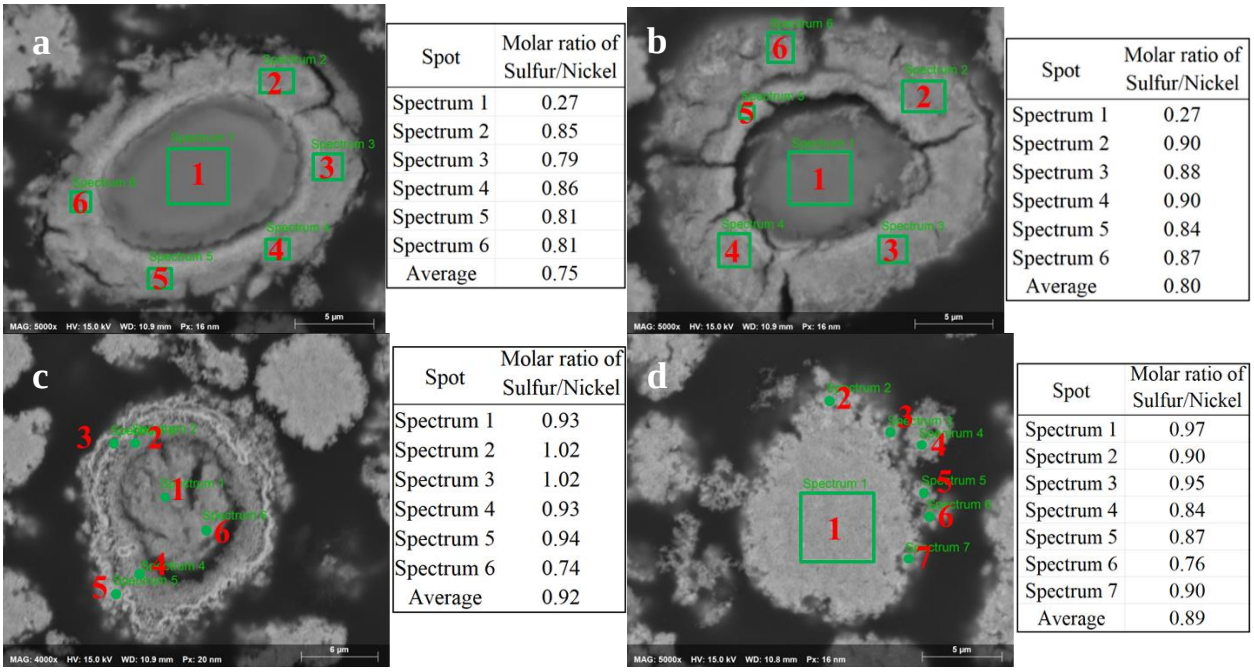

Spot	Molar ratio of Sulfur/Nickel
Spectrum 1	0.27
Spectrum 2	0.85
Spectrum 3	0.79
Spectrum 4	0.86
Spectrum 5	0.81
Spectrum 6	0.81
Average	0.75

Spot	Molar ratio of Sulfur/Nickel
Spectrum 1	0.27
Spectrum 2	0.90
Spectrum 3	0.88
Spectrum 4	0.90
Spectrum 5	0.84
Spectrum 6	0.87
Average	0.80

Spot	Molar ratio of Sulfur/Nickel
Spectrum 1	0.93
Spectrum 2	1.02
Spectrum 3	1.02
Spectrum 4	0.93
Spectrum 5	0.94
Spectrum 6	0.74
Average	0.92

Spot	Molar ratio of Sulfur/Nickel
Spectrum 1	0.97
Spectrum 2	0.90
Spectrum 3	0.95
Spectrum 4	0.84
Spectrum 5	0.87
Spectrum 6	0.76
Spectrum 7	0.90
Average	0.89

Figure 7.21 SEM-EDX images of sulfidization products between pure nickel carbonate and sodium sulfide under the conditions of 175 ℃, 1% solids content, addition of 0.09 m sodium sulfide, molar ratio of S/Ni = 1.0 for 2 hours.

The mineral carbonation process did not produce discrete nickel carbonate crystals and the sulfidization of nickel carbonate by sodium sulfide was under the product nickel sulfides product

layer diffusion control. Both results indicate that it is not reasonable to sulfidize the mineral carbonated products for the potential recovery of valuable metals.

7.2.1.2 Turnagain sample SN254

Studies into ex-situ sulfidization of the carbonated products of the high-grade olivine sample showed that this process was not suitable for nickel sulfidization. An ex-situ sulfidization test of the carbonated products of Turnagain sample SN254 with 95% mineral carbonation efficiency was carried out for comparison. The chemical composition of the mineral carbonation products from the Turnagain SN254 under the conditions of -25 μm particles, 175 ℃, PCO_2=34.5 bar, with addition of 1.5 m $NaHCO_3$ for 12 hours are shown in Table 7.6. The nickel content in the carbonated products was 0.19%.

Table 7.6 Chemical composition of the mineral carbonation products from Turnagain sample SN254 for ex-situ sulfidization.

Elements	Mg	Si	Fe	Al	Cr	Ni	Mn	Ca	Co	C
Mass, %	19.3	12.5	5.72	0.05	0.25	0.19	0.10	<0.1	0.009	8.67

The effects of temperature on the nickel conversion efficiency and molar ratio of iron/nickel sulfides are shown in Figure 7.22(a). The increase of temperature benefited the nickel conversion efficiency which increased from 22% at 25 ℃ to 30% at 175 ℃ under otherwise identical conditions of 0.012 m sodium sulfide and 0.5 m sodium chloride, 1.5% solids content for 2 hours. The corresponding molar ratio of iron/nickel sulfides increased from only 1.5 to approximately 13. Figure 7.22(b) shows that the consumption of the added sulfide ions increased with temperature in accord with the decreased pH values and correspondingly increased Eh values. It is noted that at temperature 175 ℃ the Eh values after the reaction was still less than -300 mV, which showed that there were still sulfide ions in the aqueous solution. Furthermore, the molar

ratio of iron/nickel sulfides at 25 ℃ and 90 ℃ can be limited to less than 5. Therefore, the further tests about the effects of reaction time were carried out at 25 ℃ and 90 ℃ under the same conditions, shown in Figure 7.23. At 90 ℃, the nickel conversion efficiency increased with reaction time within 12 hours up to 47%. The further increase in reaction time to 24 hours only increased the nickel conversion efficiency by another 2%. The solution pH decreased more rapidly at first, then began to level off. Likewise, solution Eh rose, and then levelled off at less than -350 mV. These trends would be consistent with the rate being controlled by diffusion through the nickel sulfides product layer. The molar ratio of iron/nickel sulfides increased to 6.0 at 12 hours and 6.6 at 24 hours, which is probably due to the fact that the nickel carbonate was intimately associated with other carbonates in the carbonated products. The reaction at 25 ℃ showed similar results but the changes were much less pronounced than at 90 ℃. The nickel conversion efficiency only rose to 33% though the molar ratio of iron/nickel sulfides was limited to less than 5.0. The smaller changes in solution pH and Eh values indicated a much slower reaction process.

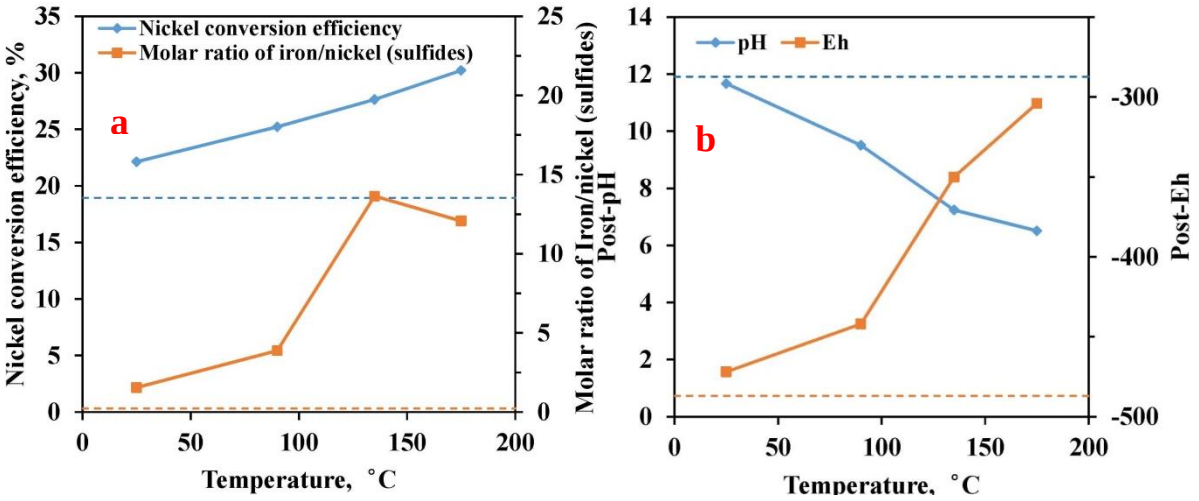

Figure 7.22 Effects of temperature on the ex-situ sulfidization of carbonated Turnagain SN254 under the conditions of 0.012 m sodium sulfide and 0.5 m sodium chloride, 1.5% solids content for 2 hours: (a) on nickel conversion efficiency and molar ratio of iron/nickel sulfides and (b) on solution pH and Eh values.

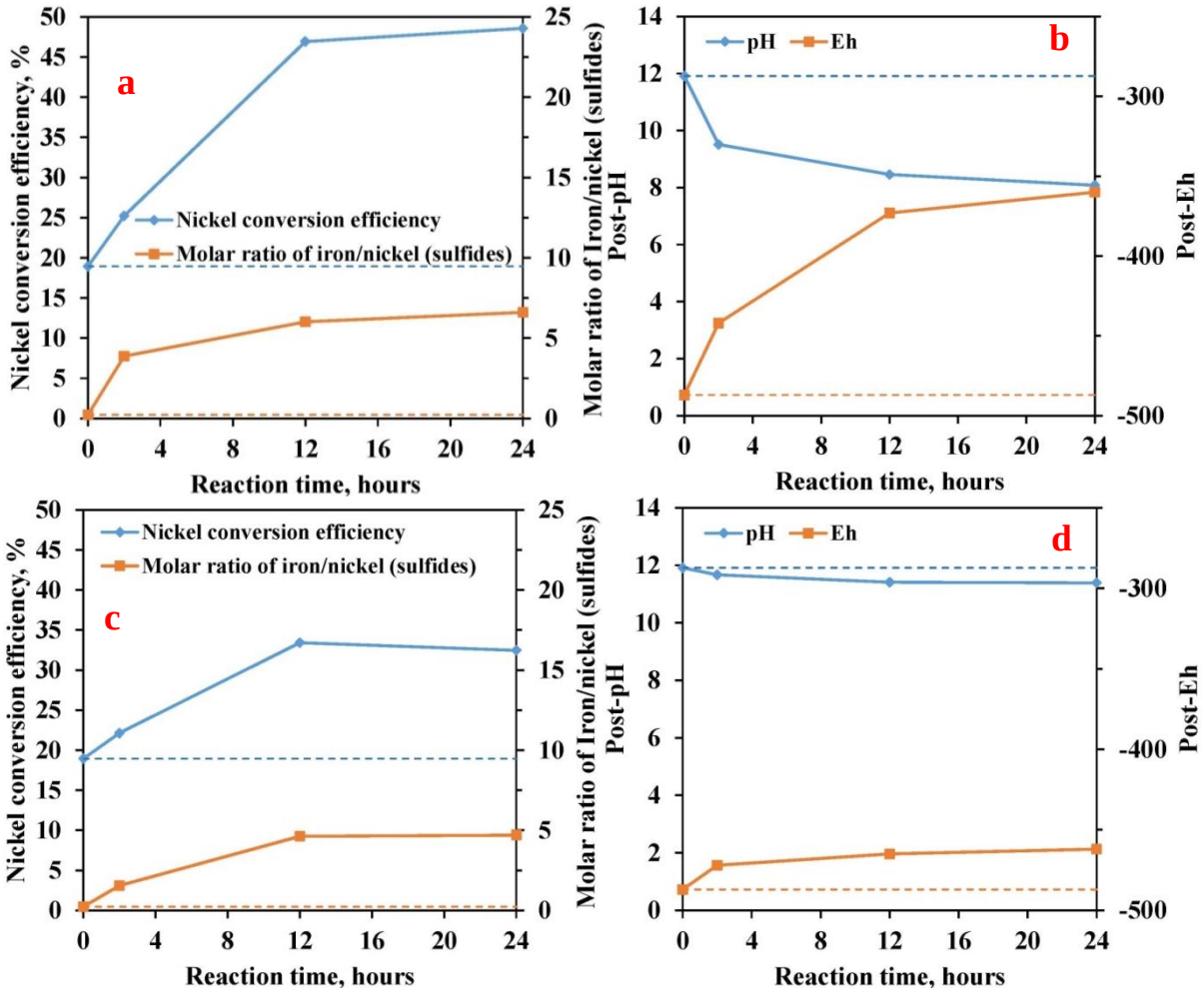

Figure 7.23 Effects of reaction time on the ex-situ sulfidization of carbonated Turnagain SN254 under the conditions of 0.012 m sodium sulfide and 0.5 m sodium chloride, 1.5% solids content for 2 hours: (a) on nickel conversion efficiency and molar ratio of iron/nickel sulfides at 90 ℃; (b) on solution pH and Eh values at 90 ℃; (c) on nickel conversion efficiency and molar ratio of iron/nickel sulfides at 25 ℃ and (d) on solution pH and Eh values at 25 ℃.

The study of the ex-situ sulfidization of carbonated high-grade olivine and carbonated Turnagain SN254 has confirmed that the ex-situ sulfidization was not suitable for efficiently forming NiS. Nickel carbonate was not present as a discrete, separate phase and even if were to be, the kinetics of sulfidization were limited by product layer diffusion control of the sulfidization process between nickel carbonate and sodium sulfide.

7.3 Conclusions

The following conclusions can be state:

(1) It is possible to in-situ sulfidize the valuable metals released from the olivine during the mineral carbonation through carefully controlling the continuous and stable supply of sulfide ions. The released magnesium, iron and nickel ions can be selectively precipitated as magnesium carbonate, iron carbonate and nickel sulfide.

(2) Ex-situ sulfidization after mineral carbonation is not suitable to enhance metal recovery. The mineral carbonation process did not produce separate, discrete nickel carbonate and the sulfidization of nickel carbonate with sodium sulfide was controlled by diffusion through product nickel sulfide layer.

(3) It was not reasonable to preload sodium sulfide for the in-situ sulfidization during mineral carbonation. Preloading sodium sulfide for the in-situ sulfidization will form sulfides of valuable metal, but failed due to the excessive formation of iron sulfides. The latter effect makes it impossible to separate out the valuable metal sulfides for potential metal recovery enhancement.

(4) The challenge of the in-situ sulfidization during mineral carbonation relates to the equipment used and the control of sulfidization conditions. Providing mixed gas of CO_2 and H_2S or specific content of iron sulfide may be woth further investigation.

8 Summary and recommendations

8.1 Research outcomes

The research conducted for this dissertation was focused on the fundamental mechanisms and kinetics of ex-situ direct mineral carbonation of magnesium silicate minerals and the utilization of mineral carbonation for the valuable metal recovery enhancement through metal sulfidization. This research has made the following achievements.

The mechanisms and kinetics of mineral carbonation of olivine have been elucidated. The most important factors affecting the mineral carbonation process were the temperature, CO_2 partial pressure, specific surface area, aqueous ionic strength and addition of sodium bicarbonate. The mechanism can vary under different conditions that mainly depended on the CO_2 partial pressure and the aqueous ionic strength. The other factors can change the carbonation reaction rate but cannot alter the kinetic rate-controlling step. When the aqueous ionic strength was low, less than 0.32 m, the mineral carbonation of olivine was controlled by diffusion through a silica-rich layer. When the aqueous ionic strength increased to more than 0.5 m, the mechanism depended on the CO_2 partial pressure. When the CO_2 partial pressure was lower than 21 bar, the mineral carbonation process was controlled by diffusion through a poorly-porous and uniform carbonate layer, rather than diffusion through a silica-rich layer. The further increase of the CO_2 partial pressure removed the uniform carbonate layer and the carbonation process was then controlled by the rate of the chemical reaction, i.e. the dissolution of olivine. Under chemical reaction control, there was a universal structure for the mineral carbonation of olivine that a porous void formed between the unreacted olivine core and a porous and well-crystallized carbonates layer.

The dissolution of olivine produced metastable aqueous silica $H_4SiO_{4(a)}$ and bivalent metal ions (e.g. Mg^{2+}, Fe^{2+}, Ni^{2+} and Co^{2+}). The increase of the aqueous ionic strength can accelerate the diffusion of the metastable aqueous silica into the aqueous solution, followed by decomposition into amorphous silica in the aqueous matrix, separate from the reacting particle. As a result, the silica rich layer did not form. The increase of the CO_2 partial pressure and preloading sodium bicarbonate can enhance the sufficient and instant supply of carbonate ions that facilitated the rapid precipitation of bivalent metal carbonates as well as the well growth of the carbonate crystals to form the porous and well-crystallized carbonate layer. The protons can easily go through the porous carbonate product layer. Under chemical reaction control, the key was the sufficient supply of protons for the dissolution of olivine. It can be also achieved by increasing the CO_2 partial pressure and sodium bicarbonate concentration. When the CO_2 partial pressure was low, the supply of carbonate ions was not sufficient and fast enough, which resulted in a uniform and poorly porous carbonate layer preventing the diffusion of protons and bivalent metal ions for the dissolution of olivine and the well-growth of carbonate crystals. The release of bivalent metal ions from the dissolution of olivine in the porous void between the unreacted core and the crystalline carbonate layer provided the opportunity to sulfidize valuable metals.

The effects of CO_2 partial pressure, specific surface area and addition of sodium bicarbonate on the mineral carbonation of olivine have been quantified to the 1.6^{th}, 0.7^{th} and 0.8^{th} power. The activation energy for the mineral carbonation olivine under chemical reaction control was approximately 48.0 kJ/mol. A kinetic formula has been successfully developed: $\alpha = (1 - (1 - k^o \times [S]^{0.7} \times [P_{CO2}]^{1.6} \times [NaHCO_3]^{0.8} \times e^{(-Ea \times 1000/RT)} \times t)^3) \times 100\%$, where k^o is the kinetic factor, related to the characteristics of materials. The suitable ranges of PCO_2, temperature and addition of $NaHCO_3$ are 28 bar – 41 bar, 100 ℃ – 175 ℃ and 0.5 m – 1.5 m, respectively. The developed

kinetic formula and the transformations can be applied to predict the mineral carbonation efficiency, the necessary requirements of reaction time, required sodium bicarbonate concentration and the relationship between the required specific surface area and CO_2 partial pressure. This kinetic formula can be widely applied to the mineral carbonation of silicate minerals in spite of variable mineral compositions, olivine content, mineral carbonation capacity, specific surface area and the particle size distribution as long as the majority of the carbonation reactions were with olivine.

The bivalent metal-containing silicate minerals other than olivine had a detrimental effect on achieving high mineral carbonation efficiency. The magnetite, iron sulfides (or metal sulfides in general), pyroxene and phologopite were not involved in the mineral carbonation reaction under the same conditions compared to olivine. Similarly, naturally occurring serpentine without heat pre-treatment had a much lower carbonation rates than olivine. The magnetite may act as a nucleation site benefiting the precipitation of the magnesium and iron ions and the carbonate ions in the aqueous solution.

Under the chemical reaction control regime, it is possible to utilize the mineral carbonation process for recovering the released valuable metal from the dissolution of olivine by in-situ sulfidization. The key for the in-situ metal sulfidization was to continuously supply suitable sulfide ions in order to effectively convert the released valuable bivalent metal ions to metal sulfide and to limit the formation of the iron sulfide as a co-precipitate. By providing a mixed gas of CO_2 and H_2S or by preloading iron sulfides into the mineral slurry, in-situ sulfidization was possible. Thus far, the challenge of the in-situ sulfidization is mainly on the equipment needed to continuously provide a suitable sulfide ion concentration into a high-temperature and high-pressure reaction system. In contrast, the metal recovery by the ex-situ sulfidization of mineral

carbonated products is not feasible. The mineral carbonation process did not produce separate, discrete valuable metal carbonate and the sulfidization of even pure nickel carbonate with sodium sulfide was controlled by diffusion through a nickel sulfide product layer.

8.2 Suggestions for future research

Mineral carbonation is the most promising method to permanently sequester CO_2 gas for the global warming mitigation. However, the high costs and unprofitability for the industry limit the application of this promising technology. Without a breakthrough of the development of an efficient catalyst or suitable carbonation equipment to markedly lower the costs, it might be pointless to carry out further research on the ex-situ mineral carbonation. At present, it is suggested to combine the mineral carbonation and the metal recovery enhancement together to offset the high capital cost of carbonation. The storage and utilization of mineral carbonation provide a perfect opportunity to make the mineral carbonation process profitable and suitable for its industrial application. In the future, the research should focus on how to successfully utilize the mineral carbonation process to efficiently recover valuable metals. In-situ metal sulfidization is one of the promising methods for the utilization of mineral carbonation. In order to successfully sulfidize valuable metals, it is worth researching the development of a high-temperature reactor which can continuously provide a suitable sulfide source to maintain on optimal sulfide concentration. However, the supply of sulfide ions also increases the risk to the environment and to human health. It may also be reasonable to seek another environmentally-friendly method to efficiently extract the valuable metals during the mineral carbonation process. As a result, the benefits of the valuable metal recovery enhancement with carbon credits can outweigh the costs of mineral carbonation, which can make the carbonation process profitable.

Then, the industries might actively apply the carbonation technology, driven by profits, with even the supports of environmental conservation organizations.

8.3 Personal reflection

This research developed the theory and practices of the ex-situ direct mineral carbonation and made progress toward the utilization of mineral carbonation to recover valuable metals from silicate minerals. This research has had a clear vision to bridge the gap between the mineral carbonation and metal recovery. Without fundamental research on the mechanisms and kinetics of mineral carbonation, it is difficult to successfully utilize the carbonation process. Similarly, without the research on the utilization of mineral carbonation for metal recovery, the promising mineral carbonation technology loses its attractiveness on the mineral industries. Though this research has not successfully developed an environmentally-friendly profitable mineral carbonation process, the understanding developed in this research strongly suggests that successful utilization is possible and it is believed that a novel, economically profitable mineral carbonation process will be successfully developed in the near future.

References

1. IPCC. *Climate Change 2014: Mitigation of climate change. Working group III contribution to the fifth assessment report of the Intergovernmental Panel on Climate Change* (2014). doi:10.1017/CBO9781107415416

2. Galán-Martín, Á. *et al.* Time for global action: An optimised cooperative approach towards effective climate change mitigation. *Energy Environ. Sci.* **11,** 572–581 (2017).

3. Bjørk, A. A. *et al.* Changes in Greenland's peripheral glaciers linked to the North Atlantic Oscillation. *Nat. Clim. Chang.* **8,** 48–52 (2018).

4. Landschützer, P., Gruber, N., Bakker, D. C. E., Stemmler, I. & Six, K. D. Strengthening seasonal marine CO_2 variations due to increasing atmospheric CO_2. *Nat. Clim. Chang.* **8,** 146–150 (2018).

5. Goodwin, P. *et al.* Pathways to 1.5 and 2 °C warming based on observational and geological constraints. *Nat. Geosci.* **11,** 1–22 (2018).

6. Kääb, A. *et al.* Massive collapse of two glaciers in western Tibet in 2016 after surge-like instability. *Nat. Geosci.* **11,** 114–120 (2018).

7. Screen, J. A. *et al.* Consistency and discrepancy in the atmospheric response to Arctic sea-ice loss across climate models. *Nat. Geosci.* **11,** 155–163 (2018).

8. Kwiatkowski, L. & Orr, J. C. Diverging seasonal extremes for ocean acidification during the twenty-first century. *Nat. Clim. Chang.* **8,** 141–145 (2018).

9. Park, C. E. *et al.* Keeping global warming within 1.5 °C constrains emergence of aridification. *Nat. Clim. Chang.* **8,** 70–74 (2018).

10. Elder, C. D. *et al.* Greenhouse gas emissions from diverse Arctic Alaskan lakes are dominated by young carbon. *Nat. Clim. Chang.* **8,** 166–171 (2018).

11. Xi, F. *et al.* Substantial global carbon uptake by cement carbonation. *Nat. Geosci.* **9,** 880–883 (2016).

12. UNFCCC. *Paris Agreement. Conference of the Parties on its twenty-first session* 32 (2015). doi:FCCC/CP/2015/L.9/Rev.1

13. Government of Canada. *Canada's 2017 Nationally determined contribution submission To the United Nations Framework.* (2017).

14. IPCC-Intergovernmental Panel on Climate Change. Available at: https://www.ipcc.ch/wp-signup.php?new=www.ipcc.ch. (Accessed: 17th February 2019)

15. Sanna, A., Uibu, M., Caramanna, G., Kuusik, R. & Maroto-Valer, M. M. A review of mineral carbonation technologies to sequester CO_2. *Chem. Soc. Rev.* **43,** 8049–8080 (2014).

16. Seifritz, W. CO_2 disposal by means of silicates. *Nature* **345,** 486 (1990).

17. Azadi, M. *et al.* Opportunities for mineral carbonation in Australia's mining industry. *Sustainability* **11,** 1250 (2019).

18. Tomkinson, T., Lee, M. R., Mark, D. F. & Smith, C. L. Sequestration of Martian CO_2 by mineral carbonation. *Nat. Commun.* **4,** 2662 (2013).

19. Renforth, P., Washbourne, C. L., Taylder, J. & Manning, D. A. C. Silicate production and availability for mineral carbonation. *Environ. Sci. Technol.* **45,** 2035–2041 (2011).

20. Jacobs, A. D. Quantifying the mineral carbonation potential of mine waste material: A new parameter for geospatial estimation. (University of British Columbia, 2014).

21. Rahman, F. A. *et al.* Pollution to solution: Capture and sequestration of carbon dioxide (CO_2) and its utilization as a renewable energy source for a sustainable future. *Renew. Sustain. Energy Rev.* **71,** 112–126 (2017).

22. Sipilä, J., Teir, S., Zevenhoven, R. Carbon dioxide sequestration by mineral carbonation: literature review update 2005-2007. Heat Engineering Laboratory, Åbo Akademi University, ISBN 978-952-12-2036-4, Turku, Finland, 2008.

23. Doucet, F. J. Scoping study on CO_2 mineralization technologies. Report No. CGS-2011-007, Pretoria, South Africa, (2011).

24. Oskierski, H. C., Dlugogorski, B. Z. & Jacobsen, G. Sequestration of atmospheric CO_2 in chrysotile mine tailings of the Woodsreef Asbestos Mine, Australia: Quantitative mineralogy, isotopic fingerprinting and carbonation rates. *Chem. Geol.* **358,** 156–169 (2013).

25. Daval, D. Carbon dioxide sequestration through silicate degradation and carbon mineralisation: promises and uncertainties. *npj Mater. Degrad.* **2,** 11 (2018).

26. Brown, J. G. E. *et al.* Geological Sequestration of CO_2 : Mechanisms and kinetics of CO_2 reactions in mafic and ultramafic rock formations, in *2009 Annual Report to the Global Climate and Energy Project* 1–27 (2009).

27. Zevenhoven, R., Fagerlund, J. Fixation of carbon dioxide into inorganic carbonates: the natural and artificial "Weathering of Silicates", in Carbon Dioxide as Chemical Feedstock (ed M. Aresta), Wiley-VCH Verlag GmbH & Co. KGaA, Weinheim, Germany, 353-379 (2010). doi: 10.1002/9783527629916.ch14.

28. Olajire, A. A. A review of mineral carbonation technology in sequestration of CO_2. *J. Pet. Sci. Eng.* **109,** 364–392 (2013).

29. Huijgen, W.J., Comans, R.N. Carbon dioxide sequestration by mineral carbonation: literature review. Energy Research Centre of the Netherlands, ECN-C--03-016, Petten, The Netherlands (2003).

30. Chizmeshya, A. V. G., Mckelvy, M. J., Squires, K., Carpenter, R. W. & Béarat, H. A

novel approach to mineral carbonation: Enhancing carbonaton while avoiding pretreatment process cost. (2007). doi:10.2172/924162

31. AMC Mining Concultants (Canada). Turnagain project Hard Creek Nickel Corporation preliminary economic assessment. (2011).

32. WARDROP A Tetra Tech Company. Technical report on the Turnagain project to Hard Creek Nickel Corporation. (2010). doi:http://www.hardcreek.com/i/pdf/2010-04-07_TurnagainTR.pdf

33. King, P. L. *et al.* Gas – Solid Reactions : Theory, experiments and case studies relevant to earth and planetary processes. *Rev. Mineral. Geochemistry* **84,** 1–56 (2018).

34. Lamadrid, H. M. *et al.* Effect of water activity on rates of serpentinization of olivine. *Nat. Commun.* **8,** 16107 (2017).

35. Power, I. M. *et al.* Carbon Mineralization: From natural analogues to engineered systems. *Rev. Mineral. Geochemistry* **77,** 305–360 (2013).

36. Matter, J. M. & Kelemen, P. B. Permanent storage of carbon dioxide in geological reservoirs by mineral carbonation. *Nat. Geosci.* **2,** 837–841 (2009).

37. Turvey, C. C. *et al.* Hydrotalcites and hydrated Mg-carbonates as carbon sinks in serpentinite mineral wastes from the Woodsreef chrysotile mine, New South Wales, Australia: Controls on carbonate mineralogy and efficiency of CO_2 air capture in mine tailings. *Int. J. Greenh. Gas Control* **79,** 38–60 (2018).

38. Tominaga, M. *et al.* Multi-scale magnetic mapping of serpentinite carbonation. *Nat. Commun.* **8,** (2017).

39. Aminu, M. D., Nabavi, S. A., Rochelle, C. A. & Manovic, V. A review of developments in carbon dioxide storage. *Applied Energy* **208,** 1389–1419 (2017).

40. Olajire, A. A. A review of mineral carbonation technology in sequestration of CO_2. *J. Pet. Sci. Eng.* **109,** 364–392 (2013).

41. Verduyna, M., Geerlingsa, H., Van-Mossel, G. & Vijayakumari, S. Review of the various CO_2 mineralization product forms. *Energy Procedia* **4,** 2885–2892 (2011).

42. Gislason, S. R. & Oelkers, E. H. Carbon storage in basalt. *Science (80).* **344,** 373–374 (2014).

43. Snæbjörnsdóttir, S. Ó., Gislason, S. R., Galeczka, I. M. & Oelkers, E. H. Reaction path modelling of in-situ mineralisation of CO_2 at the CarbFix site at Hellisheidi, SW-Iceland. *Geochim. Cosmochim. Acta* **220,** 348–366 (2018).

44. Kelemen, P. B. *et al.* Rates and mechanisms of mineral carbonation in peridotite: natural processes and recipes for enhanced, in situ CO_2 capture and storage. *Annu. Rev. Earth Planet. Sci* **39,** 545–76 (2011).

45. Kelemen, P. B. & Matter, J. In situ carbonation of peridotite for CO_2 storage, in

Proceedings of the National Academy of Sciences of the United States of America **105,** 17295–17300 (2008).

46. Dichicco, M. C. *et al.* Serpentinite carbonation for CO_2 sequestration in the Southern Apennines: preliminary study. *Energy Procedia* **76,** 477–486 (2015).

47. Gadikota, G., Matter, J., Kelemen, P. & Park, A.-H. A. Chemical and morphological changes during olivine carbonation for CO_2 storage in the presence of NaCl and $NaHCO_3$. *Phys. Chem. Chem. Phys.* **16,** 4679–93 (2014).

48. Wang, F., Dreisinger, D., Jarvis, M., Hitchins, T. & Dyson, D. Quantifying kinetics of mineralization of carbon dioxide by olivine under moderate conditions. *Chem. Eng. J.* **360,** 452–463 (2019).

49. Kasina, M., Kowalski, P. R. & Michalik, M. Mineral carbonation of metallurgical slags. *Mineralogia* **45,** 27–45 (2014).

50. Huijgen, W., Witkamp, G.J. & Comans, R. Mineral CO_2 Sequestration by Steel Slag Carbonation. *Environ. Sci. Technol.* **39,** 9676–9682 (2005).

51. Sun, J., Bertos, M. F. & Simons, S. J. R. Kinetic study of accelerated carbonation of municipal solid waste incinerator air pollution control residues for sequestration of flue gas CO_2. *Energy Environ. Sci.* **1,** 370–377 (2008).

52. Qin, S. S., Zhu, M. X., Yang, G. P. & Wang, D. A typical diagenesis of sulfur and iron in sediments of the river-dominated Bohai Sea (China). *J. Mar. Syst.* **189,** 116–126 (2019).

53. Altiner, M. Effect of Alkaline Types on the production of calcium carbonate particles from gypsum waste for fixation of CO_2 by mineral carbonation. *International Journal of Coal Preparation and Utilization* 1–19 (2018). doi:10.1080/19392699.2018.1452739

54. Polettini, A., Pomi, R. & Stramazzo, A. Carbon sequestration through accelerated carbonation of BOF slag: Influence of particle size characteristics. *Chem. Eng. J.* **298,** 26–35 (2016).

55. Oelkers, E. H., Gislason, S. R. & Matter, J. Mineral carbonation of CO_2. *Elements* **4,** 333–337 (2008).

56. Matter, J. M. *et al.* Rapid carbon mineralization for permanent disposal of anthropogenic carbon dioxide emissions. *Science (80).* **352,** 1312–1314 (2016).

57. Declercq, J. & Oelkers, E. H. CarbFix Report: PHREEQC mineral dissolution kinetics database. (2014).

58. Aradóttir, E. S. P., Sonnenthal, E. L. & Jónsson, H. Development and evaluation of a thermodynamic dataset for phases of interest in CO_2 mineral sequestration in basaltic rocks. *Chem. Geol.* **304–305,** 26–38 (2012).

59. Oelkers, E. H. *et al.* Using stable Mg isotope signatures to assess the fate of magnesium during the in situ mineralisation of CO_2 and H_2S at the CarbFix site in SW-Iceland.

Geochim. Cosmochim. Acta **245,** 542–555 (2019).

60. Alfredsson, H. A. *et al.* The geology and water chemistry of the Hellisheidi, SW-Iceland carbon storage site. *Int. J. Greenh. Gas Control* **12,** 399–418 (2013).

61. Sigfusson, B. *et al.* Solving the carbon-dioxide buoyancy challenge: The design and field testing of a dissolved CO_2 injection system. *Int. J. Greenh. Gas Control* **37,** (2015).

62. Lu, J., Mickler, P. J., Nicot, J. P., Yang, C. & Darvari, R. Geochemical impact of O_2 impurity in CO_2 stream on carbonate carbon-storage reservoirs. *Int. J. Greenh. Gas Control* **47,** 159–175 (2016).

63. Hangx, S., Bakker, E., Bertier, P., Nover, G. & Busch, A. Chemical–mechanical coupling observed for depleted oil reservoirs subjected to long-term CO_2-exposure – A case study of the Werkendam natural CO_2 analogue field. *Earth Planet. Sci. Lett.* **428,** 230–242 (2015).

64. Ahmadi, M. A., Pouladi, B. & Barghi, T. Numerical modeling of CO_2 injection scenarios in petroleum reservoirs: Application to CO_2 sequestration and EOR. *J. Nat. Gas Sci. Eng.* **30,** 38–49 (2016).

65. Kelemen Peter. Melt extraction from the mantle beneath mid-ocean ridges. *Oceanus* **41,** 23–28 (1998).

66. Marini, L. *Geological Sequestration of Carbon Dioxide: Thermodynamics, Kinetics, and Reaction Path Modeling*. (Elsevier Science, 2007).

67. Lechat, K., Lemieux, J. M., Molson, J., Beaudoin, G. & Hébert, R. Field evidence of CO_2 sequestration by mineral carbonation in ultramafic milling wastes, Thetford Mines, Canada. *Int. J. Greenh. Gas Control* **47,** 110–121 (2016).

68. Schaef, H. T. *et al.* Silicate carbonation in supercritical CO_2 containing dissolved H_2O: An in situ high pressure X-Ray diffraction and infrared spectroscopy study. *Energy Procedia* **37,** 5892–5896 (2013).

69. Zhang, S. & Liu, H. H. Porosity-permeability relationships in modeling salt precipitation during CO2 sequestration: Review of conceptual models and implementation in numerical simulations. *Int. J. Greenh. Gas Control* **52,** 24–31 (2016).

70. O'Connor, W. K., Dahlin, D. C., Nilsen, D. N., Walters, R. P. & Turner, P. C. Carbon dioxide sequestration by direct mineral carbonation with carbonic acid. in *Proceedings of the 25th International Technical Conf. On Coal Utilization & Fuel Systems* 1–15 (2000).

71. O'Connor, W. K. & Rush, G. E. Applications of mineral carbonation to geological sequestration of CO_2, in *Osti.Gov* (2005).

72. O'Connor, W.K., Dahlin, D.C., Rush, G.E., et al. Aqueous mineral carbonation: mineral availability, pretreatment, reaction parametrics and process studies. Albany Research Centre, DOE/ARC-TR-04-002, Albany, OR, USA (2004).

73. Penner, L., Connor, W. K. O., Dahlin, D. C., Gerdemann, S. & Rush, G. E. Mineral carbonation: Energy costs of pretreatment options and insigths gaines fromflow loop reation studies. Albany Research Centre, DOE/ARC--2004-042, OR, USA (2004).

74. Dahlin, D. C. *et al.* A method for permanent CO_2 mineral carbonation, in *17th Annual International Pittsburgh Coal Conference* 1–14 (2000).

75. Gerdemann, S. J., O'Connor, W. K., Dahlin, D. C., Penner, L. R. & Rush, H. Ex situ aqueous mineral carbonation. *Environ. Sci. Technol.* **41,** 2587–2593 (2007).

76. Pasquier, L. C., Mercier, G., Blais, J. F., Cecchi, E. & Kentish, S. Parameters optimization for direct flue gas CO_2 capture and sequestration by aqueous mineral carbonation using activated serpentinite based mining residue. *Appl. Geochemistry* **50,** 66–73 (2014).

77. Koukouzas, N., Gemeni, V. & Ziock, H. J. Sequestration of CO_2 in magnesium silicates, in Western Macedonia, Greece. *Int. J. Miner. Process.* **93,** 179–186 (2009).

78. Pasquier, L. C., Mercier, G., Blais, J. F., Cecchi, E. & Kentish, S. Reaction mechanism for the aqueous-phase mineral carbonation of heat-activated serpentine at low temperatures and pressures in flue gas conditions. *Environ. Sci. Technol.* **48,** 5163–5170 (2014).

79. Daval, D., Hellmann, R., Martinez, I., Gangloff, S. & Guyot, F. Lizardite serpentine dissolution kinetics as a function of pH and temperature, including effects of elevated PCO_2. *Chem. Geol.* **351,** 245–256 (2013).

80. Santos, R. M., Knops, P. C. M., Rijnsburger, K. L. & Chiang, Y. W. CO_2 Energy Reactor – Integrated mineral carbonation: Perspectives on lab-scale investigation and products valorization. *Front. Energy Res.* **4,** 1–6 (2016).

81. Giammar, D. E., Bruant, R. G. & Peters, C. A. Forsterite dissolution and magnesite precipitation at conditions relevant for deep saline aquifer storage and sequestration of carbon dioxide. *Chem. Geol.* **217,** 257–276 (2005).

82. Martinez, R. E., Weber, S. & Bucher, K. Quantifying the kinetics of olivine dissolution in partially closed and closed batch reactor systems. *Chem. Geol.* **367,** 1–12 (2014).

83. O'Connor, W. K., Dahlin, D. C., Nilsen, D. N. & Walters, R. P. Carbon dioxide sequestration by direct aqueous mineral carbonation. *osti.gov* 11 (2001).

84. Prigiobbe, V., Hänchen, M., Werner, M., Baciocchi, R. & Mazzotti, M. Mineral carbonation process for CO_2 sequestration. *Energy Procedia* **1,** 4885–4890 (2009).

85. Pokrovsky, O. S. & Schott, J. Kinetics and mechanism of forsterite dissolution at 25 ℃ and pH from 1 to 12. *Geochim. Cosmochim. Acta* **64,** 3313–3325 (2000).

86. Fabian, M. *et al.* The influence of attrition milling on carbon dioxide sequestration on magnesium-iron silicate. *Miner. Eng.* **23,** 616–620 (2010).

87. Baláž, P. *et al.* Structural changes in olivine $(Mg,Fe)_2SiO_4$ mechanically activated in high-energy mills. *Int. J. Miner. Process.* **88,** 1–6 (2008).

88. Haug, T. A., Kleiv, R. A. & Munz, I. A. Investigating dissolution of mechanically activated olivine for carbonation purposes. *Appl. Geochemistry* **25,** 1547–1563 (2010).

89. Li, J. & Hitch, M. Carbon dioxide adsorption isotherm study on mine waste for integrated CO_2 capture and sequestration processes. *Powder Technol.* **291,** 408–413 (2016).

90. Li, J. & Hitch, M. Mechanical activation of ultramafic mine waste rock in dry condition for enhanced mineral carbonation. *Miner. Eng.* **95,** 1–4 (2016).

91. Rigopoulos, I. *et al.* Carbon dioxide storage in olivine basalts: Effect of ball milling process. *Powder Technol.* **273,** 220–229 (2015).

92. Rigopoulos, I. *et al.* Enhancing the rate of ex situ mineral carbonation in dunites via ball milling. *Adv. Powder Technol.* **27,** 360–371 (2015).

93. Turianicová, E. *et al.* A comparison of the reactivity of activated and non-activated olivine with CO_2. *Int. J. Miner. Process.* **123,** 73–77 (2013).

94. Kleiv, R. A. & Thornhill, M. Mechanical activation of olivine. *Miner. Eng.* **19,** 340–347 (2006).

95. Park, A. H. A. & Fan, L. S. CO_2 mineral sequestration: Physically activated dissolution of serpentine and pH swing process. *Chem. Eng. Sci.* **59,** 5241–5247 (2004).

96. Turianicová, E. *et al.* Interaction of natural and thermally processed vermiculites with gaseous carbon dioxide during mechanical activation. *Appl. Clay Sci.* **88–89,** 86–91 (2014).

97. Santos, R. *et al.* Nickel extraction from olivine: Effect of carbonation pre-treatment. *Metals (Basel).* **5,** 1620–1644 (2015).

98. Hamilton, J. L. The fate of transition metals during enhanced weathering and development of geochemical treatments for accelerated carbonation of ultramafic mine tailings. (Monash University, 2018).

99. Hamilton, J. L. *et al.* Fate of transition metals during passive carbonation of ultramafic mine tailings via air capture with potential for metal resource recovery. *Int. J. Greenh. Gas Control* **71,** 155–167 (2018).

100. Energy Reactor©: http://www.innovationconcepts.eu/CO2EnergyReactor.htm. Accessed by May 1st, 2019.

101. Power, I. M., Harrison, A. L., Dipple, G. M. & Southam, G. Carbon sequestration via carbonic anhydrase facilitated magnesium carbonate precipitation. *Int. J. Greenh. Gas Control* **16,** 145–155 (2013).

102. Harrison, A. L., Power, I. M. & Dipple, G. M. Accelerated carbonation of brucite in mine tailings for carbon sequestration. *Environ. Sci. Technol.* **47,** 126–134 (2013).

103. Power, I. M., Harrison, A. L. & Dipple, G. M. Accelerating mineral carbonation using carbonic anhydrase. *Environ. Sci. Technol.* **50,** 2610–2618 (2016).

104. Carbonic anhydrase, Sigma-Aldrich. Avaible at: https://www. sigmaaldrich.com. Accessed: April 24th, 2019.

105. Huijgen, W., Witkamp, G. J. & Comans, R. Mineral CO_2 sequestration in alkaline solid residues. *Greenh. Gas Control Technol.* 2415–2418 (2005). doi:10.1016/B978-008044704-9/50344-X

106. Mayoral, M. C., Andrés, J. M. & Gimeno, M. P. Optimization of mineral carbonation process for CO_2 sequestration by lime-rich coal ashes. *Fuel* **106,** 448–454 (2013).

107. Hosseini, T., Haque, N., Selomulya, C. & Zhang, L. Mineral carbonation of Victorian brown coal fly ash using regenerative ammonium chloride - Process simulation and techno-economic analysis. *Appl. Energy* **175,** 54–68 (2016).

108. Nyambura, M. G., Mugera, G. W., Felicia, P. L. & Gathura, N. P. Carbonation of brine impacted fractionated coal fly ash: Implications for CO_2 sequestration. *J. Environ. Manage.* **92,** 655–664 (2011).

109. Tamilselvi Dananjayan, R. R., Kandasamy, P. & Andimuthu, R. Direct mineral carbonation of coal fly ash for CO_2 sequestration. *J. Clean. Prod.* **112,** 4173–4182 (2016).

110. Han, S. J., Im, H. J. & Wee, J. H. Leaching and indirect mineral carbonation performance of coal fly ash-water solution system. *Appl. Energy* **142,** 274–282 (2015).

111. Reynolds, B., Reddy, K. J. & Argyle, M. D. Field application of accelerated mineral carbonation. *Minerals* **4,** 191–207 (2014).

112. Ji, L. *et al.* Insights into carbonation kinetics of fly ash from Victorian lignite for CO_2 sequestration. *Energy & Fuels* **32,** 4569–4578 (2018).

113. Santos, R. M., François, D., Mertens, G., Elsen, J. & Gerven, T. Van. Ultrasound-intensified mineral carbonation. *Appl. Therm. Eng.* **57,** 154–163 (2013).

114. Su, T. H., Yang, H. J., Shau, Y. H., Takazawa, E. & Lee, Y. C. CO_2 sequestration utilizing basic-oxygen furnace slag: Controlling factors, reaction mechanisms and V-Cr concerns. *J. Environ. Sci. (China)* **41,** 99–111 (2016).

115. Fernández Bertos, M., Li, X., Simons, S. J. R., Hills, C. D. & Carey, P. J. Investigation of accelerated carbonation for the stabilisation of MSW incinerator ashes and the sequestration of CO_2. *Green Chem.* **6,** 428–436 (2004).

116. Araizi, P. K., Hills, C. D., Maries, A., Gunning, P. J. & Wray, D. S. Enhancement of accelerated carbonation of alkaline waste residues by ultrasound. *Waste Manag.* **50,** 121–129 (2016).

117. Munz, I. A. *et al.* A continuous process for manufacture of magnesite and silica from olivine, CO_2 and H_2O. *Energy Procedia* **1,** 4891–4898 (2009).

118. Meyer, N. A. *et al.* Mineral carbonation of PGM mine tailings for CO_2 storage in South Africa: A case study. *Miner. Eng.* **59,** 45–51 (2014).

119. Kemache, N. *et al.* Aqueous mineral carbonation of serpentinite on a pilot scale: The effect of liquid recirculation on CO_2 sequestration and carbonate precipitation. *Appl. Geochemistry* **67,** 21–29 (2016).

120. Sanna, A., Dri, M. & Maroto-Valer, M. Carbon dioxide capture and storage by pH swing aqueous mineralisation using a mixture of ammonium salts and antigorite source. *Fuel* **114,** 153–161 (2013).

121. Sanna, A. *et al.* Enhancing Mg extraction from lizardite-rich serpentine for CO_2 mineral sequestration. *Miner. Eng.* **49,** 135–144 (2013).

122. Azdarpour, A. *et al.* A review on carbon dioxide mineral carbonation through pH-swing process. *Chem. Eng. J.* **279,** 615–630 (2015).

123. Romão, I. S., Gando-Ferreira, L. M., Da Silva, M. M., & Zevenhoven, R. CO_2 sequestration with serpentinite and metaperidotite from Northeast Portugal. *Miner. Eng.* **94,** 104–114 (2016).

124. Zevenhoven, R., Slotte, M., Åbacka, J. & Highfield, J. A comparison of CO_2 mineral sequestration processes involving a dry or wet carbonation step. *Energy* **117,** 604–611 (2015).

125. Huijgen, W. J, Comans, R. N. Carbon dioxide sequestration by mineral carbonation: literature review update 2003-2004. Energy Research Centre of the Netherlands, ECN-C--05-022, Petten, The Netherlands (2004).

126. Mazzotti, M., Abanades, J. C., Allam, R., et al. Mineral carbonation and industrial uses of carbon dioxide. In: B. Eliasson and R.T.M. Sutamihardja, editor. Carbon dioxide capture and storage. Cambridge, United Kingdom: Cambridge University Press, 2005. p. 319-338.

127. Teir, S., Eloneva, S., Fogelholm, C. J. & Zevenhoven, R. Stability of calcium carbonate and magnesium carbonate in rainwater and nitric acid solutions. *Energy Convers. Manag.* **47,** 3059–3068 (2006).

128. Zevenhoven, R. & Fagerlund, J. Mineral sequestration for CCS in Finland and abroad. in *World Renewable Energy Congress 2011-Sweden, Climate Change Issues (CC)* 660–667 (2011).

129. Pasquier, L. C., Mercier, G., Blais, J. F., Cecchi, E. & Kentish, S. Technical & economic evaluation of a mineral carbonation process using southern Québec mining wastes for CO_2 sequestration of raw flue gas with by-product recovery. *Int. J. Greenh. Gas Control* **50,** 147–157 (2016).

130. Gabbard, A. Coal combustion: Nuclear resource or danger. *ORNL Rev.* **26,** 1–9 (1993).

131. Song, K. *et al.* Effect of polyacrylic acid on direct aqueous mineral carbonation of flue gas desulfurization gypsum. *Chem. Eng. J.* **301,** 51–57 (2016).

132. Song, K., Kim, W., Bang, J. H., Park, S. & Jeon, C. W. Polymorphs of pure calcium carbonate prepared by the mineral carbonation of flue gas desulfurization gypsum. *Mater.*

Des. **83,** 308–313 (2015).

133. Xuan, D., Zhan, B. & Poon, C. S. Development of a new generation of eco-friendly concrete blocks by accelerated mineral carbonation. *J. Clean. Prod.* **133,** 1235–1241 (2016).

134. Ben Ghacham, A., Cecchi, E., Pasquier, L. C., Blais, J. F. & Mercier, G. CO_2 sequestration using waste concrete and anorthosite tailings by direct mineral carbonation in gas-solid-liquid and gas-solid routes. *J. Environ. Manage.* **163,** 70–77 (2015).

135. Lewis, A. E. Review of metal sulphide precipitation. *Hydrometallurgy* **104,** 222–234 (2010).

136. AMC Mining Concultants (Canada) Ltd. Turnagain nickel project mineral processing and metallurgical testing status report (2012).

137. Wang, F., Dreisinger, D. B., Jarvis, M. & Hitchins, T. The technology of CO_2 sequestration by mineral carbonation: current status and future prospects. *Can. Metall. Q.* **57,** 46–58 (2018).

138. Klock, P. R., Czamanske, G. K., Foose, M. & Pesek, J. Selective chemical dissolution of sulfides: An evaluation of six methods applicable to assaying sulfide-bound nickel. *Chem. Geol.* 157–163 (1986).

139. Penttinen, U., Palosaari, V. & Siura, T. Selective dissolution and determination of sulphides in nickel ores by the bromine-methanol method. *Bull Geol Soc Finl.* **49,** 79–84 (1977).

140. Falini, G. *et al.* Tubular-shaped stoichiometric chrysotile nanocrystals. *Chem. - A Eur. J.* **10,** 3043–3049 (2004).

141. Scarlett, N. V. Y. & Madsen, I. C. Quantification of phases with partial or no known crystal structures. *Powder Diffr.* **21,** 278–284 (2006).

142. Mellini, M. The crystal structure of lizardite 1T: hydrogen bonds and polytypism. *American Mineralogist* **67,** (1982).

143. Wang, F., Dreisinger, D., Jarvis, M. & Hitchins, T. Kinetics and mechanism of mineral carbonation of olivine for CO_2 sequestration. *Miner. Eng.* **131,** 185–197 (2019).

144. Gharabaghi, M., Irannajad, M. & Azadmehr, A. R. Leaching kinetics of nickel extraction from hazardous waste by sulphuric acid and optimization dissolution conditions. *Chem. Eng. Res. Des.* **91,** 325–331 (2013).

145. Habashi, F. *Kinetics of Metallurgical Processes*. (Métallurgie Extractive Publishing, 1999).

146. Huijgen, W. J. J., Witkamp, G. & Comans, R. N. J. Mechanisms of aqueous wollastonite carbonation as a possible CO_2 sequestration process. *Chem. Eng. Sci.* **61,** 4242–4251 (2006).

147. Levenspiel, O. *Chemical Reaction Engineering*. (Wiley, 1999). doi:10.1016/0009-2509(64)85017-X

148. Boot-Handford, M. E. *et al.* Carbon capture and storage update. *Energy Environ. Sci.* **7,** 130–189 (2014).

149. Hamid, R. D., Swedlund, P. J., Song, Y. & Miskelly, G. M. Ionic strength effects on silicic acid (H_4SiO_4) sorption and oligomerization on an iron oxide surface: An interesting interplay between electrostatic and chemical forces. *Langmuir* **27,** 12930–12937 (2011).

150. O'Connor, W. K., Dahlin, D. C., Rush, G. E., Dahlin, C. L. & Collins, W. K. Carbon dioxide sequestration by direct mineral carbonation: Process mineralogy of feed and products. in *Minerals and Metallurgical Processing* **19,** 95–101 (2002).

151. Wang, F. *et al.* A mechanism of calcium fluoride-enhanced vanadium leaching from stone coal. *Int. J. Miner. Process.* **145,** 87–93 (2015).

152. Long, H. & Dixon, D. G. Pressure oxidation of pyrite in sulfuric acid media: A kinetic study. *Hydrometallurgy* **73,** 335–349 (2004).

153. Xu, H. *et al.* Sulfuric acid leaching of zinc silicate ore under pressure. *Hydrometallurgy* **105,** 186–190 (2010).

154. Dreisinger, D. *Silica chemistry for hydrometallurgy*. Department of Materials Engineering, University of British Columbia, Vancouver, BC, Canada (2019).

155. Wood, C. E., Qafoku, O., Loring, J. S. & Chaka, A. M. Role of Fe(II) content in olivine carbonation in wet supercritical CO_2. *Environ. Sci. Technol. Lett.* (2019). doi:10.1021/acs.estlett.9b00496

156. Davidson, J. M. & Glass, D. H. Nucleation kinetics in the reactions of nickel basic carbonates with hydrogen sulfide: The carbonate precipitation reactions of divalent nickel. *Ind. Eng. Chem. Res.* **46,** 4772–4777 (2007).

157. Dixon, D. *Modeling of leaching reactors*. Department of Materials Engineering, University of British Columbia, Vancouver, BC. Canada (2019).

Appendixes

Appendix A Procedures of bromine-methanol digestion for nickel sulfide analysis

The following are the detailed steps for the bromine-methanol digestion and atomic absorption analysis (AAS)[138,139].

(1) Add 80 mL of anhydrous methanol and 5 mL of bromine to a 500 mL glass shaking bottle;

(2) Cool and add 1000 mg of sample; (3) Shake gently on a wrist-action shaker for 1 h (150 rpm);

(4) In a fume hood, filter into a 250 mL beaker by 0.2 μm membrane filter, washing with methanol three times;

(5) Heat the filtrate to around 25 mL on a steam bath (Attention: do not make the temperature setting over 300 ℃. Otherwise, there will be a fire! Methanol is flammable!);

(6) Cool down the filtrate and add 10 mL concentrated nitric acid, continue to carefully heat to dryness on the steam bath. (Attention: wear suitable gloves or use a plier! It is highly toxic! In the end of this stage, heat it very slowly, otherwise the dryness will splash everywhere resulting in the loss of nickel);

(7) Add 1 mL hydrochloric acid and heat again to dryness. (heat it very slowly to prevent the dryness of splashing);

(8) Add 5 mL of hydrochloric acid to completely dissolve the dryness with some deionized water, if necessary with some heat;

(9) Cool it down and transfer all into a 50 mL volumetric flask;

(10) Dilute the solution for AAS analysis;

(11) Analyze the nickel, iron and cobalt sulfides contents and calculate the molar ratio of iorn/nickel sulfides in the products.

Appendix B Concentration of nickel, cobalt, magnesium and iron in aqueous solution after mineral carbonation

The mineral carbonation tests were carried out in a 2-Litre titanium autoclave (No. 4520, Parr Instrument) under conditions of under the conditions of P_{80} = 30 ± 3 μm, 185 ± 2 ℃, PCO_2 = 20.7 bar, 15% solids content, 1 m $NaHCO_3$+1 m NaCl, 700 rpm for 5 hours. The mineral carbonation efficiency for all samples was varied from 9% to 29%, which was dependent on the olivine content in sample. After mineral carbonation reaction for each sample, the slurry was taken and followed by the liquid/solid separation of filtration through a qualitative Whatman™ filter paper. For each aqueous sample, 5 mL was taken and diluted 5 times into 2% nitric acid for ICP-OES where the standard solutions were the Ni, Co, Mg and Fe mixture with the matrix of nitric acid. The concentrations of Ni, Co, Mg and Fe in aqueous solutions after mineral carbonation of samples and the corresponding dissolution efficiencies of the four elements are shown in Table Appendix B-1.

Table B-1 Concentration of nickel, cobalt, magnesium and iron in aqueous solution after mineral carbonation

Samples	Concentration in solution after MC, mg/L				Dissolution efficiency, %			
	Ni	Co	Mg	Fe	Ni	Co	Mg	Fe
High-grade Olivine	0.37	-	70.83	0.79	0.07	-	0.20	0.008
SN254	0.34	0.010	38.95	0.96	0.07	0.05	0.09	0.008
SN255	0.33	-	43.40	0.84	0.07	-	0.10	0.007
SN256	0.21	0.017	65.10	0.29	0.04	0.05	0.17	0.002
SN257	0.24	-	23.86	0.33	0.04	-	0.06	0.002
SN258	0.09	-	27.26	0.30	0.01	-	0.07	0.002
SN259	0.20	-	39.61	0.33	0.05	-	0.12	0.002
SN260	0.28	-	38.18	0.68	0.02	-	0.12	0.002
SN261	1.08	0.016	41.89	0.44	0.19	0.05	0.12	0.003
SN262	0.35	0.021	34.46	0.80	0.05	0.06	0.09	0.005

Mineral carbonation conditions: P_{80}=30±3 μm of particle size (size reduction by a pulveriser), 185 ℃, PCO_2=20.7 bar, 15% solids content, 1 m $NaHCO_3$, 1 m NaCl, 700 rpm, 5 hours within a 2 liter titanium autoclave reactor No. 4522 and temperature control system No. 4842.

According to Table Appendix B-1, there were but trace concentrations of Ni, Co and Fe (all less than 1 mg/L) in the solutions of the 10 samples after mineral carbonation except that Mg was higher concentration than the other three elements but still less than 100 mg/L. The dissolution efficiencies of all the four elements were always lower than 0.2%. Therefore, it can be considered that all the bivalent metals have been converted into stable carbonates during mineral carbonation.

Appendix C △G for formation of aqueous H_4SiO_4 during mineral carbonation

Table C-1 △G for formation of aqueous H_4SiO_4 during mineral carbonation.

Reactions	$2CO_{2(g)} + Mg_2SiO_4 + 2H_2O_{(l)} = 2MgCO_3 + H_4SiO_{4(a)}$	
Temperature, ℃	△G °, kJ/mol	△G, kJ/mol
110	6.721	-34.218
115	8.466	-33.007
120	10.211	-31.796
125	11.956	-30.585
130	13.701	-29.375
135	15.445	-28.164
140	17.190	-26.954
145	18.934	-25.744
150	20.679	-24.533
155	22.423	-23.323
160	24.168	-22.113
165	25.913	-20.902
170	27.658	-19.691
175	29.404	-18.480
180	31.149	-17.268
185	32.896	-16.056
190	34.642	-14.844
195	36.389	-13.631
200	38.137	-12.417

CO_2 partial pressure is considered as 34.5 bar; concentration of aqueous H_4SiO_4 is considered as 300 mg/L according to Figure 5.9; and all the other △G° data are from HSC 7.1.

Appendix D Verification of reliability and representativeness of samples through continuous sampling kit during mineral carbonation

The comparison of mineral carbonation efficiency through the developed Equation 4.7 based on continuous sampling and through the traditional Equation 4.3 based on change of weight has been shown in Figure D-1. The comparison was carried out under various conditions (PCO_2 varied from 20.7 bar to 34.5 bar and temperature varied between 185 ℃ and 175 ℃) for various samples which have different mineral compositions. It can be seen that the difference of mineral carbonation efficiencies based on the two methods was only less than 1.5%. It confirms that the samples taken through the continuous sampling kit during mineral carbonation are reliable and representative and the developed Equation 4.7 are suitable for the calculation of mineral carbonation efficiency.

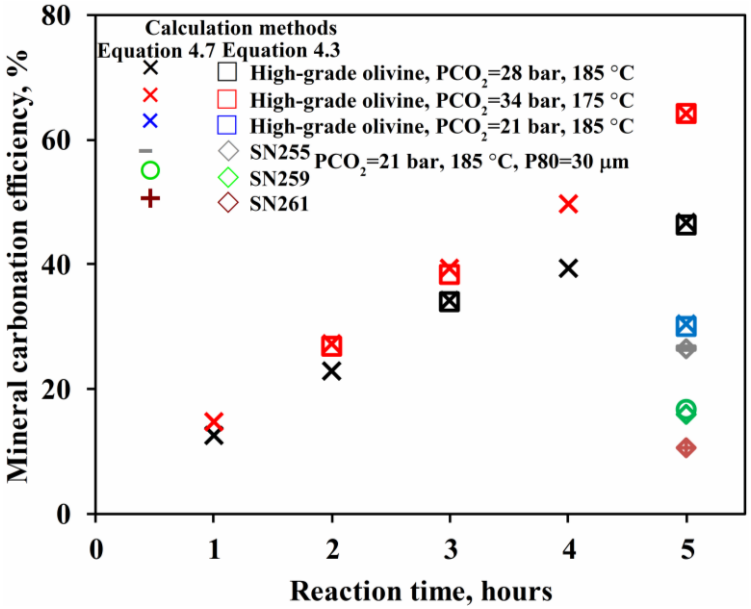

Figure D-1 Comparison of mineral carbonation efficiency through Equation 4.7 based on continuous sampling and through Equation 4.3 based on change of weight. Mineral carbonation conditions: -25 µm high-grade olivine, 700 rpm, 10% solids content, with addition of 1 m $NaHCO_3$ + 1 m NaCl.

Appendix E Relationship between rate constant of chemical reaction control model and average particle size

For the classical SCM model, the rate constant k_2 for chemical reaction control model should be linear to the reciprocal of initial particle size with slope=1[157]. In addition to the relationship of logarithm of specific surface area of narrow-sized particles versus logarithm of rate constant for chemical reaction control model which is shown in Chapter 5, the relationship between rate constant k_2 and 1/Daverage was further analyzed to confirm the suitability of chemical reaction model for all narrow-sized particles of high-grade olivine, especially for -25 μm fractions which had a wide range of particle size distribution. Table E-1 shows the initial particle size of high-grade olivine particle fractions, -25 μm, 25 – 38 μm, 38 – 53 μm, and 53 – 75 μm. The particle size was based on three types, D50, D[4,3] and D[3,2], which can be obtained through laser particle size analysis (Malvern Masersizer 2000). There was obvious difference between D[4,3] and D[3,2], as shown in Table E-1. The difference even became more obvious for smaller size fractions. It means that the high-grade olivine particles were not very regular sphere.

Table E-1 Initial particle size of high-grade olivine particle fractions

$D_{average}$, μm	-25	25 – 38	38 – 53	53 – 75
D50	13.3	39.6	51.1	76.9
D[4,3]	15.7	37.3	53.0	79.6
D[3,2]	3.9	22.3	49.2	74.2

Figure E-1 reveals that there was always linear relationship between k_2 and 1/D for all D50, D[4,3] and D[3,2] with R^2 more than 0.99. It is to say that -25 μm olivine particle fractions were suitable for kinetic analysis of carbonation despite of the wide distribution of particle size and

irregular shape of particles. In addition, the slope of k_2 versus D[4,3] was 1. D[4,3] may be more suitable to represent the initial particle size of narrow-sized olivine particle fractions.

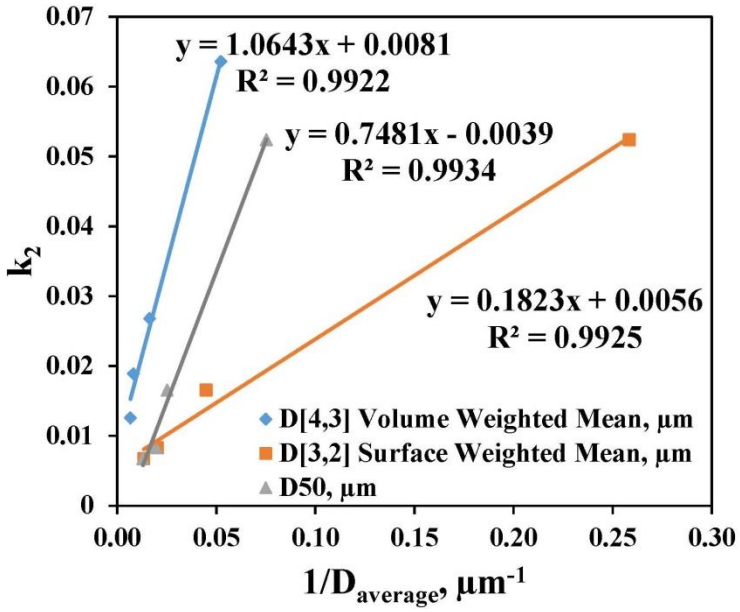

Figure E-1 Relationship of rate constant k_2 of chemical reaction control model versus $1/D_{average}$ for mineral carbonation of high-grade olivine particle fractions: -25 µm, 25 – 38 µm, 38 – 53 µm, and 53 – 75 µm.